

DEVELOPMENT OF MULTIBAND MICROSTRIP ANTENNAS FOR GPS  
APPLICATIONS

A THESIS SUBMITTED TO  
THE GRADUATE SCHOOL OF NATURAL AND APPLIED SCIENCES  
OF  
MIDDLE EAST TECHNICAL UNIVERSITY

BY

MUSTAFA CANER ÖNDER

IN PARTIAL FULFILLMENT OF THE REQUIREMENTS  
FOR  
THE DEGREE OF MASTER OF SCIENCE  
IN  
ELECTRICAL AND ELECTRONICS ENGINEERING

SEPTEMBER 2019



Approval of the thesis:

**DEVELOPMENT OF MULTIBAND MICROSTRIP ANTENNAS FOR GPS APPLICATIONS**

submitted by **MUSTAFA CANER ÖNDER** in partial fulfillment of the requirements for the degree of **Master of Science in Electrical and Electronics Engineering Department, Middle East Technical University** by,

Prof. Dr. Halil Kalıpçılar  
Dean, Graduate School of **Natural and Applied Sciences** \_\_\_\_\_

Prof. Dr. İlkay Ulusoy  
Head of Department, **Electrical and Electronics Engineering** \_\_\_\_\_

Prof. Dr. Özlem Aydın Çivi  
Supervisor, **Electrical and Electronics Engineering** \_\_\_\_\_

**Examining Committee Members:**

Prof. Dr. Sencer Koç  
Electrical and Electronics Engineering, METU \_\_\_\_\_

Prof. Dr. Özlem Aydın Çivi  
Electrical and Electronics Engineering, METU \_\_\_\_\_

Prof. Dr. Şimşek Demir  
Electrical and Electronics Engineering, METU \_\_\_\_\_

Prof. Dr. Asım Egemen Yılmaz  
Electrical and Electronics Engineering, Ankara University \_\_\_\_\_

Assoc. Prof. Dr. Lale Alatan  
Electrical and Electronics Engineering, METU \_\_\_\_\_

Date: 04.09.2019

**I hereby declare that all information in this document has been obtained and presented in accordance with academic rules and ethical conduct. I also declare that, as required by these rules and conduct, I have fully cited and referenced all material and results that are not original to this work.**

Name, Surname: Mustafa Caner Önder

Signature :

## ABSTRACT

### DEVELOPMENT OF MULTIBAND MICROSTRIP ANTENNAS FOR GPS APPLICATIONS

Önder, Mustafa Caner

M.S., Department of Electrical and Electronics Engineering

Supervisor: Prof. Dr. Özlem Aydın Çivi

SEPTEMBER 2019, 143 pages

In this thesis study, the design, fabrication and measurements of dualband and triband circularly polarized microstrip antennas for GPS applications are presented. Characteristic mode analysis technique is applied to get an insight into circularly polarized patch antennas. A design flow is presented for a circularly polarized L1 GPS band microstrip antenna by using characteristic mode analysis.

A single fed L1/L2 GPS band right hand circularly polarized four-slotted patch antenna is designed by using reactive loading technique. A novel zigzag four-slotted patch is designed to operate at L1/L2 GPS bands without the need of reactive loading and designed antenna is fabricated. The frequency ratio of 1.31 is achieved with zigzag four-slotted patch. The axial ratios 7.5 dB and 8.1 dB are measured at lower and higher operating bands, respectively.

An L1/L2/L5 GPS band single fed right hand circularly polarized two-layer stacked antenna is designed and fabricated. In measurements, it is seen that the impedance bandwidths of 58 MHz, 28 MHz and 11 MHz are achieved at operating frequencies.

The axial ratios of 0.7 dB, 8 dB and 7.5 dB are measured at operating frequencies.

An L1/L2/L5 GPS band single fed right hand circularly polarized three-layer stacked antenna is designed and fabricated. In measurements, the impedance bandwidths of 71.1 MHz, 4 MHz and 32 MHz are achieved at the center frequencies of L5, L2 and L1 GPS bands, respectively. The axial ratios of 0.7 dB and 3-dB axial ratio bandwidth of 5 MHz are measured at L1 GPS band. The lowest axial ratios of 1.5 dB and 8.9 dB are measured at the lowest and the middle operating frequencies, respectively.

Keywords: microstrip antenna, multiband, dualband, triband, circular polarization, stacked antenna, GPS antenna, characteristic mode analysis

## ÖZ

### **KKS UYGULAMALARI İÇİN ÇOK BANTLI MİKROŞERİT ANTENLERİN GELİŞTİRİLMESİ**

Önder, Mustafa Caner

Yüksek Lisans, Elektrik ve Elektronik Mühendisliği Bölümü

Tez Yöneticisi: Prof. Dr. Özlem Aydın Çivi

Eylül 2019 , 143 sayfa

Bu tez çalışmasında, KKS uygulamaları için iki bantlı ve üç bantlı dairesel polarize mikroşerit antenlerin tasarımı, üretimi ve ölçümleri sunulmaktadır. Dairesel polarize yama antenlerin iç yüzünü anlamak için karakteristik mod analiz tekniği uygulandı. Karakteristik mod analizi kullanılarak L1 KKS bandında çalışan dairesel polarize bir mikroşerit anten için bir tasarım akışı sunuldu.

Reaktif yükleme tekniği kullanılarak tek beslemeli L1/L2 KKS bantlarında sağ el dairesel polarize dört-yarıklı yama antena tasarlandı. Reaktif yüklemeye ihtiyaç duymadan L1/L2 KKS bantlarında çalışan özgün zikzak dört-yarıklı yama tasarlandı ve tasarlanan anten üretildi. Zikzak dört-yarıklı yama ile 1.31 frekans oranı elde edildi. Sırasıyla, düşük ve yüksek çalışma bantlarında 7.5 dB ve 8.1 dB eksenel oran ölçüldü.

L1/L2/L5 KKS bantlarında çalışan tek beslemeli sağ el dairesel polarize iki katlı bir yığın anten tasarlandı ve üretildi. Ölçümlerde, çalışma bantlarında 58 MHz, 28 MHz ve 11 MHz empedans bant genişliği elde edildiği görüldü. Çalışma bantlarında 0.7 dB, 8 dB ve 7.5 dB eksenel oran ölçüldü.

L1/L2/L5 KKS bantlarında çalışan tek beslemeli sađ el dairesel polarize üç katlı bir yığın anten tasarlandı ve üretildi. Ölçümlerde, sırasıyla L5, L2 ve L1 GPS bantları merkez frekanslarında 71.1 MHz, 4 MHz ve 32 MHz empedans bant genişliği elde edildi. L1 KKS bandında 0.7 dB aksel oran ve 5 MHz 3-dB aksel oran bant genişliği ölçüldü. Sırasıyla, en düşük ve orta çalışma frekanslarında en düşük aksel oran değeri 1.5 dB ve 8.9 dB olarak ölçüldü.

Anahtar Kelimeler: mikroşerit anten, çok bantlı, iki bantlı, üç bantlı, dairesel polarizasyon, yığın anten, KKS anteni, karakteristik mod analizi

*to Bilge...*

## ACKNOWLEDGMENTS

First of all, I would like to express my gratitude to my advisor, Prof. Dr. Özlem Aydın Çivi, for her guidance and patience.

I would like to thank to ROKETSAN Inc. and METU Electrical and Electronics Engineering Department for supports and assistance during the simulations, fabrication and measurements of antennas.

I would like to thank to Ozan Koroğlu for his guidance and supports in academic issues.

I would like to thank to my dear friend, Caner Yiğit, for the helps in the process of prototyping of antennas.

I sincerely thank to my wife, my love, my chance, my Bilge, for her emotional supports and eternal love... I love you dear!

I would like to thank to my mother, Fatma ÖNDER, my father, Ali ÖNDER, my brother, Anıl ÖNDER and the rest of all my family members for their supports and understanding during the thesis works. Sorry for my absence!

And finally, I sincerely express my gratitude to my grandfather, Hüseyin Önder, for his wisely vision on education and life...

## TABLE OF CONTENTS

ABSTRACT . . . . .	v
ÖZ . . . . .	vii
ACKNOWLEDGMENTS . . . . .	x
TABLE OF CONTENTS . . . . .	xi
LIST OF TABLES . . . . .	xiv
LIST OF FIGURES . . . . .	xvii
LIST OF ABBREVIATIONS . . . . .	xxviii
CHAPTERS	
1 INTRODUCTION . . . . .	1
1.1 Objectives and Structure of the Thesis . . . . .	2
1.2 Microstrip Patch Antenna . . . . .	4
1.3 Circular Polarization in Microstrip Antennas . . . . .	6
1.4 Multiband Operation in Microstrip Antenna . . . . .	11
1.5 Multiband and Circularly Polarized Microstrip Antennas . . . . .	14
2 DESIGN OF CIRCULARLY POLARIZED MICROSTRIP PATCH AN- TENNA WITH CHARACTERISTIC MODE ANALYSIS . . . . .	21
2.1 Characteristic Mode Theory . . . . .	22
2.2 Physical Explanation of Characteristic Modes . . . . .	24

2.3	Circular Polarization Definition with CMA Parameters . . . . .	28
2.4	Design Flow of CP L1 GPS Band Single Fed Microstrip Patch Antenna with CMA Method . . . . .	29
2.5	Summary and Discussions . . . . .	40
3	DESIGN, FABRICATION AND MEASUREMENT OF A NOVEL L1/L2 DUALBAND MICROSTRIP ANTENNA FOR GPS APPLICATIONS . . .	43
3.1	THE PARAMETRIC ANALYSIS ON FOUR-EDGE SLOTTED PATCH ANTENNA . . . . .	44
3.1.1	Effect of the Dielectric Constant and the Height of the Substrate	47
3.1.2	Effect of Slot Length . . . . .	49
3.1.3	Effect of Slot Width . . . . .	49
3.1.4	Parametric Analysis on Slot Offset . . . . .	51
3.1.5	Summary of Parametric Analysis . . . . .	51
3.2	CIRCULAR POLARIZATION ON FOUR-SLOTTED PATCH . . . .	52
3.3	CAPACITIVELY LOADED L1/L2 BAND GPS ANTENNA . . . . .	53
3.4	L1/L2 BAND GPS ANTENNA with MODIFIED SLOTS . . . . .	60
3.4.1	Design and Simulations . . . . .	61
3.4.2	Fabrication of the Antenna . . . . .	72
3.4.3	Measurement Results of Fabricated Antenna . . . . .	73
3.5	SUMMARY and DISCUSSION . . . . .	77
4	DESIGN, FABRICATION AND MEASUREMENT OF L1/L2/L5 TRIBAND MICROSTRIP ANTENNAS FOR GPS APPLICATIONS . . . . .	79
4.1	L1/L2/L5 TRIBAND TWO-LAYER STACKED ANTENNA for GPS APPLICATIONS . . . . .	80
4.1.1	Design and Simulations . . . . .	80

4.1.2	Fabrication of the Antenna . . . . .	94
4.1.3	Measurement Results of Fabricated Antenna . . . . .	98
4.2	L1/L2/L5 TRIBAND THREE-LAYER STACKED ANTENNA for GPS APPLICATIONS . . . . .	103
4.2.1	Design and Simulations . . . . .	103
4.2.2	Fabrication of the Antenna . . . . .	118
4.2.3	Measurement Results of Fabricated Antenna . . . . .	120
4.3	SUMMARY and DISCUSSIONS . . . . .	131
5	CONCLUSION, ACHIEVEMENTS AND FUTURE WORKS . . . . .	135
	REFERENCES . . . . .	139

## LIST OF TABLES

### TABLES

Table 1.1	Feeding methods of microstrip antennas. . . . .	5
Table 1.2	Circular polarization performance of dualband and triband antennas in literature. . . . .	20
Table 2.1	Parameters of rectangular patch antenna for CMA simulations. . . .	25
Table 2.2	Initial parameters of CP corner truncated patch antenna for CMA simulations. . . . .	29
Table 2.3	Change of truncation length between 0 and 6 mm in CMA simulations.	33
Table 2.4	Change of truncation length between 4.1 and 4.9 mm in CMA sim- ulations. . . . .	34
Table 2.5	Change of patch length in CMA simulations. . . . .	36
Table 2.6	Final parameters of L1 GPS band CP corner truncated patch antenna.	40
Table 3.1	Initial design parameters of parametric analysis on four-edge slotted patch. . . . .	45
Table 3.2	The effect of slot width on frequency ratio. . . . .	51
Table 3.3	Summary of parametric analysis on four-edge slotted patch. . . . .	52
Table 3.4	Initial parameters for capacitive loaded patch antenna. . . . .	54
Table 3.5	Frequency ratio vs capacitance . . . . .	55

Table 3.6	Geometry of L1/L2 dualband four-edge slotted patch. . . . .	56
Table 3.7	Final Parameters of the Capacitively Loaded L1-L2 GPS Dualband Four-Edge Slotted Patch Antenna . . . . .	57
Table 3.8	Initial parameters of zigzag slot section inserted patch simulations. .	62
Table 3.9	Effects of the lengths of inserted zigzag slots between 5 mm and 35 mm. . . . .	63
Table 3.10	Effects of the lengths of inserted zigzag slots between 15 mm and 25 mm. . . . .	65
Table 3.11	Parameters of multiple zigzag slot inserted simulations. . . . .	66
Table 3.12	Effects of the multiple zigzag slot insertion. . . . .	67
Table 3.13	Change of bandwidth and frequency ratio when the parameters of slot offset and slot width are changed. . . . .	68
Table 3.14	Final design parameters of L1/L2 dualband GPS antenna with 7- Sector zigzag slotted patch. . . . .	70
Table 4.1	Initial parameters of nearly square patch simulations. . . . .	82
Table 4.2	Simulation parameters of CP nearly square patch antenna operates at L5 GPS band. . . . .	87
Table 4.3	Initial parameters of the two layered stacked antenna structure. . . .	90
Table 4.4	Final design parameters of the two-layer stacked antenna which op- erates CP at L1/L2/L5 GPS bands. . . . .	93
Table 4.5	Initial parameters of the parameter analysis on corner truncated an- tenna. . . . .	105
Table 4.6	The parameters of the L5 band circularly polarized truncated antenna.	108
Table 4.7	The parameters of the L5 band circularly polarized truncated stacked antenna . . . . .	110

Table 4.8	Summary of final simulation results of two-layer stacked antenna.	. . . 131
Table 4.9	Summary of measurement results of two-layer stacked antenna.	. . . 132
Table 4.10	Summary of final simulation results of three-layer stacked antenna.	. . . 133
Table 4.11	Summary of measurement results of three-layer stacked antenna.	. . . 133

## LIST OF FIGURES

### FIGURES

Figure 1.1	Structure of microstrip antenna. . . . .	5
Figure 1.2	Feeding methods of microstrip antennas [3]. . . . .	6
Figure 1.3	Representation of circularly polarized wave. . . . .	7
Figure 1.4	Trace of tip of electric field vectors for elliptical polarization. . .	7
Figure 1.5	Double fed CP microstrip antenna configurations for rectangular patches. . . . .	8
Figure 1.6	Double fed CP microstrip antenna configuration for circular patches.	8
Figure 1.7	Single Fed Circularly Polarized Patch Geometries . . . . .	9
Figure 1.8	Feed configurations for RHCP and LHCP on corner truncated patches. . . . .	9
Figure 1.9	Patch configurations for RHCP and LHCP on nearly square patches. . . . .	10
Figure 1.10	Patch configurations for RHCP and LHCP on asymmetrical cross-shaped slot patch. . . . .	11
Figure 1.11	Structure of stacked microstrip patch antenna for multiband operations. . . . .	12
Figure 1.12	Stacked microstrip antenna with air gap. . . . .	12
Figure 1.13	Multiband slot loaded patches. . . . .	13

Figure 1.14	Current distribution of $TM_{10}$ and $TM_{30}$ modes on dual edge slot patch, [32]. . . . .	14
Figure 1.15	Corner truncated stacked L1/L2 dualband GPS antenna. . . . .	15
Figure 1.16	Triband circularly polarized corner truncated stacked antenna. . .	16
Figure 1.17	Corner truncated stacked L1/L2 dualband GPS antenna with air gap. . . . .	17
Figure 1.18	Triband Circularly Polarized Stacked Antenna Configuration, (a) Upper Patch, (b) Middle Patch, (c) Lower Patch . . . . .	17
Figure 1.19	Center-cross and four edge slotted patch. . . . .	18
Figure 1.20	T-slot and Y-slot circularly polarized dualband microstrip antennas.	18
Figure 1.21	T-element loaded circularly polarized dualband antenna. . . . .	19
Figure 1.22	Slot loaded corner truncated circularly polarized dualband antenna.	19
Figure 2.1	Current distribution for rectangular patch of five modes . . . . .	23
Figure 2.2	Geometry of rectangular patch antenna for CMA simulations. . .	25
Figure 2.3	Eigenvalue vs Frequency graph of a rectangular patch antenna . .	26
Figure 2.4	MS graph of the rectangular patch antenna. . . . .	27
Figure 2.5	CA graph of the rectangular patch antenna. . . . .	28
Figure 2.6	CP corner truncated patch antenna for CMA simulations. . . . .	29
Figure 2.7	Graph of modal significance. . . . .	30
Figure 2.8	Graph of characteristic angle. . . . .	30
Figure 2.9	Design flow of CP L1 GPS band antenna with CMA method . .	31
Figure 2.10	MS result for square patch. . . . .	32
Figure 2.11	MS result for the change of truncation length. . . . .	32

Figure 2.12	MS result for the change of truncation length. . . . .	33
Figure 2.13	MS Curves of Mode-1. . . . .	35
Figure 2.14	MS Curves of Mode-2. . . . .	35
Figure 2.15	MS graph for the change of patch length in CMA simulations. . .	36
Figure 2.16	CA graph of the CP L1 GPS band corner truncated antenna in CMA simulation. . . . .	37
Figure 2.17	Location of coaxial probe on corner truncated patch. . . . .	37
Figure 2.18	$S_{11}$ of parametric analysis on the feed position of corner truncated patch. . . . .	38
Figure 2.19	Axial ratio of the corner truncated patch when $Y_f = 11.5$ mm. . .	39
Figure 2.20	Final axial ratio of CP corner truncated patch antenna at L1 GPS band with CMA method. . . . .	39
Figure 2.21	Final $S_{11}$ of CP corner truncated patch antenna at L1 GPS band with CMA method. . . . .	40
Figure 3.1	The geometry of four-edge slotted patch. . . . .	44
Figure 3.2	$S_{11}$ of four-edge slotted patch with initial parameters. . . . .	45
Figure 3.3	$TM_{10}$ mode surface current of four-edge slotted patch with ini- tial parameters at 1227 MHz. . . . .	46
Figure 3.4	$TM_{30}$ mode surface current of four-edge slotted patch with ini- tial parameters at 1632 MHz. . . . .	46
Figure 3.5	Radiation pattern of the $TM_{10}$ mode (at 1227 MHz), (a) Azimuth Pattern ( $\phi = 0^\circ$ ), (b) Elevation Pattern ( $\phi = 90^\circ$ ). . . . .	47
Figure 3.6	Radiation pattern of the $TM_{30}$ mode (at 1632 MHz), (a) Azimuth Pattern ( $\phi = 0^\circ$ ), (b) Elevation Pattern ( $\phi = 90^\circ$ ). . . . .	47

Figure 3.7	$S_{11}$ of parametric analysis on dielectric constant of substrates. . .	48
Figure 3.8	$S_{11}$ of parametric analysis on height of substrate. . . . .	49
Figure 3.9	$S_{11}$ of parametric analysis on slot length. . . . .	50
Figure 3.10	$S_{11}$ of parametric analysis on slot width. . . . .	50
Figure 3.11	$S_{11}$ of parametric analysis on slot offset. . . . .	51
Figure 3.12	The representation of horizontal and vertical slots and edges on four-edge slotted patch. . . . .	53
Figure 3.13	Capacitive loaded four-edge slotted patch. . . . .	54
Figure 3.14	$S_{11}$ of different capacitance loaded patch. . . . .	55
Figure 3.15	$S_{11}$ of LP L1/L2 dualband capacitively loaded patch. . . . .	57
Figure 3.16	Axial ratio of the capacitively loaded CP L1/L2 dualband four- edge slotted patch antenna for GPS applications. . . . .	58
Figure 3.17	$S_{11}$ of the capacitively loaded CP L1/L2 dualband four-edge slot- ted patch antenna for GPS applications. . . . .	58
Figure 3.18	Radiation patterns of the capacitively loaded CP L1/L2 dualband four-edge slotted patch antenna at 1227.6 MHz, (a) Azimuth Pattern ( $\phi = 0^\circ$ ), (b) Elevation Pattern ( $\phi = 90^\circ$ ). . . . .	59
Figure 3.19	Radiation patterns of the capacitively loaded CP L1/L2 dualband four-edge slotted patch antenna at 1575.42 MHz, (a) Azimuth Pattern ( $\phi = 0^\circ$ ), (b) Elevation Pattern ( $\phi = 90^\circ$ ). . . . .	59
Figure 3.20	Geometry of zigzag four-edge slotted patch. . . . .	60
Figure 3.21	Geometry of zigzag slot section inserted four-edge slotted patch. . . . .	61
Figure 3.22	$S_{11}$ of the comparison simulations on the effects of zigzag slot usage. . . . .	62
Figure 3.23	$S_{11}$ of different length of inserted zigzag slot usage. . . . .	63

Figure 3.24	$S_{11}$ graph of different length of inserted zigzag slot usage at lower band. . . . .	64
Figure 3.25	$S_{11}$ graph of different length of inserted zigzag slot usage at higher band. . . . .	64
Figure 3.26	The representation of multiple zigzag slot sectors. . . . .	65
Figure 3.27	The construction of multiple zigzag slots. . . . .	66
Figure 3.28	$S_{11}$ Result of Comparison Simulation of Zigzag Slots Number . .	67
Figure 3.29	$S_{11}$ graph when SlotOffset = 0.8 mm and $W_s = 0.8$ mm. . . . .	68
Figure 3.30	$S_{11}$ graph of L1/L2 dualband linearly polarized zigzag slotted antenna. . . . .	69
Figure 3.31	$S_{11}$ of L1/L2 dualband RHCP zigzag slotted GPS antenna. . . . .	69
Figure 3.32	Axial Ratio of L1/L2 dualband RHCP zigzag slotted GPS antenna.	71
Figure 3.33	RHCP and LHCP radiation patterns of the L1/L2 dualband RHCP zigzag slotted GPS antenna. . . . .	71
Figure 3.34	Front View of Zigzag Slotted Patch Antenna . . . . .	72
Figure 3.35	$S_{11}$ comparison graph of simulation and measurement of zigzag slotted antenna. . . . .	74
Figure 3.36	Representation of " <i>t_milling</i> " parameter in extra milling simulations on zigzag slotted antenna. . . . .	74
Figure 3.37	$S_{11}$ graph of extra milling simulations on zigzag slotted antenna.	75
Figure 3.38	Measurements of radiation pattern in the anechoic chamber. . . .	76
Figure 3.39	Comparison of simulated and measured radiation patterns at lower band. . . . .	76
Figure 3.40	Comparison of simulated and measured radiation patterns at higher band. . . . .	77

Figure 3.41	Axial ratio measurement results at 1238 MHz and 1621 MHz. . . . .	77
Figure 4.1	Side view of two-layer triband GPS antenna. . . . .	81
Figure 4.2	Geometry of the nearly square patch. . . . .	81
Figure 4.3	$S_{11}$ results of patch width simulations on square patch. . . . .	82
Figure 4.4	Axial ratio graph for the simulations of changing DiffWidth parameter on nearly square patch. . . . .	83
Figure 4.5	$S_{11}$ graph for the simulations of changing DiffWidth parameter on nearly square patch. . . . .	84
Figure 4.6	$S_{11}$ results for the simulations of feed position on nearly square patch. . . . .	85
Figure 4.7	Axial ratio results for the simulations of feed position on nearly square patch. . . . .	85
Figure 4.8	$S_{11}$ results for the simulations of dimensions of nearly square patch. . . . .	86
Figure 4.9	Axial ratio results for the simulations of dimensions of nearly square patch. . . . .	86
Figure 4.10	$S_{11}$ results of L5 GPS band CP nearly square patch. . . . .	87
Figure 4.11	Axial ratio results of L5 GPS band CP nearly square patch. . . . .	88
Figure 4.12	Top view of two-layer triband GPS antenna structure. . . . .	89
Figure 4.13	Representation of the patch transfer in stacked structures. . . . .	89
Figure 4.14	$S_{11}$ results of the initial simulation on the two-layer stacked antenna. . . . .	90
Figure 4.15	Representation of the conducting cove on coved four-slotted patch. . . . .	91

Figure 4.16	$S_{11}$ of the simulations on the width of the inserted conducting cove. . . . .	91
Figure 4.17	$S_{11}$ of the simulations on the length of the inserted conducting cove. . . . .	92
Figure 4.18	$S_{11}$ simulation result of the L1/L2/L5 triband CP two-layer stacked antenna. . . . .	94
Figure 4.19	Axial ratio simulation result of the L1/L2/L5 triband CP two- layer stacked antenna. . . . .	94
Figure 4.20	Co-polar and cross-polar radiation patterns of the two-layer stacked antenna at L1/L2/L5 GPS bands. . . . .	95
Figure 4.21	Coved four-slotted patch of the two layered stacked antenna. . .	96
Figure 4.22	Ground plane of the two layered stacked antenna. . . . .	96
Figure 4.23	Assembly of the layers of the two-layer stacked antenna. . . . .	97
Figure 4.24	Top view of the integrated two-layer stacked antenna. . . . .	97
Figure 4.25	Side view of the integrated two-layer stacked antenna. . . . .	98
Figure 4.26	The $S_{11}$ comparison graph between simulation and measurement of the L1/L2/L5 triband two-layer stacked GPS antenna. . . . .	99
Figure 4.27	Comparison of simulated and measured normalized radiation patterns of L1/L2/L5 triband two-layer stacked GPS antenna at first band (1176 MHz). . . . .	99
Figure 4.28	Comparison of simulated and measured normalized radiation patterns of L1/L2/L5 triband two-layer stacked GPS antenna at second band (1259 MHz). . . . .	100
Figure 4.29	Comparison of simulated and measured normalized radiation patterns of L1/L2/L5 triband two-layer stacked GPS antenna at third band (1623 MHz). . . . .	100

Figure 4.30	Axial ratio measurement result of two-layer stacked antenna . . .	101
Figure 4.31	Representation of tuned covered four-slotted patch. . . . .	102
Figure 4.32	$S_{11}$ comparison of the tuned antenna and fabricated covered four-slotted patch antenna. . . . .	102
Figure 4.33	Side view of three-layer triband GPS antenna. . . . .	104
Figure 4.34	Top view of three-layer triband GPS antenna. . . . .	104
Figure 4.35	$S_{11}$ versus frequency for different patch lengths on square patch.	106
Figure 4.36	Axial ratio versus frequency for different truncation lengths on square patch. . . . .	106
Figure 4.37	$S_{11}$ versus frequency for different truncation lengths on square patch. . . . .	107
Figure 4.38	Axial ratio graph related to the change of feed position on square patch. . . . .	107
Figure 4.39	$S_{11}$ of L5 GPS band circular polarized corner truncated antenna.	109
Figure 4.40	Axial ratio of L5 GPS band circular polarized corner truncated antenna. . . . .	109
Figure 4.41	$S_{11}$ of linearly polarized L1/L2/L5 GPS band corner truncated stacked antenna. . . . .	110
Figure 4.42	Axial Ratio of the change of truncation length on bottom patch in corner truncated stacked antenna. . . . .	111
Figure 4.43	$S_{11}$ of the change of truncation length on bottom patch in corner truncated stacked antenna. . . . .	111
Figure 4.44	$S_{11}$ of the change of Xf parameter on bottom patch in corner truncated stacked antenna. . . . .	112

Figure 4.45	Axial ratio of the change of Xf parameter on bottom patch in corner truncated stacked antenna. . . . .	112
Figure 4.46	Axial Ratio of the change of W_Bottom on bottom patch in corner truncated stacked antenna. . . . .	113
Figure 4.47	$S_{11}$ of the change of W_Bottom parameter on bottom patch in corner truncated stacked antenna. . . . .	113
Figure 4.48	Axial ratio of the change of T2 parameter on middle patch in corner truncated stacked antenna. . . . .	114
Figure 4.49	Axial ratio of the change of x_trans_middle parameter on middle patch in corner truncated stacked antenna. . . . .	115
Figure 4.50	Axial ratio of the change of W_Middle and W_Bottom parameters in corner truncated stacked antenna. . . . .	115
Figure 4.51	$S_{11}$ of the change of W_Middle and W_Bottom parameters in corner truncated stacked antenna. . . . .	116
Figure 4.52	Axial ratio of the change of T1_Middle parameters in corner truncated stacked antenna. . . . .	116
Figure 4.53	Axial ratio of the change of W_Top parameters in corner truncated stacked antenna. . . . .	117
Figure 4.54	Axial ratio of the final tuning of W_Top and T1 parameters in corner truncated stacked antenna. . . . .	117
Figure 4.55	$S_{11}$ of the final tuning of W_Top and T1 parameters in corner truncated stacked antenna. . . . .	118
Figure 4.56	Co-polar and cross-polar radiation patterns of the three layered antenna at L1/L2/L5 GPS bands. . . . .	119
Figure 4.57	Fabricated bottom patch of the three-layer antenna at L1/L2/L5 GPS bands. . . . .	120

Figure 4.58	Fabricated middle patch of the three-layer antenna at L1/L2/L5 GPS bands. . . . .	120
Figure 4.59	Fabricated top patch of the three-layer antenna at L1/L2/L5 GPS bands. . . . .	121
Figure 4.60	Side view of the fabricated three-layer antenna at L1/L2/L5 GPS bands. . . . .	121
Figure 4.61	$S_{11}$ comparison of the corner truncated three-layer stacked antenna.	122
Figure 4.62	$S_{11}$ comparison between PEC and copper materials on corner truncated three-layer stacked antenna. . . . .	122
Figure 4.63	Axial ratio comparison between PEC and copper materials on corner truncated three-layer stacked antenna. . . . .	123
Figure 4.64	Tuning studies of the three-layer stacked antenna at L1/L2/L5 GPS bands. . . . .	123
Figure 4.65	Tuned three-layer stacked antenna at L5 GPS band. . . . .	124
Figure 4.66	$S_{11}$ measurement results of tuning on three-layer stacked antenna at L5 GPS band. . . . .	124
Figure 4.67	Pre-measurement setup for the measurement of axial ratio in tuning studies. . . . .	125
Figure 4.68	Tuned three-layer stacked antenna at L2 GPS band. . . . .	126
Figure 4.69	$S_{11}$ measurement results of tuning on three-layer stacked antenna at L2 GPS band. . . . .	127
Figure 4.70	Tuned three-layer stacked antenna at L1 GPS band. . . . .	127
Figure 4.71	$S_{11}$ measurement results of tuning on three-layer stacked antenna at L1 GPS band. . . . .	128
Figure 4.72	Comparison of $S_{11}$ measurement results of early fabricated and tuned three-layer stacked antennas. . . . .	128

Figure 4.73	Radiation pattern of the first frequency band of three-layer stacked antenna. . . . .	129
Figure 4.74	Radiation pattern of the second frequency band of three-layer stacked antenna. . . . .	129
Figure 4.75	Radiation pattern of the third frequency band of three-layer stacked antenna. . . . .	130
Figure 4.76	Axial ratio measurement result of the tuned three-layer stacked antenna. . . . .	130

## LIST OF ABBREVIATIONS

### ABBREVIATIONS

AR	<b>Axial Ratio</b>
AUT	<b>Antenna Under Test</b>
BW	<b>Bandwidth</b>
CA	<b>Characteristic Angle</b>
CP	<b>Circularly Polarized</b>
CMA	<b>Characteristic Mode Analysis</b>
CNAV	<b>Civil Navigation</b>
DoD	<b>Department of Defense</b>
EFIE	<b>Electric Field Integral Equation</b>
ESA	<b>European Space Agency</b>
FDTD	<b>Finite Difference Time Domain</b>
FEM	<b>Finite Element Method</b>
GLONASS	<b>Global Navigation Satellite Systems</b>
GNSS	<b>Global Navigation Satellite Systems</b>
GPS	<b>Global Positioning System</b>
HPBW	<b>Half Power Beamwidth</b>
MoM	<b>Method of Moments</b>
MS	<b>Modal Significance</b>
PCB	<b>Printed Circuit Board</b>
PEC	<b>Perfectly Electric Conducting</b>
PMC	<b>Perfectly Magnetic Conducting</b>
UAV	<b>Unmanned Aerial Vehicle</b>

US

United States

USRR

Union of Soviet Socialist Republics



## CHAPTER 1

### INTRODUCTION

Antenna is one of the main components of wireless communication systems. The operational performance of the antenna affects whole system performance directly. The requirements of bandwidth, gain, beamwidth, polarization and multiple frequency operability may change according to the application area of the antenna. Circularly polarized multiband low-profile antennas are preferred in many wireless communication systems such as satellite communication, Global Navigation Satellite Systems (GNSS), radio frequency identification, wireless power transmission, wireless local area networks, etc. [1].

“GNSS” covers all satellite-based navigation systems such as GPS, GLONASS, and Galileo. These satellite systems generate circularly polarized radio navigation signals. The polarization of the electromagnetic waves changes due to ionized gases or earth magnetic field. This effect, known as Faraday Rotation, causes rotation in the orientation of the linear polarized wave. In order to minimize this effect, Right Hand Circularly Polarized (RHCP) signals are used in satellite navigation systems [1].

GPS is the first GNSS constellation developed by US Department of Defense (DoD). GPS has 24 satellites at 6 orbits around the earth at altitude of 20200 km. Civil navigation signals were composed of L1 (1575.42 MHz) and L2 (1227.60 MHz) until 2014. After 2014, with the usage of the next generation GPS satellites “GPS Block-IIF”, L5 (1176.45 MHz) frequency is activated to be used as pre-operational Civil Navigation (CNAV) by civilian users [2].

GLONASS constellation is another navigation satellite system developed by Union of Soviet Socialist Republics (USSR). It is fully operational orbiting around earth

with 24 satellites since 1996. GLONASS supplies two kinds of navigation service as “standard positioning service” which is open to civilian usage and “precise positioning service” which is only open to military applications. There are three operating GLONASS frequency band as G1 (1602 MHz), G2 (1246 MHz) and G3 (1204.704 MHz). G1 and G2 frequency bands are open to civilian usage since 1996 [2].

Galileo constellation is another GNSS which has been developed by European Space Agency (ESA) since May 1999. The complete system will comprise 30 satellites (24 operational and 6 spares for each orbital plane). Five frequency bands are used for navigational signal transmission as E1 (1575.42 MHz), E6 (1278.75 MHz), E5 (1191.795 MHz), E5a (1176.45 MHz) and E5b (1207.14 MHz). Galileo will have four different service choices as Open Service, Commercial Service, Safe-of-life Service, and Public Regulated Service. E5a, E5b, and E1 frequency bands will be open to free usage in Open Service [2].

Combinational usage of the GNSS signals improves the accuracy and robustness of all navigation systems. Additionally, multiband GNSS usage also makes the system robust against jamming signals. Therefore, using multi navigational signal usage becomes more important to improve the reliability of positioning [2].

## **1.1 Objectives and Structure of the Thesis**

In this study, dualband and triband GPS antennas are designed, fabricated and measured to receive the transmitted radio navigation signals by GPS satellites at multi civilian frequency bands as L1, L2 and L5. In accordance with this purpose, below studies are performed and presented;

- The literature survey is carried out on multiband microstrip antennas developed for navigation purposes to get information about circular polarization and multiband operation techniques on microstrip antennas.
- An L1 band antenna is designed by using Characteristic Mode Analysis (CMA) technique to get a physical insight into circularly polarized microstrip antennas.

A design work flow is presented about obtaining circular polarization on corner truncated microstrip antenna by using CMA technique.

- Parametric analysis is performed on the four-edge slotted microstrip patch antenna for dualband operation. The parameters which directly effects the performance of antenna resonance are summarized to get an insight into four-edge slotted patch geometry.
- An L1/L2 dualband GPS antenna is designed by using capacitive loading technique on the slots of the four-slotted patch.
- An L1/L2 dualband GPS antenna is designed, fabricated and measured. In this study, a novel zigzag shaped four-slotted patch is designed to decrease the frequency ratio of the dualband antenna.
- An L1/L2/L5 triband GPS antenna is designed, fabricated and measured. In this study, two microstrip antennas are stacked to operate at L1/L2/L5 GPS bands. A novel slotted patch and a nearly square patch is designed and diagonally fed with a single coaxial feed to get circular polarization.
- An L1/L2/L5 triband GPS antenna is designed as three layer stacked structure. Three corner truncated patches are stacked and fed with a single coaxial feed. Designed antenna is fabricated and measured. Tuning processes is applied on the antenna to meet the requirements.

In Chapter 1, the objectives of the thesis and the literature survey on circularly polarized multiband microstrip patch antennas are given.

In Chapter 2, characteristic mode theory and related literature survey are presented. The physical explanations are given to comment on the outputs of the CMA. The design work flow on the L1 band circularly polarized microstrip antenna which is designed by using CMA technique is explained in this chapter.

In Chapter 3, the studies about L1/L2 dualband GPS antennas are presented. In these studies, L1 and L2 GPS bands are achieved on a single patch with a single coaxial feed. Reactive loading is applied on the slots of a four-slotted patch to decrease the frequency ratio. And, a novel zigzag four-slotted patch is proposed to decrease the

frequency ratio without reactive loading. Designed antenna is fabricated and measured. Results and evaluations are presented about studies on L1/L2 dualband GPS antennas.

In Chapter 4, the studies about L1/L2/L5 triband GPS antennas are presented. Two kinds of microstrip stacked antennas are designed as two-layer and three-layer to operate at L1, L2 and L5 GPS bands. In two-layer antenna, two microstrip layers are stacked to carry out triband operation. One of the microstrip layers has a novel covered four-slotted patch to achieve dualband on a single patch, and the third frequency band is achieved with a nearly square patch. In three-layer antenna, three corner truncated microstrip layers are stacked to get triband operability at L1, L2 and L5 GPS bands. The studies on design, simulation, fabrication, measurement and tuning of triband antennas are given in this chapter.

In Chapter 5, the conclusion of the thesis and the achievements during the thesis study are presented. In addition, the planned future works are given in Chapter 5.

In this thesis study, CST Microwave Studio<sup>®</sup> is used for electromagnetic simulations.

## **1.2 Microstrip Patch Antenna**

The microstrip patch antenna is one of the best candidates to meet the multiple frequency operability, circular polarization and low-profile requirements for a GPS antenna. When a specific patch geometry is used to generate desired modes, microstrip patch antennas are very versatile in terms of resonant frequency, polarization, pattern, and impedance. On the other hand, microstrip patch antennas have some disadvantages like low efficiency, spurious feed radiation, and very narrow bandwidth. However, there are some methods to minimize these disadvantages, for instance increasing the thickness of the substrate can increase the bandwidth and efficiency. But increasing the thickness can also introduce unwanted surface waves which degrade the radiation performance of the antenna [3]. Surface wave degradations can be minimized with using some photonic bandgap structures [4]. In addition to the use of thicker substrate, there are some methods to increase bandwidth such as slot loading on patch, different feeding techniques (i.e. aperture coupled feed), stacked structures,

parasitic patches, and other multimoding techniques [4].

As shown in Figure 1.1, microstrip antennas are consist of three main layers as ground, substrate and conducting patch. The thickness of the substrate is usually a small fraction of wavelength ( $0.003\lambda \leq h \leq 0.05\lambda$ ). The geometry of the conducting patch can be rectangular, circular or any other geometrical shape. For a rectangular conducting patch, the length of the patch is usually in the interval of  $\lambda/3 < h < \lambda/2$ . Substrates are dielectric materials and their dielectric constants are usually in the range of  $2.2 \leq \epsilon \leq 12$ . The bandwidth of the antenna decreases with the increase of the dielectric constant of the substrate. [3].

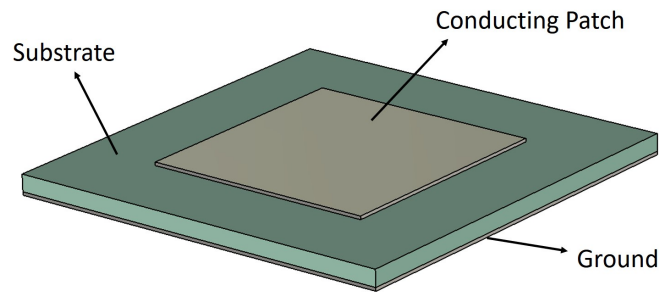


Figure 1.1: Structure of microstrip antenna.

There are four common feeding methods as microstrip line, coaxial probe, aperture coupling and proximity coupling for microstrip antennas. These feeding structures are shown in Figure 1.2. In Table 1.1, feeding methods are compared with respect to bandwidth. Despite the low bandwidth, the feeding techniques of coaxial probe and microstrip line are implemented more frequently [4].

Table 1.1: Feeding methods of microstrip antennas.

	<b>Coaxial Probe</b>	<b>Microstrip Line</b>	<b>Aperture Coupled</b>	<b>Proximity Coupled</b>
<b>Bandwidth</b>	2 - 5%	2 - 5%	20 - 25%	10 - 15%

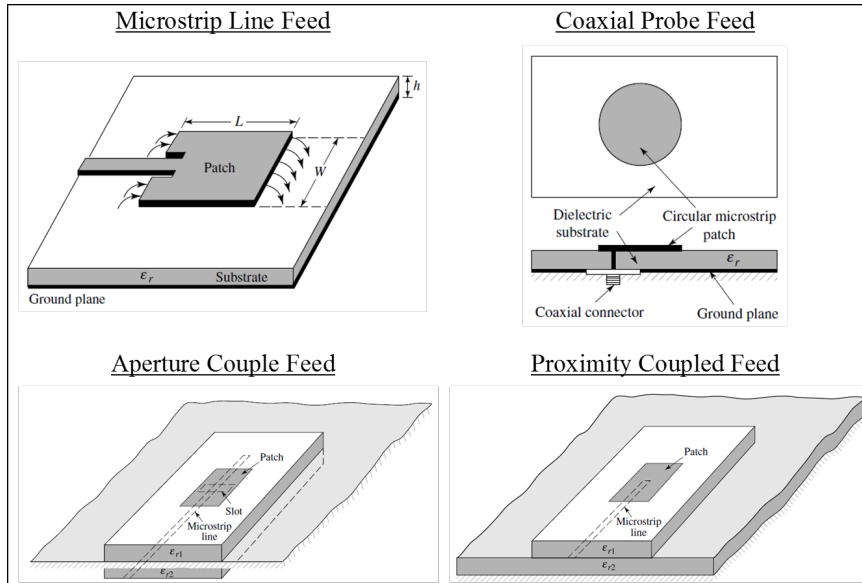


Figure 1.2: Feeding methods of microstrip antennas [3].

### 1.3 Circular Polarization in Microstrip Antennas

In linearly polarized systems, transmission losses can occur because of misalignment of the transmitting and receiving antennas. Circular polarization reduces transmission losses that occur due to misalignment between transmitting and receiving terminals. In addition, the multipath interference is another problem of concern in wireless communication [5]. Circular polarization avoids multipath fading by introducing polarization diversity in radio propagation environment thus providing a high probability of a successful link, enhances weather penetration, superior mobility, spectral efficiency, and improved system performance [6].

The polarization of an antenna is related to the orientation of electric fields radiated by the antenna. If the electrical fields are vertically or horizontally oriented above the earth, the polarization of the antenna is called vertical or horizontal polarized, respectively. Both vertical and horizontal polarizations are called as linear polarization.

For circular polarization, two orthogonal components of the electric field which have the same amplitudes and  $90^\circ$  phase difference between orthogonal components are required in the far field region. For a circularly polarized wave, the trace of the

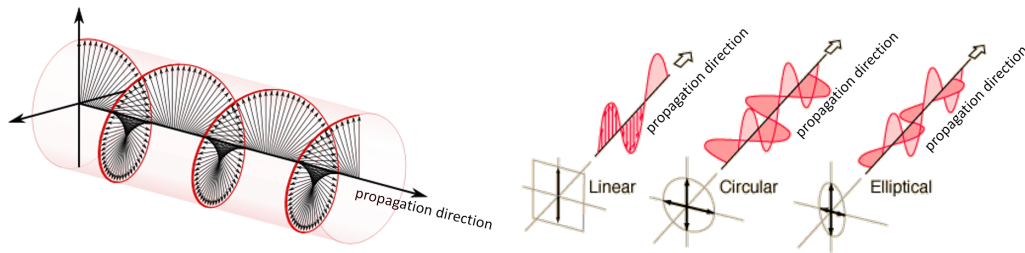


Figure 1.3: Representation of circularly polarized wave.

electric field vector at a given point in space as a function of time is a circle as shown in Figure 1.3. If the electric field vector rotates in a right-hand sense with respect to the direction of propagation, the wave is Right Hand Circularly Polarized (RHCP); if the electric field vector rotates in a left-hand sense with respect to the direction of propagation, the wave is Left Hand Circularly Polarized (LHCP).

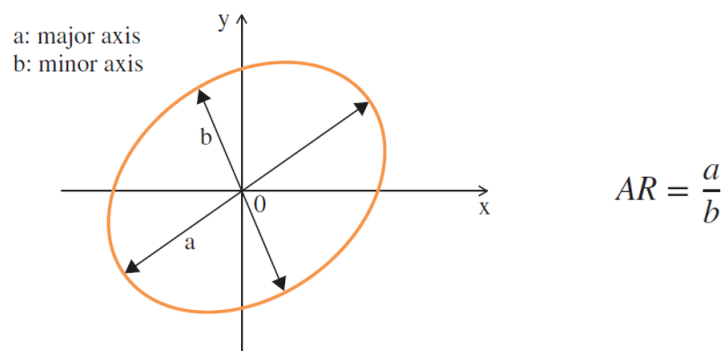


Figure 1.4: Trace of tip of electric field vectors for elliptical polarization.

It is hard to achieve a perfect circular polarization in real life, thus the curve traced at a given position as a function of time is usually an ellipse, as shown in Figure 1.4. This type of polarization is called elliptical polarization. Lines “a” and “b” denote the major axis and the minor axis of polarization ellipse, respectively. The ratio of the major axis to the minor axis of the ellipse is termed as the Axial Ratio (AR). AR is a key parameter for measuring the circular polarization. Usually, AR is required to be below 3 dB for a CP antenna [1].

Circular polarization can be achieved in microstrip patch antennas with two different feed configurations as single fed and double fed [1]. 90° phase difference between

two orthogonal modes is provided with an external passive microwave component (power divider, hybrid coupler, etc.) in double fed circularly polarized microstrip antennas.  $TM_{10}$  and  $TM_{01}$  modes are used as orthogonal modes for rectangular patch geometries as shown in Figure 1.5. Double fed configuration can also be used in circular patches as shown in Figure 1.6.  $TM_{11}$  mode is used to get circular polarization on circular patches.

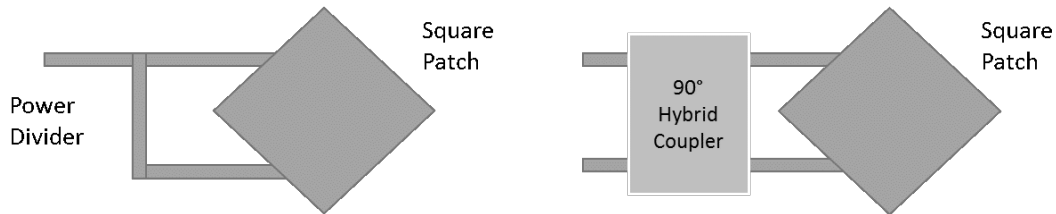


Figure 1.5: Double fed CP microstrip antenna configurations for rectangular patches.

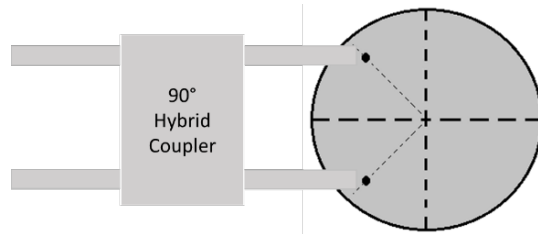


Figure 1.6: Double fed CP microstrip antenna configuration for circular patches.

Even if there are several studies in the literature [7–10], double fed circularly polarized antennas are not preferred in most of the applications because of increasing the complexity, mass, and cost of the system with installing extra components.

In single fed circularly polarized microstrip antennas, it is needed to perturb the orthogonal modes to get  $90^\circ$  phase difference between orthogonal modes.

Different patch geometries such as truncated [11, 12], arc-shaped edge [13], nearly square [11], elliptical [14], center-cross and four edge slotted [15], asymmetrical slot loaded [16, 17], symmetric slot loaded [18], asymmetric U-slot loaded [19], E-shaped slot loaded [20], corner truncated and slit loaded [21, 22] patches are applied to get circular polarization in literature. Some of these patches are shown in Figure 1.7.

In single fed circularly polarized rectangular patches, orthogonal modes ( $TM_{10}$  and  $TM_{01}$  modes) are needed to be excited with  $90^\circ$  phase difference from a single point.

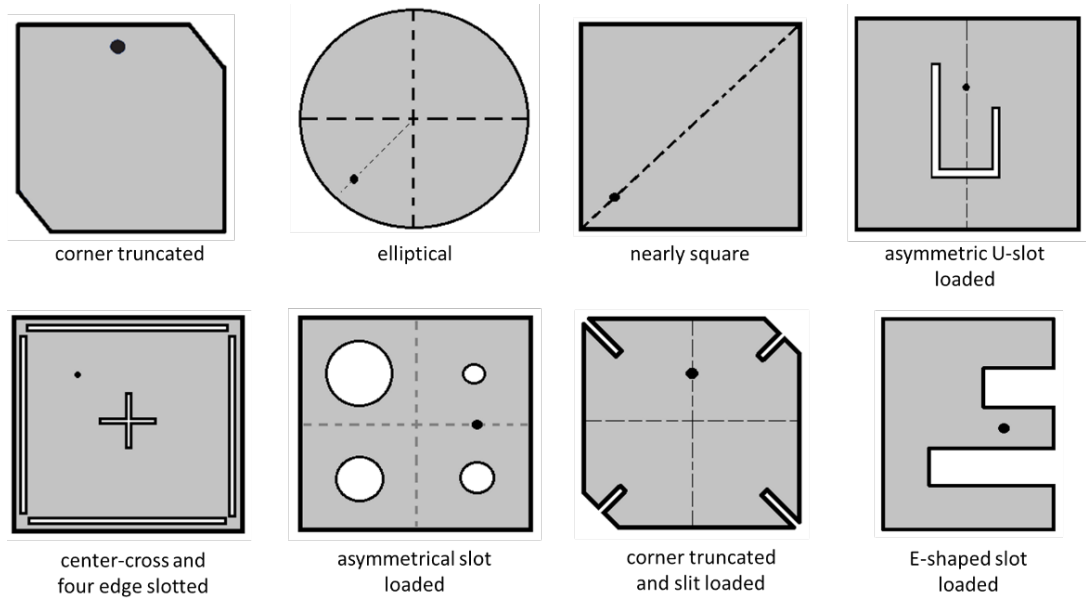


Figure 1.7: Single Fed Circularly Polarized Patch Geometries

In references [11, 12, 21, 22], corner truncation is applied on rectangular patch to get circular polarization. RHCP or LHCP can be obtained according to the location of feed point. The feed configurations that provide RHCP and LHCP are given in Figure 1.8.

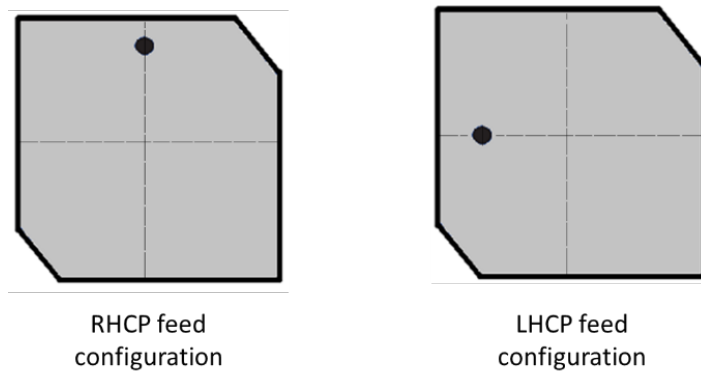


Figure 1.8: Feed configurations for RHCP and LHCP on corner truncated patches.

If a square patch is fed diagonally, orthogonal modes are excited in phase. The length of the vertical and horizontal edges are changed slightly to get  $90^\circ$  phase difference between orthogonal modes and the square patch becomes nearly square [11]. The patch configurations that provides RHCP and LHCP are given in Figure 1.9.

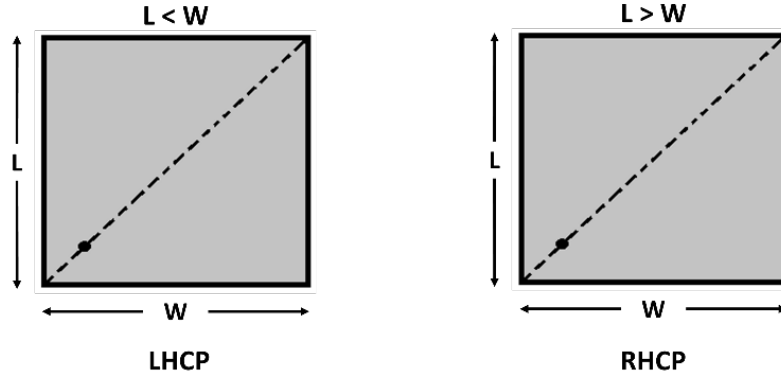


Figure 1.9: Patch configurations for RHCP and LHCP on nearly square patches.

A center cross slot is applied to get circular polarization and four-edge slotted patch is fed diagonally in [15].

Circular patches can be made elliptical with changing an axis length of the circle to obtain  $90^\circ$  phase difference in the single fed configuration [14].

U-slot loading is known as a method of increasing bandwidth in microstrip antennas. In [23], U-slot is applied to a rectangular patch to increase the bandwidth of the linearly polarized antenna. In [19], asymmetrical U-slot is applied on the rectangular patch to get circular polarization. Asymmetrical U-slot is obtained with changing the length of one arm of U-slot. If the left arm of the U-slot is longer than the right one, LHCP is obtained; if the right arm of the U-slot is longer than the left one, RHCP is obtained.

The loading of E-shaped slot on rectangular patch is another method to increase the bandwidth in microstrip antennas [24]. In [24], symmetrical E-shape is used, and linear polarization is obtained. In [20], the length of one slot is changed to get circular polarization.

The loading of asymmetric slots on rectangular patch is another method for circular polarization [16, 17]. In these studies, slightly varying circular slots are placed along diagonal directions to get circular polarization.

In [15], the asymmetrical cross-shaped slot is placed at the center of the patch to obtain circular polarization. RHCP and LHCP can be obtained according to which

slot is longer as given in Figure 1.10.

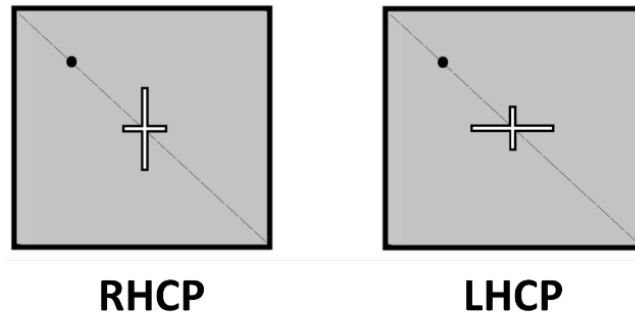


Figure 1.10: Patch configurations for RHCP and LHCP on asymmetrical cross-shaped slot patch.

Most of the previously mentioned patch antennas have low axial ratio bandwidth. Slit and slot loaded patches have 3 dB axial ratio bandwidth smaller than 1% [15, 16, 21, 22]. Corner truncated, nearly square diagonally fed and circular patch geometries have approximately 3 dB axial ratio bandwidth of 1% [11, 14]. In order to increase the axial ratio bandwidth, U-slot and E-slot patches are used and these patch configurations achieved approximately 3 dB axial ratio bandwidth of 4% [19, 20].

Single fed circularly polarized microstrip antennas are preferred in many safety-critical applications which have strict mechanical requirements as compared to double fed circularly polarized microstrip antennas, because of their compact sizes and less complexity. From the viewpoint of cost, single fed antennas are also less expensive than double fed ones, because they do not need any extra passive components.

#### 1.4 Multiband Operation in Microstrip Antenna

Many wireless communication systems use different frequency bands. Single frequency operating antennas can be used for each frequency band separately. However, this case will lead to a large size, mass and high cost. Therefore, multiband antennas are preferred in multiband operating applications [6].

In accordance with objectives of the thesis, the literature of the multiband microstrip antenna is examined in this section. There is a vast amount of literature on multiband

antennas. Since stacking and loading methods are used in this thesis, literature survey is limited to multiband antennas realized by these techniques.

Stacking method is applied with stacking microstrip layers on each other as shown in Figure 1.11. In this configuration, coaxial probe is connected to the upper patch, the lower patch is coupled electromagnetically (parasitically) with the upper patch. Each microstrip layer operates its own resonant frequency and the whole antenna with two layers operates multiband.

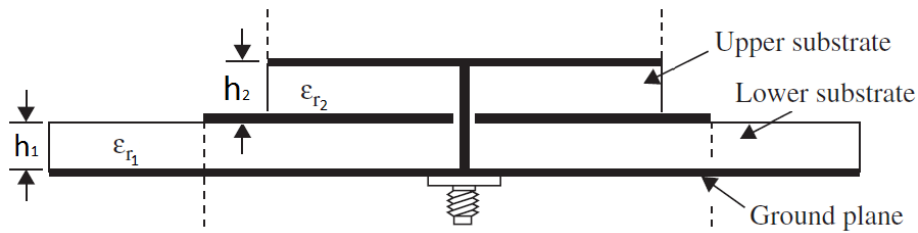


Figure 1.11: Structure of stacked microstrip patch antenna for multiband operations.

There are several studies on the stacking method to get multiband operations in microstrip antennas [6, 25–31]. Stacked antennas have broader impedance bandwidth and axial ratio bandwidth than loaded microstrip antennas [29, 30]. Having a small frequency ratio between operating frequencies is a quite a challenging issue for loaded microstrip antennas, but stacked antennas can achieve dualband operations with the frequency ratio smaller than 1.5 [6]. Stacked antennas can be also used to increase the bandwidth with stacking patches which operates at close frequencies [31].

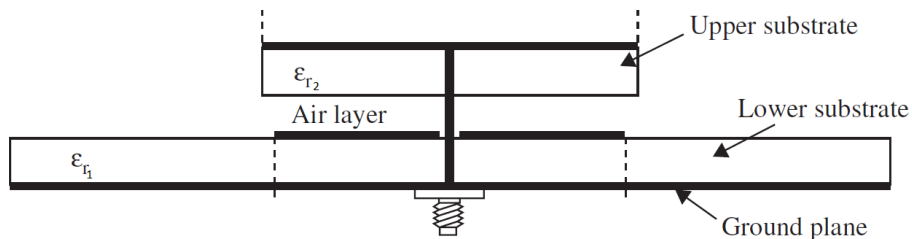


Figure 1.12: Stacked microstrip antenna with air gap.

The air gap can be used in a stacked antennas to get good impedance matching and increase the bandwidth and efficiency of the antenna [25], [30]. Stacked antenna with air gap is shown in Figure 1.12.

Loading method is used on the patches for size reduction, control of polarization, control of radiation pattern and dualband operations in microstrip antennas. The patch can be loaded with stubs, slots, shorting vias and capacitors to obtain required resonance frequency, radiation pattern, polarization, bandwidth, and so on [4].

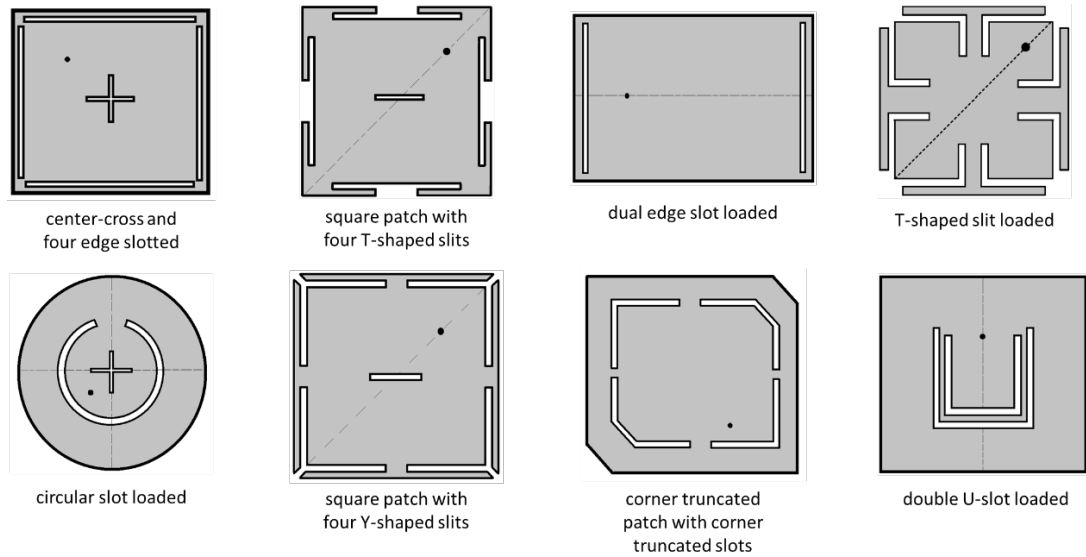


Figure 1.13: Multiband slot loaded patches.

Different shaped slots are applied to achieve multiband operations in literature [15, 32–37]. The geometries of center-cross and four edge slotted [15], dual edge slot loaded [32], square patch with four T-shaped slits [33], square patch with four Y-shaped slits [33], T-shaped slit loaded [34], corner truncated patch with corner truncated slots [35], double U-slot loaded [36] and circular slot loaded [37] patches are shown in Figure 1.13.

Dualband operation is obtained with perturbation of  $TM_{10}$  and  $TM_{30}$  modes on dual edge slot loaded patch [32]. If slots are placed close to radiating edges,  $TM_{10}$  mode is perturbed slightly. Therefore, the resonance frequency of  $TM_{10}$  mode changes slightly. The current distribution of  $TM_{10}$  is given in Figure 1.14-(a). The second resonance frequency is obtained with perturbation of  $TM_{30}$  mode. Slots are placed where the unperturbed  $TM_{30}$  mode current is significant as shown in Figure 1.14-(b). Therefore, the perturbed  $TM_{30}$  mode becomes like  $TM_{10}$  mode. The resonance frequency of  $TM_{30}$  mode decreases and have boresight radiation with no sidelobe. This radiation mechanism also explains the way of obtaining multiband operations

on other patch geometries which have slots close to edges as studied in [15, 33, 35].

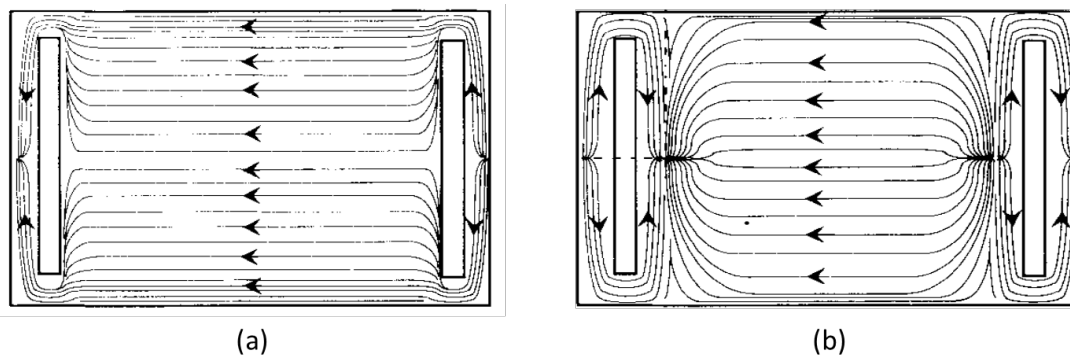


Figure 1.14: Current distribution of  $TM_{10}$  and  $TM_{30}$  modes on dual edge slot patch, [32].

The loading of multiple U-slot on rectangular patch is another method to get multi-band operability in microstrip antennas. Linearly polarized triband is obtained with double U-slot loaded configuration [36].

Slot loading can also be used on circular patches.  $TM_{11}$  and  $TM_{12}$  modes are used for boresight dualband operations. In circular slot loaded patch, the circular patch is divided as inner and outer patches which have own resonance frequencies [37].

## 1.5 Multiband and Circularly Polarized Microstrip Antennas

In previous sections, the ways of getting circular polarization and multiband operations on microstrip antennas are given separately. In this section, circularly polarized multiband microstrip antennas are examined and presented.

It is needed to merge the methods of circular polarization and multiband operation to design circularly polarized multiband microstrip antennas. First, the number of feed points is chosen to get circular polarization. A passive component or circuit that provides  $90^\circ$  phase difference is needed in the double fed antennas. In single fed antennas,  $90^\circ$  phase difference is obtained with perturbation of orthogonal modes. In this thesis study, it is aimed to get circular polarization with single feed without extra passive components. After decision on the number of feed, the technique of multiband operation is chosen. Both stacking and slot loading methods are suitable

for single feed configurations. Therefore, single fed circularly polarized multiband antennas are researched in the literature survey.

In [25,27–30], multiband operation is obtained with stacking method. Circular polarization is obtained with different patch geometries. In [25], [28] and, [30], truncated patches are used for each frequency bands. In [25], two truncated patch antennas are stacked as operating at 1575.4 MHz and 1227.6 MHz (L1 and L2 GPS bands, respectively) as shown in Figure 1.15. Corner truncation is used for circular polarization at each frequency bands. The air layer is used to tune the frequency ratio. Antenna is fed by a single coaxial probe which is soldered to upper patch and lower patch is fed parasitically. According to measurement results, 15 MHz and 17 MHz circular polarization bandwidth is obtained at L2 and L1 bands, respectively.

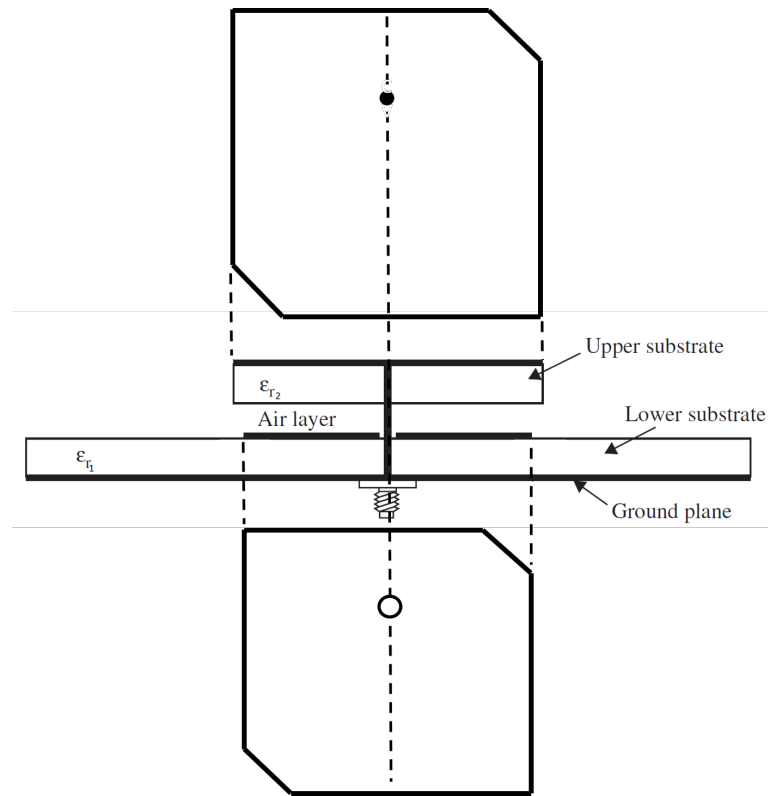


Figure 1.15: Corner truncated stacked L1/L2 dualband GPS antenna.

In [28], a triband corner truncated antenna is designed to operate at GPS L1/Galileo E1 (1.575 GHz), Galileo E5b (1.207 GHz) and GPS L5/Galileo E5a (1.176 GHz) frequency bands as shown in Figure 1.16. Corner truncation is used for circular polarization at each frequency. Antenna is fed by a single coaxial cable which is sol-

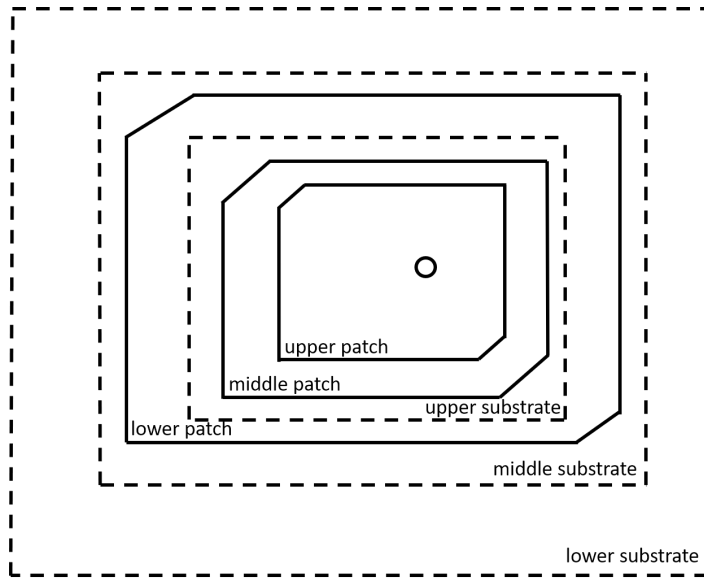


Figure 1.16: Triband circularly polarized corner truncated stacked antenna.

dered to upper patch. Middle and lower patches are fed parasitically. According to given simulation results, 3 dB axial ratio bandwidth of 12.6 MHz (0.8%), 4.83 MHz (0.4%) and 94 MHz (8%) are obtained at the center frequencies of GPS L1/Galileo E1, Galileo E5b and GPS L5/Galileo E5a bands, respectively.

In [30], an L1 and L2 GPS band operating truncated patch antenna is designed and measured. The structure of the antenna is shown in Figure 1.17. Corner truncation is used for circular polarization at each frequency. Antenna is fed by a single coaxial probe which is soldered to lower patch. Upper patch is placed with an air gap from lower substrate and excited parasitically. The height of the air gap is used to tune the frequency ratio. According to results, if the height of the air gap increases, the frequency ratio decreases.

In [27], three square patches are stacked with different geometries as shown in Figure 1.18. Antenna is designed to operate at L1, L2 and L5 GPS frequency bands. Antenna is fed by a single coaxial probe that is soldered to top patch. Other patches are fed parasitically. Circular polarization is obtained with corner truncation on upper patch for L1 band operation. Four symmetric cross-shaped slots are used to get circular polarization on middle patch for L2 band operation. Symmetric slits are placed on the corner of the lower patch to obtain circular polarization for L5 band operation.

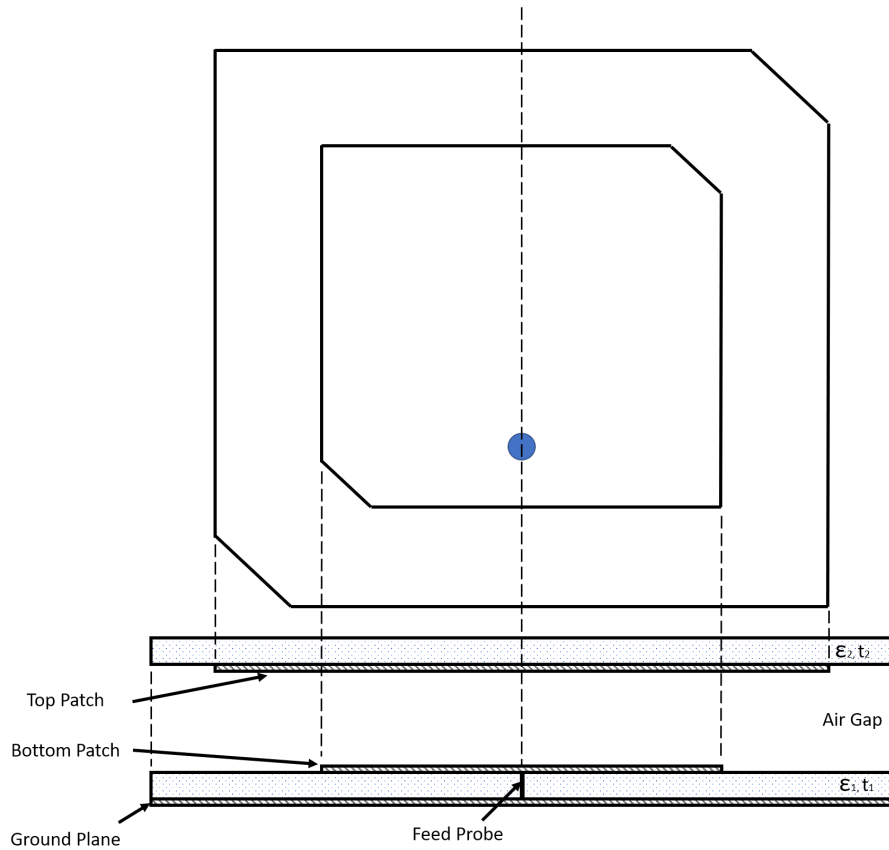


Figure 1.17: Corner truncated stacked L1/L2 dualband GPS antenna with air gap.

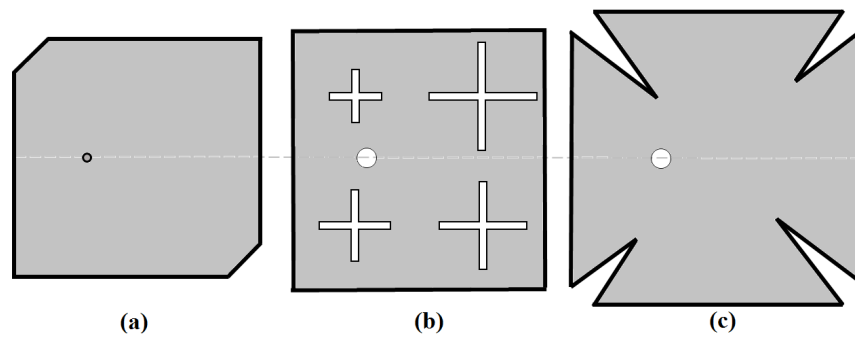


Figure 1.18: Triband Circularly Polarized Stacked Antenna Configuration,  
 (a) Upper Patch, (b) Middle Patch, (c) Lower Patch

In [15], [33–35], multiband operation is obtained with loading of slots and circular polarization is obtained with perturbation of the patch geometry. In [15], dualband is obtained with slots close to edges (edge slots) and circular polarization is obtained with the center cross slot and diagonal feed as shown in Figure 1.19. In [15], antenna

is designed to operate circularly polarized at 1575.4 MHz and 1227.6 MHz. The length of the edge slots controls the resonance frequency of the  $TM_{30}$  mode. However, there is limited place on the patch. Therefore, the patch is loaded with short circuit stubs from the edges of the patch to decrease the frequency ratio.

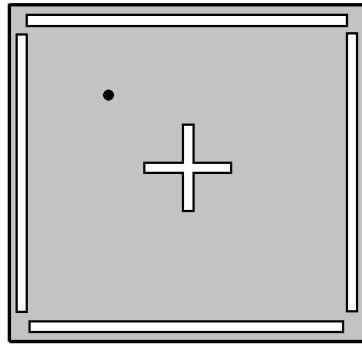


Figure 1.19: Center-cross and four edge slotted patch.

In [33], T-slot and Y-slot loaded patches are studied as dualband circularly polarized microstrip antenna with single feed as shown in Figure 1.20. In a similar manner with [15], the resonance frequency of  $TM_{30}$  mode is decreased with slots to get dualband. Circular polarization is obtained with center slot on the patch with diagonal feed. The antennas are not designed for a specific application. The frequency ratio of 1.984 and 1.766 are obtained on T-slot and Y-slot patches, respectively [33].

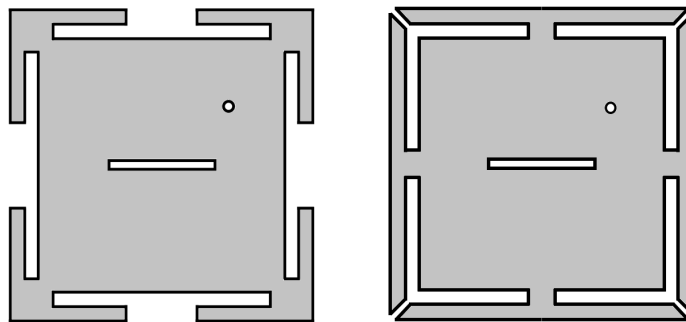


Figure 1.20: T-slot and Y-slot circularly polarized dualband microstrip antennas.

In [34], L1 and L2 GPS bands are achieved with loading of T-elements to patch as shown in Figure 1.21. The frequency ratio is decreased with inset slits and Y-slots. This approach can be defined as similar to the study in [34] (Y-slot loading). Circular polarization is achieved with diagonal feeding the nearly square patch for

lower frequency band ( $TM_{10}$ , fundamental mode). The lengths of the T-elements are slightly perturbed to get circular polarization at higher frequency band ( $TM_{30}$  mode). 3 dB axial ratio bandwidth of 2 MHz is obtained in simulations.

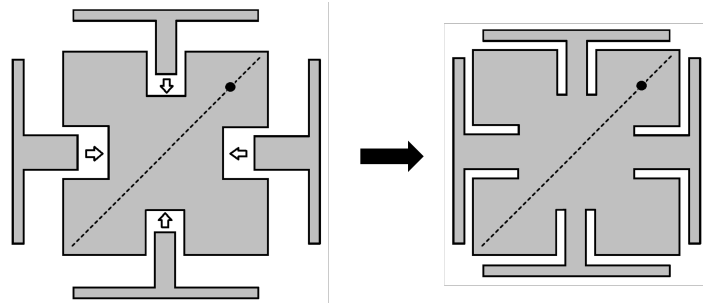


Figure 1.21: T-element loaded circularly polarized dualband antenna.

In [35], slots are loaded on corner truncated patch to get circularly polarized dual-band microstrip antenna as shown in Figure 1.22. In this study, slots are used to get dualband and corner truncation is used for circular polarization. The antenna is designed for L1 GPS band (1575 MHz) and Digital Multimedia Broadcasting frequencies (2.6 GHz).

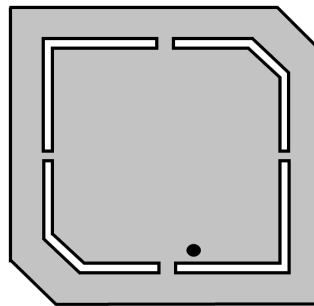


Figure 1.22: Slot loaded corner truncated circularly polarized dualband antenna.

The literature survey is carried out to examine the studies on circularly polarized multiband microstrip antennas. The circular polarization performance of examined dualband and triband antennas are summarized in Table 1.2. Obtained information in literature survey is summarized in this chapter and applied to design studies on multiband GPS antennas that are presented in following chapters.

Table 1.2: Circular polarization performance of dualband and triband antennas in literature.

Reference	Number of Bands	Multiband Operation	CP Operation	AR BW of Band #1	AR BW of Band #2	AR BW of Band #3
[25]	Dualband	Stacked	Corner Truncation	15 MHz (1227.6 MHz)	17 MHz (1575.4 MHz)	-
[28]	Triband	Stacked	Corner Truncation	94 MHz (1176.45 MHz)	4.83 MHz (1207 MHz)	12.6 MHz (1575.4 MHz)
[30]	Dualband	Stacked	Corner Truncation	52.5 MHz (1227.6 MHz)	71.75 MHz (1575.4 MHz)	-
[33]	Dualband	Slot Loaded	Perturbation of Patch	18 MHz (1538 MHz)	32 MHz (3050 MHz)	-
[34]	Dualband	SloL loaded	Perturbation of Patch	2 MHz (1227 MHz)	2 MHz (1575 MHz)	-

## CHAPTER 2

### DESIGN OF CIRCULARLY POLARIZED MICROSTRIP PATCH ANTENNA WITH CHARACTERISTIC MODE ANALYSIS

There are three main methods of analysis for microstrip antennas as Transmission Line, Cavity and Full Wave methods. Transmission Line model is the easiest and less accurate method when compared to other methods. But it gives good physical insight to the designers [3] at the beginning of the design. Cavity model assumes that the microstrip patch is a dielectric loaded cavity. According to cavity model, microstrip patch antenna is assumed as having Perfectly Electric Conducting (PEC) walls at the top and bottom surfaces, and Perfectly Magnetic Conducting (PMC) walls for periphery surfaces for thin dielectric substrates ( $h \ll \lambda$ ) [3]. Cavity model is also useful for getting a first insight about the antenna geometry. If the cavity model is compared with transmission line model, it gives chance to the designer about the visualization of fields beneath patch. This could be useful for the applications requiring specific radiation pattern.

Transmission line and cavity models give quite accurate results for simple shaped (rectangular, circular) patches. However, complex shaped patches could not be analyzed accurately with these models. Full wave analysis methods can be applied to any kind of patch geometry and give more accurate results than other methods. Some of the full wave analysis methods are Method of Moments (MoM), Finite Difference Time Domain (FDTD), Finite Element Method (FEM). These methods are based on the solution of the Maxwell equations under various constitutive relations of media, and boundary conditions. The accuracy of the computational methods depends on the mesh size. Smaller mesh size (dense mesh) yields more accurate simulation results.

With the increase of the computational resource capabilities, full wave methods be-

came the most preferable methods for the antenna designers. However, using full wave methods requires the knowledge of the details of applied method, intuition and experience. To get physical insight before the design of antennas, characteristic mode analysis is applied to CP antenna.

In this chapter; a brief information is given about the theory of characteristic modes and physical explanations are presented. Then, a circularly polarized patch antenna that operates at L1 GPS band is designed with the method of CMA.

## 2.1 Characteristic Mode Theory

The term of “characteristic mode” was first used by Garbacz in 1968 [38]. In that study, characteristic modes are defined with eigenvectors of a weighted eigenvalue equation. Harrington and Mautz developed a simpler derivation of characteristic modes for conducting bodies with arbitrary shapes in 1971 [39]. Then, Harrington extended the formulation for dielectric and magnetic structures [40].

Characteristic modes can be defined as the current modes for arbitrarily shaped conducting bodies. These modes provide valuable physical insight into antenna radiation characteristic. Characteristic modes only depend on the shape and size of the conducting body and are independent of any kind of feeding. Therefore, the shape optimization of a conducting body can be performed to obtain the required radiation pattern. The optimization of the feed point can also be performed using characteristic modes [41, 42].

Real and imaginary parts of impedance matrix obtained by EFIE MoM formulation of conducting body is defined as Equation (2.1).

$$\mathbf{Z} = \mathbf{R} + j\mathbf{X} \quad (2.1)$$

Characteristic currents (eigencurrents) can be defined as real currents on conducting

body. Characteristic modes are represented in matrix form in Equation (2.2),

$$\mathbf{X}\mathbf{J}_n = \lambda_n\mathbf{R}(\mathbf{J}_n) \quad (2.2)$$

where the  $\mathbf{J}_n$  is the eigencurrent (eigenfunction),  $\lambda_n$  is the eigenvalue,  $\mathbf{R}$  and  $\mathbf{X}$  are the real and imaginary parts of the impedance matrix obtained by Electric Field Integral Equation (EFIE) MoM formulation of the conducting body as given in Equation 2.2. Characteristic current ( $\mathbf{J}_n$ ) and eigenvalues ( $\lambda_n$ ) can be obtained by solving the generalized eigenvalue equation given in Equation 2.2. In [39], the details about the formulation are given.

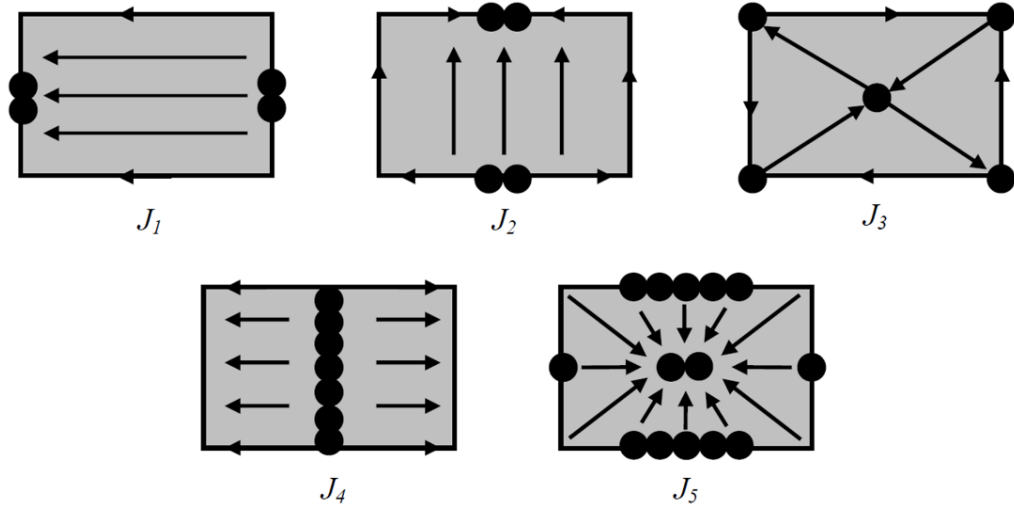


Figure 2.1: Current distribution for rectangular patch of five modes

The characteristic current solutions of a rectangular conducting patch are represented in Figure 2.1 [41]. Minimum current densities are represented with black points and arrows show the direction of the surface current.  $J_1$  and  $J_2$  characteristic currents are the horizontal and vertical currents, respectively. These characteristic currents are used most frequently in rectangular shaped patch applications to generate fundamental modes which radiate to boresight.  $J_3$ ,  $J_4$ , and  $J_5$  characteristic currents generate higher order modes at higher frequencies.

The characteristic currents on the conducting patch produce electric fields, called as

characteristic fields. Characteristic fields can be defined as given in Equation 2.3.

$$\begin{aligned}
\mathbf{E}_n \mathbf{J}_n &= \mathbf{Z} \mathbf{J}_n \\
&= \mathbf{R} \mathbf{J}_n + j \mathbf{X} \mathbf{J}_n \\
&= \mathbf{R} \mathbf{J}_n (1 + j \lambda_n)
\end{aligned} \tag{2.3}$$

The characteristic modes radiate independently because of orthogonality property. Therefore, characteristic modes can be used as a basis set to obtain the total surface current  $\mathbf{J}$  as given in Equation 2.4.

$$\mathbf{J} = \sum_n \frac{V_n^i |\mathbf{J}_n|}{1 + j \lambda_n} \tag{2.4}$$

The term  $V_n^i$  is called as modal-excitation coefficient [39], and it is defined as given in Equation 2.5.

$$V_n^i = \langle \mathbf{J}_n^*, \mathbf{E}^i \rangle = \int_n \mathbf{J}_n \mathbf{E}^i ds \tag{2.5}$$

Modal-excitation coefficient gives information about the effects of the position, phase and magnitude of excitation to total current for each mode. The term of  $\lambda_n$  stands for the eigenvalue which respect to  $n^{\text{th}}$  characteristic mode. Eigenvalues give important information about resonance characteristic of the conducting bodies. In general, eigenvalue changes between negative infinity to infinity ( $-\infty < \lambda_n < \infty$ ). When eigenvalue is equal to zero,  $|\lambda_n = 0|$ ,  $n^{\text{th}}$  characteristic mode resonates if excited properly. Additionally, the sign of the eigenvalue indicates whether related mode contributes to store electrical energy ( $\lambda_n < 0$ ) or magnetic energy ( $\lambda_n > 0$ ) [42].

## 2.2 Physical Explanation of Characteristic Modes

In this section, CMA simulations are performed on a rectangular patch antenna which is given in Figure 2.2 and simulation results are reviewed to get physical explanation

of characteristic modes. CMA solver tool of CST Microwave Studio® is used in simulations. Initial simulation parameters are given in Table 2.1.

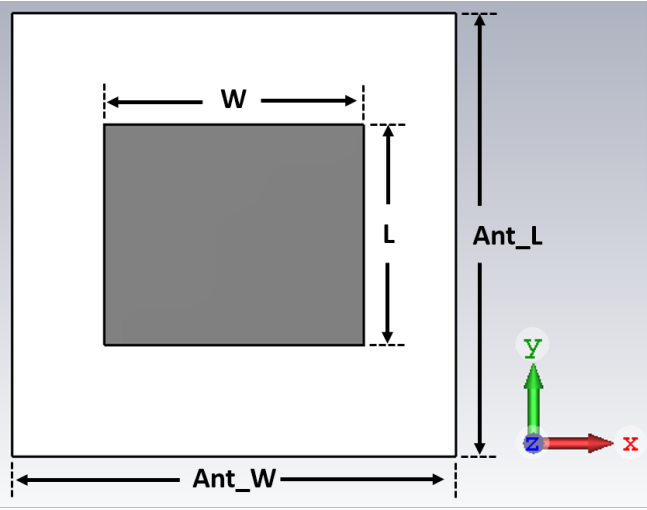


Figure 2.2: Geometry of rectangular patch antenna for CMA simulations.

Table 2.1: Parameters of rectangular patch antenna for CMA simulations.

Parameter	Description	Value
Eps	Dielectric constant of substrate	2.2
Ant_W	Width of antenna	120 mm
Ant_L	Length of antenna	120 mm
W	Width of patch	70 mm
L	Length of patch	60 mm
h	Height of substrate	1.575 mm

As explained in previous section, eigenvalues give helpful information about resonance and radiation characteristics of the characteristic modes. However, the eigenvalue versus frequency graphs as given in Figure 2.3 are not easy to understand the resonance behaviour of the characteristic modes. Therefore, alternative representations are presented to analyze the eigenvalues.

Modal Significance (MS) is one of these representations which gives more precise information about resonance frequency and the radiation bandwidth of the related

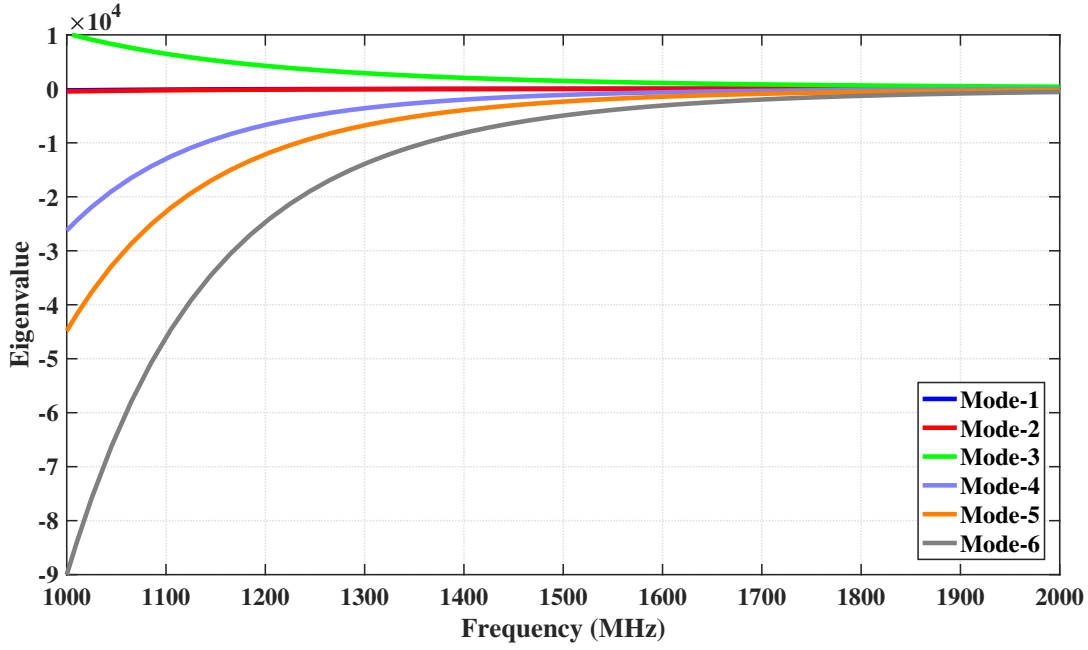


Figure 2.3: Eigenvalue vs Frequency graph of a rectangular patch antenna

characteristic mode that contributes to radiation. MS is formulated as in Equation 2.7.

$$MS = \frac{1}{|1 + j\lambda|} \quad (2.7)$$

As mentioned before, when the eigenvalue of the  $n^{\text{th}}$  mode is equal to zero ( $|\lambda_n = 0|$ ),  $n^{\text{th}}$  characteristic mode resonates at that frequency. Therefore, when MS is equal to 1 ( $MS = 1$ ), related characteristic mode resonates.

In Figure 2.4, simulated MS values of the rectangular patch antenna are given. It is seen in Figure 2.4 that, 1<sup>st</sup> and 2<sup>nd</sup> characteristic modes resonate at 1418 MHz and 1643 MHz, respectively.

Radiation bandwidth is an important design parameter to estimate the radiation performance of characteristic modes. MS graph also gives information about the radiation bandwidth of resonating characteristic modes. Radiation bandwidth is formulated as in Equation 2.8.

$$MS_{\text{HP}_n} = \frac{1}{|1 + j\lambda|} = \frac{1}{\sqrt{2}} = 0.707 \quad (2.8)$$

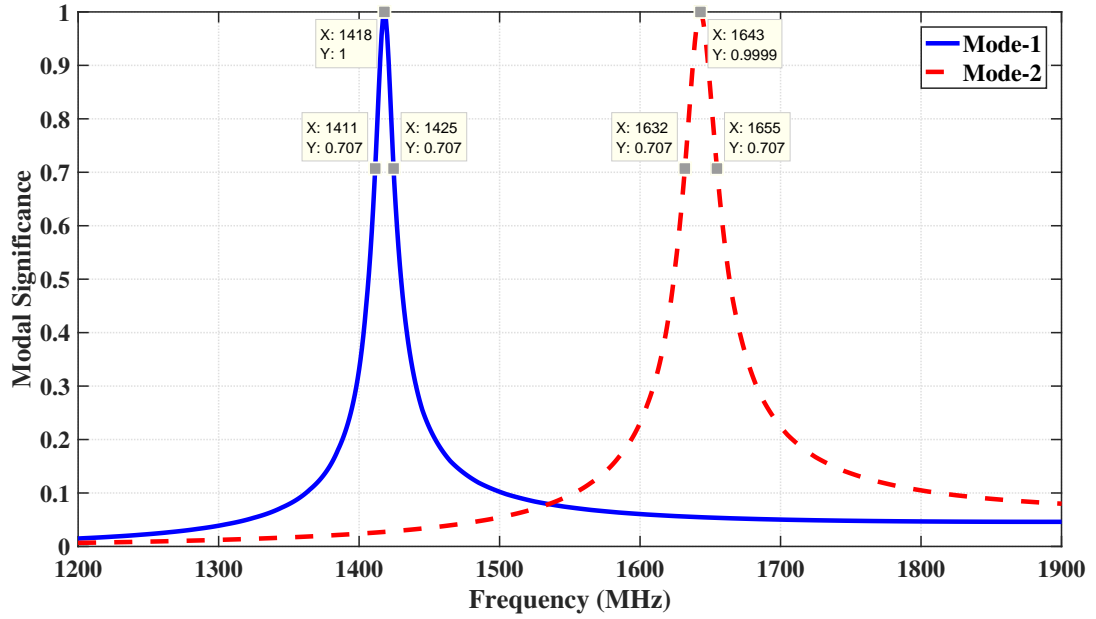


Figure 2.4: MS graph of the rectangular patch antenna.

In Figure 2.4, the quantities of radiating bandwidth are signed with markers for 1<sup>st</sup> and 2<sup>nd</sup> characteristic modes.

Characteristic Angle (CA) is another representation parameter in CMA to define the phase angle between characteristic current and the related characteristic field. CA is defined as in Equation 2.9 [43].

$$\alpha_n = 180^\circ - \tan^{-1}(\lambda_n) \quad (2.9)$$

As mentioned before, characteristic modes resonate when eigenvalue is equal to zero. Therefore, characteristic mode resonates when CA is equal to  $180^\circ$  ( $\alpha_n = 180^\circ$ ). When CA is near to  $90^\circ$  or  $270^\circ$ , mode stores energy.

CA simulation result of the rectangular patch antenna is given in Figure 2.5. It is observed that 1<sup>st</sup> and 2<sup>nd</sup> characteristic modes resonate at 1418 MHz and 1643 MHz, respectively. This result is compatible with MS simulation result. The radiation bandwidth is defined as the frequency range between  $135^\circ$  and  $225^\circ$  angles in CA graphs. The slope of the CA curve also gives information about radiating bandwidth at first view. Steeper slope refers to narrower bandwidth or vice versa.

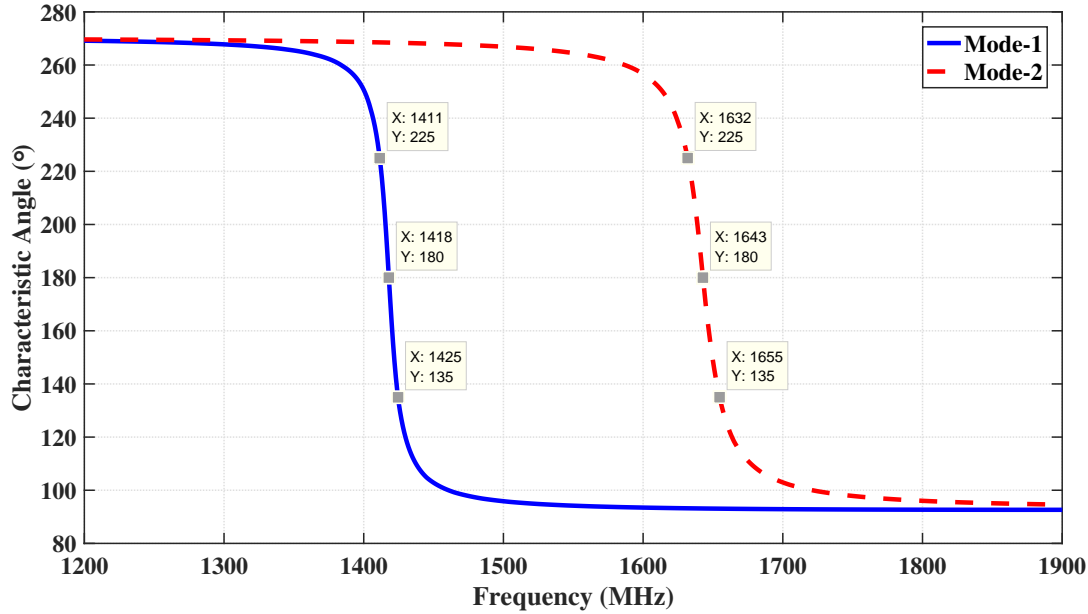


Figure 2.5: CA graph of the rectangular patch antenna.

### 2.3 Circular Polarization Definition with CMA Parameters

As mentioned before, two linearly polarized orthogonal modes should have equal amplitude and  $90^\circ$  phase difference at the required frequency to get circular polarization on a patch antenna. MS and CA parameters are used to determine amplitude and phase difference features, respectively. Two orthogonal modes should have the same MS and  $90^\circ$  CA difference to get circular polarization at the required frequency that is defined as the crossover frequency [44].

MS and CA parameters are explained on a circularly polarized corner truncated patch antenna that operates at 1575 MHz. The antenna structure is given in Figure 2.6. Simulation parameters of the antenna are listed in Table 2.2.

MS and CA results of the CMA simulations are given in Figure 2.7 and Figure 2.8, respectively. It is seen that orthogonal modes resonate at different frequencies and there is a  $90^\circ$  CA difference at the crossover frequency (1575 MHz) which is defined previously as the frequency that has same MS value for each characteristic modes. This means that simulated patch antenna radiates circularly polarized at 1575 MHz if two orthogonal modes (Mode-1 and Mode-2) are excited properly.

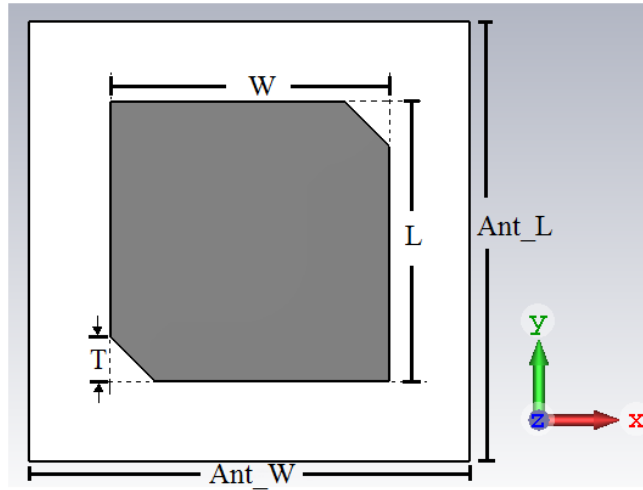


Figure 2.6: CP corner truncated patch antenna for CMA simulations.

Table 2.2: Initial parameters of CP corner truncated patch antenna for CMA simulations.

Parameter	Description	Value
Eps	Dielectric constant of substrate	2.2
Ant_W	Width of antenna	100 mm
Ant_L	Length of antenna	100 mm
W	Width of patch	63.4 mm
L	Length of patch	63.4 mm
h	Height of substrate	1.575 mm
T	Length of truncation	4.65 mm

## 2.4 Design Flow of CP L1 GPS Band Single Fed Microstrip Patch Antenna with CMA Method

In this section, a design flow is proposed for a single fed circularly polarized corner truncated patch antenna by using CMA method. Corner truncated patch is one of the well-known circularly polarized patch geometries [11, 12]. Design is performed on a Rogers RT5880 ( $\epsilon_r = 2.2$ ) dielectric substrate with the thickness of 1.575 mm.

In design process, the effects of "patch length" parameter which is used to adjust the resonance frequency and "truncation length" parameter which controls the circular polarization performance of the antenna are examined primarily. The design flow

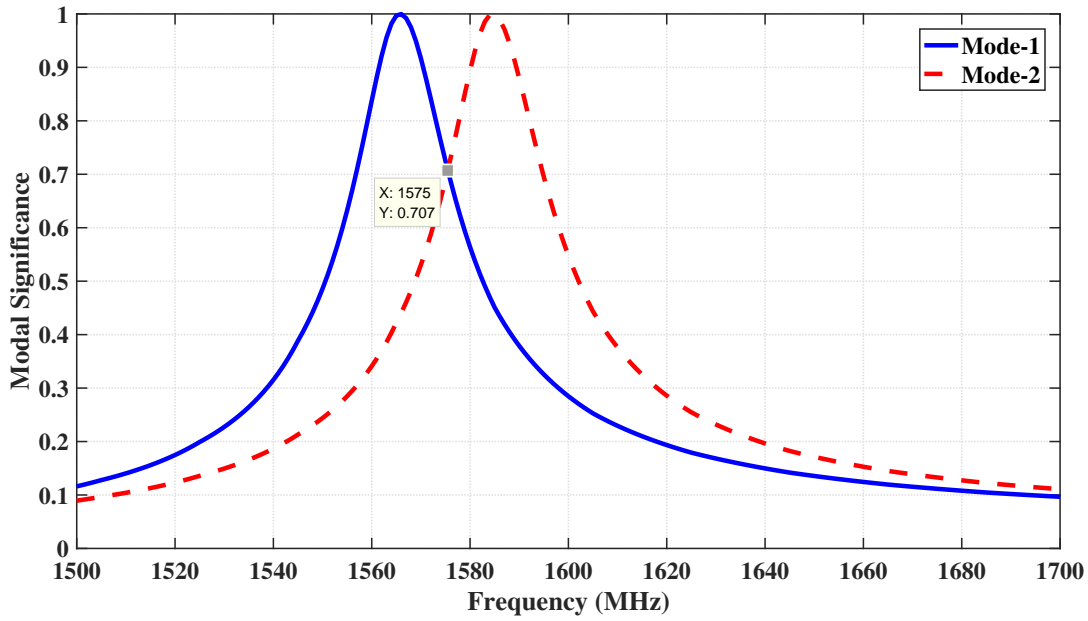


Figure 2.7: Graph of modal significance.

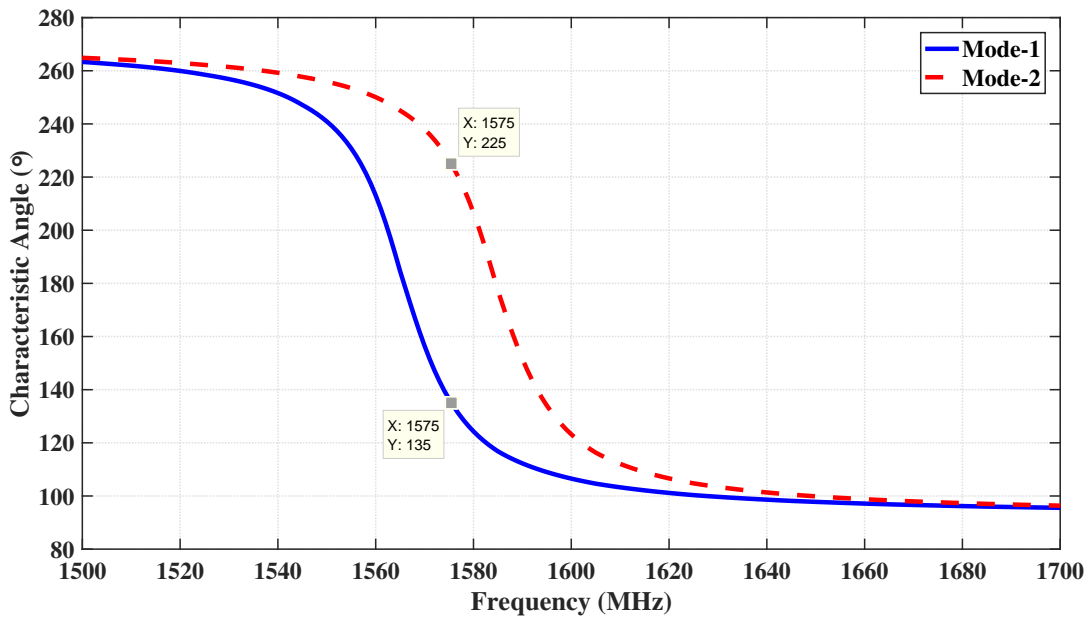


Figure 2.8: Graph of characteristic angle.

which is followed to design CP L1 GPS band antenna is summarized in Figure 2.9 and steps of the design flow are explained below:

**Examination of Patch Length:** The patch length of a square patch is calculated as 63.4 mm to resonate at L1 GPS band with the analytical formulas given in [3]. CMA

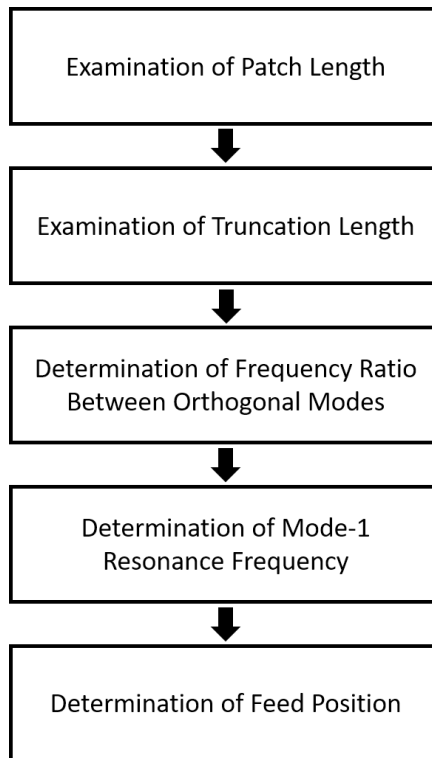


Figure 2.9: Design flow of CPL L1 GPS band antenna with CMA method

simulations are performed to verify the analytical solution. MS graph is given in Figure 2.10. As seen in MS curve, both Mode-1 and Mode-2 resonate at 1555 MHz. Analytical calculation and simulation results differ about 20 MHz with respect to the resonance frequency. However, the exact solution of the resonance frequency is not required at this stage of the design. Therefore, design process is continued with the patch length of 63.4 mm.

**Examination of Truncation Length:** The corners of the patch are truncated with different length to see the effects on characteristic modes. Truncation length is changed from 0 to 6 mm in CMA simulations. MS and CA results are given in Figure 2.11 and Figure 2.12, respectively. According to results, the resonance frequency of Mode-2 increases when the truncation length increases. However, Mode-1 is not affected from the change of truncation of corners. This information is used at the tuning process of the antenna.

The crossover frequencies of MS values are noted to get same current amplitude for each mode in Table 2.3. The CA values are also noted to see the phase difference

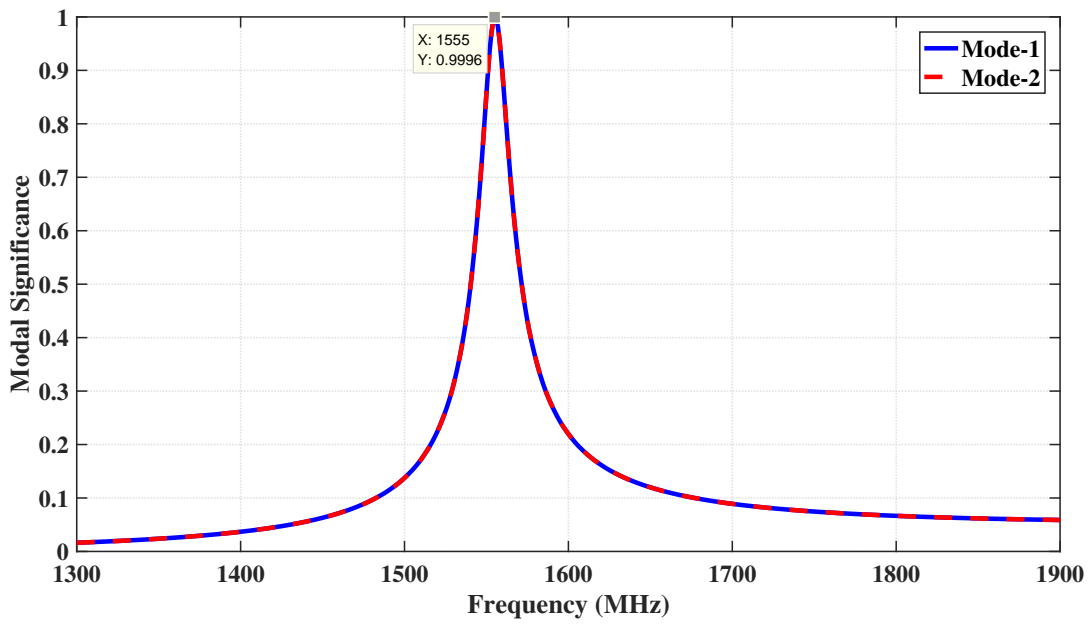


Figure 2.10: MS result for square patch.

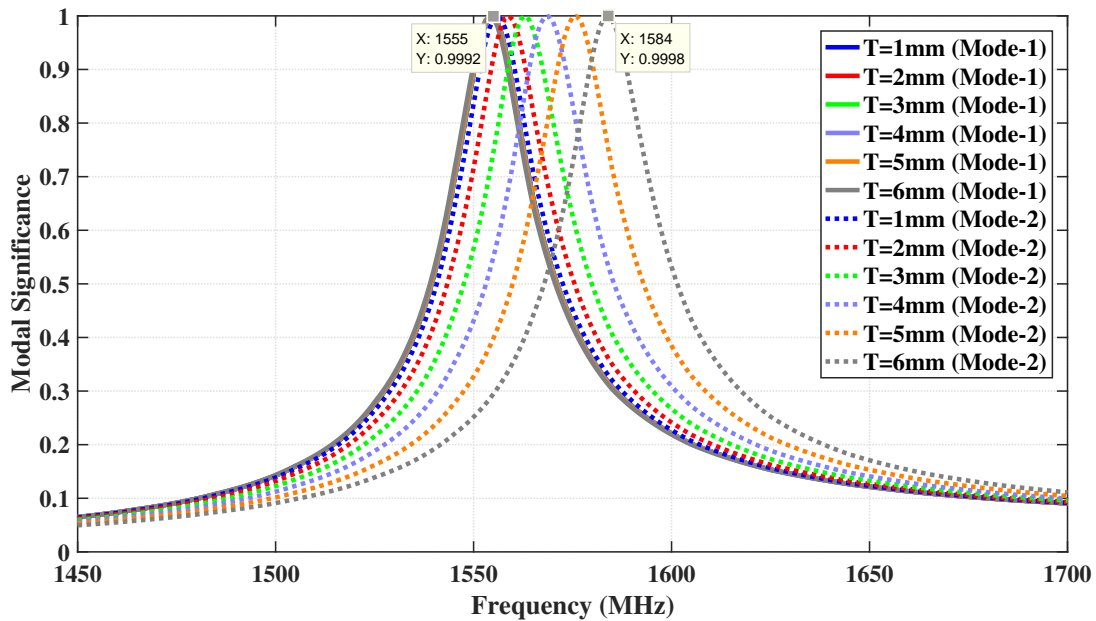


Figure 2.11: MS result for the change of truncation length.

between orthogonal modes at crossover frequencies. According to results,  $90^\circ$  phase difference is obtained between the length of 4 and 5 mm. Therefore, this interval is simulated more precisely and results are given in Table 2.4. According to Table 2.4,  $90^\circ$  phase difference is obtained when the truncation length is between 4.6 and 4.7

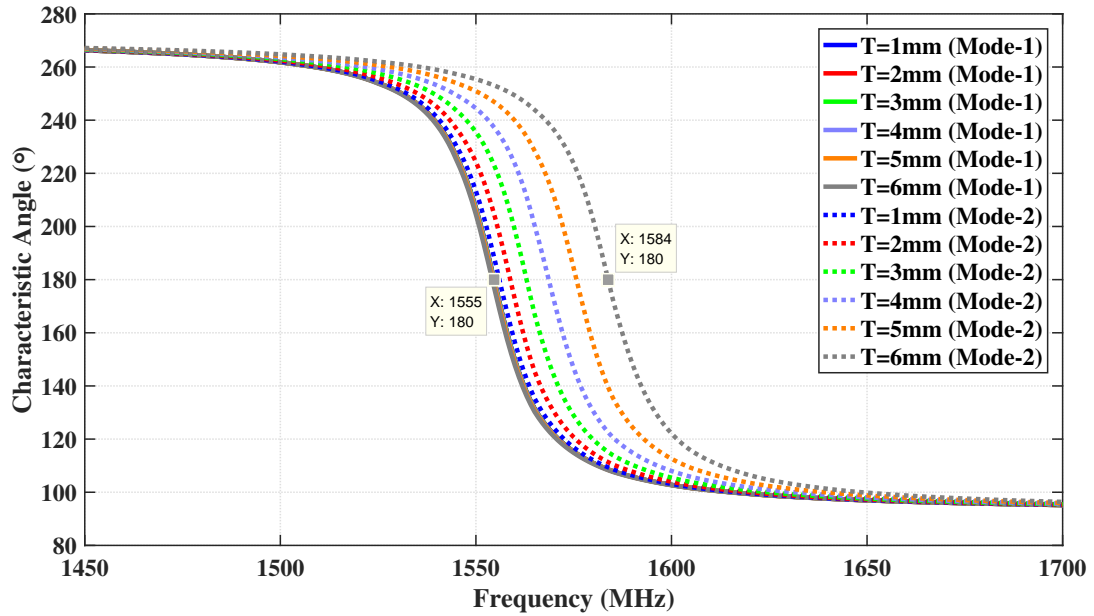


Figure 2.12: MS result for the change of truncation length.

mm. Therefore, it is supposed that 4.65 mm truncation length will ensure  $90^\circ$  phase difference and simulations shows that 4.65 mm ensures  $90^\circ$  phase difference. The rest of the simulations are performed with the truncation length of 4.65 mm.

Table 2.3: Change of truncation length between 0 and 6 mm in CMA simulations.

Truncation Length (mm)	Mode-1 Resonance Frequency (MHz)	Mode-2 Resonance Frequency (MHz)	Crossover Frequency (MHz)	Mode-1 CA at Crossover Frequency (MHz)	Mode-2 CA at Crossover Frequency (MHz)	Phase Difference (Degree)
0	1555	1555	1555	-	-	
1	1555	1556	1555.3	175.6	184.3	8.7
2	1555	1559	1556.7	167.3	193	25.7
3	1555	1563	1558.8	155.4	205	49.6
4	1555	1569	1561.3	142.4	217.2	74.8
5	1555	1576	1564.9	131.1	228.8	97.7
6	1555	1584	1569.2	122.1	237.7	115.6

**Determination of Frequency Ratio Between Orthogonal Modes:** According to Table 2.4, the frequency ratio between the resonance frequencies of Mode-1 and Mode-2 is noted as 1.012. In other words, the frequency ratio of 1.012 provides  $90^\circ$  phase difference.

Table 2.4: Change of truncation length between 4.1 and 4.9 mm in CMA simulations.

Truncation Length (mm)	Mode-1 Resonance Frequency (MHz)	Mode-2 Resonance Frequency (MHz)	Crossover Frequency (MHz)	Mode-1 CA at Crossover Frequency (MHz)	Mode-2 CA at Crossover Frequency (MHz)	Phase Difference (Degree)
4.1	1555	1569.4	1561.9	141.2	218.5	77.3
4.2	1555	1570	1562.2	140	219.8	79.8
4.3	1555	1570.6	1562.5	138.9	221.1	82.2
4.4	1555	1571.2	1562.7	137.9	222.3	84.4
4.5	1555	1572	1563.2	136.5	223.2	86.7
4.6	1555	1572.7	1563.5	135.4	224.4	89
4.65	1555	1573.1	1563.6	135	225	90
4.7	1555	1573.4	1563.8	134.5	225.6	91.1
4.8	1555	1574.1	1564.2	133.3	226.6	93.3
4.9	1555	1575	1564.5	132.3	227.8	95.5

**Determination of Mode-1 Resonance Frequency:** As seen in previous examinations, 90° difference is obtained at 1563.6 MHz. It is needed to tune the crossover frequency to 1575.4 MHz. Therefore, the patch length is changed in simulations and the effect on frequency ratio is examined.

The patch length is changed from 55 mm to 65 mm when truncation length is equal to 4.65 mm. MS curves of the Mode-1 and Mode-2 are given in Figure 2.13 and Figure 2.14, respectively. Resonance frequencies, frequency difference and frequency ratio are tabulated in Table 2.5. According to Table 2.5, if the patch length is changed as 1 mm, the frequency ratio changes in the order of 0.001. Therefore, the required frequency ratio which ensures 90° phase difference could be tuned to required crossover frequency (1575.42 MHz).

Equation 2.10 is derived to calculate the resonance frequency of mode-1 which ensures the crossover frequency at 1575.42 MHz. In Equation 2.10, required crossover frequency ( $f_{cr}$ ) and frequency ratio ( $r$ ) are assigned as 1575.42 MHz and 1.012. Then, resonance frequency of mode-1 ( $f_{mode_1}$ ) is calculated as 1566 MHz.

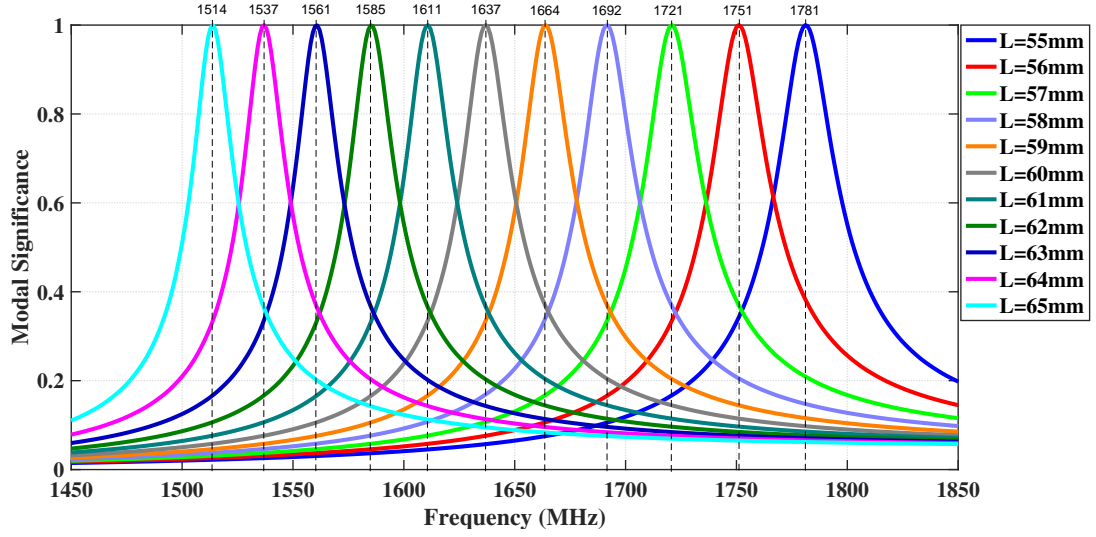


Figure 2.13: MS Curves of Mode-1.

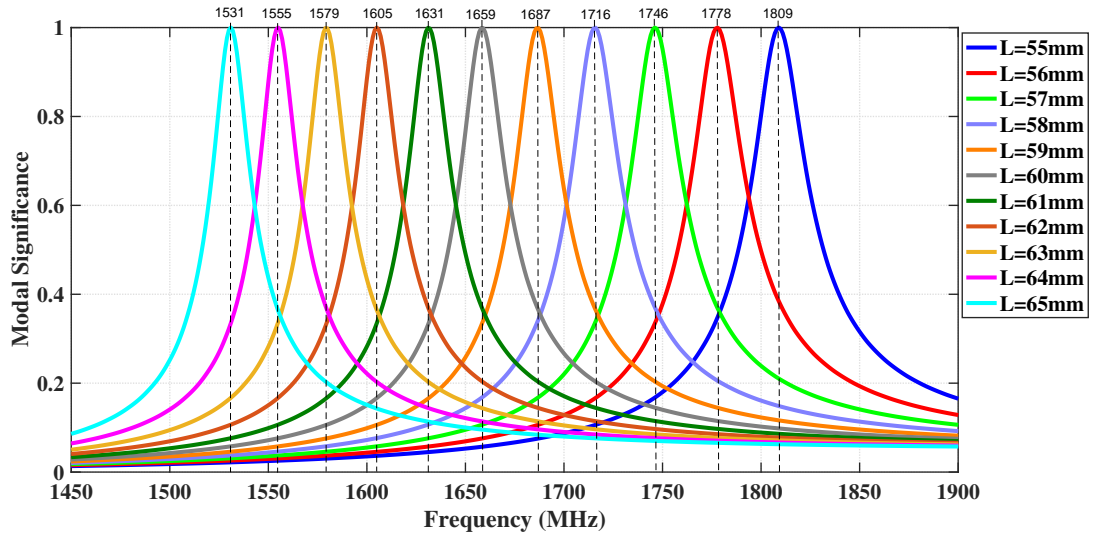


Figure 2.14: MS Curves of Mode-2.

$$f_{mode1} = \frac{2 f_{cr}}{1 + r} \quad (2.10)$$

It is seen that in Table 2.5, the patch length should be between 62 mm and 63 mm to get the resonance frequency of mode-1 as 1566 MHz. The patch length is changed between 62.4 and 62.8 mm in CMA simulations and modal significance is given in 2.15. It is seen in Figure 2.15, if the patch length is equal to 62.8 mm, mode-1 resonates at 1566 MHz.

Table 2.5: Change of patch length in CMA simulations.

Truncation Length (mm)	Patch Length (mm)	Mode-1 Resonance Frequency (MHz)	Mode-2 Resonance Frequency (MHz)	Frequency Difference (MHz)	Frequency Ratio
4.65	55	1781	1809	28	1.015722
4.65	56	1751	1778	27	1.015420
4.65	57	1721	1746	25	1.014526
4.65	58	1692	1716	24	1.014184
4.65	59	1664	1687	23	1.013822
4.65	60	1637	1658	21	1.012828
4.65	61	1611	1631	20	1.012415
4.65	62	1585	1605	20	1.012618
4.65	63	1561	1579	18	1.011531
4.65	64	1537	1555	18	1.011711
4.65	65	1514	1531	17	1.011229

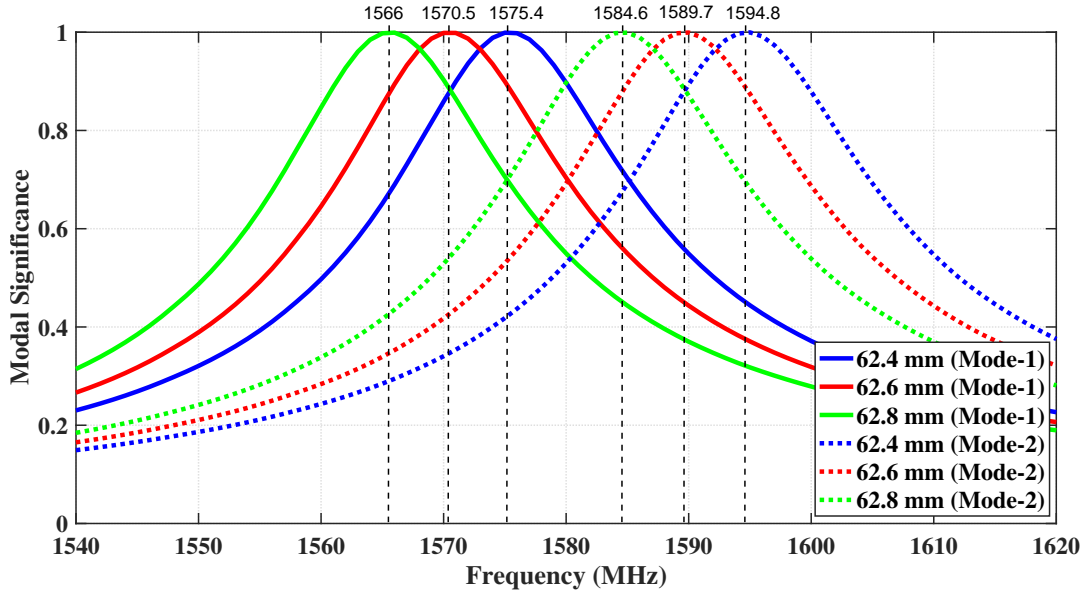


Figure 2.15: MS graph for the change of patch length in CMA simulations.

The crossover frequency of the orthogonal modes is 1575.4 as seen in Figure 2.15 and the phase difference is  $90^\circ$  as seen in Figure 2.16. According to CMA simulations, the corner truncated patch antenna could be defined as circularly polarized at 1575.4 MHz when the patch length and the truncation length are equal to 62.8 mm and 4.65 mm, respectively.

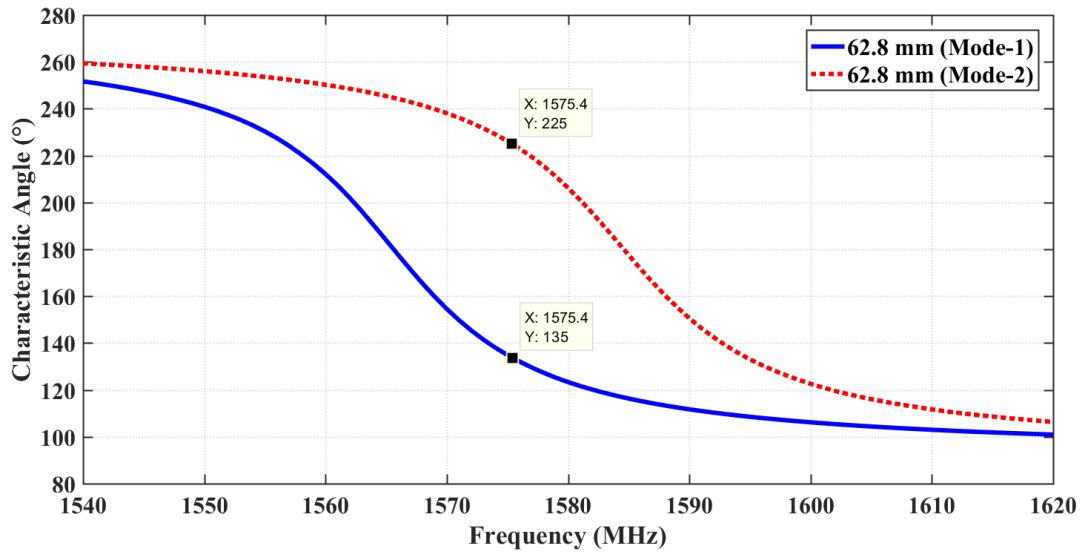


Figure 2.16: CA graph of the CP L1 GPS band corner truncated antenna in CMA simulation.

**Determination of Feed Position:** The common feeding techniques of the microstrip antennas are mentioned in Section 1.2. The coaxial feeding is used in this design study. Therefore, the location of the feed is important for the performance of the microstrip patch antenna. Simulations are carry out to determine the feed position in "Transient Solver" of CST Microwave Studio®, because excitation source is not allowed to use in CMA simulations.

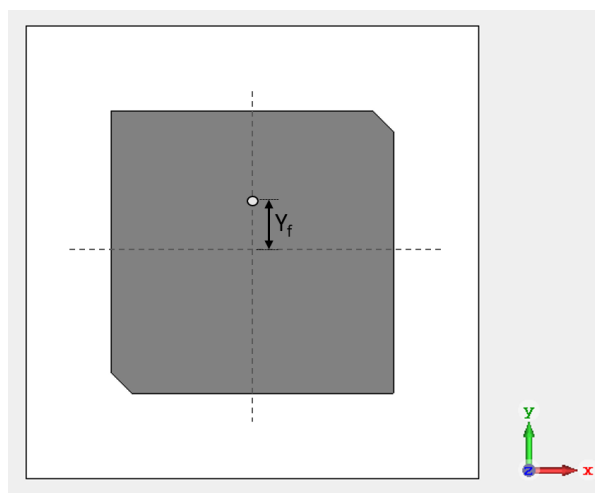


Figure 2.17: Location of coaxial probe on corner truncated patch.

Simulations are carried out with the parameters which ensure CP at L1 GPS band with CMA technique. Coaxial is located along the y-axis to get RHCP on the corner truncated patch as shown in Figure 2.17. So, the parameter of  $Y_f$  is assigned to define the location of the feed along y-axis. Then, parametric analysis is performed to get the best impedance matching case.  $Y_f$  is changed from 5 mm to 14 mm.  $S_{11}$  of the parametric analysis is given in Figure 2.18.

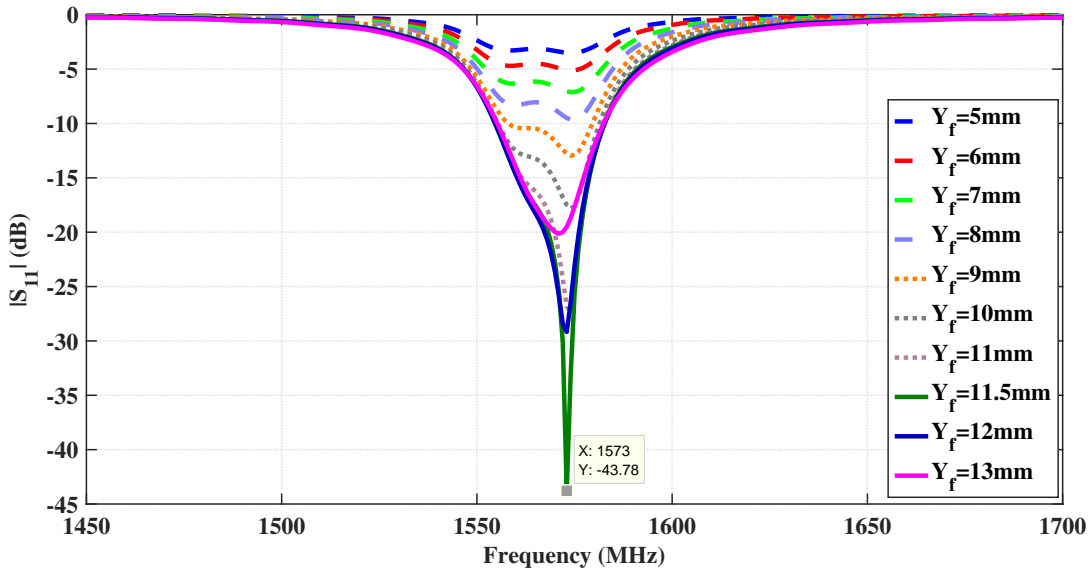


Figure 2.18:  $S_{11}$  of parametric analysis on the feed position of corner truncated patch.

According to Figure 2.18, the best impedance matching is obtained when  $Y_f$  is equal to 11.5 mm. The -10 dB impedance bandwidth (The term of "impedance bandwidth" is defined as  $S_{11}$  is lower than -10 dB in the rest of the thesis.) of 28 MHz is obtained around the center frequency of 1568.6 MHz. The  $S_{11}$  is equal to -24.26 dB at the frequency of 1575.4 MHz. Simulation results meet the bandwidth requirements ( $\geq 2.046$  MHz) of the L1 GPS band signals.

It is seen in Figure 2.19 that the axial ratio of 8 dB is obtained at 1575.4 MHz. Fine tuning is applied by changing the patch length slightly. The final parameters of designed antenna is given in Table 2.6. The axial ratio and  $S_{11}$  graphs are given in Figure 2.20 and Figure 2.21, respectively. According to results, the axial ratio of 1 dB is obtained at 1575.4 MHz when the patch length is equal to 62.41 mm. As a consequence,

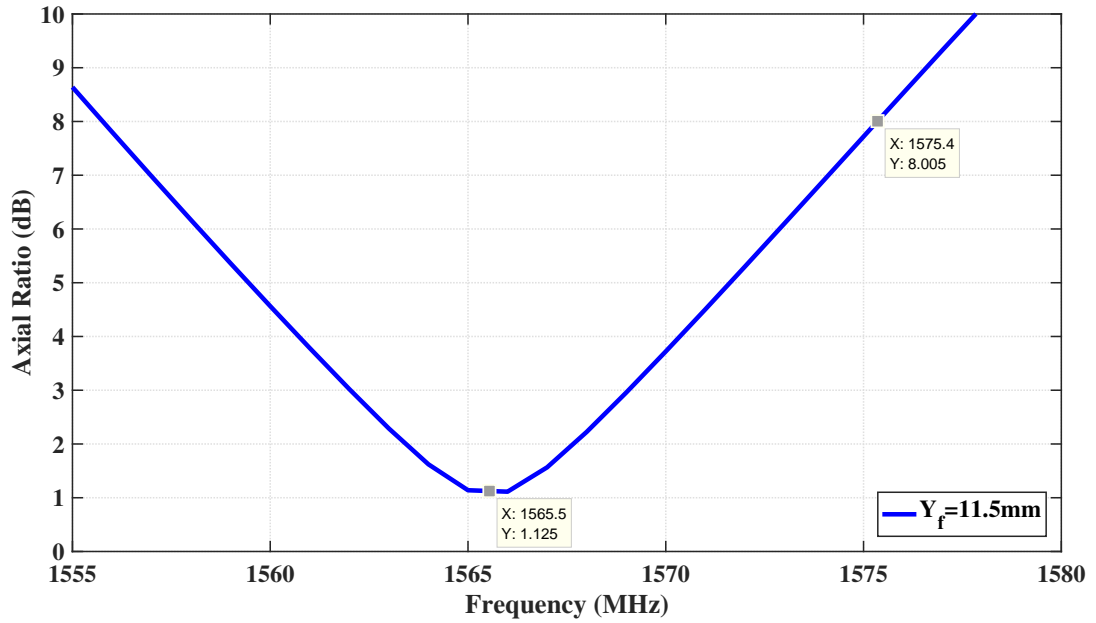


Figure 2.19: Axial ratio of the corner truncated patch when  $Y_f = 11.5$  mm.

a single fed circularly polarized corner truncated patch antenna is designed to operate at L1 GPS band by means of CMA technique.

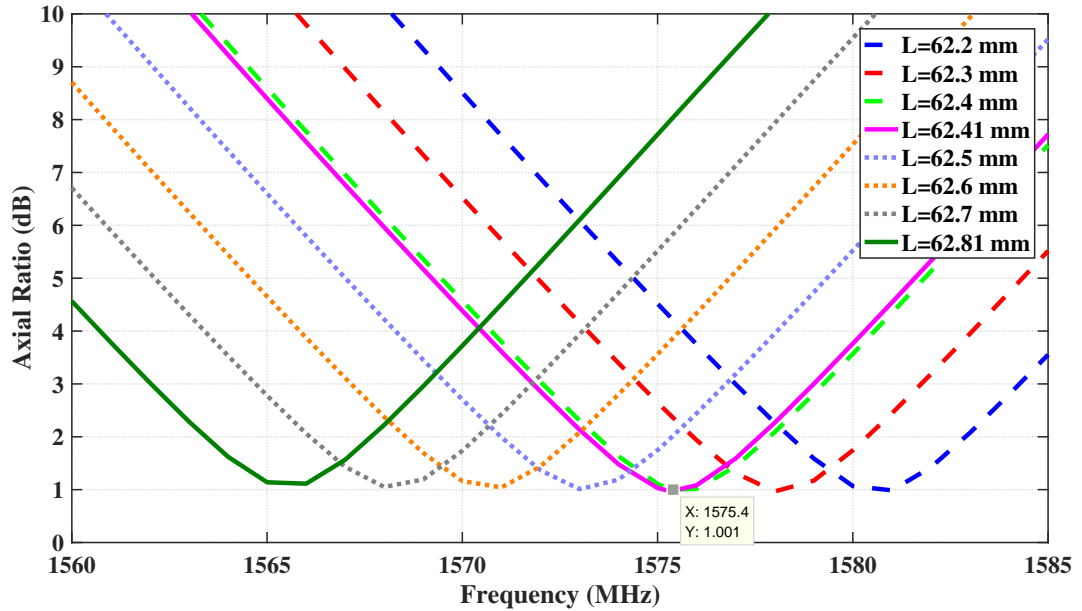


Figure 2.20: Final axial ratio of CP corner truncated patch antenna at L1 GPS band with CMA method.

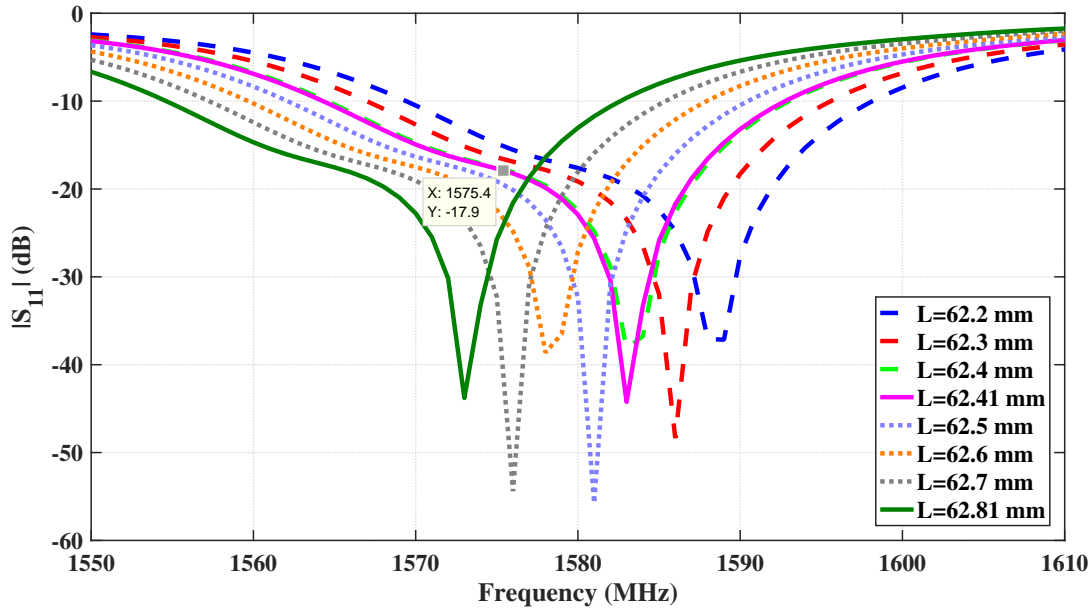


Figure 2.21: Final  $S_{11}$  of CP corner truncated patch antenna at L1 GPS band with CMA method.

Table 2.6: Final parameters of L1 GPS band CP corner truncated patch antenna.

Parameter	Description	Value
Eps	Dielectric constant of substrate	2.2
Ant_W	Width of antenna	100 mm
Ant_L	Length of antenna	100 mm
W	Width of patch	62.41 mm
L	Length of patch	62.41 mm
h	Height of substrate	1.575 mm
T	Length of truncation	4.65 mm
Xf	Feed distance along the x-axis	0 mm
Yf	Feed distance along the y-axis	11.5 mm

## 2.5 Summary and Discussions

In this section, the theory of characteristic mode and physical explanations are presented to comment on MS and CA outputs of CMA. A design flow is proposed to design a single fed circularly polarized L1 GPS band microstrip antenna by means of

CMA technique.

CMA technique allows to antenna designers to see the characteristics of the radiating and non-radiating modes on the antenna without any excitation. This feature is very useful for the designers to see the behaviour of the antenna structure in the preliminary phases of the design. In presented study, circular polarization is examined on a corner truncated conducting patch. The characteristic of modes are observed clearly when the length of truncation is changed and design flow is formed based on the changes of characteristics modes.



## CHAPTER 3

### DESIGN, FABRICATION AND MEASUREMENT OF A NOVEL L1/L2 DUALBAND MICROSTRIP ANTENNA FOR GPS APPLICATIONS

As mentioned in the Chapter 1, there are two active GPS frequency bands for civil usage. These civilian GPS bands are operating at L1 (1575.42 MHz) and L2 (1227.60 MHz) frequencies and both bands have the signal bandwidth of 2.046 MHz. The frequency ratio between L1 and L2 bands is considered as small in literature [15]. In most of the studies, the "slot loading" method is used to achieve dualband operability on a single patch which has a small frequency ratio [32]. Placing the slots close to the edges of the patch is used frequently to get small frequency ratio in dualband operations [15, 32, 33, 35]. Therefore, the four-edge slotted square patch antenna structure is chosen as an initial geometry to design a GPS antenna operating at L1 and L2 bands with a single feed.

In this chapter, studies on the single fed dualband microstrip antenna which are implemented with *reactive loading* and *slot loading* methods are presented. The parametric analysis of four-edge slotted patch geometry is given and, reactive loading (capacitive loading) is applied to decrease the frequency ratio in dualband operation. A novel four-edge slotted (*zigzag four-edge slotted*) patch is proposed to decrease the frequency ratio without using capacitive loading. This novel patch is designed to operate circularly polarized at L1 and L2 GPS bands with a single coaxial feed. Designed antenna is fabricated and measured. Results and evaluations are presented related to "*zigzag four-edge slotted*" patch antenna.

### 3.1 THE PARAMETRIC ANALYSIS ON FOUR-EDGE SLOTTED PATCH ANTENNA

In order to get an insight for the design of the four-edge slotted patch antenna, a parametric analysis is performed. In the parametric analysis, effects of dielectric constant ("Eps") and the height of the substrate ("h"), slot length ("L\_slot"), slot width ("Ws") and slot offset ("SlotOffset") parameters are examined. The geometry of the patch is given in Figure 3.1.

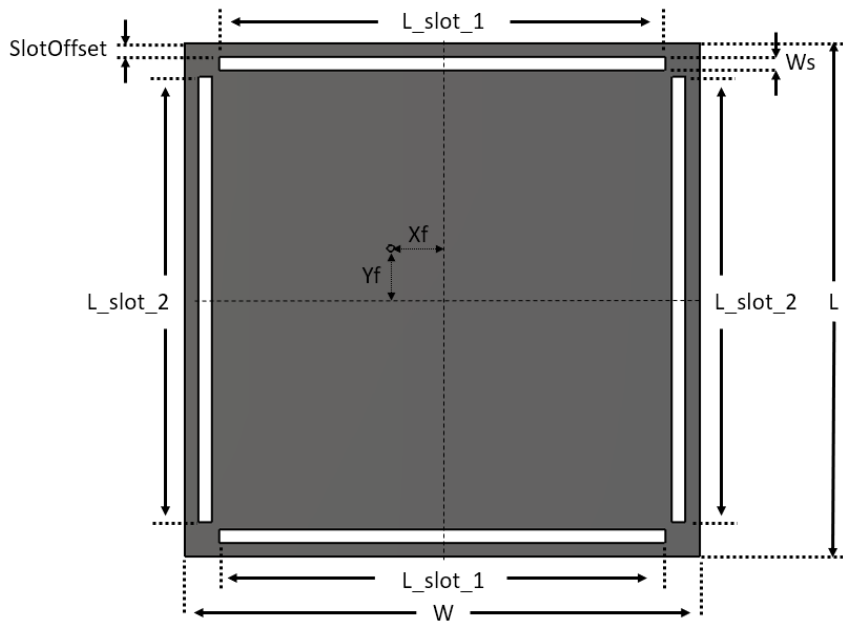


Figure 3.1: The geometry of four-edge slotted patch.

As mentioned in Section 1.4,  $TM_{10}$  and  $TM_{30}$  modes radiate boresight. These two modes are used in dualband operations on a single patch. The resonance frequency of the  $TM_{30}$  mode decreases to lower frequencies with loading slots close to edges. Because, the placement of slots close to edges causes to perturb the  $TM_{30}$  mode more than  $TM_{10}$  mode.

Simulations are started with the initial parameters given in Table 3.1 and  $S_{11}$  graph is given in Figure 3.2. According to  $S_{11}$  graph, lower band ( $TM_{10}$ ) resonates at 1227 MHz and higher band ( $TM_{30}$ ) resonates at 1632 MHz. The surface currents of the  $TM_{10}$  and  $TM_{30}$  modes are given in Figure 3.3 and Figure 3.4, respectively .

Table 3.1: Initial design parameters of parametric analysis on four-edge slotted patch.

Parameter	Value	Description
Eps	2.2	Dielectric constant of the substrate
Ant	120 mm	Length of the antenna substrate
h	1.575 mm	Height of the substrate
L	75.9 mm	Length of the patch
W	75.9 mm	Width of the patch
L_slot_1	71.7 mm	Length of the horizontal slots
L_slot_2	71.7 mm	Length of the vertical slots
SlotOffset	1 mm	Distance between patch edge and slot edge
Ws	1 mm	Width of the edge slots
Xf	7.5 mm	Feed distance along the x-axis
Yf	7.5 mm	Feed distance along the y-axis

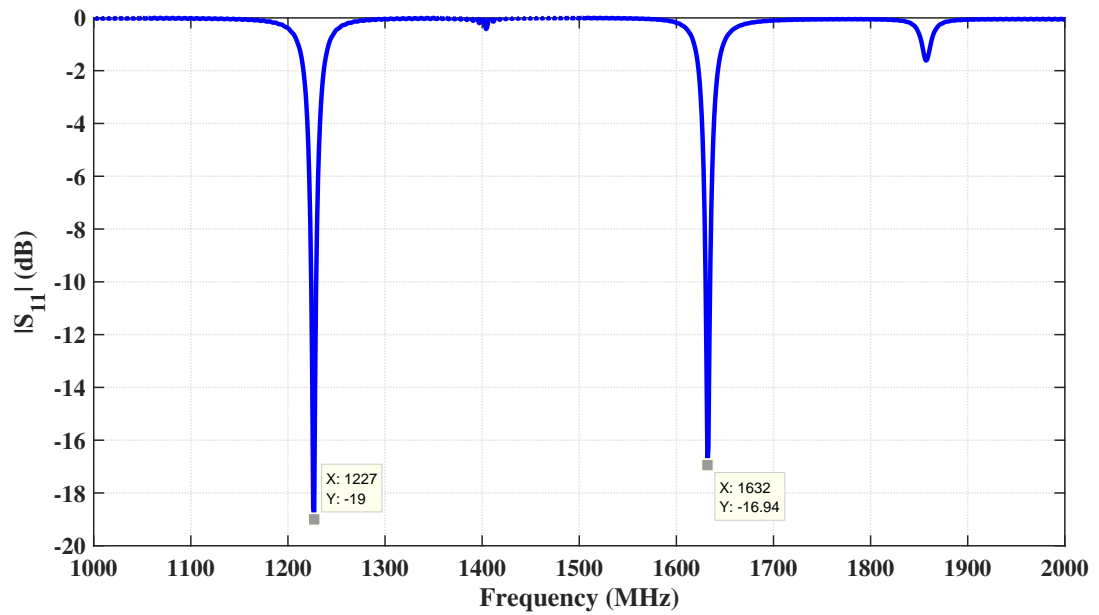


Figure 3.2:  $S_{11}$  of four-edge slotted patch with initial parameters.

Radiation patterns of  $TM_{10}$  mode and  $TM_{30}$  mode are given in Figure 3.5 and in Figure 3.6 as azimuth and elevation pattern, respectively. As expected,  $TM_{10}$  and  $TM_{30}$  modes radiate to boresight of the antenna.

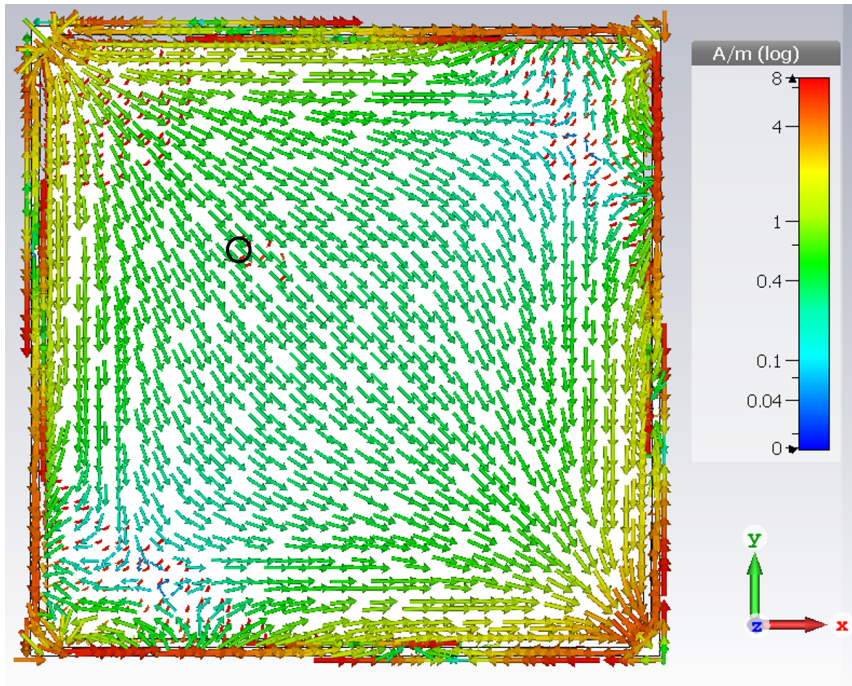


Figure 3.3:  $TM_{10}$  mode surface current of four-edge slotted patch with initial parameters at 1227 MHz.

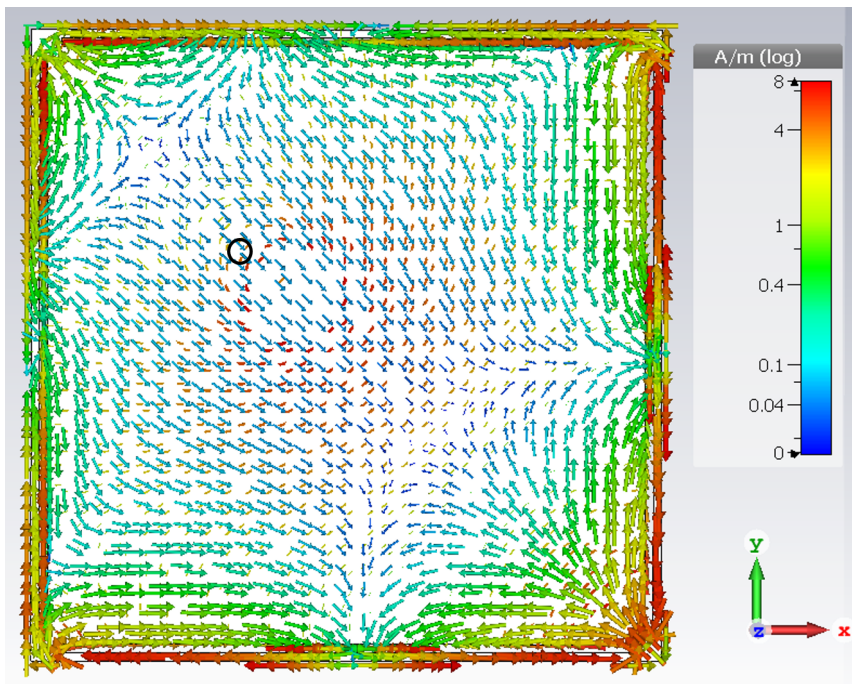


Figure 3.4:  $TM_{30}$  mode surface current of four-edge slotted patch with initial parameters at 1632 MHz.

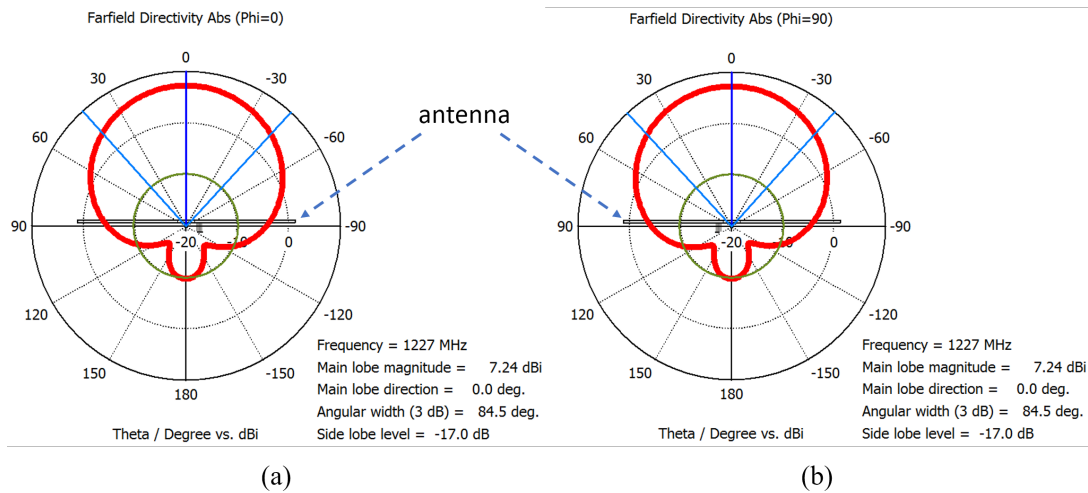


Figure 3.5: Radiation pattern of the  $TM_{10}$  mode (at 1227 MHz),  
 (a) Azimuth Pattern ( $\phi = 0^\circ$ ), (b) Elevation Pattern ( $\phi = 90^\circ$ ).

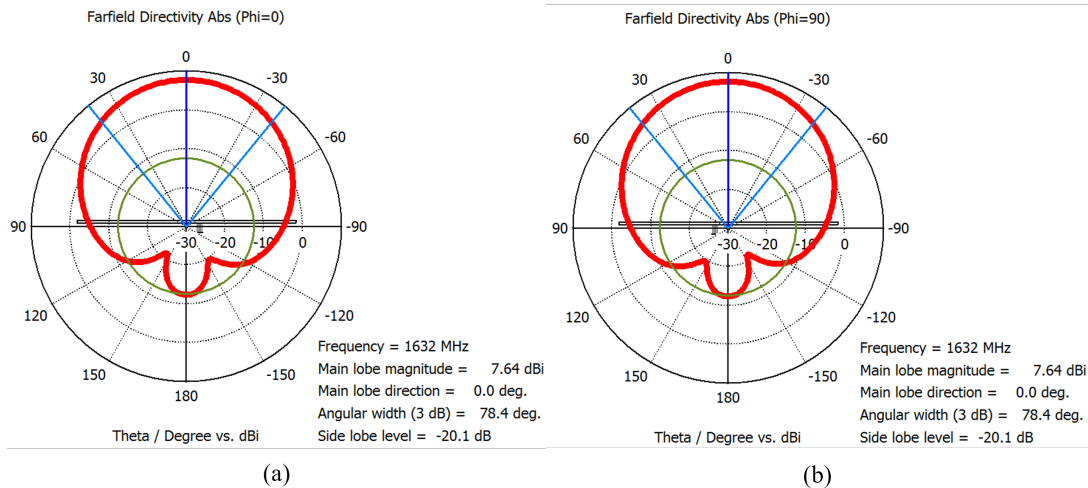


Figure 3.6: Radiation pattern of the  $TM_{30}$  mode (at 1632 MHz),  
 (a) Azimuth Pattern ( $\phi = 0^\circ$ ), (b) Elevation Pattern ( $\phi = 90^\circ$ ).

In the following subsections, parametric analysis is presented on four-edge slotted patch to get an insight into the design of four-edge slotted patch.

### 3.1.1 Effect of the Dielectric Constant and the Height of the Substrate

The type and height of the substrate is specified according to requirements in the design process of microstrip antennas. Therefore, parametric analysis is performed

on two different substrates which have the relative dielectric constants of 2.2 and 3 to determine the substrate which allows small frequency ratio. Lower dielectric constants are chosen to get broader bandwidth. The lower resonance frequency is tuned to 1227.6 MHz (L2 GPS band) for each substrate with changing the lengths of patch and slots. The initial parameters which are given in Table 3.1 are used to tune the lower band at 1227.6 MHz on a substrate with the relative dielectric constant of 2.2. When the relative dielectric constant is increased the electrical length of the patch increases, and therefore the resonance frequencies decrease. The patch length is decreased to increase the resonance frequencies. The patch length is assigned to 65.5 mm and slot length is shortened to 61.3 mm. The difference between the patch length and slot length is fixed as 4.2 mm. When the relative dielectric constant of the substrate is increased to 3, higher band increases (i.e. the frequency ratio is decreased) as shown in Figure 3.7. Therefore, Rogers RT5880 substrate ( $\epsilon_r = 2.2$ ) which is frequently used in microstrip applications is chosen.

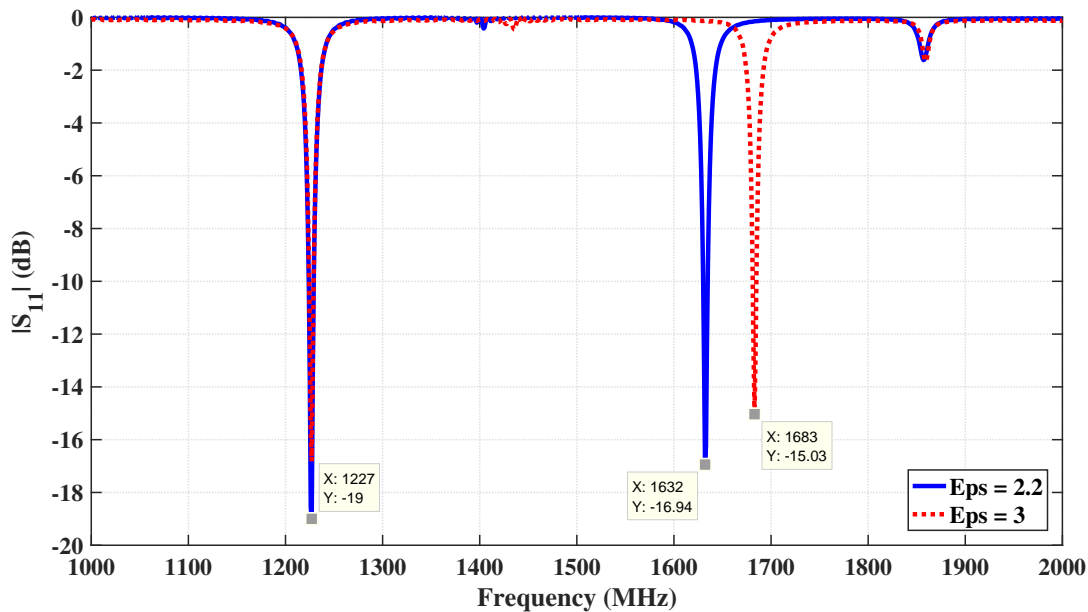


Figure 3.7:  $S_{11}$  of parametric analysis on dielectric constant of substrates.

In order to determine the height of the substrate, simulations are performed with two different heights as 1.575 mm and 3.18 mm. Previous simulations were performed with the height of 1.575 mm. Then, the height of the substrate is increased to 3.18 mm and simulations are performed without changing other parameters given in Table 3.1. According to Figure 3.8, the frequency of lower band decreases and higher band in-

creases when the height of the substrate increases (i.e. the frequency ratio increases). As a consequence, the thinner substrate allows to get smaller frequency ratio. Therefore, the substrate with the height of 1.575 mm is chosen to be used in the design.

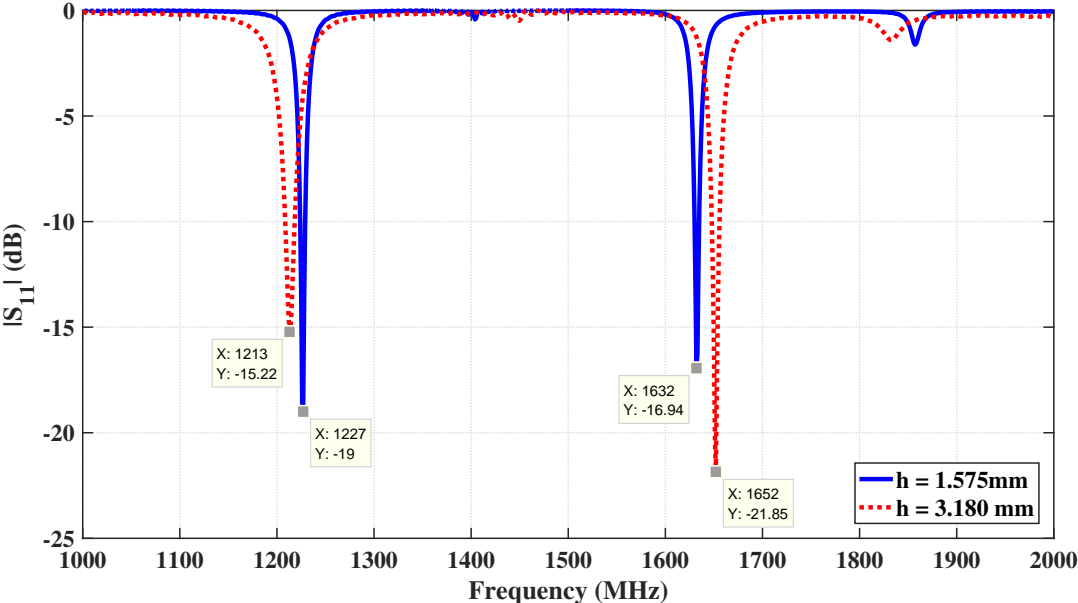


Figure 3.8:  $S_{11}$  of parametric analysis on height of substrate.

### 3.1.2 Effect of Slot Length

Parametric analysis are performed to see the effect of the change in the slot length. Slot length is changed from 71.7 mm to 65.7 mm. According to Figure 3.9, when the slot length increases both resonance frequencies decreases. But, it is seen that the frequency of higher band decreases more than lower frequency. Therefore, the frequency ratio decreases. As mentioned in Section 1.4, the placement of the slots to close the edge of the patch perturbs the  $TM_{30}$  mode mostly. Therefore, the resonance frequency of the  $TM_{30}$  is effected from the change of slot length more than  $TM_{10}$  mode.

### 3.1.3 Effect of Slot Width

In this analysis, slot width is changed from 0.5 mm to 1.5 mm with the steps of 0.5 mm. The slot length is assigned to 69.5 mm, because the slots intersect to each

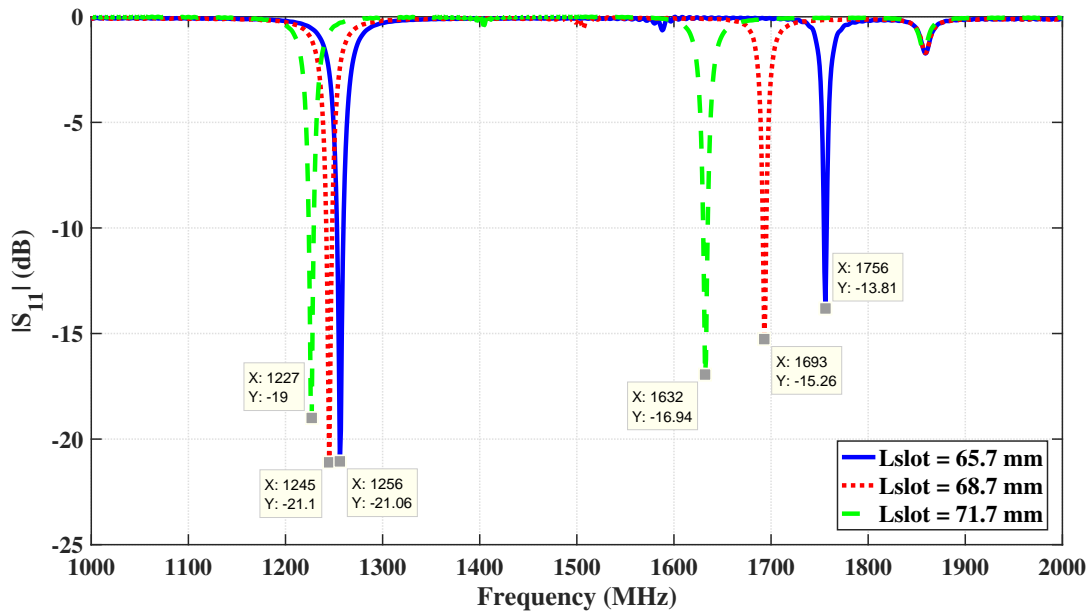


Figure 3.9:  $S_{11}$  of parametric analysis on slot length.

other when the slot width is equal to 1.5 mm. According to Figure 3.10, there is not a dramatical change on frequency ratio. If the results are examined detailed, it is seen that increasing the width of the slot increases the frequency ratio slightly as given in Table 3.2.

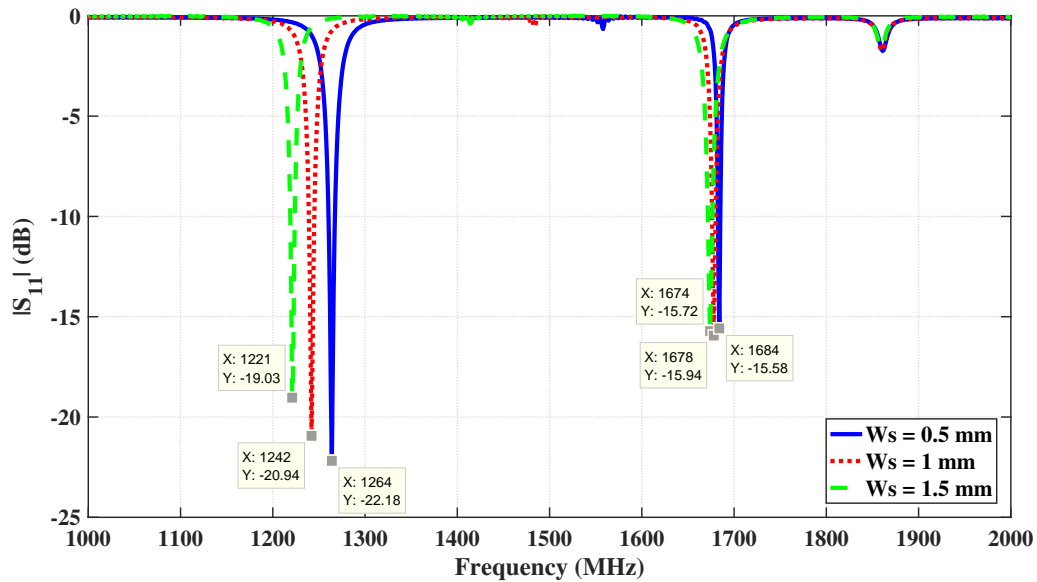


Figure 3.10:  $S_{11}$  of parametric analysis on slot width.

Table 3.2: The effect of slot width on frequency ratio.

Slot Width (mm)	Frequency Difference (MHz)	Frequency Ratio
0.5	420	1.33
1	436	1.35
1.5	453	1.37

### 3.1.4 Parametric Analysis on Slot Offset

The slot offset is changed from 0.5 mm to 1.5 mm with steps of 0.5 mm when the patch length is equal to 69.5 mm. According to Figure 3.11, both resonance frequencies decreases but the lower band is affected mostly from the change of the slot offset. Therefore, the frequency ratio decreases when slot offset decreases.

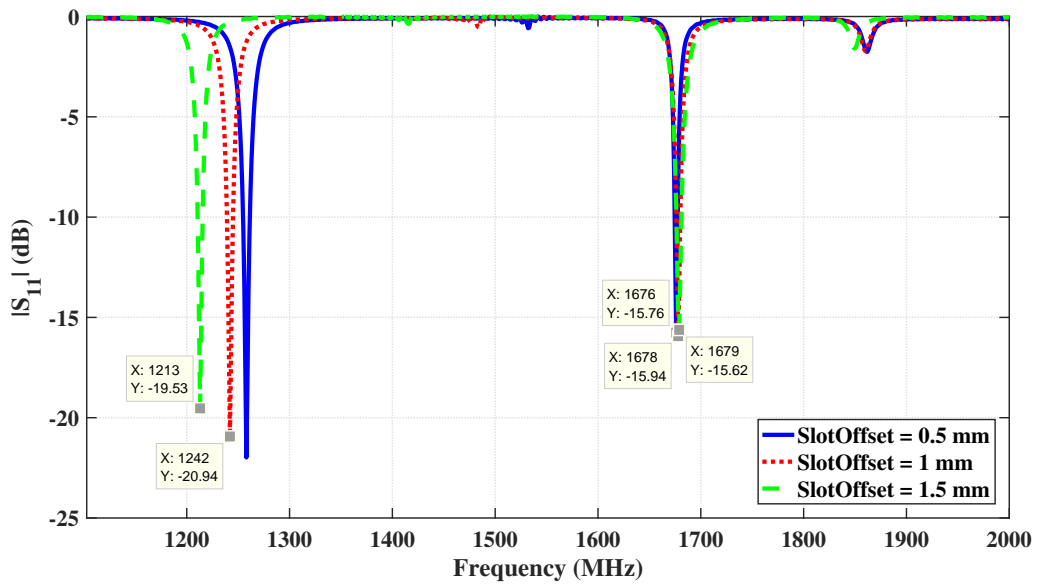


Figure 3.11:  $S_{11}$  of parametric analysis on slot offset.

### 3.1.5 Summary of Parametric Analysis

Outputs of parametric analysis on four-edge slotted patch are summarized in Table 3.3. A substrate which has low dielectric constant and low thickness is needed to achieve small frequency ratio on four-edge slotted patch. Slots must be placed close

to edges and slot length must be as long as possible to decrease the frequency ratio. In addition, the width of the slots should be narrow to get small frequency ratio.

Table 3.3: Summary of parametric analysis on four-edge slotted patch.

Parameter	Change	Lower Resonance Frequency	Higher Resonance Frequency	Frequency Ratio
Dielectric Constant	↑	↓	↓	↑
Thickness of Substrate	↑	↓	↓	↑
Sloth Length	↑	↓	↓↓↓	↓
Slot Width	↑	↓↓	↓	↑
Slot Offset	↑	↓↓↓	-	↑

### 3.2 CIRCULAR POLARIZATION ON FOUR-SLOTTED PATCH

The patch is needed to be perturbed to get circular polarization on single fed structures. Perturbation process is based on changing the length of slots and edges on four-edge slotted patch. Slots and edges are defined as vertical and horizontal as shown in Figure 3.12. Then margin parameters are defined as "MarEdge" and "MarSlot". The parameter of MarEdge expresses the absolute length difference between the lengths of horizontal and vertical edges. In a similar manner, the margin parameter of MarSlot expresses the absolute length difference between the lengths of horizontal and vertical slots.

Below conditions must be applied to get right hand circular polarization at each frequency band on four-slotted patch;

- length of horizontal edge > length of vertical edge,
- length of vertical slot > length of horizontal slot.

The parameter of MarEdge controls the axial ratio at lower band, and the parameter

of MarSlot controls the axial ratio at higher band. The parameters of MarEdge and MarSlot are changed iteratively according to axial ratio simulation results. Different approaches are studied and the best way is determined to control the axial ratio of the frequency bands. According to this approach, at first, MarEdge is increased slightly, then MarSlot is increased until the axial ratio of higher frequency band is not going to be better. After that, MarEdge is increased slightly, then MarSlot parameter is increased until the best axial ratio again. This iterative process continues until getting required axial ratio at required frequencies.

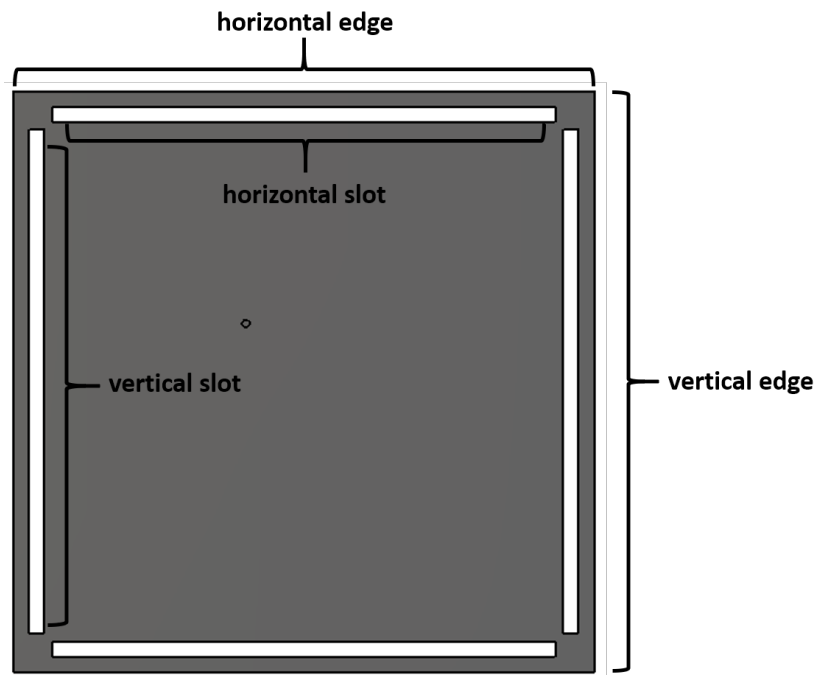


Figure 3.12: The representation of horizontal and vertical slots and edges on four-edge slotted patch.

The process of getting circular polarization is applied to four-slotted patch antennas as described in this section. The simulation results are presented in the design sections of dualband and triband antennas.

### 3.3 CAPACITIVELY LOADED L1/L2 BAND GPS ANTENNA

In this section, an L1/L2 dualband GPS antenna is designed on a four-edge slotted patch with capacitive loading of slots. The initial parameters are given in Table 3.4.

The type and height of substrate, slot width and slot offset are chosen to get small frequency ratio and satisfy the bandwidth requirements of L1 and L2 GPS bands.

Table 3.4: Initial parameters for capacitive loaded patch antenna.

<b>Substrate Type</b>	Rogers RT5880
<b>Relative Dielectric Constant</b>	2.2
<b>Substrate Height</b>	1.575 mm
<b>Slot Width</b>	1 mm
<b>Slot Offset</b>	1 mm

As mentioned in section 3.1.2, the frequency ratio decreases when slot length increases. Therefore, slot length is increased as far as possible in the physical condition of the patch and lower band is tuned to 1227 MHz as performed in parameter analysis with the given parameter in Table 3.1. As seen in the  $S_{11}$  graph in Figure 3.2, higher band resonates at 1632 MHz. There is 57 MHz between L1 GPS band frequency (1575 MHz) and 1632 MHz.

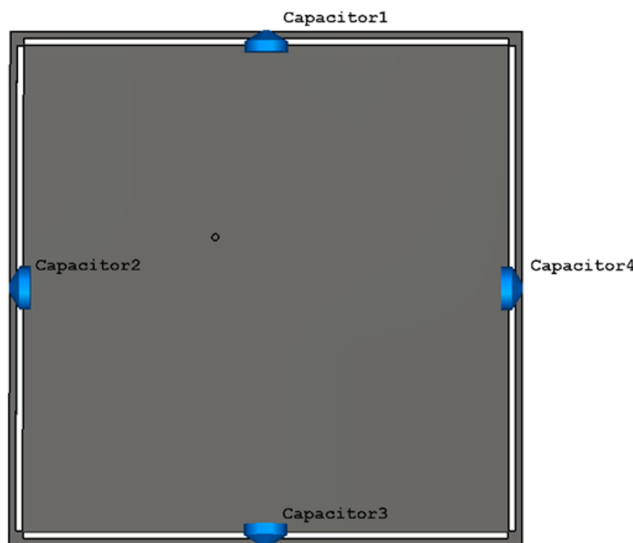


Figure 3.13: Capacitive loaded four-edge slotted patch.

Capacitive loading is applied on slots to decrease the frequency ratio as shown in Figure 3.13. Different capacitance values are selected from procurable surface mount components from the market and assigned as lumped element in simulations.

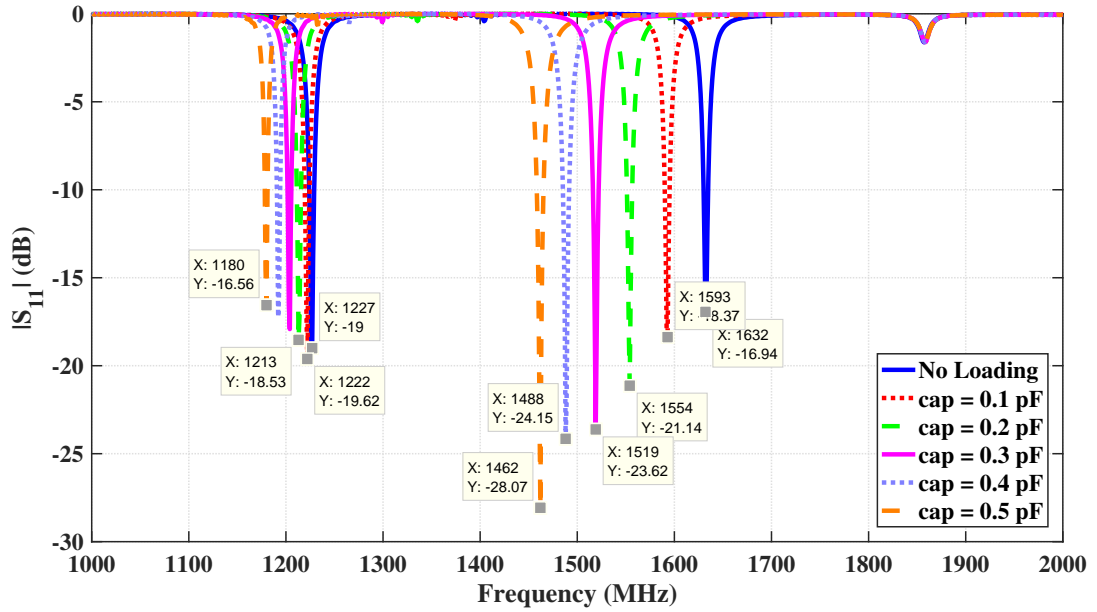


Figure 3.14:  $S_{11}$  of different capacitance loaded patch.

The capacitance of the capacitors are changed from 0 to 0.5 pF in simulations.  $S_{11}$  graph is given in Figure 3.14. Resonance frequencies and frequency ratio between lower and higher band are listed in Table 3.5.

Table 3.5: Frequency ratio vs capacitance

Capacitance (pF)	Lower Resonance Frequency (MHz)	Higher Resonance Frequency (MHz)	Frequency Ratio
0	1227	1632	1.330
0.1	1222	1593	1.304
0.2	1213	1554	1.281
0.3	1204	1519	1.262
0.4	1192	1488	1.248
0.5	1180	1462	1.239

It is expected that the increase of the capacitance decreases the frequency ratio. Because, when the slots are loaded with capacitors the electrical length of the slots behaves as if they are increased.

There is a frequency ratio of 1.283 between L1 and L2 GPS bands. Therefore, capacitances should be selected near or slightly bigger than the capacitance which satisfies the frequency ratio of 1.283. According to Table 3.5, the frequency ratio of 1.262 is

obtained when capacitance is equal to 0.3 pF. This capacitance satisfies the required frequency ratio and rest of the design is performed with 0.3 pF capacitors loaded to slots.

Table 3.6: Geometry of L1/L2 dualband four-edge slotted patch.

Parameter	Value	Description
Eps	2.2	Dielectric constant of the substrate
Cap	0.3 pF	Capacitance of the loaded capacitors
Ant	120 mm	Simulated antenna border length
h	1.575 mm	Height of the substrate
L	76.6 mm	Length of the patch
W	76.6 mm	Width of the patch
L_slot_1	67.3 mm	Length of the horizontal slots
L_slot_2	67.3 mm	Length of the vertical slots
SlotOffset	1 mm	Distance between patch edge and slot edge
Ws	1 mm	Width of the edge slots
Xf	7.5 mm	Feed distance along the x-axis
Yf	7.5 mm	Feed distance along the y-axis

By means of choosing the capacitance properly to satisfy the required frequency ratio, the length of the slots is decreased to increase the higher band to 1575 MHz. When the slot length decreases the resonance frequency of lower band also increases (i.e. lower band is detuned). Therefore, an iterative tuning process is started with changing of the lengths of slots and patch to adjust both bands. As a result of the tuning process, lower and higher bands are tuned to 1227.6 MHz and 1575.4 MHz as shown in Figure 3.15 with the given parameters in Table 3.6.

The tuned antenna radiates linearly polarized at L1 and L2 GPS bands. Patch geometry is perturbed as described in Section 3.2 to get circular polarization. Required axial ratios are achieved at both bands with tuning the MarEdge and MarSlot parameters. The final parameters of the designed antenna is given in Table 3.7.

3-dB axial ratio bandwidth of 3 MHz is achieved at both L1 and L2 GPS bands as shown in Figure 3.16. According to  $S_{11}$  graph in Figure 3.17, impedance bandwidths of 12.2 MHz and 7.2 MHz are obtained in L2 and L1 GPS bands, respectively. Ob-

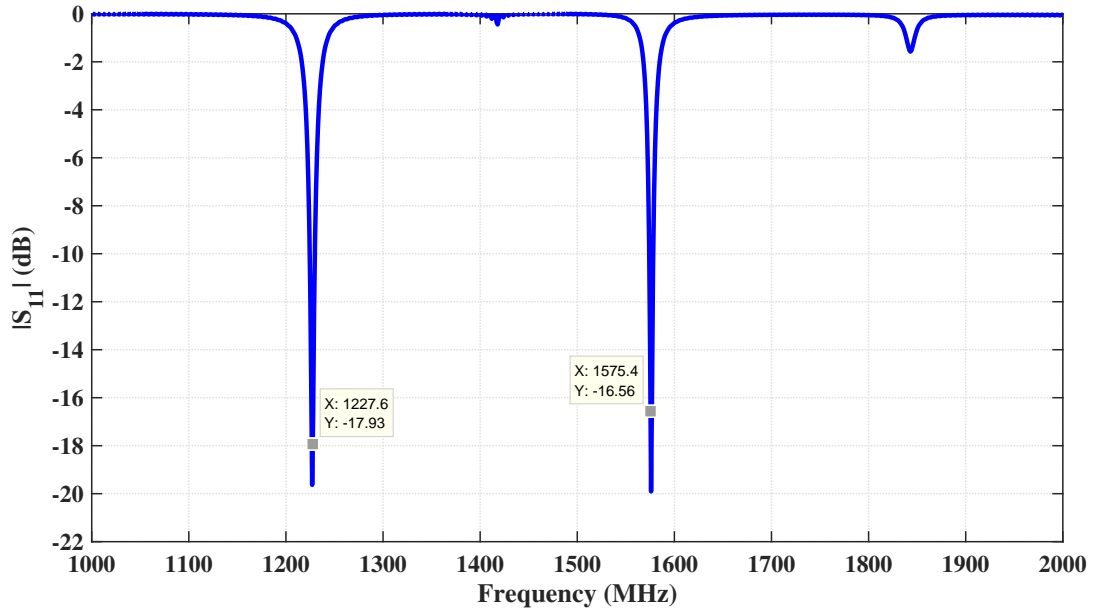


Figure 3.15:  $S_{11}$  of LP L1/L2 dualband capacitively loaded patch.

Table 3.7: Final Parameters of the Capacitively Loaded L1-L2 GPS Dualband Four-Edge Slotted Patch Antenna

Parameter	Value	Description
Eps	2.2	Dielectric constant of the substrate
Cap	0.3 pF	Capacitance of the loaded capacitors
MarEdge	0.35 mm	Difference between the horizontal and vertical edges
MarSlot	0.1 mm	Difference between the horizontal and vertical slots
Ant	120 mm	Simulated antenna border length
h	1.575 mm	Height of the substrate
L	75.89 mm	Length of the patch
W	76.24 mm	Width of the patch
L_slot_1	67.2 mm	Length of the horizontal slots
L_slot_2	67.3 mm	Length of the vertical slots
SlotOffset	1 mm	Distance between patch edge and slot edge
Ws	1 mm	Width of the edge slots
Xf	7.5 mm	Feed distance along the x-axis
Yf	7.5 mm	Feed distance along the y-axis

tained  $S_{11}$  and axial ratio bandwidths are acceptable for civilian L1 and L2 band GPS applications.

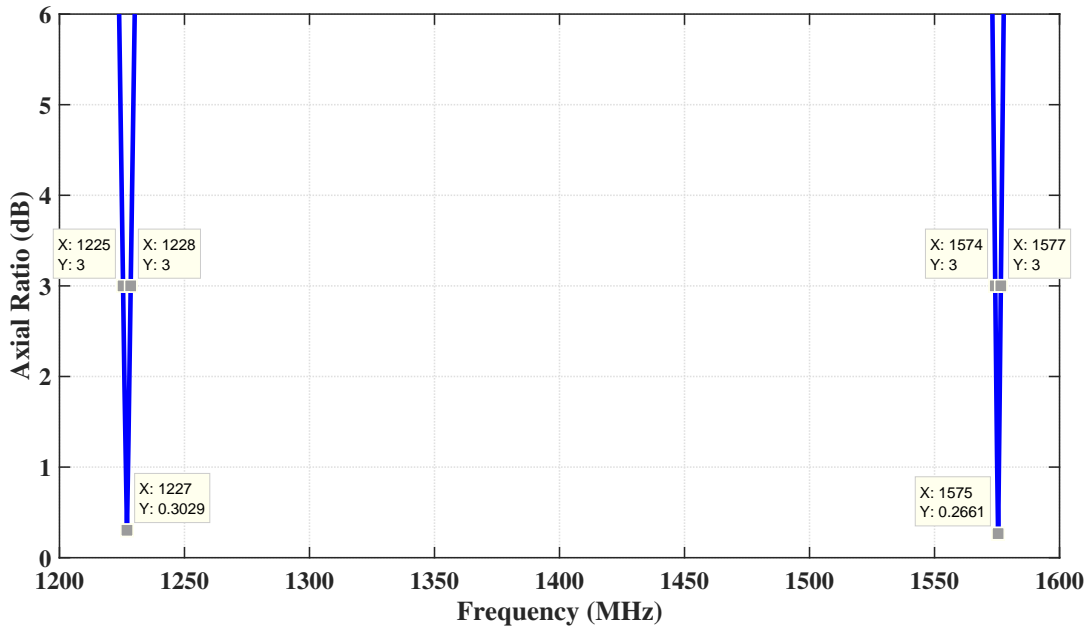


Figure 3.16: Axial ratio of the capacitively loaded CP L1/L2 dualband four-edge slotted patch antenna for GPS applications.

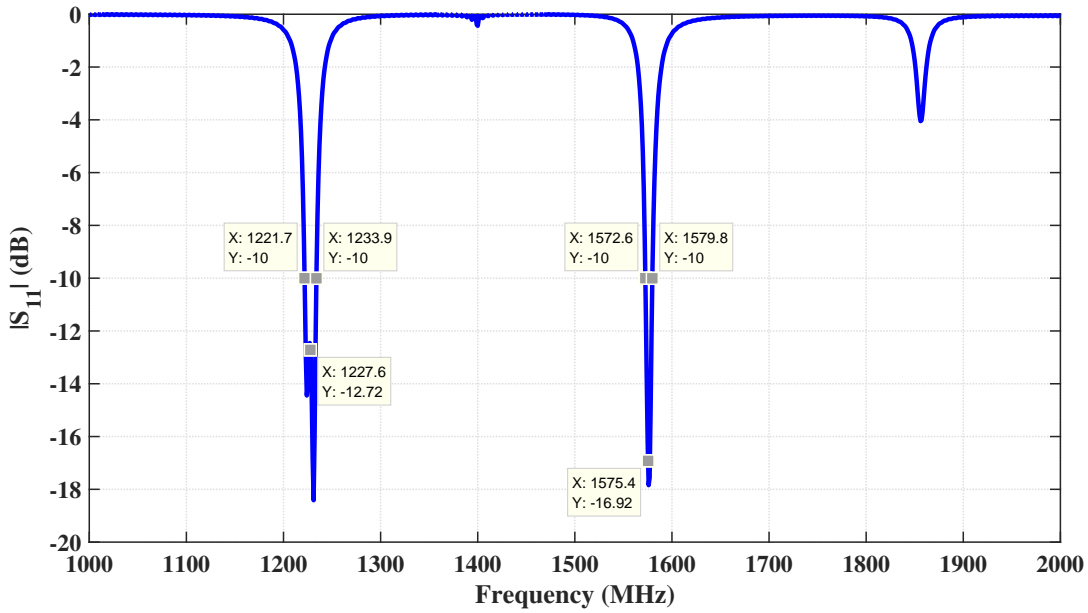


Figure 3.17:  $S_{11}$  of the capacitively loaded CP L1/L2 dualband four-edge slotted patch antenna for GPS applications.

Radiation patterns at L2 and L1 GPS bands are given in Figure 3.18 and Figure 3.19, respectively. As seen in figures, the directivities of 7.23 dBi and 7.6 dBi are achieved at L2 and L1 GPS bands, respectively. 3dB beamwidths of 84.7° and 84.3° are ob-

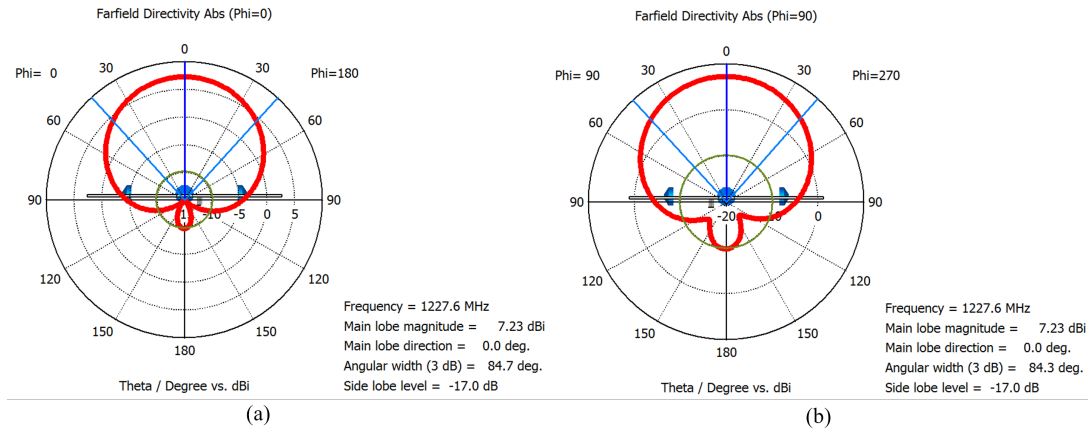


Figure 3.18: Radiation patterns of the capacitively loaded CP L1/L2 dualband four-edge slotted patch antenna at 1227.6 MHz,  
 (a) Azimuth Pattern ( $\phi = 0^\circ$ ), (b) Elevation Pattern ( $\phi = 90^\circ$ ).

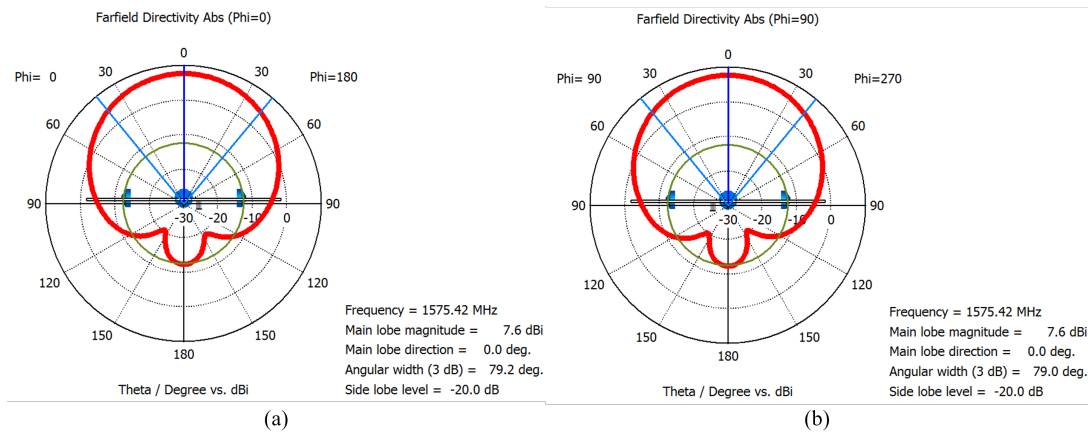


Figure 3.19: Radiation patterns of the capacitively loaded CP L1/L2 dualband four-edge slotted patch antenna at 1575.42 MHz,  
 (a) Azimuth Pattern ( $\phi = 0^\circ$ ), (b) Elevation Pattern ( $\phi = 90^\circ$ ).

tained at L2 GPS band on azimuth ( $\phi = 0^\circ$ ) and elevation ( $\phi = 90^\circ$ ) planes, respectively. 3-dB beamwidths of  $79.2^\circ$  and  $79^\circ$  are obtained at L1 GPS band on azimuth and elevation planes, respectively.

In the following section, a novel patch geometry is proposed to decrease the frequency ratio without loading capacitively the slots to get L1/L2 dualband GPS antenna.



### 3.4.1 Design and Simulations

As mentioned in early sections, slots close to edges control the resonance frequency of higher mode in dualband operations. The length of the slots should be increased as far as possible in the limits of the patch to decrease the higher resonance frequency. Because, the longer current paths result in lower resonance frequency. However, there is limited physical space on the patch to increase the length of slots. Therefore, a zigzag slot section is inserted to the center of each slots to increase the length of current path as shown in Figure 3.21.

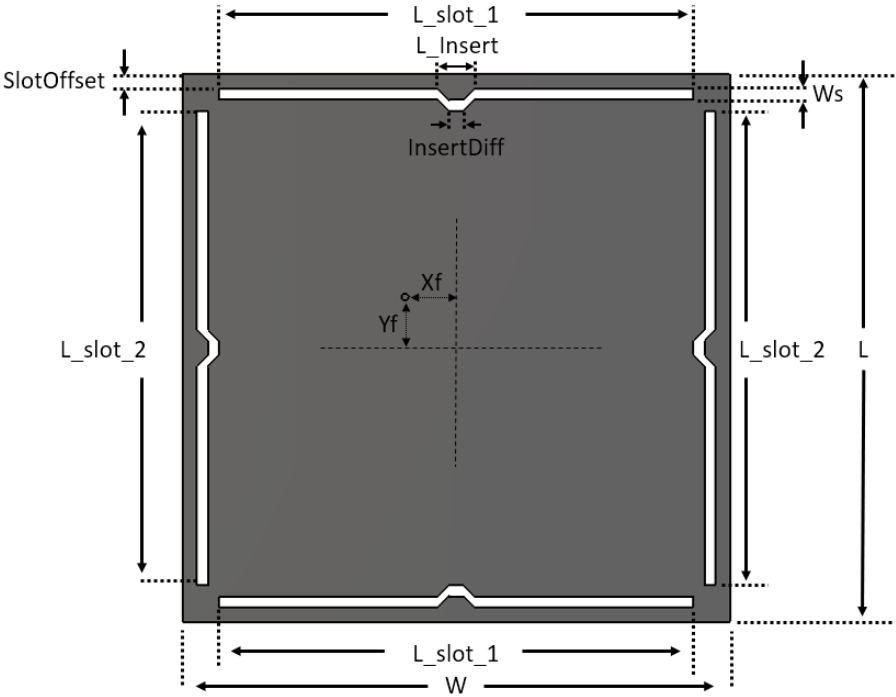


Figure 3.21: Geometry of zigzag slot section inserted four-edge slotted patch.

Simulations are performed to see the effects of the inserted zigzag slot on the patch. Rogers RT5880 type substrate is used in simulations. Initial simulation parameters are listed in Table 3.8. Four-edge slotted patch is compared with the addition of zigzag slots in simulation. As seen in Figure 3.22, the resonance frequency of the higher band decreases and therefore, the frequency ratio decreases from 1.41 to 1.38.

After observing the decreases in the frequency ratio with inserted zigzag slots on the patch, the length of the inserted slots are increased to see the effect of the inserted

Table 3.8: Initial parameters of zigzag slot section inserted patch simulations.

Parameter	Value (mm)	Description
Ant	120	Simulated antenna border length
h	1.575	Height of the substrate
L	75	Length of the patch
W	75	Width of the patch
L_slot_1	65	Length of the horizontal slots
L_slot_2	65	Length of the vertical slots
SlotOffset	1	Distance between patch edge and slot edge
Ws	1	Width of the edge slots
L_Insert	5	Length of the inserted zigzag slot section
InsertDiff	3	Inner side length of the inserted zigzag slots
Xf	7	Feed distance along the x-axis
Yf	7	Feed distance along the y-axis

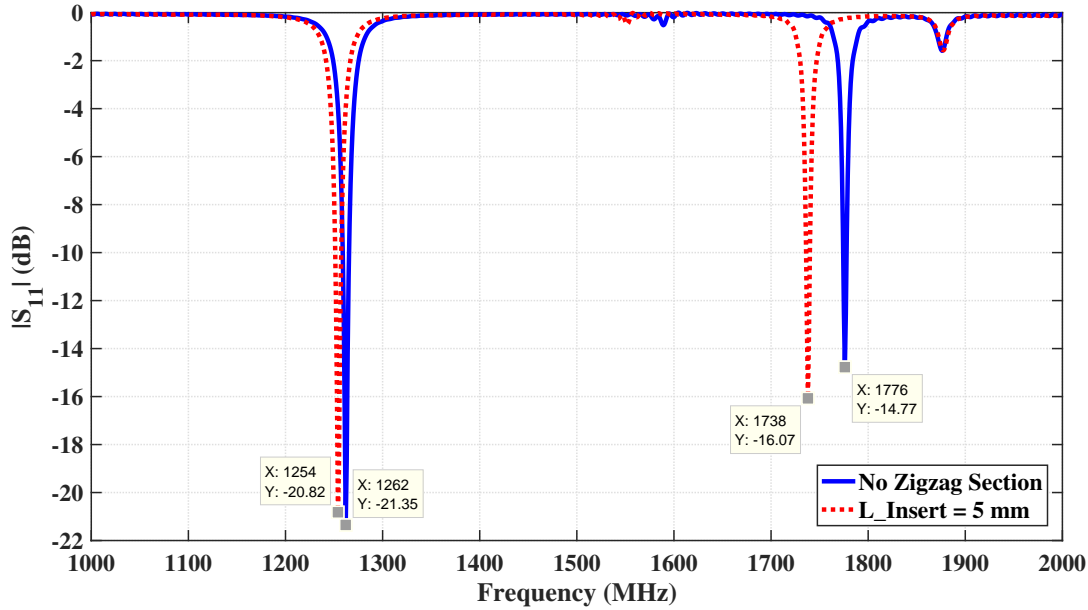


Figure 3.22:  $S_{11}$  of the comparison simulations on the effects of zigzag slot usage.

slots. The length of the inserted zigzag slot is increased from 5 mm to 35 mm and  $S_{11}$  graph is given in Figure 3.23. The resonance frequencies and the frequency ratio are listed in Table 3.9. As seen in Table 3.9, frequency ratio decreases until a certain length, then increases. Therefore, the lengths of zigzag slots increased from 15 mm to 25 mm in simulations. In order to see the results clearly,  $S_{11}$  graphs of lower

and higher bands are given in Figure 3.24 and Figure 3.25, respectively. Resonance frequencies and frequency ratios are listed in Table 3.10.

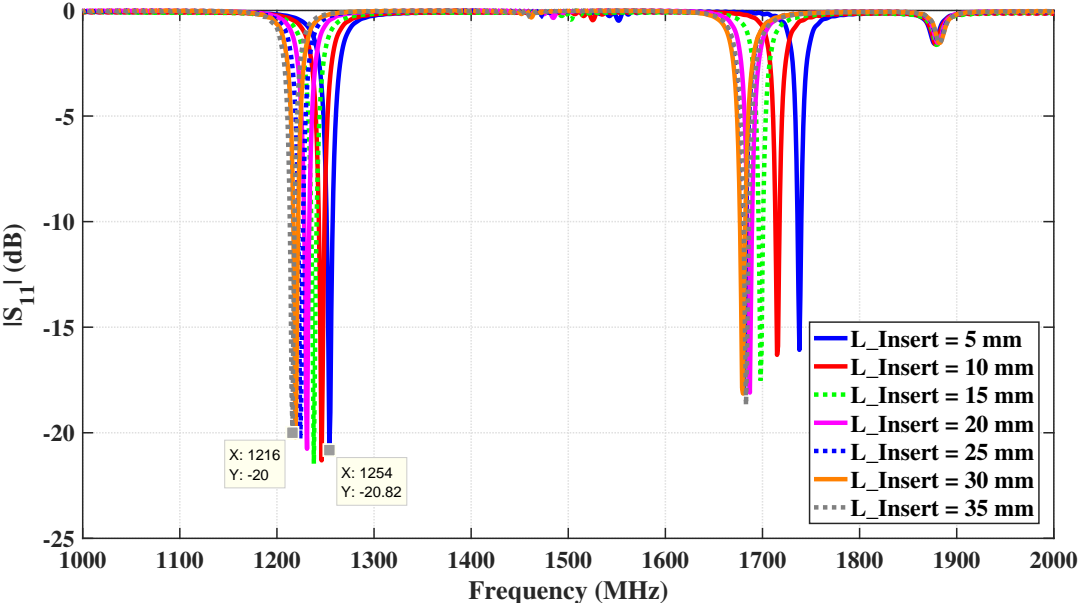


Figure 3.23:  $S_{11}$  of different length of inserted zigzag slot usage.

Table 3.9: Effects of the lengths of inserted zigzag slots between 5 mm and 35 mm.

Inserted Slot Length (mm)	Lower Resonance Frequency (MHz)	Higher Resonance Frequency (MHz)	Frequency Ratio
5	1254	1738	1.38596
10	1246	1715	1.37640
15	1238	1698	1.37157
20	1231	1687	1.37043
25	1224	1681	1.37337
30	1219	1680	1.37818
35	1216	1683	1.38405

The lowest frequency ratio is achieved with the inserted zigzag slot length of 20 mm as seen in Table 3.10. The frequency ratio increases when the inserted zigzag slot length is longer than 20 mm. This information is used in design process as a constraint for inserted slots.

As mentioned before, the required frequency ratio between L1 and L2 GPS bands is 1.283. However, the frequency ratio could not be decreased to required frequency ratio with increasing the inserted zigzag slot length and therefore, the number of the

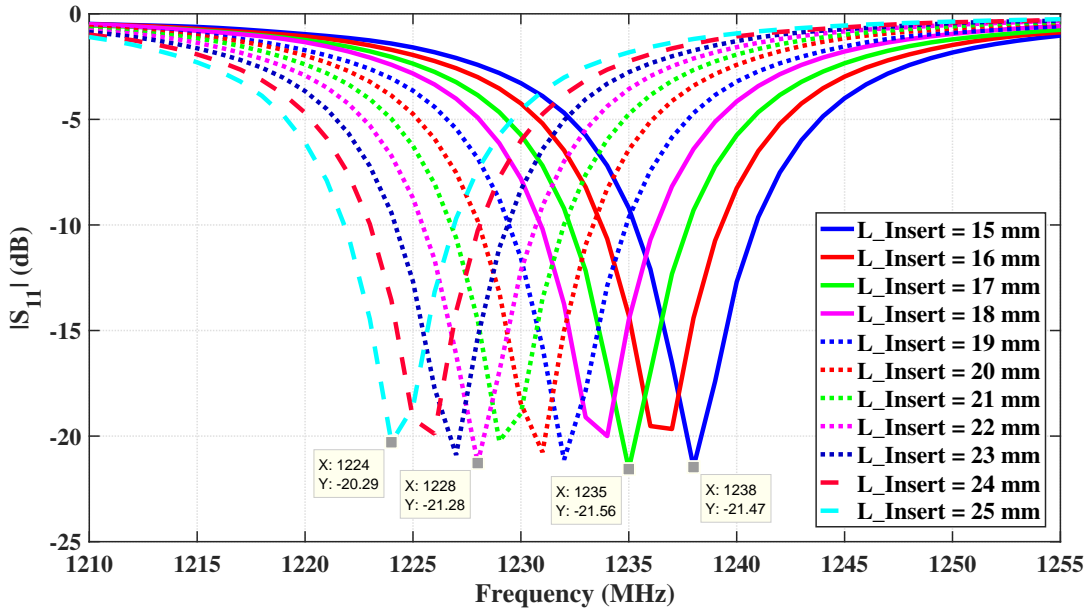


Figure 3.24:  $S_{11}$  graph of different length of inserted zigzag slot usage at lower band.

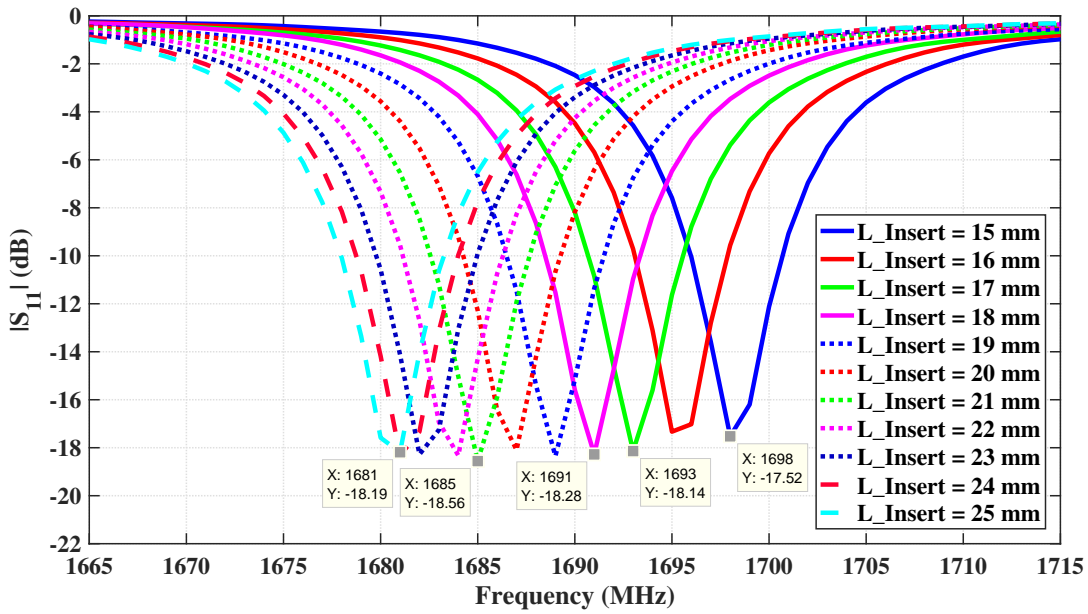


Figure 3.25:  $S_{11}$  graph of different length of inserted zigzag slot usage at higher band.

inserted zigzag slots are increased as shown in Figure 3.26. Each section is called as "sector" in this patch geometry.

Multiple zigzag slot sectors are constructed with additional parameter of "SlotTrans"

Table 3.10: Effects of the lengths of inserted zigzag slots between 15 mm and 25 mm.

Inserted Slot Length (mm)	Lower Resonance Frequency (MHz)	Higher Resonance Frequency (MHz)	Frequency Ratio
15	1238	1698	1.37157
16	1235	1693	1.37085
17	1233.6	1691	1.37078
18	1232.1	1689	1.37083
19	1230.7	1687	1.37076
20	1229.5	1685	1.37048
21	1228	1683.7	1.37109
22	1227	1682.6	1.37131
23	1225.5	1681.5	1.37209
24	1224.5	1680.5	1.37240
25	1224	1681	1.37337

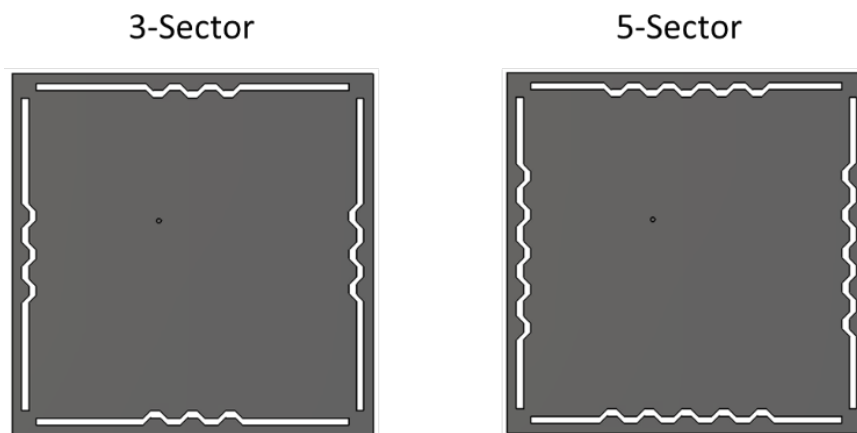


Figure 3.26: The representation of multiple zigzag slot sectors.

as shown in Figure 3.27. The zigzag slot is transferred to both side as the parameter of SlotTrans. The number of sectors is increased from 3 to 11 in simulations with the given parameters in Table 3.11 and  $S_{11}$  graphs are given in Figure 3.28. Resonance frequencies and frequency ratio are listed in Table 3.12.

As seen in Table 3.12, the lowest frequency ratio (1.3183) is obtained with the number of 7 zigzag slot sectors. This frequency ratio does not satisfy the requirement of 1.283, therefore slot offset (SlotOffset) and slot width ( $W_s$ ) parameters are decreased to get

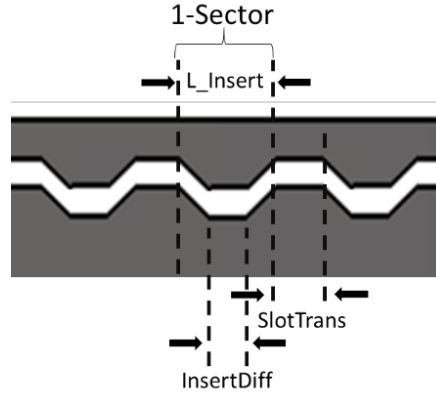


Figure 3.27: The construction of multiple zigzag slots.

Table 3.11: Parameters of multiple zigzag slot inserted simulations.

Parameter	Value	Description
Ant	120 mm	Simulated antenna border length
h	1.575 mm	Height of the substrate
L	75 mm	Length of the patch
W	75 mm	Width of the patch
L_slot_1	70 mm	Length of the horizontal slots
L_slot_2	70 mm	Length of the vertical slots
SlotOffset	1 mm	Distance between patch edge and slot edge
SlotTrans	1 mm	Length of transferred slots sector
InsertDiff	1 mm	Length of inner side of zigzag slots
Ws	1 mm	Width of the edge slots
L_Insert	3 mm	Length of the inserted zigzag slot section
Xf	7 mm	Feed distance along the x-axis
Yf	7 mm	Feed distance along the y-axis

smaller frequency ratio. SlotOffset and Ws parameters are changed between 0.7 mm and 1 mm in simulations. The simulation results are listed in Table 3.13 with respect to bandwidth and frequency ratio at both lower and higher bands. It is seen that there are four different combinations of parameter which satisfy the frequency ratio requirement. The highest bandwidth is obtained within these combinations when the slot offset is equal to 0.8 mm and slot width is equal to 0.8 mm as shown in Figure 3.29. The rest of the design is performed with these parameter values.

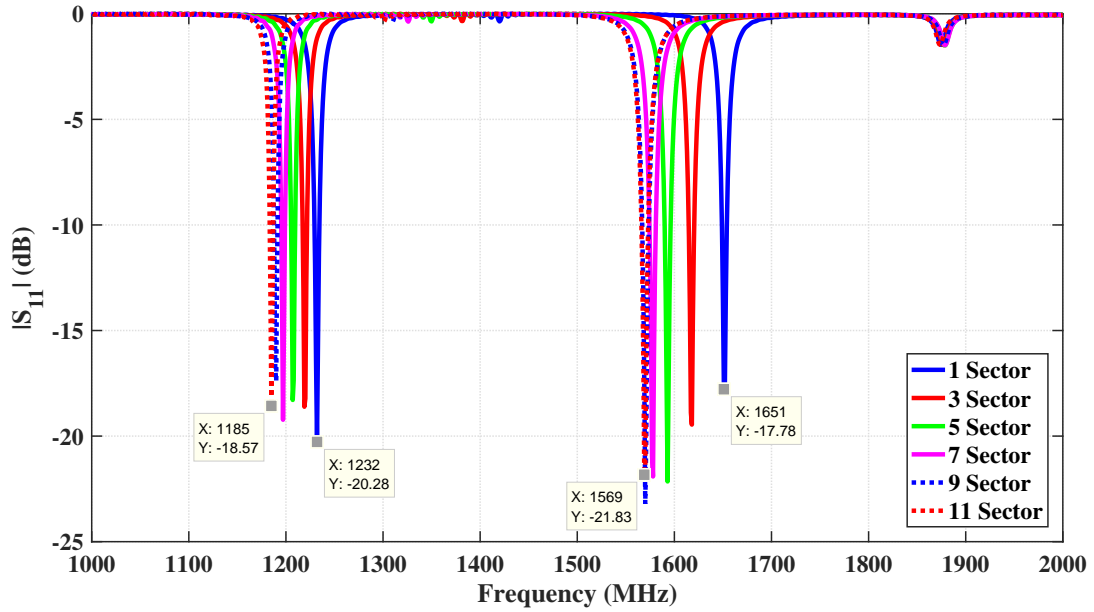


Figure 3.28:  $S_{11}$  Result of Comparison Simulation of Zigzag Slots Number

Table 3.12: Effects of the multiple zigzag slot insertion.

Number of Sectors	Lower Resonance Frequency (MHz)	Higher Resonance Frequency (MHz)	Frequency Ratio
1	1232	1651	1.3401
3	1219	1618	1.3273
5	1207	1593	1.3198
7	1197	1578	1.3183
9	1190	1570	1.3193
11	1185	1569	1.3241

According to  $S_{11}$  graph in Figure 3.29, the lower band resonates at 1229 MHz and higher band resonates at 1576 MHz. Fine tuning is applied on slot length and patch length to achieve L1 and L2 GPS bands. The antenna is tuned to resonate at L1 and L2 GPS bands when the patch length is equal to 75.1 mm and the slot length is equal to 70.05 mm as given in Figure 3.30.

The antenna radiates linearly polarized at L1 and L2 GPS bands. Because, the patch geometry is square, slot lengths are equal and the feed position is on the diagonal direction of the patch. Each orthogonal modes ( $TM_{10}$  and  $TM_{01}$ ) resonate at same frequency, but there is not any phase difference between orthogonal modes.

Table 3.13: Change of bandwidth and frequency ratio when the parameters of slot offset and slot width are changed.

Slot Offset (mm)	Slot Width (mm)	Bandwidth of Lower Band (%)	Bandwidth of Higher Band (%)	Frequency Ratio
1.0	0.7	0.3412	0.3522	1.2916
1.0	0.8	0.3434	0.3783	1.2968
1.0	0.9	0.3539	0.4106	1.3029
1.0	1.0	0.3716	0.4282	1.3113
0.9	0.7	0.3404	0.3468	1.2853
0.9	0.8	0.3507	0.3669	1.2896
0.9	0.9	0.3610	0.4053	1.2953
0.9	1.0	0.3633	0.4378	1.3014
0.8	0.7	0.3395	0.3350	1.2789
0.8	0.8	0.3499	0.3617	1.2823
0.8	0.9	0.3679	0.3933	1.2891
0.8	1.0	0.3621	0.4201	1.2930
0.7	0.7	0.3387	0.3169	1.2726
0.7	0.8	0.3653	0.3499	1.2760
0.7	0.9	0.3837	0.3886	1.2834
0.7	1.0	0.3777	0.4148	1.2865

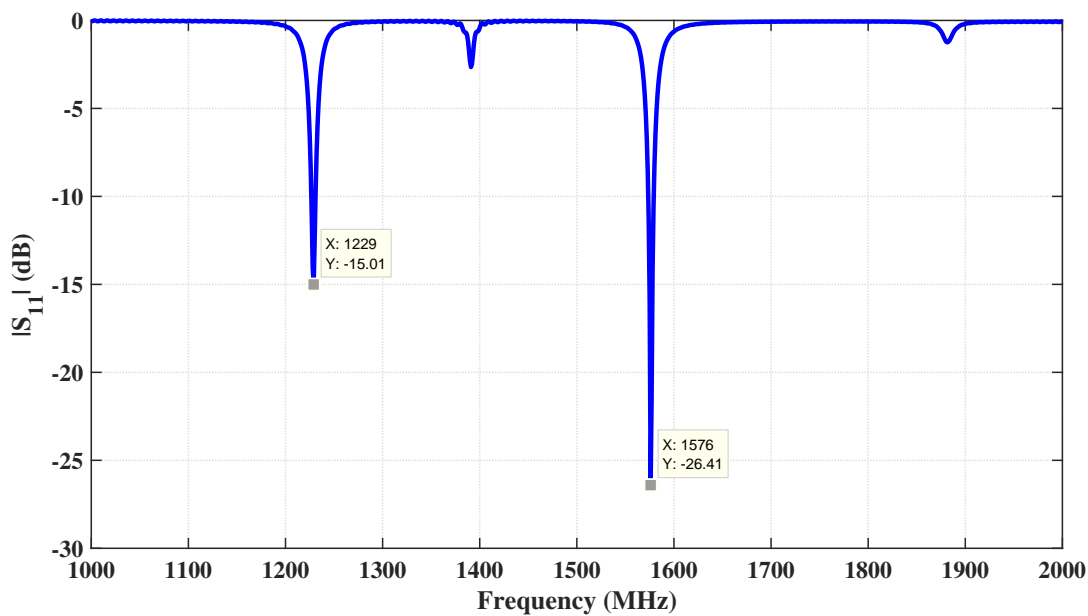


Figure 3.29:  $S_{11}$  graph when SlotOffset = 0.8 mm and  $W_s = 0.8$  mm.

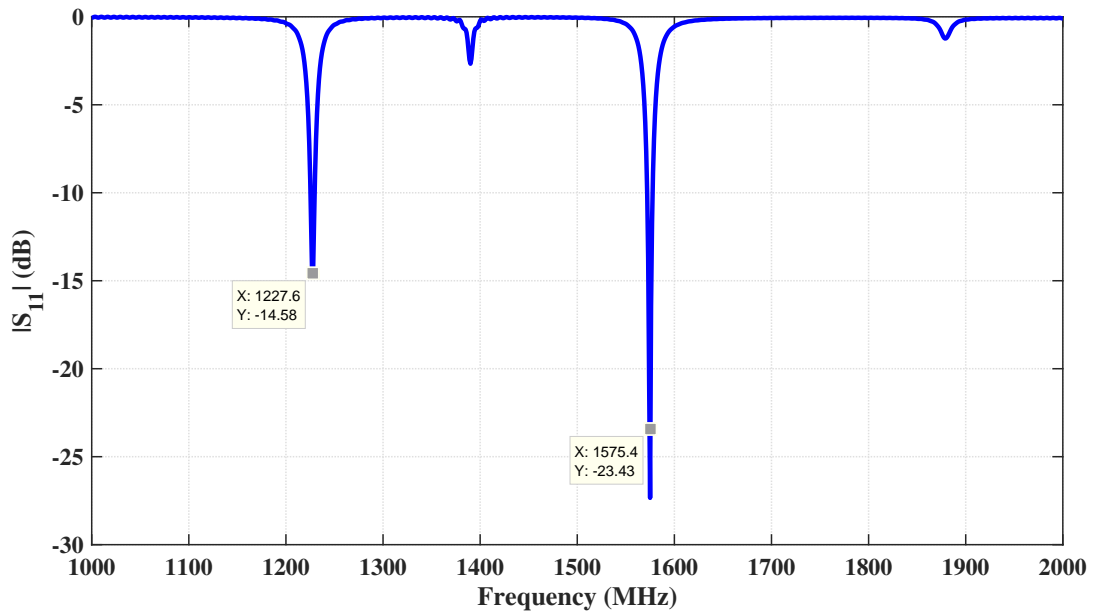


Figure 3.30:  $S_{11}$  graph of L1/L2 dualband linearly polarized zigzag slotted antenna.

Patch geometry is perturbed to get RHCP with the described method in Section 3.2. Margin parameters are assigned to control the perturbation process on slot lengths (MarSlot) and edge lengths (MarEdge) as defined in the design on *Four-Edge Slotted Patch* geometry. Additional margin parameter is also defined to get the best impedance matching at each frequency bands for feed position as "MarFeed".

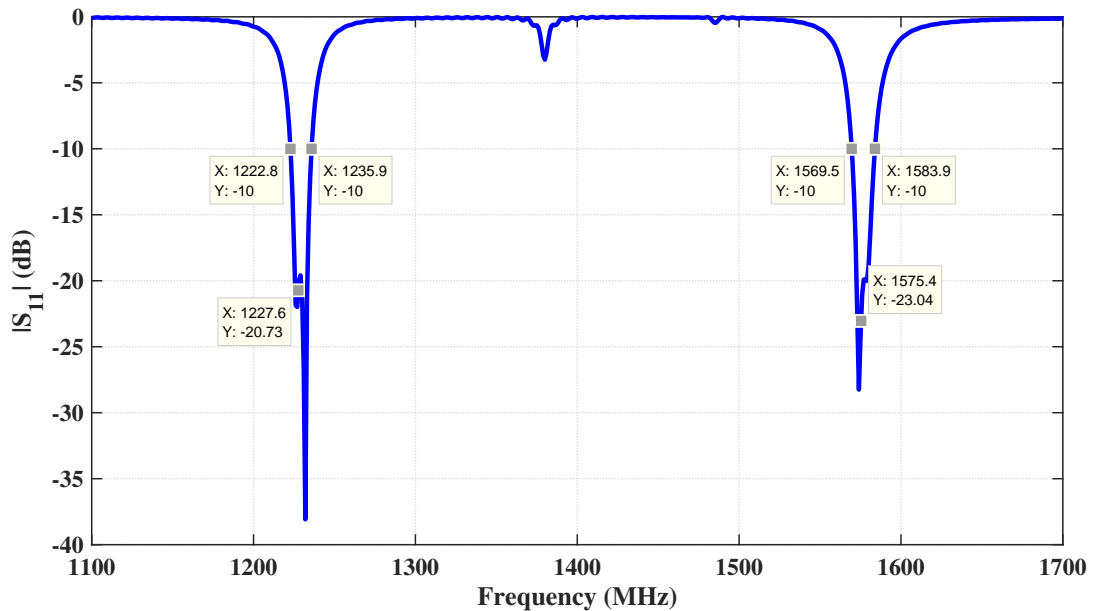


Figure 3.31:  $S_{11}$  of L1/L2 dualband RHCP zigzag slotted GPS antenna.

RHCP L1/L2 dualband GPS antenna is achieved with the given parameters in Table 3.14. The  $S_{11}$  and axial ratio graphs are given in Figure 3.31 and Figure 3.32, respectively. According to simulation results, impedance bandwidth of 13.1 MHz (1.07%) and 3-dB axial ratio bandwidth of 3.1 MHz (0.25%) are achieved at L2 GPS band; and impedance bandwidth of 14.4 MHz (0.91%) and 3-dB axial ratio bandwidth of 3.2 MHz (0.2%) are achieved at L1 GPS band. Obtained bandwidths are defined as very narrow, but these values satisfy the civilian GPS applications which operate at L1 and L2 bands.

Table 3.14: Final design parameters of L1/L2 dualband GPS antenna with 7-Sector zigzag slotted patch.

Parameter	Value	Description
Ant	120 mm	Simulated antenna border length
h	1.575 mm	Height of the substrate
L	74.65 mm	Length of the patch
W	74.75 mm	Width of the patch
L_slot_1	70.07 mm	Length of the horizontal slots
L_slot_2	70.7 mm	Length of the vertical slots
MarFeed	0.7 mm	Margin between feed points
MarEdge	0.1 mm	Margin between edge lengths
MarSlot	0.63 mm	Margin between slot lengths
SlotOffset	0.8 mm	Distance between patch edge and slot edge
SlotTrans	1 mm	Length of transfered slots sector
InsertDiff	1 mm	Length of inner side of zigzag slots
Ws	0.8 mm	Width of the edge slots
L_Insert	3 mm	Length of the inserted zigzag slot section
Xf	11.5 mm	Feed distance along the x-axis
Yf	10.8 mm	Feed distance along the y-axis

The RHCP and LHCP patterns are given in Figure 3.33. The radiation patterns of L2 and L1 bands are given in the first two rows of the table as azimuth plane ( $\phi = 0^\circ$ ) and elevation plane ( $\phi = 90^\circ$ ) patterns, respectively. According to radiation patterns, directivity of 6.86 dB and 7.25 dB are achieved at L2 and L1 bands, respectively. According to RHCP and LHCP patterns, cross polarization of 34.16 dB and 22.07 dB are achieved on both azimuth and elevation planes, respectively.

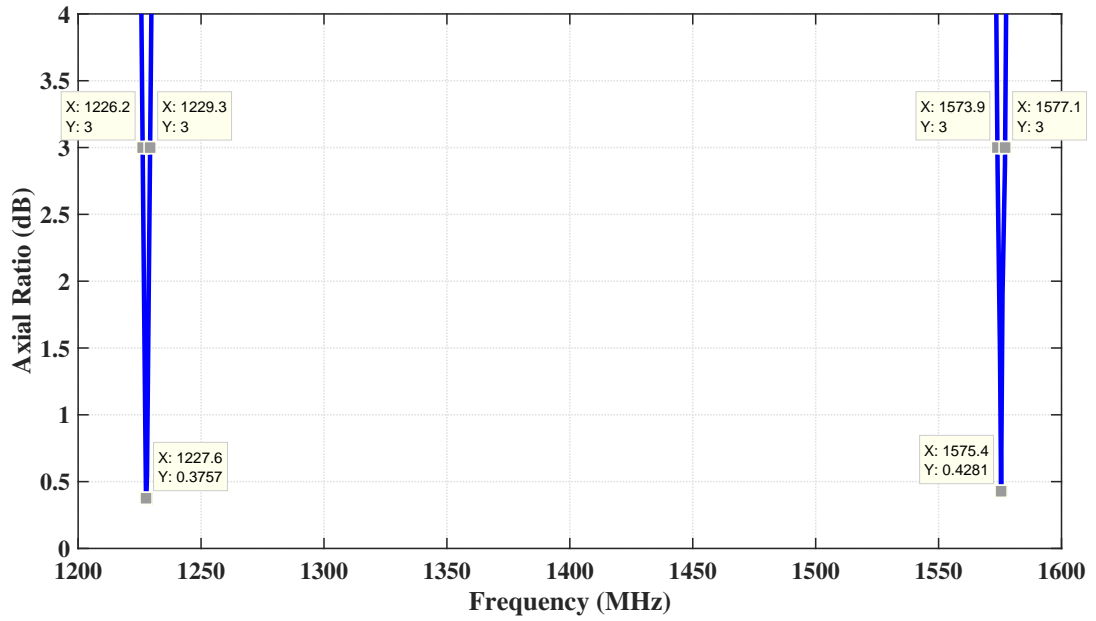


Figure 3.32: Axial Ratio of L1/L2 dualband RHCP zigzag slotted GPS antenna.

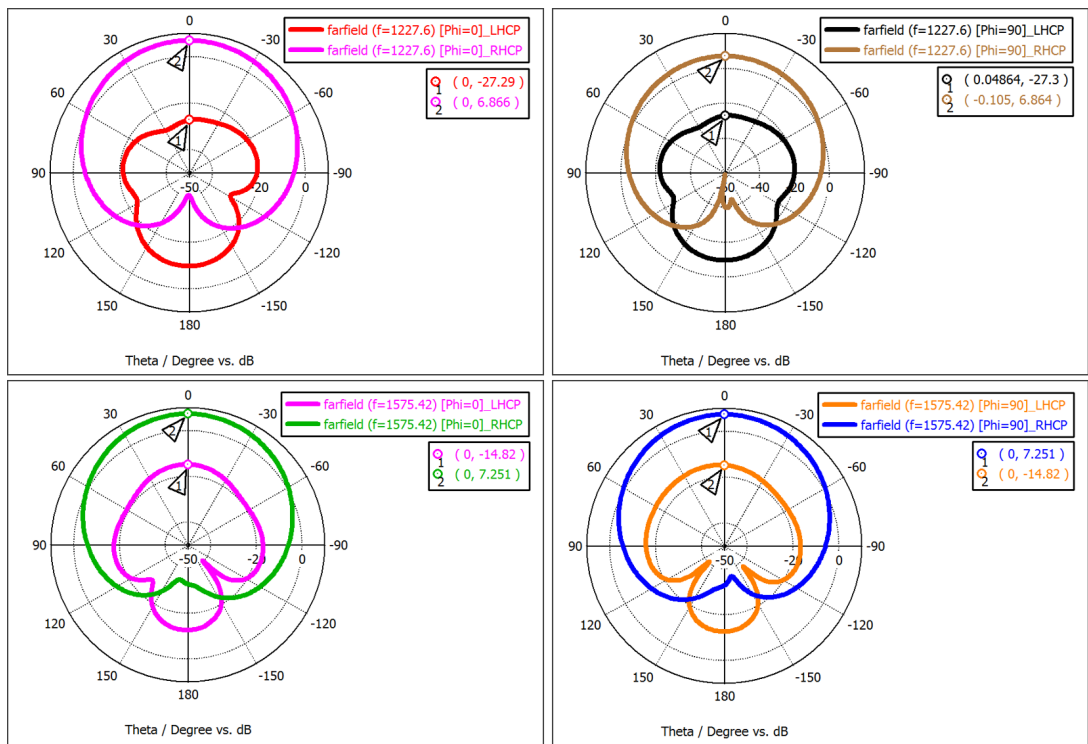


Figure 3.33: RHCP and LHCP radiation patterns of the L1/L2 dualband RHCP zigzag slotted GPS antenna.

### 3.4.2 Fabrication of the Antenna

Designed antenna is fabricated with a circuit board plotter machine (LPKF ProtoMat S103) which is used in PCB prototyping works. This machine performs the board shaping process with milling technique. RF mills and drills are used in prototyping process of the antenna. As mentioned in Section 3.4.1, Rogers RT5880 type substrate with the thickness of 1.575 mm (conductor thickness is 0.035 mm) is used in the fabrication process. Fabrication is performed with the given final design parameters in Table 3.14.

As mentioned in previous sections, slot width and slot offset parameters directly affect the resonance frequencies. In the order of 0.1 mm changes causes to the change of resonance frequencies about 10 MHz in simulations. Therefore, the accurate fabrication of the slots can be required as the most important part of the fabrication process. The thickness of the milling is another important parameter in fabrication with LPKF prototyping machine. Because, if the milling thickness is not adjusted properly the thickness of the substrate decreases with extra milling. This situation also causes to change the resonance frequencies.

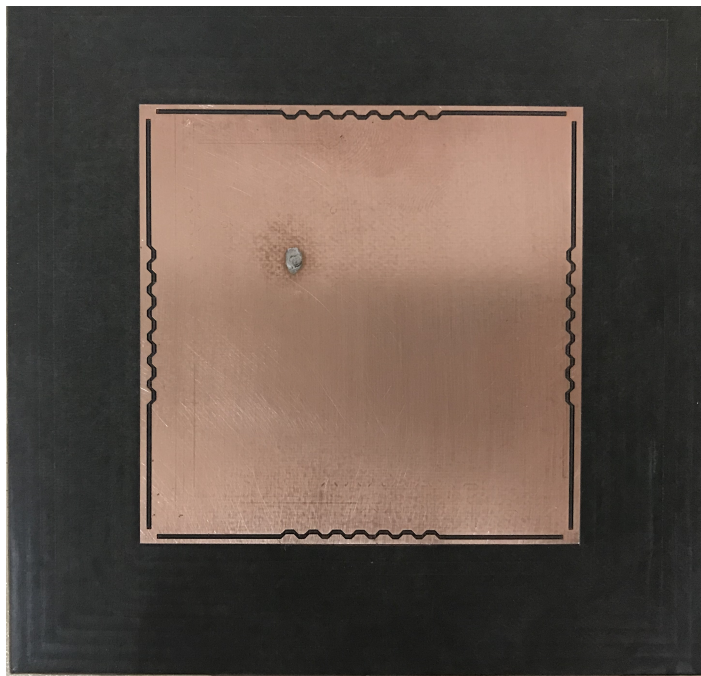


Figure 3.34: Front View of Zigzag Slotted Patch Antenna

Designed antenna is fabricated as shown in Figure 3.34 and coaxial feed is soldered to the patch. Soldering is another important fabrication issue that effects the performance of the antenna with respect to impedance matching. The inner conductor of the coaxial connector should be cut as the same level with the patch conductor and then soldered to patch. The solder should be spread homogeneously over inner conductor and patch.

A panel type coaxial SMA connector is used to feed the antenna. The ground panel of the coaxial connector is soldered to the ground plane of the antenna. The flat surface of the connector should contact to the ground plane of the microstrip antenna as much as possible to achieve a good grounding.

### 3.4.3 Measurement Results of Fabricated Antenna

The s-parameter and radiation pattern measurements are performed to see the performance of the fabricated antenna. The s-parameter measurements are performed with a network analyzer (Keysight PNA-X N52244A). The comparison graph of simulation and measurement is given in Figure 3.35. According to  $S_{11}$  measurements, lower and higher bands resonate at 1238 MHz and 1621 MHz, respectively. It is seen in the measurement result, the lower band is shifted as 11 MHz and the higher band is shifted as 46 MHz when it is compared to simulation result.

The fabrication errors could cause the shift in resonance frequencies. As mentioned in Section 3.4.2, the milling thickness should be adjusted as the thickness of the conductor on the substrate. Otherwise, the thickness of the substrate will decrease. As a result of this fabrication error, the resonance behaviour of the antenna changes.

Simulations are performed to see the effects of extra milling on the substrate. The milling is applied in simulations with a parameter of milling thickness and this parameter is applied as in Figure 3.36. Simulations are performed with different thickness of milling and  $S_{11}$  graph is given in Figure 3.37. As seen in  $S_{11}$  graph, the resonance frequencies increase with the increase of the milling thickness. Therefore, extra milling on the substrate can cause to detune the resonance frequencies of the antenna.

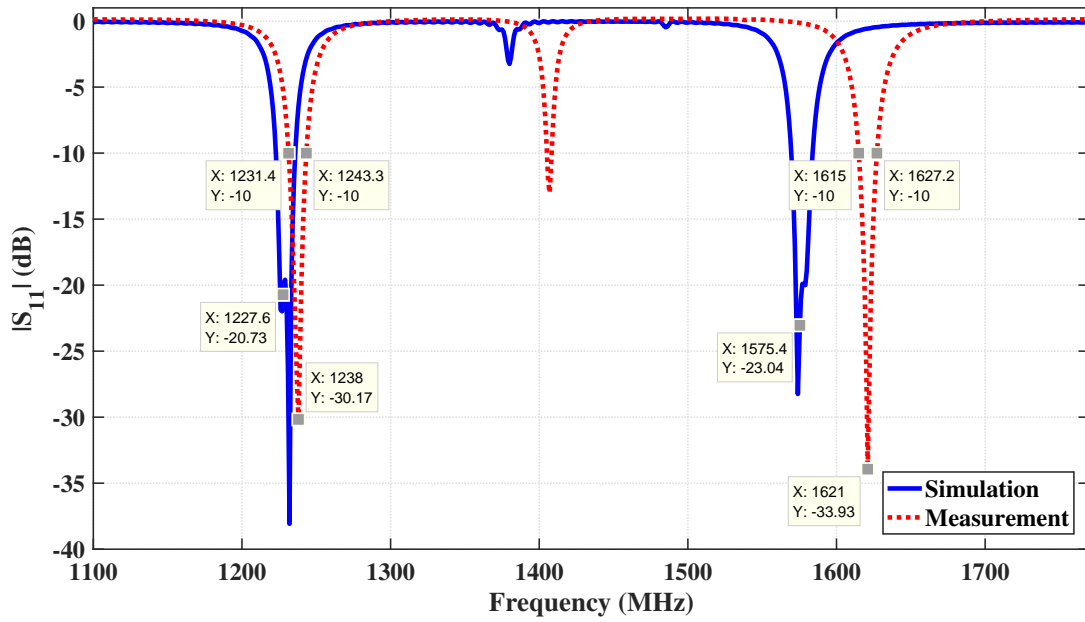


Figure 3.35:  $S_{11}$  comparison graph of simulation and measurement of zigzag slotted antenna.

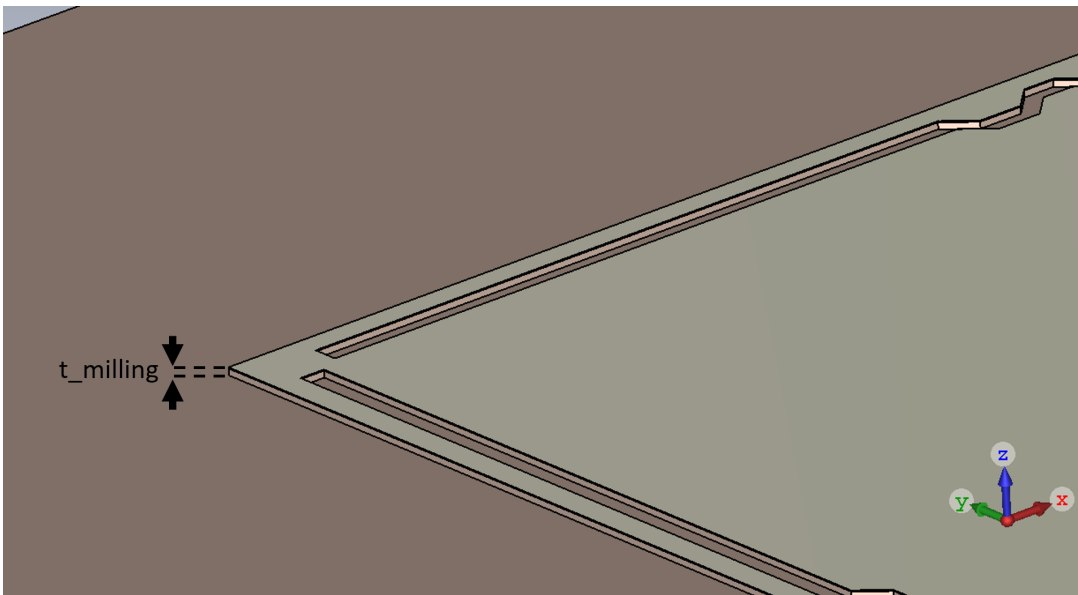


Figure 3.36: Representation of " $t_{milling}$ " parameter in extra milling simulations on zigzag slotted antenna.

Measurements of farfield radiation pattern are performed to see the radiation performance of the fabricated antenna at 1238 MHz and 1621 MHz frequencies that the antenna resonates. The anechoic chamber which is located in the METU - Ayaslı

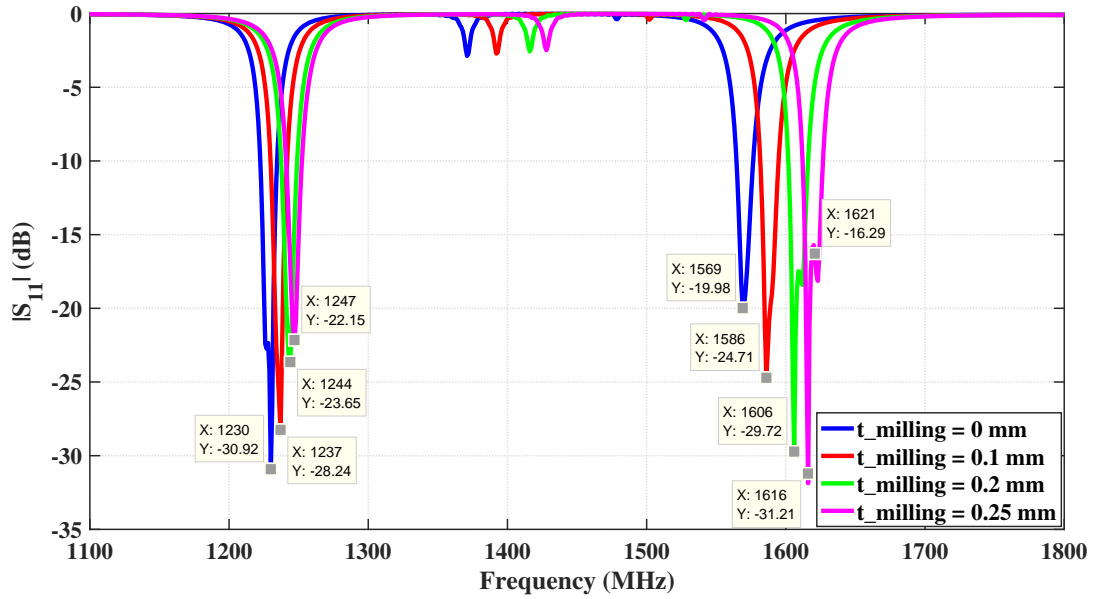


Figure 3.37:  $S_{11}$  graph of extra milling simulations on zigzag slotted antenna.

Research Center is used in measurements of radiation pattern. A picture is shown in Figure 3.38 related to measurements of radiation pattern.

Radiation patterns are measured on azimuth ( $\phi = 0^\circ$ ) and elevation ( $\phi = 90^\circ$ ) planes. The comparisons of simulation and measurement radiation patterns at lower and higher operating bands are given in Figure 3.39 and Figure 3.40, respectively. HPBW of  $95^\circ$  and  $86^\circ$  are measured at 1238 MHz on azimuth and elevation planes, respectively. HPBW of  $104^\circ$  and  $85^\circ$  are measured at 1621 MHz on azimuth and elevation planes, respectively. It is seen in the comparison graphs, the radiation characteristics in the measurements are quiet consistent with simulations.

In order to see the circular polarization performance of the antenna, the axial ratio measurements are performed at each operating band. The antenna is rotated around the roll axis (along the surface normal vector of patch) of the antenna continuously. Measurement results are given in Figure 3.41. In simulations, the axial ratio was obtained smaller than 0.5 dB at both frequency bands. However, the axial ratio of 8 dB is measured in measurements at both frequency bands. The difference between simulation and measurement can be arisen from the fabrication errors.

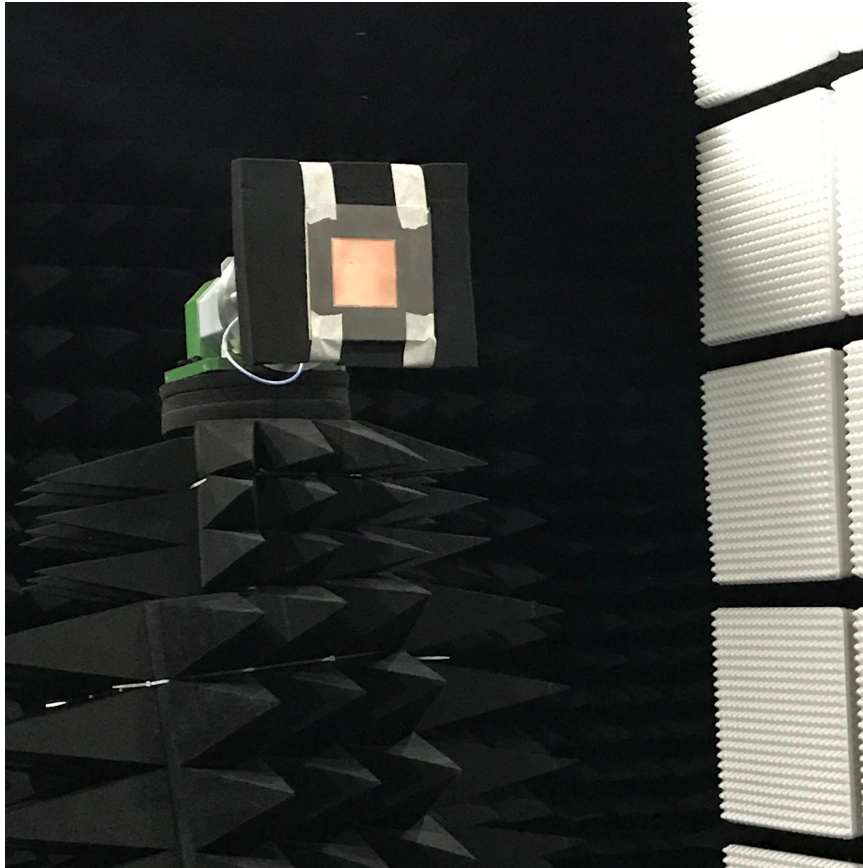


Figure 3.38: Measurements of radiation pattern in the anechoic chamber.

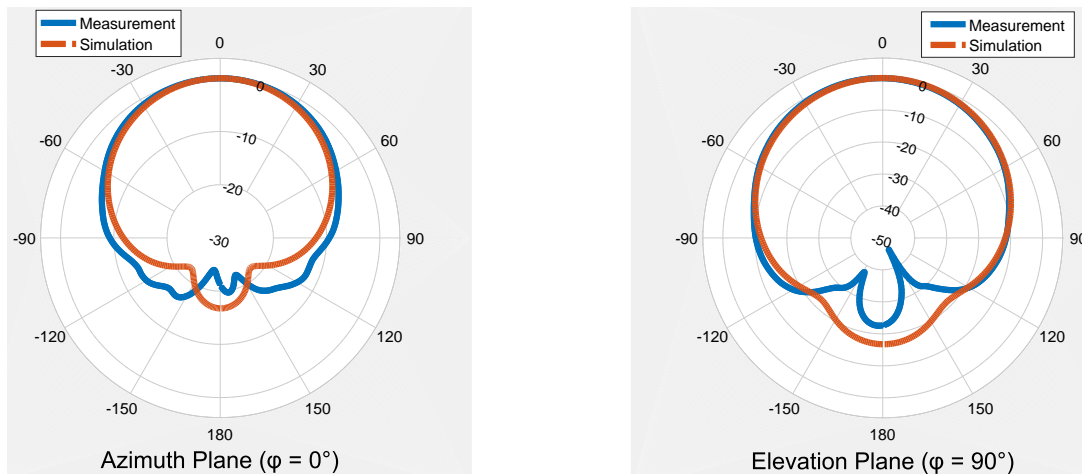


Figure 3.39: Comparison of simulated and measured radiation patterns at lower band.

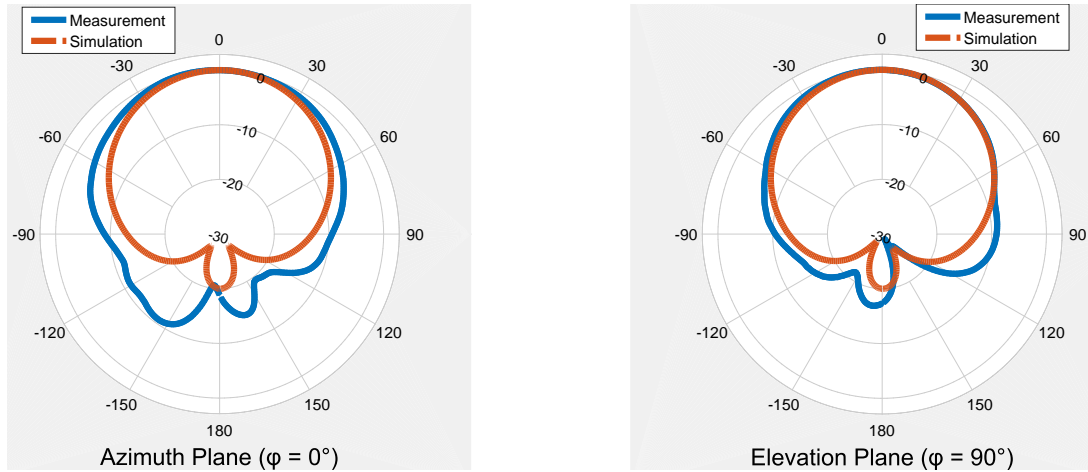


Figure 3.40: Comparison of simulated and measured radiation patterns at higher band.

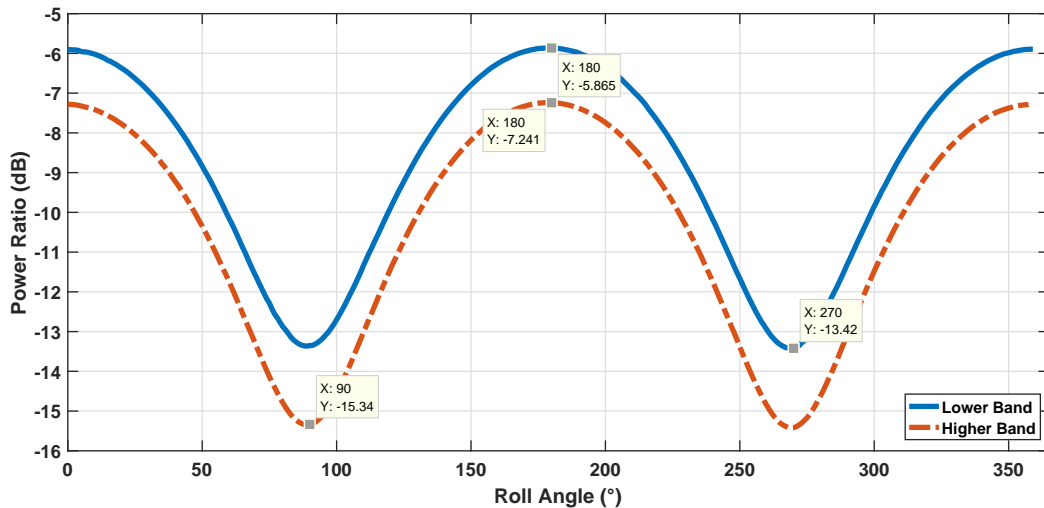


Figure 3.41: Axial ratio measurement results at 1238 MHz and 1621 MHz.

### 3.5 SUMMARY and DISCUSSION

In this chapter, the studies on design, fabrication and measurement of CP L1/L2 dual-band GPS antenna are presented. In this manner, four-edge slotted patch is examined with the study of parametric analysis. Capacitive loading is applied on four-edge slotted patch to decrease the frequency ratio to achieve L1/L2 GPS bands. A single fed CP patch antenna is designed to operate at L1/L2 GPS bands with loading slots capacitively. Then, a novel modified four-edge slotted patch (zigzag four-slotted patch)

geometry is proposed to decrease the frequency ratio without using capacitive loading and it is seen that the proposed novel patch achieves the required frequency ratio between L1 and L2 GPS bands. This antenna structure is fabricated and measured. Simulations and measurement results are compared and outcomes are given.

The operating frequencies of the fabricated antenna are shifted as 11 MHz and 46 MHz at lower and higher bands, respectively. The axial ratio is measured as 8 dB at both operating frequency bands. The frequency ratio of 1.31 is achieved with zigzag four-slotted patch. Extra milling simulations show that the difference between simulation and measurements are mostly originated from the fabrication, i.e. extra milling causes the increase of the resonance frequencies. Addition to extra milling, slight changes on the lengths of slots can cause detune of the antenna.

The measured radiation patterns are consistent with simulated ones. The antenna radiates boresight and HPBW of  $80^\circ$  is obtained at both operating frequency bands.

It is shown that the zigzag slots can be used to decrease the frequency ratio in dual-band operations. The frequency ratio between L1 and L2 bands can be achieved with proper fabrication methods like PCB processing with UV lasers. The axial ratio of 8 dB is obtained at both operating frequency bands with a single coaxial feed. It is thought that, the axial ratio can also be decreased with better fabrication.

## CHAPTER 4

### DESIGN, FABRICATION AND MEASUREMENT OF L1/L2/L5 TRIBAND MICROSTRIP ANTENNAS FOR GPS APPLICATIONS

As mentioned in the Chapter 1, the combinational usage of the GNSS signals improves the accuracy and robustness of all navigation systems. In addition, the usage of multiband GNSS signal also makes the system robust for jamming signals. So, the multiple navigational signal is required in the applications which need accurate position information. Aviation systems (missile, UAV, etc.) are one of these applications. In aviation systems there are limited spaces to place the avionics units and therefore multiple signal usage capability in one unit is a desired function for avionics systems.

L5 GPS band is the third civilian GPS band. This band is applied to meet the requirements for safety of life transportation and high performance applications. L5 GPS signal uses the center frequency of 1176.45 MHz. L5 signal features broader bandwidth ( $\geq 20.46$  MHz) and higher power [2].

In this study, L5 GPS signal is aimed to be added to operating bands of the multiband GPS antenna. Therefore, two kind of microstrip patch antennas are designed to operate at L1/L2/L5 GPS bands with a single coaxial feed. One of these antennas is designed as two-layer stacked antenna and the other one is designed as three-layer stacked antenna. These two antennas are fabricated and measured.

## 4.1 L1/L2/L5 TRIBAND TWO-LAYER STACKED ANTENNA for GPS APPLICATIONS

The studies related to L1/L2/L5 triband GPS antenna is presented in this section. The antenna is designed by stacking two microstrip patches. A novel four-slotted patch is designed to operate at L1 and L2 GPS bands and placed at the top of the stacked antenna structure. A nearly square patch is used to resonate at L5 GPS band and placed as lower patch. The stacked antenna is fed by a single coaxial feed diagonally to achieve circular polarization at all three bands. The coaxial probe is connected to upper patch by soldering and the lower patch is fed by parasitically.

The details of the design, simulations, fabrication and measurement are given in following subsections.

### 4.1.1 Design and Simulations

As seen from the studies in Chapter 3, modified four-slotted patch can operate circularly polarized at L1/L2 GPS bands. Starting from this point, it is decided to use another novel modified four-slotted patch in stacked antenna to operate at L1/L2 GPS bands. The four-slotted patch is fed diagonally to achieve circular polarization. Therefore, a patch geometry which can be fed diagonally to get circular polarization should be chosen to operate at L5 GPS band without using any extra feeds. Nearly square patch geometry is chosen as the lower patch for the third frequency band. Because, it is mentioned that the nearly square patches can be fed diagonally to get circular polarization in Section 1.3.

As mentioned before, the L5 GPS signal has a broader bandwidth as 20.46 MHz. Therefore, it is decided that the substrates which has a lower dielectric constant is used to meet bandwidth requirement for L5 band. In addition to lower dielectric constant, the height of the substrate should be high to meet the bandwidth requirements.

Foam is used as a substrate to provide the lowest dielectric constant ( $\epsilon_r \approx 1$ ). In addition to foam, Rogers RT5880 dielectric substrate with a dielectric constant as  $\epsilon_r = 2.2$  which is procurable in market is used for L5 GPS band. These two substrates are

used in the structure of two-layer stacked antenna. The Rohacell 31 HF<sup>®</sup> ( $\epsilon_r = 1.05$ ) type foam substrate with the thickness of 6 mm is used as the substrate over ground plane. Rogers RT5880 substrates with the thickness of 1.575 mm are used under conducting patches. The side view of the stacked antenna is given in Figure 4.1. The conducting patches are located on the Rogers RT5880 substrates.

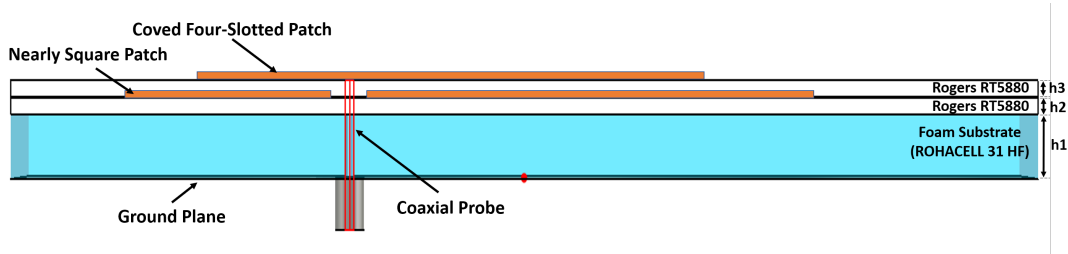


Figure 4.1: Side view of two-layer triband GPS antenna.

Design process begins by the validating that nearly square patch meets the bandwidth requirement of L5 GPS band. The bandwidth requirement is assigned as 5-dB axial ratio bandwidth of 20.46 MHz when the center frequency is equal to 1176.45 MHz.

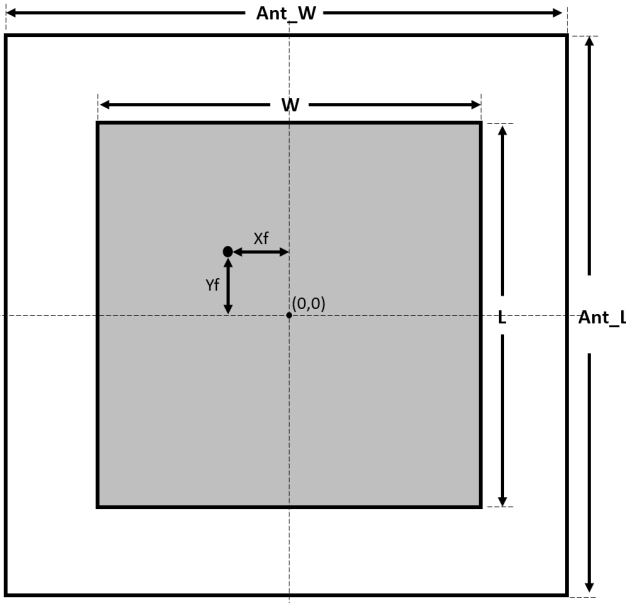


Figure 4.2: Geometry of the nearly square patch.

The nearly square patch antenna is simulated as a single patch antenna in the simulations which are performed to see the axial ratio bandwidth. The patch geometry is shown in Figure 4.1. Foam and Rogers RT5800 substrates are stacked under the

patch. The geometry and initial simulation parameters are given in Figure 4.2 and Table 4.1, respectively.

Table 4.1: Initial parameters of nearly square patch simulations.

Parameter	Value (mm)	Description
Ant_W	150	Width of the Substrate
Ant_L	150	Length of the Substrate
W	127	Width of the patch
L	127	Length of the patch
Xf	10	Feed distance along the x-axis
Yf	10	Feed distance along the y-axis
h1	6	Height of the foam
h2	1.575	Height of the Rogers RT5880 substrate

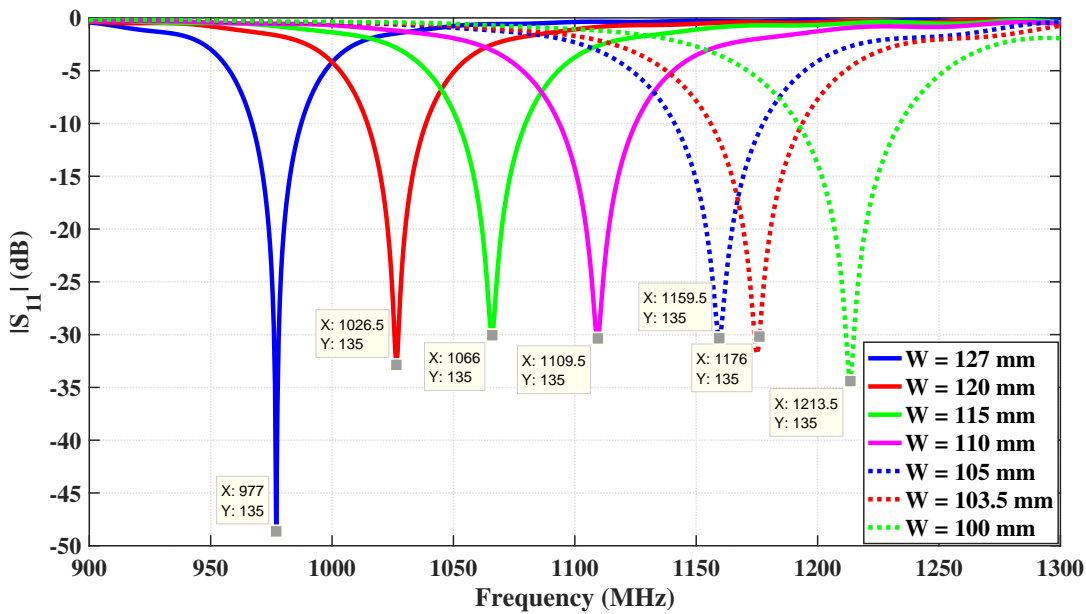


Figure 4.3:  $S_{11}$  results of patch width simulations on square patch.

First, linearly polarized square patch antenna is designed. The initial value of the patch width is chosen as the half of the free space wavelength at 1176.45 MHz ( $\lambda/2 \approx 127$  mm). The patch width parameter is changed to tune the antenna at 1176.45 MHz. According to Figure 4.3, the antenna resonates at 1176 MHz when the patch width is equal to 103.5 mm and the impedance bandwidth of 38 MHz is obtained around the center frequency of 1176 MHz.

Square patch is perturbed slightly to get circular polarization and nearly square patch is obtained with the parameter of "DiffWidth" which represents the difference between patch width and patch length ( $\text{DiffWidth} = W - L$ ). In other words, when the DiffWidth parameter increases, the patch length (L) decreases.

DiffWidth is changed in simulations and axial ratio outputs are given in Figure 4.4. As seen in the axial ratio graph, 1 dB axial ratio is obtained at 1180 MHz with changing the length of the patch slightly.

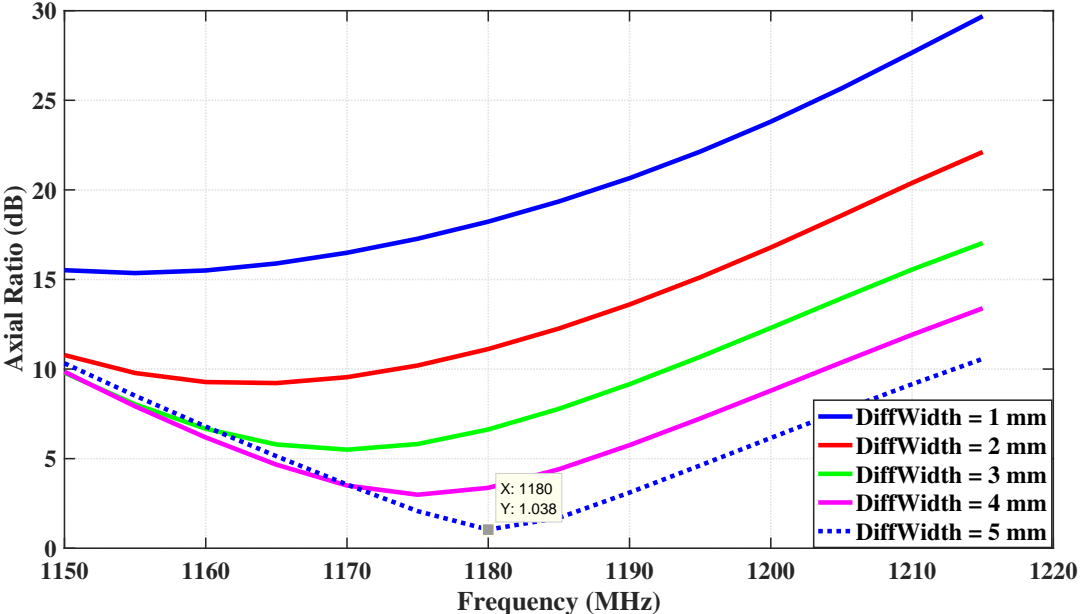


Figure 4.4: Axial ratio graph for the simulations of changing DiffWidth parameter on nearly square patch.

When the DiffWidth parameter is increased, the  $S_{11}$  of the antenna is changed as given in Figure 4.5. The decrease of the patch length causes to increase of the resonance frequency which originates from the fundamental mode ( $\text{TM}_{01}$  mode) along y-axis as shown in Figure 4.5.

The position of the feed is critical in the coaxially fed microstrip antennas to provide required return loss and impedance bandwidth. In addition, the position of the feed also tunes the notch frequency of the axial ratio ("the notch frequency of the axial ratio" is defined as the frequency at which the antenna has the lowest axial ratio in the rest of the study). Therefore, the position of the feed is changed to enhance the

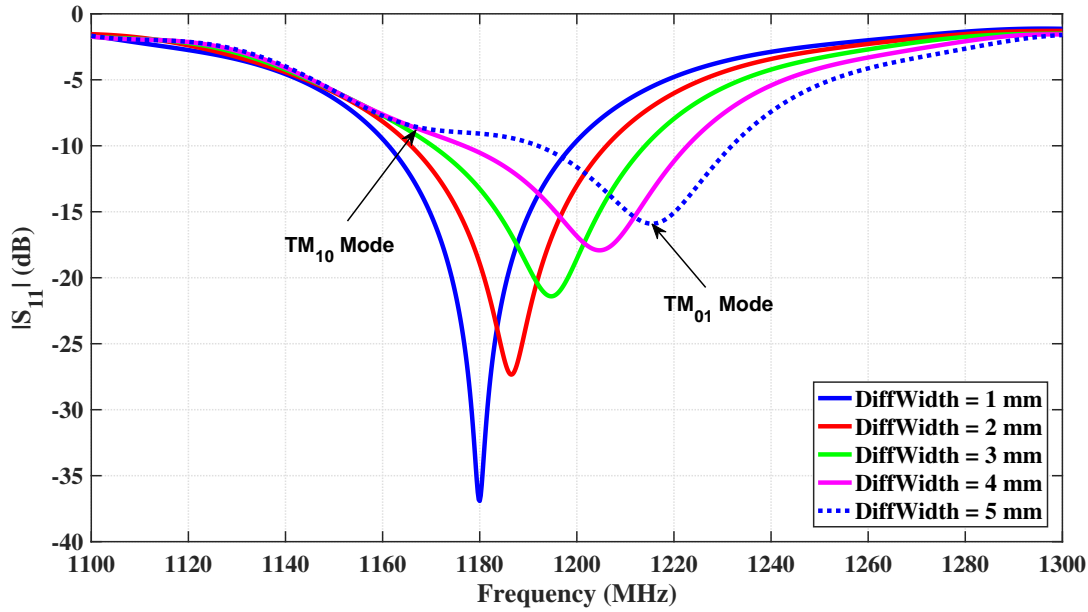


Figure 4.5:  $S_{11}$  graph for the simulations of changing DiffWidth parameter on nearly square patch.

return loss and tune the frequency which has the lowest axial ratio. The position of the feed is changed along x and y axes in simulations. The results of  $S_{11}$  and axial ratio are given in Figure 4.6 and Figure 4.7, respectively. According to results, when the position of the feed is increased along the x axis, the return loss of the  $TM_{10}$  mode is getting better and the notch frequency of the axial ratio tunes to higher frequencies. In addition, in the case of increase in the feed position in y axis, the return loss of the  $TM_{01}$  mode is getting better and the notch frequency of the axial ratio goes to lower frequencies.

In addition to the change of the feed position, the dimensions of the patch also directly effects the resonance frequencies and the notch frequency of the axial ratio. The dimensions of the patch are changed and simulations are performed.  $S_{11}$  and axial ratio results are given in Figure 4.8 and Figure 4.9, respectively. As it is expected, the resonance frequencies of the fundamental modes decrease when the patch dimensions increase, and vice versa. The change on the patch dimensions effects the axial ratio in a similar manner. When the dimensions of the patch increase, the notch frequency of the axial ratio increases.

The nearly square patch is tuned to operate circularly polarized at L5 GPS band with

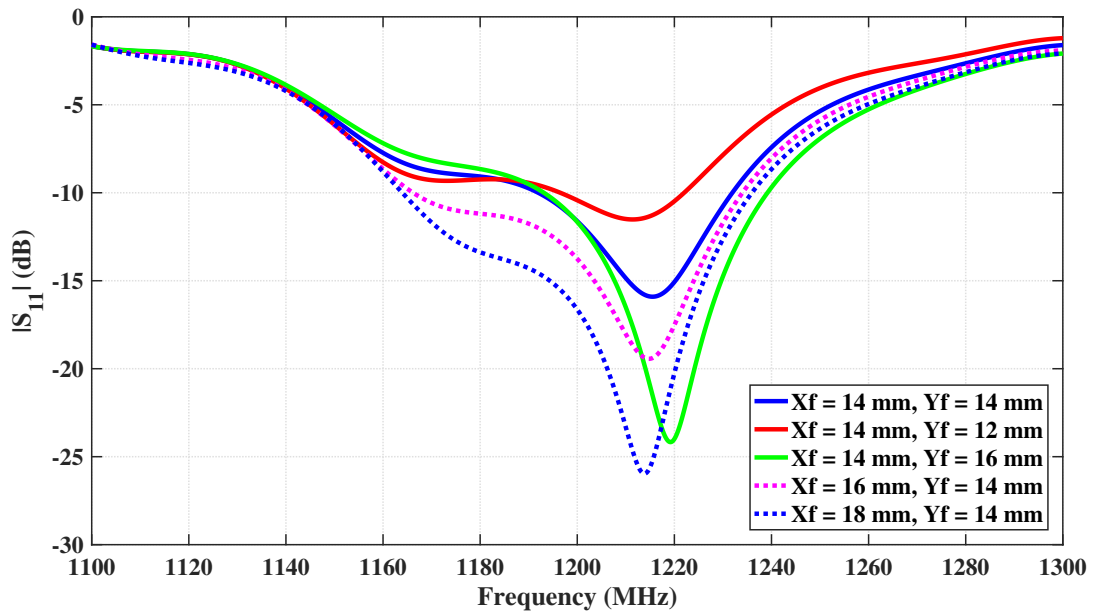


Figure 4.6:  $S_{11}$  results for the simulations of feed position on nearly square patch.

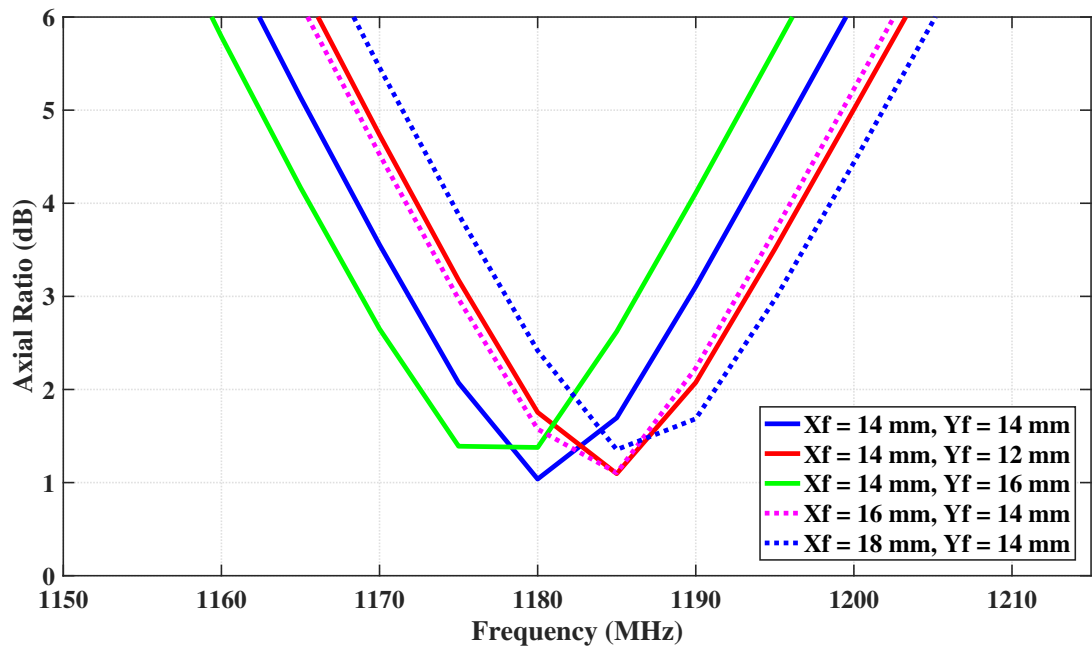


Figure 4.7: Axial ratio results for the simulations of feed position on nearly square patch.

given parameters in Table 4.2.  $S_{11}$  and axial ratio results are given in Figure 4.10 and Figure 4.11, respectively. According to simulation results, impedance bandwidth of 76.4 MHz (6.5%) and 5-dB axial ratio bandwidth of 32.7 MHz (2.8%) is achieved

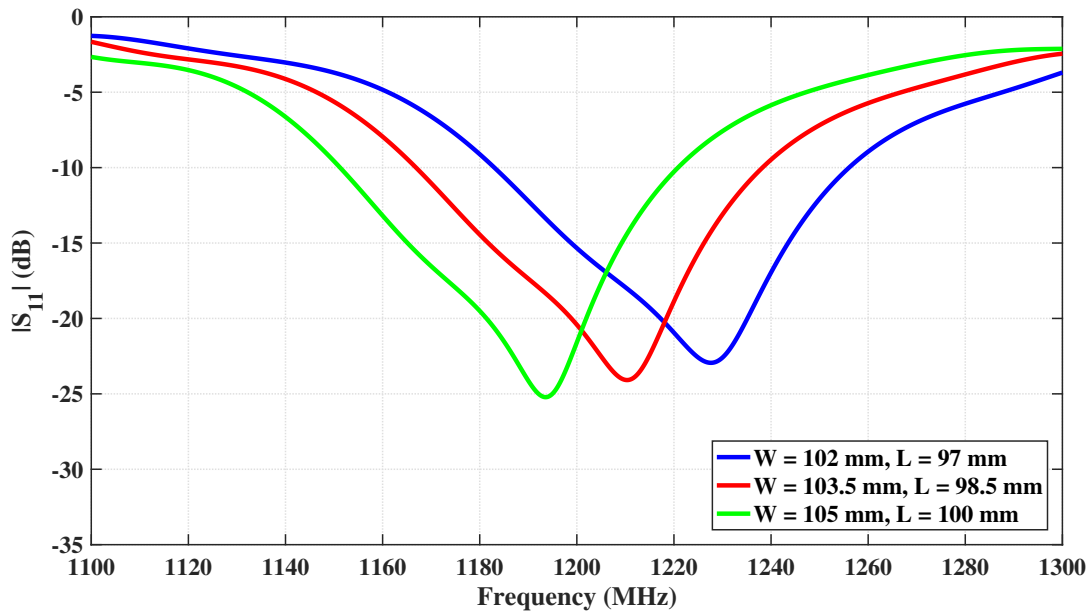


Figure 4.8:  $S_{11}$  results for the simulations of dimensions of nearly square patch.

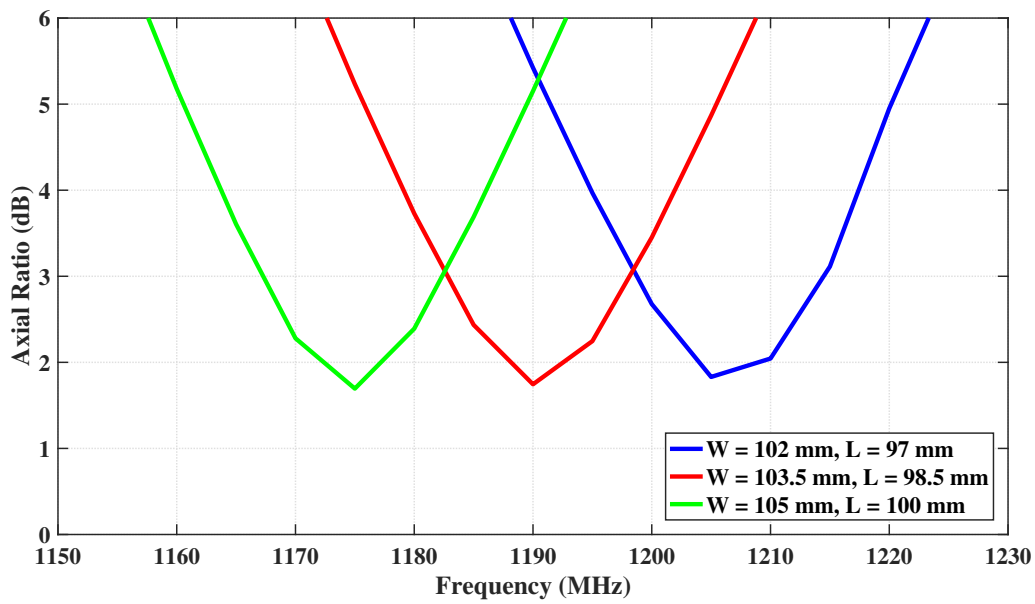


Figure 4.9: Axial ratio results for the simulations of dimensions of nearly square patch.

around 1176.45 MHz. The obtained bandwidths meet the bandwidth requirements of the L5 GPS signal.

After designing nearly square circularly polarized patch antenna at L5 GPS band, a modified four-slotted patch antenna is placed on the nearly square patch as shown in

Table 4.2: Simulation parameters of CP nearly square patch antenna operates at L5 GPS band.

Parameter	Value (mm)	Description
Ant_W	150	Width of the Substrate
Ant_L	150	Length of the Substrate
W	105.5	Width of the patch
L	99.5	Length of the patch
DiffWidth	6	Difference between length and width of the patch
Xf	22	Feed distance along the x-axis
Yf	14	Feed distance along the y-axis
h1	6	Height of the foam
h2	1.575	Height of the Rogers RT5880 substrate

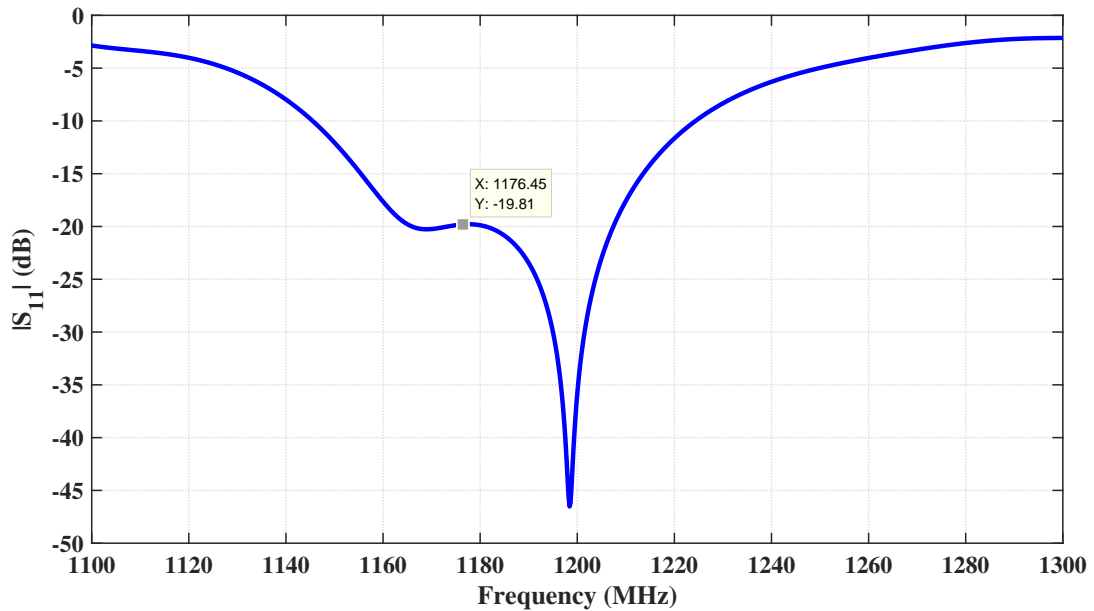


Figure 4.10:  $S_{11}$  results of L5 GPS band CP nearly square patch.

Figure 4.12 to operate L1 and L2 GPS bands as designed in Chapter 3. In this stacked configuration, the modified four-slotted patch is named as the top patch and the nearly square patch is named as bottom patch.

The top patch is fed by the coaxial probe and the bottom patch is fed parasitically from the top patch (i.e. the bottom patch is not contacting to coaxial probe). A feed offset is defined as the parameter of "r\_FeedOffset" on the nearly square patch to avoid conduction between coaxial probe and bottom patch.

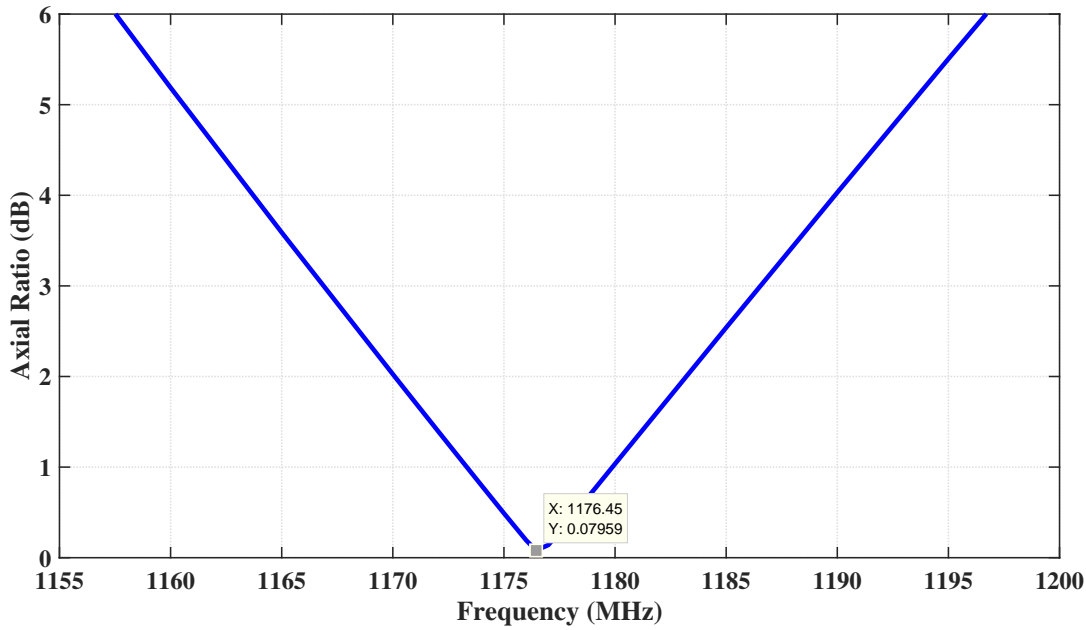


Figure 4.11: Axial ratio results of L5 GPS band CP nearly square patch.

As seen in the Figure 4.12, the top patch is not placed at the center of the antenna structure. The top patch is transferred to the position which provides better impedance matching. The parameters of transfer are defined as "x\_trans" and "y\_trans" as represented in Figure 4.13.

The top patch is placed over the bottom patch as shown in Figure 4.1. The initial simulation parameters which are shown in Figure 4.12 are listed in Table 4.3. The initial parameters related to four-slotted patch are set with the heritage from the previous design which operates at L1 and L2 GPS bands. The  $S_{11}$  result which is obtained with the given initial parameters is given in Figure 4.14. It is seen that the lowest frequency band (the first frequency band) shifted to lower frequencies from the frequency of L5 band. In addition, the second and the third frequency bands resonate at 1233 MHz and 1636 MHz, respectively. The frequency ratio between the second and the third frequencies is 1.33 and it should be decreased to 1.28 to achieve the L1 and L2 GPS bands.

The structure of the four-slotted patch is modified with a new kind of slot geometry to decrease the frequency ratio as performed in Chapter 3. Related patch geometry is named as "coved four-slotted patch", because of the conducting cove at the center of

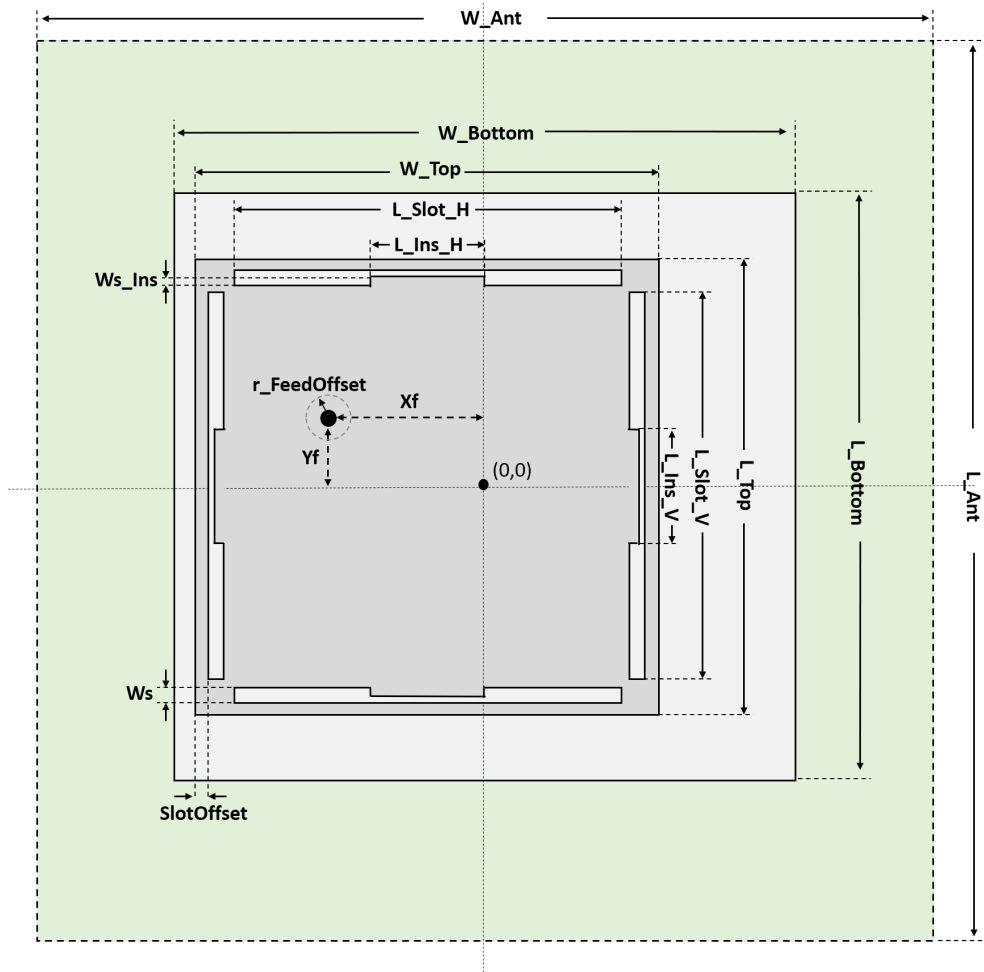


Figure 4.12: Top view of two-layer triband GPS antenna structure.

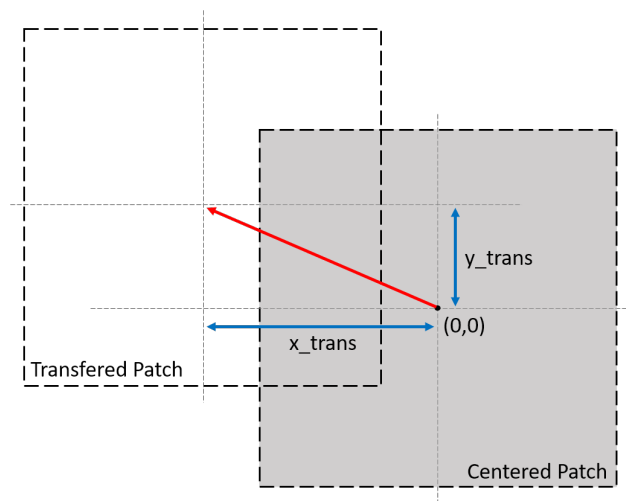


Figure 4.13: Representation of the patch transfer in stacked structures.

Table 4.3: Initial parameters of the two layered stacked antenna structure.

Parameter	Value (mm)	Description
W_Ant	150	Width of the substrate
L_Ant	150	Length of the substrate
W_Bottom	105.5	Width of the bottom patch
L_Bottom	99.5	Length of the bottom patch
W_Top	77.5	Width of the top patch
L_Top	77.5	Length of the top patch
L_Slot_H	72.2	Length of the horizontal slot
L_Slot_V	72.2	Length of the vertical slot
Ws	0.8	Width of the slots
L_Ins_H	0	Length of the inserted conducting cove in horizontal direction
L_Ins_V	0	Length of the inserted conducting cove in horizontal direction
Ws_Ins	0	Width of the inserted conducting cove
SlotOffset	0.8	Distance between edges of patch and slot
r_FeedOffset	1	Distance between bottom patch and coaxial probe
Xf	22	Distance of the coaxial probe along the x-axis
Yf	14	Distance of the coaxial probe along the y-axis
x_trans	5	Transfer distance of the top patch along x-axis
y_trans	5	Transfer distance of the top patch along y-axis

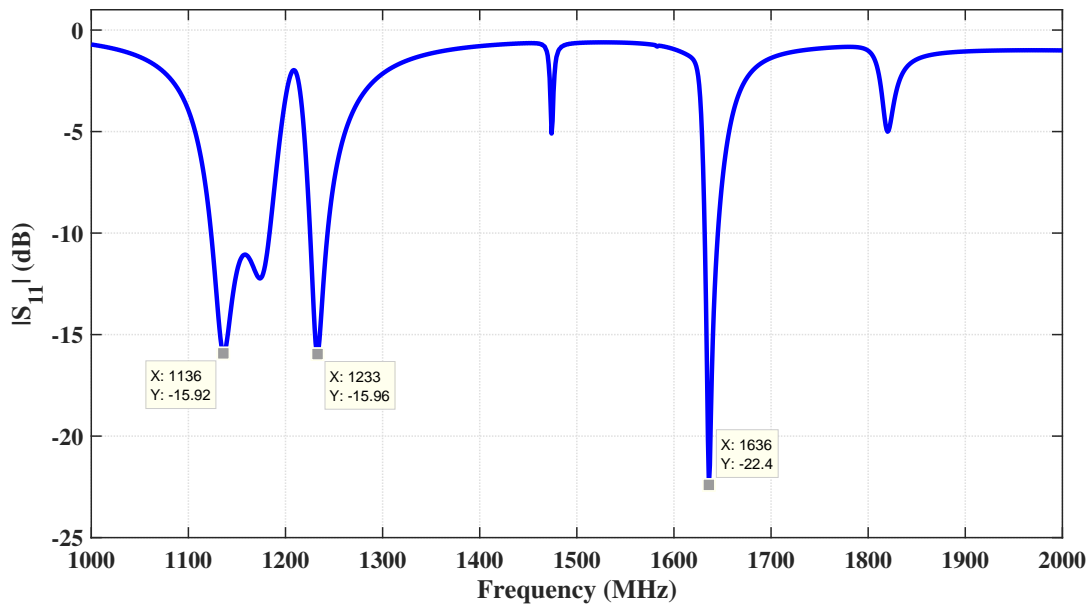


Figure 4.14:  $S_{11}$  results of the initial simulation on the two-layer stacked antenna.

each slots as shown in Figure 4.15.

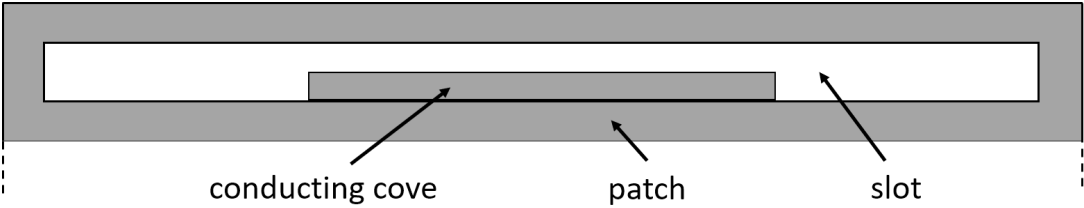


Figure 4.15: Representation of the conducting cove on coved four-slotted patch.

The conducting cove is placed to increase the electrical length of the slot and to increase the capacitive effect of the slot. The simulations are performed to see the effect of the inserted conducting cove to the patch. At first, the width of the cove is analyzed in simulations. The width of the cove ( $W_{s\_Ins}$ ) is increased from 0 to 0.4 mm when the length of the cove is equal to 10 mm. As seen in Figure 4.16, the frequency ratio decreases with the increase of the width of the cove. Because, the capacitive effect of the slot is increased with the addition of the conducting cove on the slots.

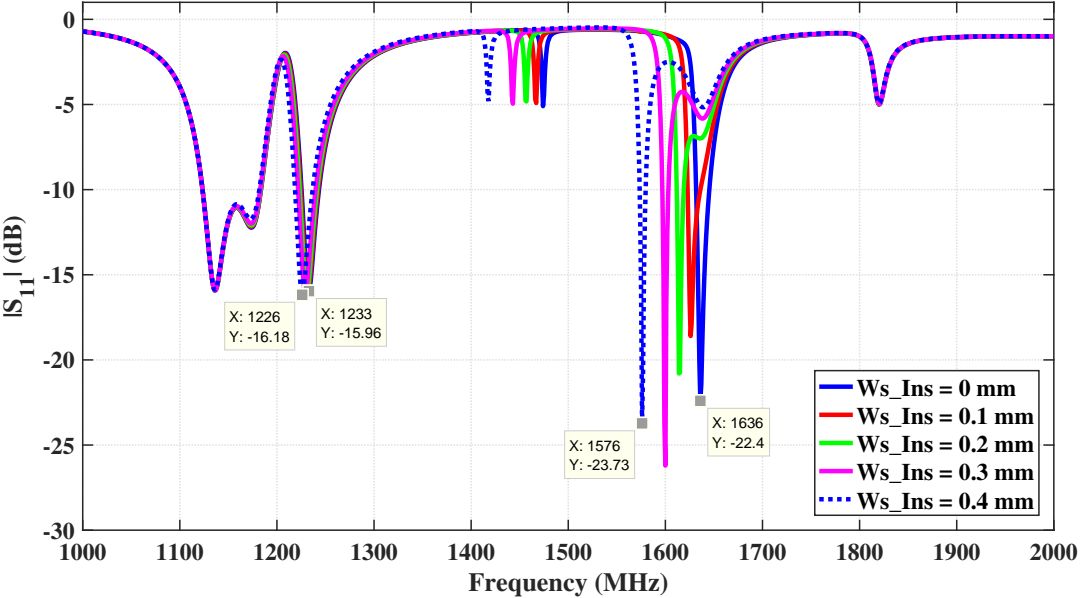


Figure 4.16:  $S_{11}$  of the simulations on the width of the inserted conducting cove.

The increase of the length of the cove also increases the capacitive effect of the slot as shown in the  $S_{11}$  graph in Figure 4.17. The simulations show that the frequency ratio can be decreased to 1.28 by adjusting the length and width of the conducting cove.

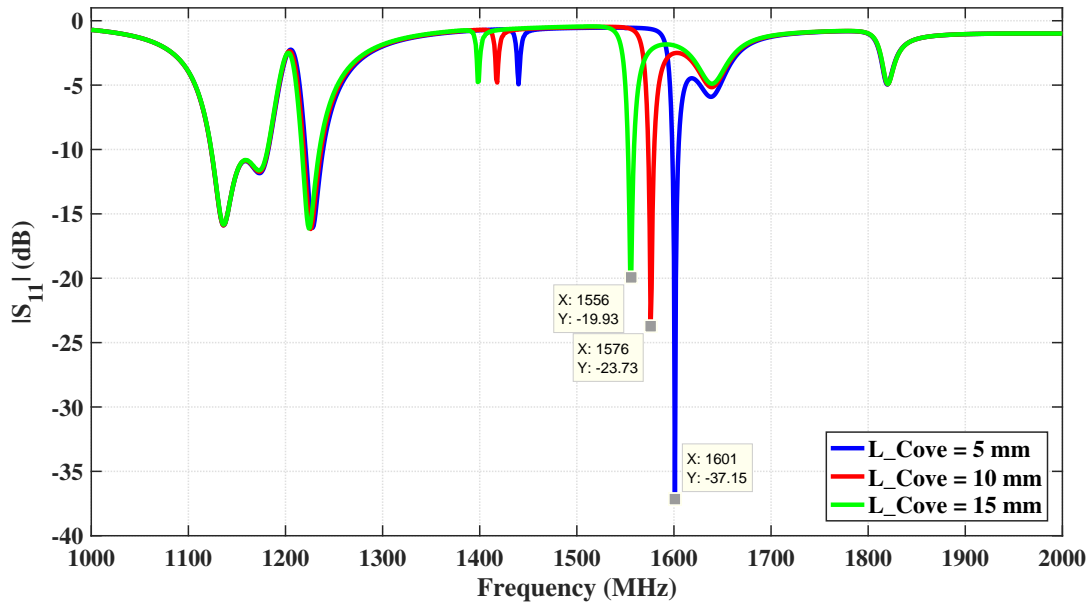


Figure 4.17:  $S_{11}$  of the simulations on the length of the inserted conducting cove.

The tuning process of the antenna is started from the lowest band to highest band. In this manner, the dimensions of the nearly square patch is decreased to increase the resonance frequency to 1176.45 MHz. Then, the notch frequency of the axial ratio is tuned to 1176.45 MHz with adjusting feed position as described before.

The resonance frequencies of the coved four-slotted patch are tuned to L2 and L1 GPS bands with adjusting the dimensions of the conducting coves. At first, the second frequency band is tuned to L2 band and then the third frequency band is tuned to L1 band. Top patch is perturbed to get circular polarization at L1 and L2 GPS bands. The perturbation process is carried out with defining the margin parameters as in the design of zigzag four-slotted patch. The dimensions of the horizontal and the vertical slots are changed to get 90° phase difference between orthogonal modes at operating bands.

The design of the L1/L2/L5 band GPS antenna is achieved with given parameters in Table 4.4. The graphs of the  $S_{11}$  and the axial ratio of the triband antenna are given in Figure 4.18 and Figure 4.19, respectively.

According to the simulation results of the final design, the -10 dB impedance bandwidth of 43.4 MHz and the 3 dB axial ratio bandwidth of 16 MHz (5 dB axial ratio

Table 4.4: Final design parameters of the two-layer stacked antenna which operates CP at L1/L2/L5 GPS bands.

Parameter	Value (mm)	Description
W_Ant	150	Width of the substrate
L_Ant	150	Length of the substrate
W_Bottom	103.8	Width of the bottom patch
L_Bottom	97.8	Length of the bottom patch
W_Top	77.5	Width of the top patch
L_Top	75.9	Length of the top patch
L_Slot_H	72.2	Length of the horizontal slot
L_Slot_V	71.8	Length of the vertical slot
Ws	0.8	Width of the slots
L_Cove_H	16.6	Length of the inserted conducting cove in horizontal direction
L_Cove_V	17.6	Length of the inserted conducting cove in horizontal direction
Ws_Cove	0.4	Width of the inserted conducting cove
SlotOffset	0.8	Distance between edges of patch and slot
r_FeedOffset	1	Distance between bottom patch and coaxial probe
Xf	26	Distance of the coaxial probe along the x-axis
Yf	11.5	Distance of the coaxial probe along the y-axis
x_trans	9	Transfer distance of the top patch along x-axis
y_trans	0.5	Transfer distance of the top patch along y-axis

bandwidth is equal to 26.2 MHz) are achieved at the center frequency of 1176.45 MHz. The -10 dB impedance bandwidth of 33.4 MHz and the 3 dB axial ratio bandwidth of 2.8 MHz are achieved at the center frequency of 1227.6 MHz. The -10 dB impedance bandwidth of 12.5 MHz and the 3 dB axial ratio bandwidth of 2.4 MHz are achieved at the center frequency of 1575.42 MHz. Therefore the designed antenna meets the bandwidth requirements of L1, L2 and L5 GPS bands.

The RHCP and LHCP patterns are given in Figure 4.20 at L5,L2 and L1 bands, respectively. According to RHCP and LHCP patterns, the cross polarizations are obtained as 43.12 dB, 37.5 dB and 36 dB at L5, L2 and L1 bands, respectively. Therefore, the antenna radiates RHCP to boresight of the antenna.

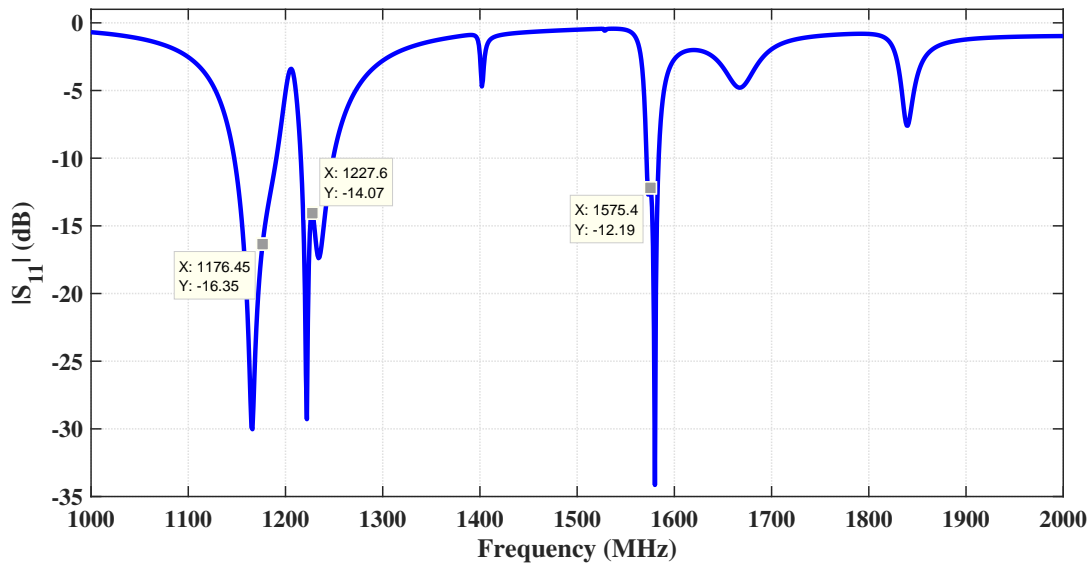


Figure 4.18:  $S_{11}$  simulation result of the L1/L2/L5 triband CP two-layer stacked antenna.

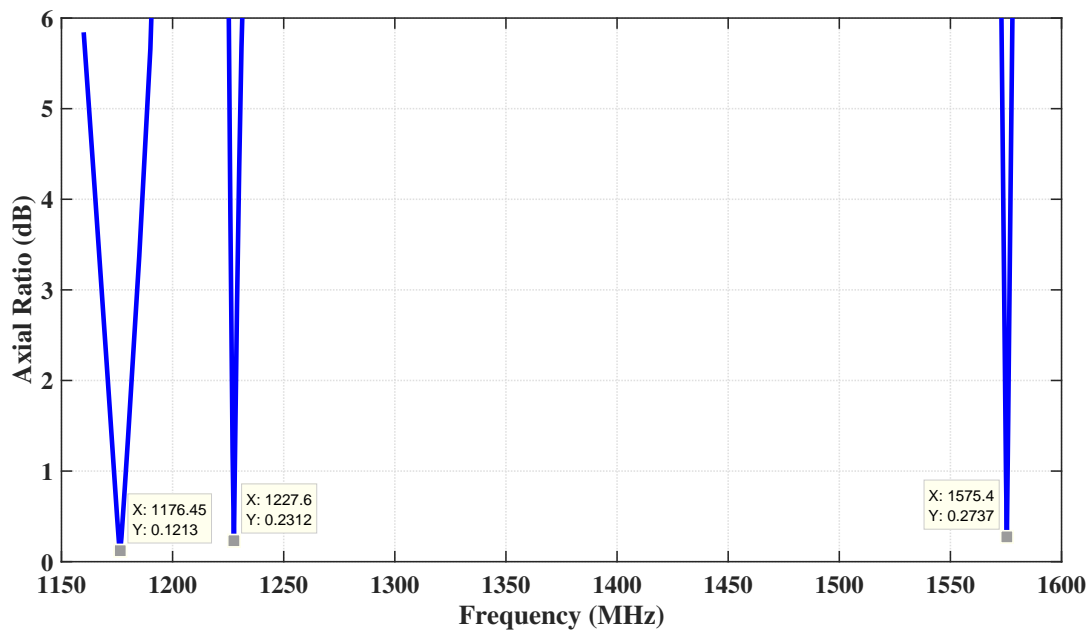


Figure 4.19: Axial ratio simulation result of the L1/L2/L5 triband CP two-layer stacked antenna.

#### 4.1.2 Fabrication of the Antenna

The structure of the stacked antenna is given in Figure 4.1. As seen from the figure, there are four layers as ground plane, foam substrate and two Rogers RT5880

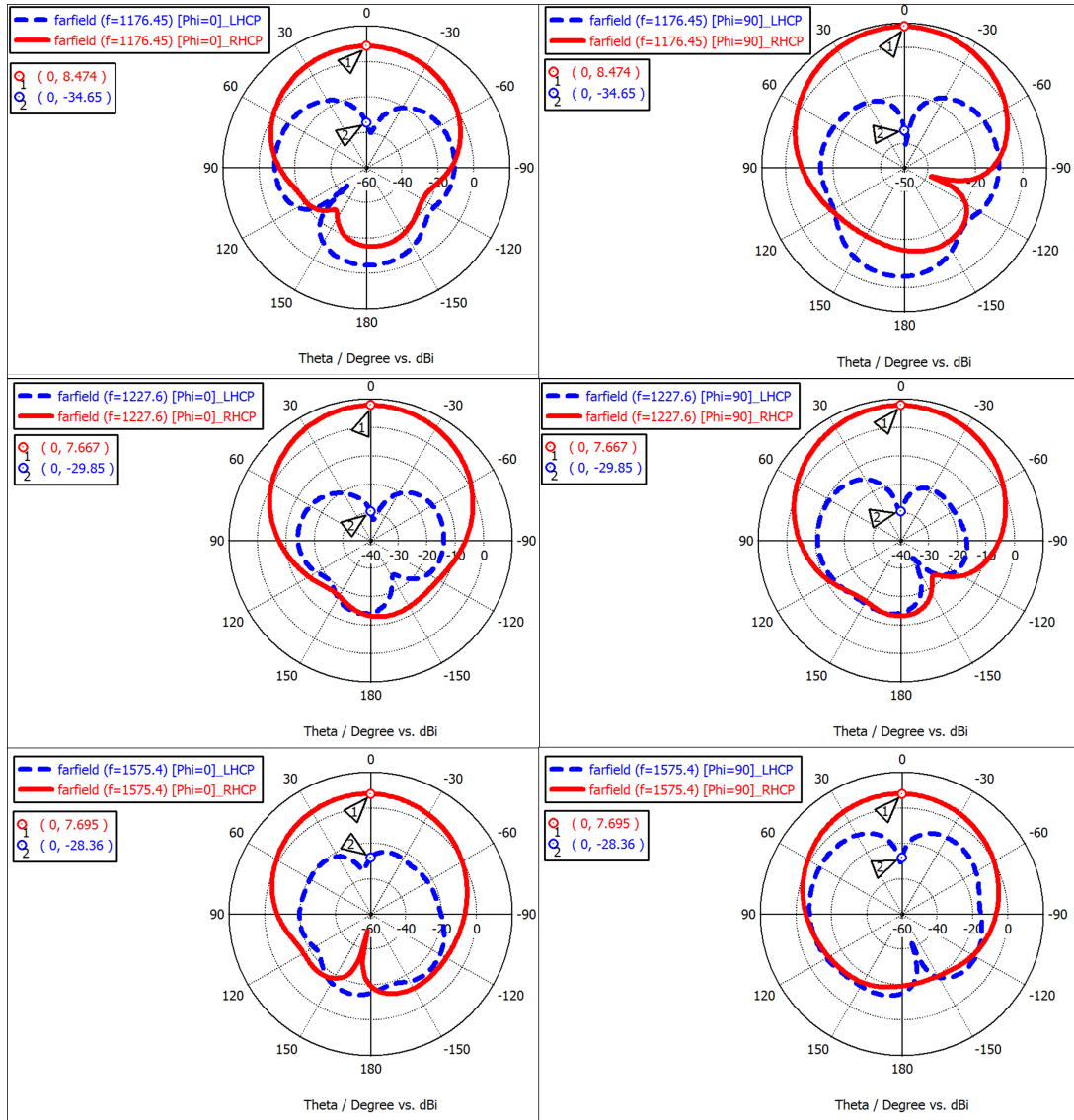


Figure 4.20: Co-polar and cross-polar radiation patterns of the two-layer stacked antenna at L1/L2/L5 GPS bands.

substrates in the structure of stacked antenna. Patches are placed on the substrates of Rogers RT5880. In order to fabricate the designed patches, the PCB prototyping machine is used as in the Section 3.4.2. Double sided substrates are used in the fabrication process. One side of the substrates are fully milled and the other side is shaped according to the shape of the designed patch with the PCB prototyping machine. The fabricated covered four-slotted patch is shown in Figure 4.21.

The Rohacell 31 HF foam substrate with the height of 6 mm is used as the first sub-

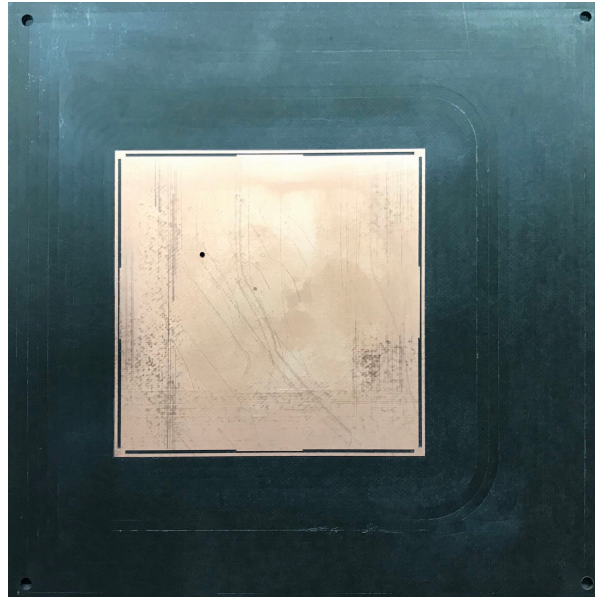


Figure 4.21: Coved four-slotted patch of the two layered stacked antenna.

strate above the ground plane. Drilling process is not applied with any drilling tool. Because, the foam material is soft and the need of drilling is met by hand. Conducting plane of a single sided FR4 substrate is used as the ground plane.



Figure 4.22: Ground plane of the two layered stacked antenna.

The panel type SMA coaxial connector is used to feed the antenna. The length of the inner conductor is chosen according to the total height of the stacked antenna. The exceeding part of the inner conductor is cut as to be flat of the top surface of the top patch. A window is cut out from the FR4 substrate to install the coaxial connector

and the ground panel of the connector is soldered to the ground plane as shown in Figure 4.22.

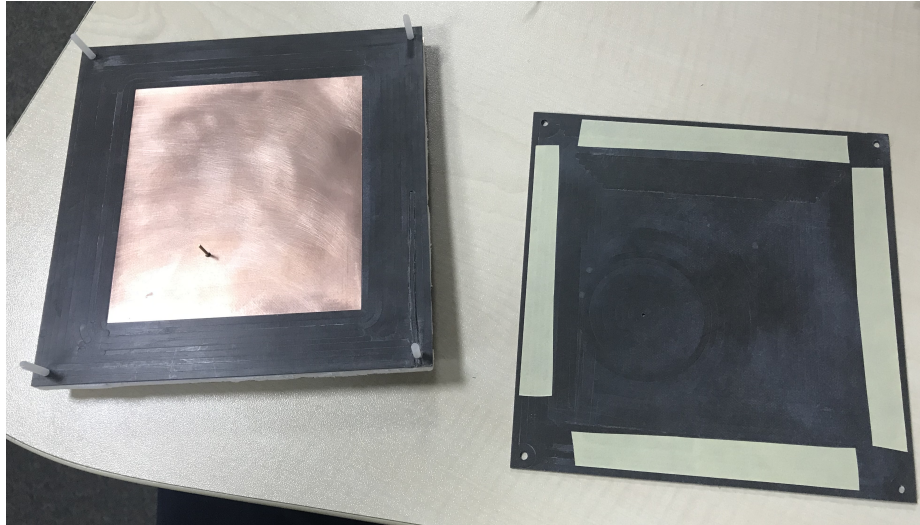


Figure 4.23: Assembly of the layers of the two-layer stacked antenna.

The corners of the layers are drilled to place the nonconducting screws to integrate the stacked antenna. Double-sided tapes are used to stick the layers as shown in Figure 4.23. The top view and the side view of the integrated stacked antenna are shown in Figure 4.24 and Figure 4.25.

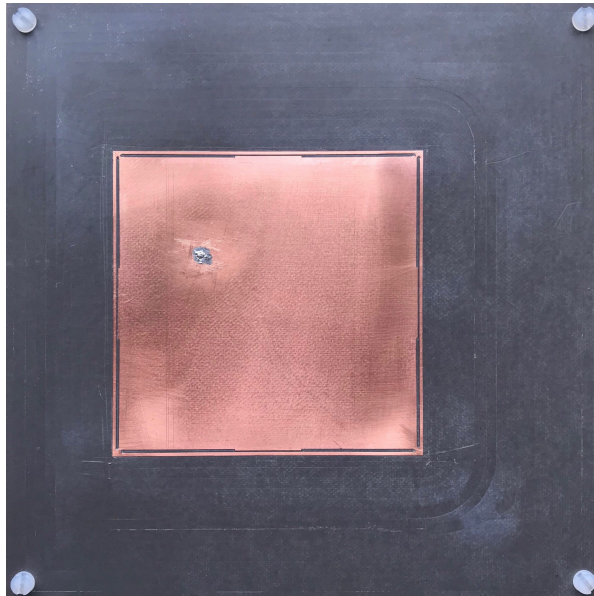


Figure 4.24: Top view of the integrated two-layer stacked antenna.



Figure 4.25: Side view of the integrated two-layer stacked antenna.

### 4.1.3 Measurement Results of Fabricated Antenna

The measurements of the  $S_{11}$  and the radiation pattern of the fabricated antenna are carried out. The graph which indicates the  $S_{11}$  measurement and the simulation results is given in Figure 4.26. According to measurement results, fabricated antenna operates at three bands, however the operating frequencies of the fabricated antenna is shifted to the frequencies of 1178 MHz, 1259 MHz and 1623 MHz. The impedance bandwidths of 58 MHz, 28 MHz and 11 MHz are achieved at the center frequencies of 1178 MHz, 1259 MHz and 1623 MHz, respectively. The measurement of  $S_{11}$  shows that the fabricated antenna meets the requirements of the L5 band GPS signal, but the antenna does not operate at L1 and L2 GPS bands as designed in simulations. The errors on the fabrication and integration may cause the shift of the operating frequencies.

Measurements of radiation pattern are carried out at the frequencies of 1176 MHz, 1259 MHz and 1623 MHz. The measured radiation patterns are compared with simulations. The comparison graphs of the lowest band to highest band are given in Figure 4.27, Figure 4.28 and Figure 4.29, respectively.

According to the results of radiation pattern measurements, fabricated antenna radiates to boresight at all three operating bands. In the measurements at the first band, the HPBW of  $63^\circ$  and  $69^\circ$  are achieved on azimuth and elevation planes, respectively. In simulations, the HPBW of  $69^\circ$  and  $72^\circ$  are obtained at the first band on azimuth and elevation planes, respectively. In the measurements at the second band, the HPBW of  $77^\circ$  and  $71^\circ$  are achieved on azimuth and elevation planes, respectively. In simulations, the HPBW of  $76^\circ$  and  $81^\circ$  are obtained at the second band on azimuth and elevation planes, respectively. In the measurements at the third band, the HPBW

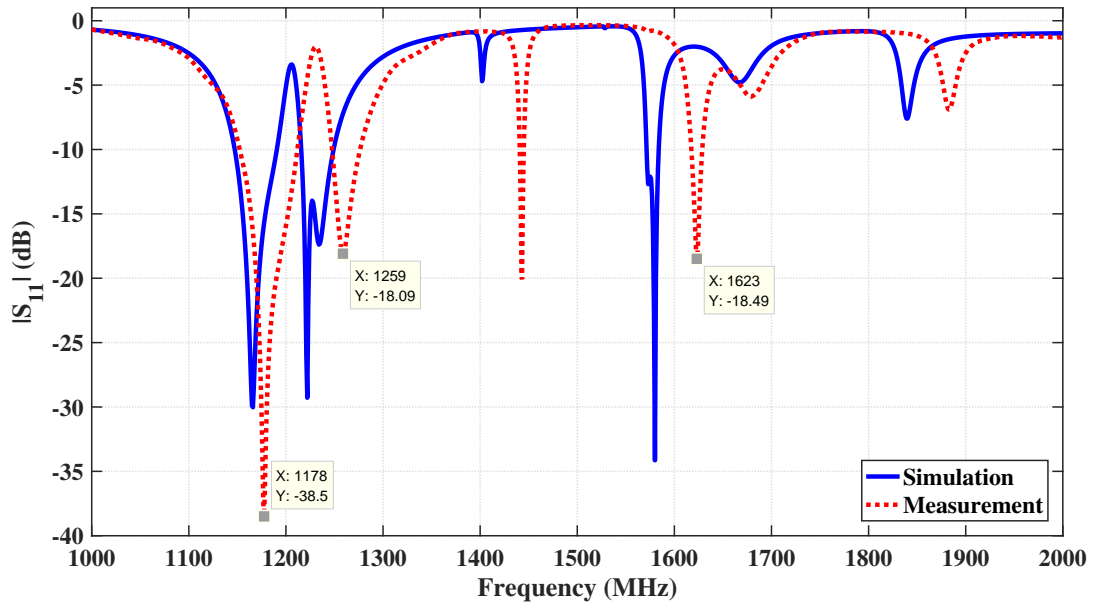


Figure 4.26: The  $S_{11}$  comparison graph between simulation and measurement of the L1/L2/L5 triband two-layer stacked GPS antenna.

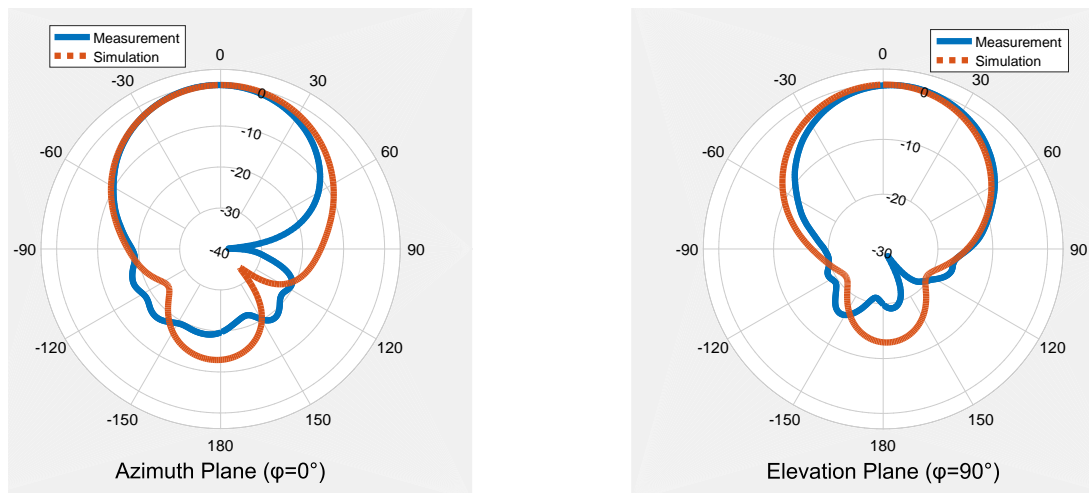


Figure 4.27: Comparison of simulated and measured normalized radiation patterns of L1/L2/L5 triband two-layer stacked GPS antenna at first band (1176 MHz).

of  $82^\circ$  and  $88^\circ$  are achieved on azimuth and elevation planes, respectively. In simulations, the HPBW of  $74^\circ$  and  $77^\circ$  are obtained at the third band on azimuth and elevation planes, respectively. When measured and simulated radiation patterns are compared, measured radiation patterns are quite consistent with simulation results.

The measurement of the axial ratio is carried out to see the circular polarization per-

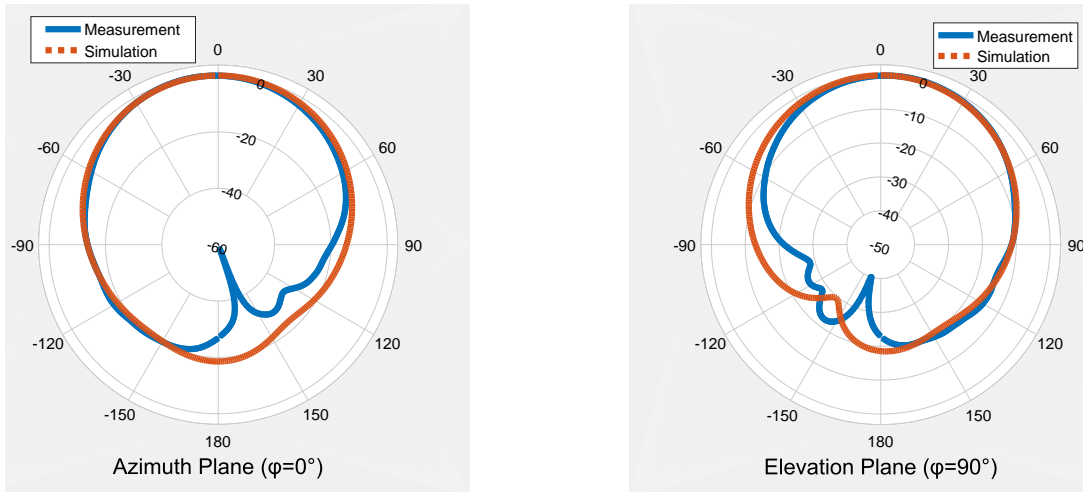


Figure 4.28: Comparison of simulated and measured normalized radiation patterns of L1/L2/L5 triband two-layer stacked GPS antenna at second band (1259 MHz).

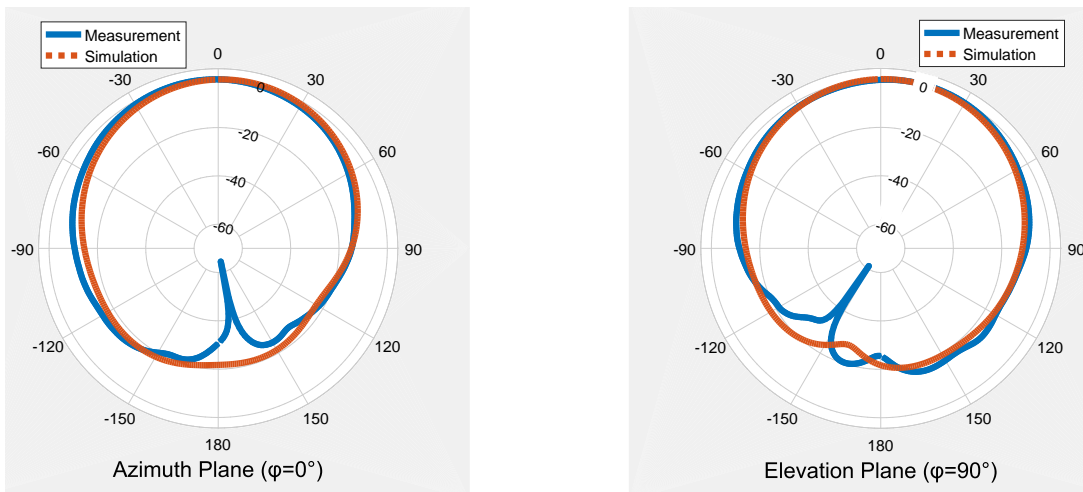


Figure 4.29: Comparison of simulated and measured normalized radiation patterns of L1/L2/L5 triband two-layer stacked GPS antenna at third band (1623 MHz).

formance of the antenna. The antenna is turned around the roll axis (roll axis is defined as the axis which is normal to the top surface of the antenna) of the antenna in measurements. The measurements of the axial ratio are performed around the operating frequencies of the fabricated antenna.

The measured axial ratio around the operating bands is given in Figure 4.30. The axial ratio of 3.9 dB is achieved at 1176 MHz. The lowest axial ratio is measured as 0.7 dB at the frequency of 1187 MHz. The 5-dB axial ratio bandwidth of 27.3 MHz

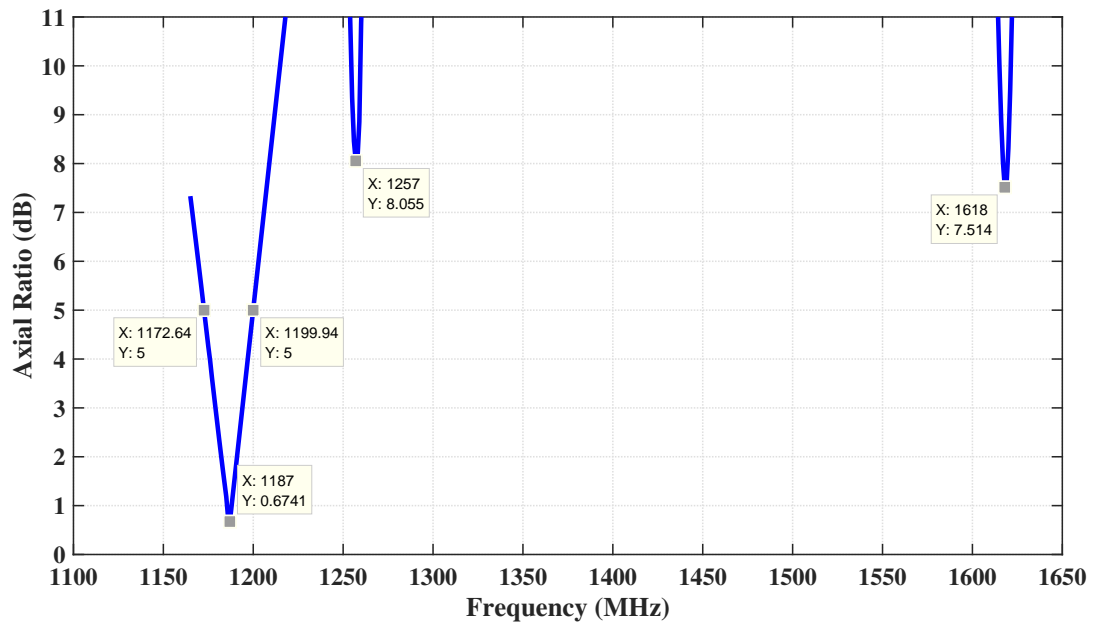


Figure 4.30: Axial ratio measurement result of two-layer stacked antenna

is achieved around the center frequency of 1187 MHz.

The lowest axial ratios are measured as 8 dB and 7.5 dB at the frequencies of 1257 MHz and 1618 MHz, respectively. It is seen from the results, the fabricated antenna does not radiate circularly polarized as required at second and third operating bands. It is thought that the difference between simulation and the measurements may be originated from the errors in fabrication and the integration of the stacked antenna.

In summary, fabricated antenna resonates at the center frequency of the L5 GPS band with the axial ratio of 3.9 dB. The notch frequency of the axial ratio is shifted to higher frequencies for lowest operating band of the antenna. But, the antenna does not meet the requirements of the L2 and L1 GPS bands. Because of this reason, top patch is experimentally modified to tune the resonance frequencies to L2 and L1 GPS bands. As mentioned before, the frequency ratio can be controlled with the parameters of L\_Cove (length of the conducting coves), W\_Cove (width of the conducting coves), L\_Slot (length of the slots), W\_Slot (width of the slots) and SlotOffset. L\_Cove is the only parameter which can be changed with a controlled way. The length of the conducting cove should be increased to decrease the frequency ratio. The copper tape is used on the top patch as shown in Figure 4.31. The length of the conducting cove

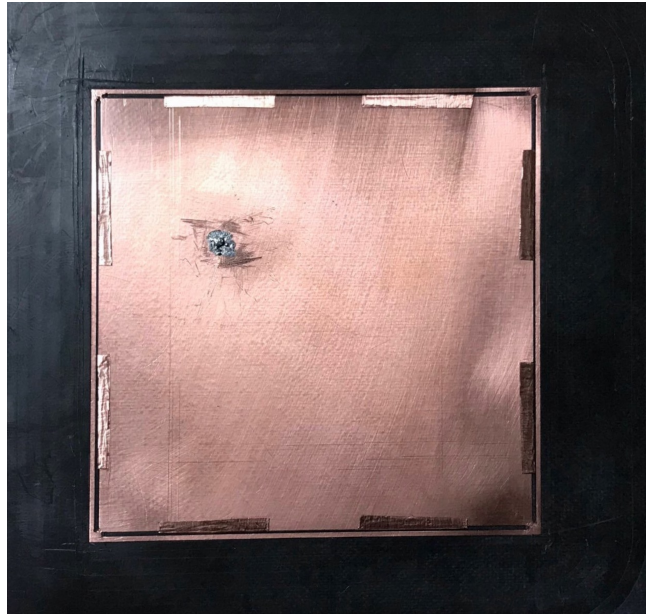


Figure 4.31: Representation of tuned covered four-slotted patch.

is increased to 45 mm on every slots.

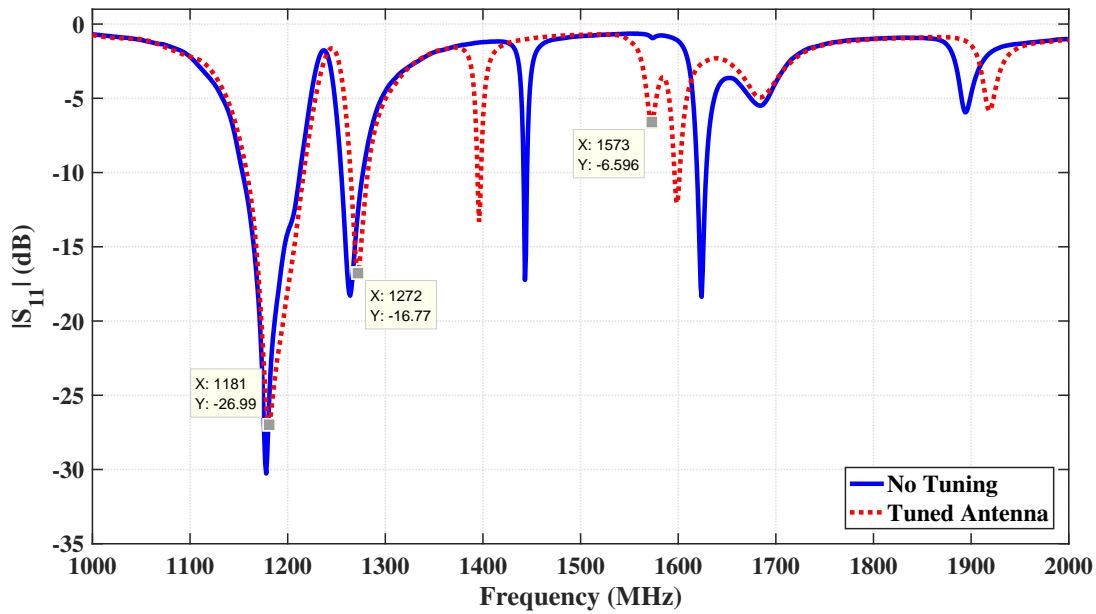


Figure 4.32:  $S_{11}$  comparison of the tuned antenna and fabricated covered four-slotted patch antenna.

The  $S_{11}$  comparison graph of the tuned patch is given in Figure 4.32. As expected, the frequency ratio is decreased between the middle frequency band and the highest

frequency band. It is seen from the comparison graph that the antenna resonates around L1 GPS band. But the return loss is not good as required at 1575 MHz. The position of the feed point should be changed to enhance the impedance matching of the antenna at L1 GPS band. But, to change the feed position new antenna should be fabricated.

The shifts in the resonance frequencies of the fabricated antenna can be tuned by re-fabrication of the antenna.

## **4.2 L1/L2/L5 TRIBAND THREE-LAYER STACKED ANTENNA for GPS APPLICATIONS**

In this section, the studies about the design of L1/L2/L5 triband GPS antenna which consists of three microstrip layers are presented. Corner truncated patches are used on each microstrip layer to operate circularly polarized at L1, L2 and L5 GPS bands. The stacked antenna is fed by a single coaxial probe. The coaxial probe is connected to the top patch by soldering and lower patches are fed by parasitically.

The details about the design, simulations, fabrication and measurements are given in the following subsections.

### **4.2.1 Design and Simulations**

As mentioned in Section 1.3, corner truncated patches can be used to achieve circular polarization on microstrip antennas. RHCP and LHCP can be obtained according to the position of the feed point (see Figure 1.8). Therefore, corner truncated patches are used to operate circularly polarized at L1, L2 and L5 GPS bands in the structure of stacked antenna.

There are two main design parameters on the truncated patches. One of these parameters is the dimensions of the patch. The length of the edges controls the resonance frequencies of the patches. And the other parameter is the length of the truncation. The truncation length is used to control the circular polarization of the patches.

The configuration of the stacked antenna is formed as given in Figure 4.33. The microstrip layer which is used to operate at L5 GPS band is placed as the lowest layer and that patch is named as the bottom patch. Rogers RT5880 substrate is chosen to get broader bandwidth. The height of the substrate is increased with stacking two substrates with the height of 3.18 mm to increase the bandwidth. Therefore, the total height of the lowest substrate becomes 6.36 mm ( $h_1 = 6.36$  mm).

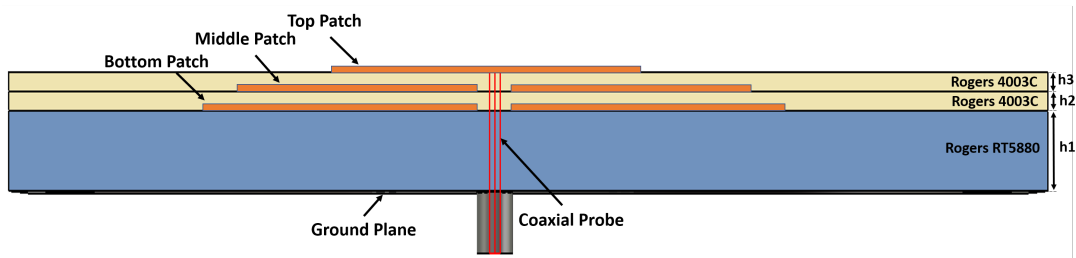


Figure 4.33: Side view of three-layer triband GPS antenna.

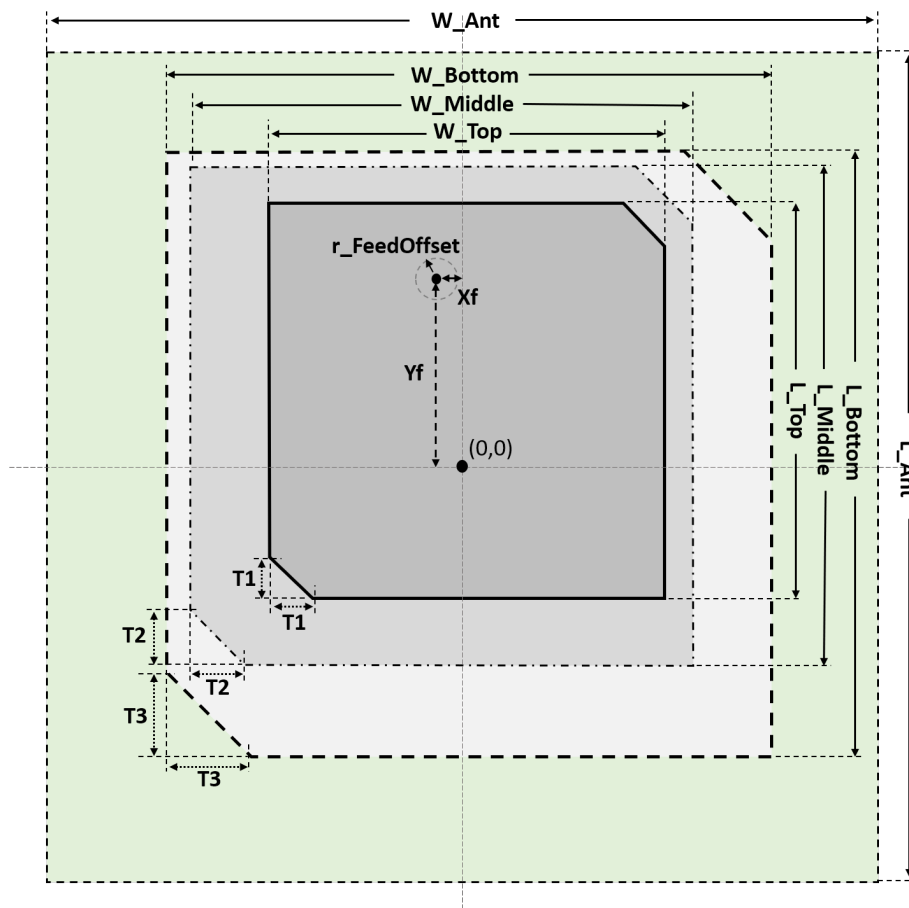


Figure 4.34: Top view of three-layer triband GPS antenna.

Rogers 4003C substrate is used in middle and top microstrip layers. The thickness of the middle and the top layer are chosen as 1.52 mm ( $h_2 = 1.52$  mm,  $h_3 = 1.52$  mm).

The stacked antenna is fed by a single coaxial probe which is connected to the top patch. The other patches are fed by parasitically as performed in the previous design.

The design parameters are given in Figure 4.34 which shows the configuration of the triband stacked antenna from the top view.

The design is performed with an iterative way. At first, the stacked antenna is designed as linearly polarized at L1, L2 and L5 GPS bands with square patches. Then, square patches are perturbed with cutting the corners to achieve circular polarization at L1, L2 and L5 GPS bands. The process of realizing circular polarization is begun from the lowest band to highest one.

Table 4.5: Initial parameters of the parameter analysis on corner truncated antenna.

Parameter	Value (mm)	Description
W_Ant	150	Width of the substrate
L_Ant	150	Length of the substrate
W_Bottom	85	Width of the bottom patch
L_Bottom	85	Length of the bottom patch
T3	0	Truncation length of the bottom patch
Xf	0	Distance of the coaxial probe along the x-axis
Yf	16	Distance of the coaxial probe along the y-axis

Before starting to design, parametric analysis is carried out on corner truncated patch antenna to learn the effects of the parameters on antenna performance. The patch length, truncation length and position of the feed is examined within the study of parameter analysis. A corner truncated patch antenna is designed to operate circularly polarized at L5 GPS band within the study of parameter analysis. In addition, the circular polarization performance of the corner truncated patch is examined at L5 GPS band in terms of bandwidth requirements.

The initial design parameters are given in Table 4.5. The initial value of the patch length is chosen as the half of the wavelength which is calculated for the substrate with the dielectric constant of 2.2 at 1176.45 MHz ( $\lambda/2 \approx 85$  mm). Simulations are

performed and the resonance frequency of the square patch is tuned to 1176.45 MHz with the patch length of 79.7 mm as shown in Figure 4.35.

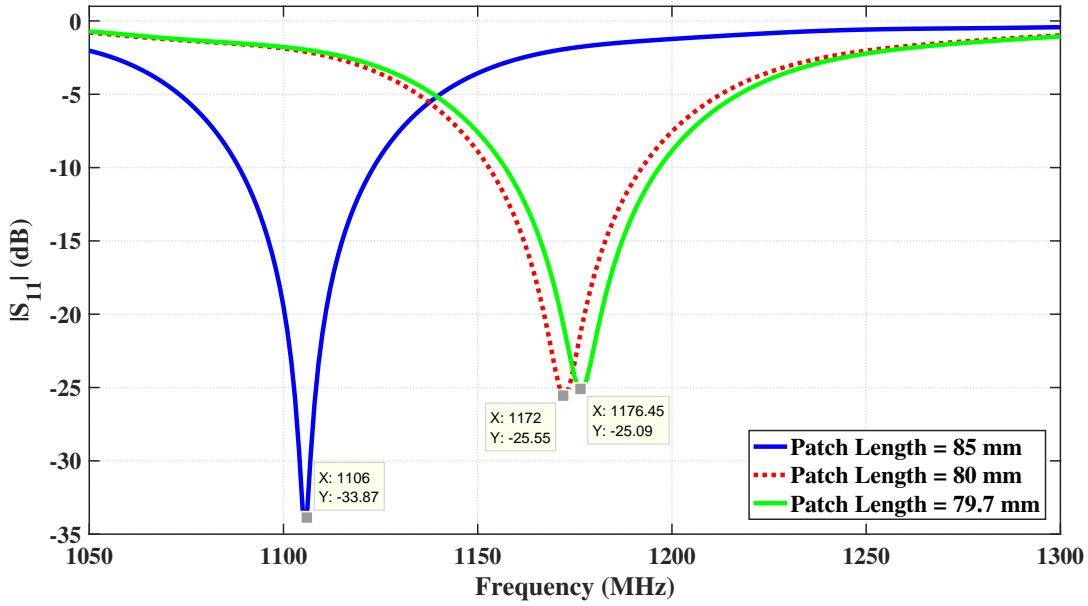


Figure 4.35:  $S_{11}$  versus frequency for different patch lengths on square patch.

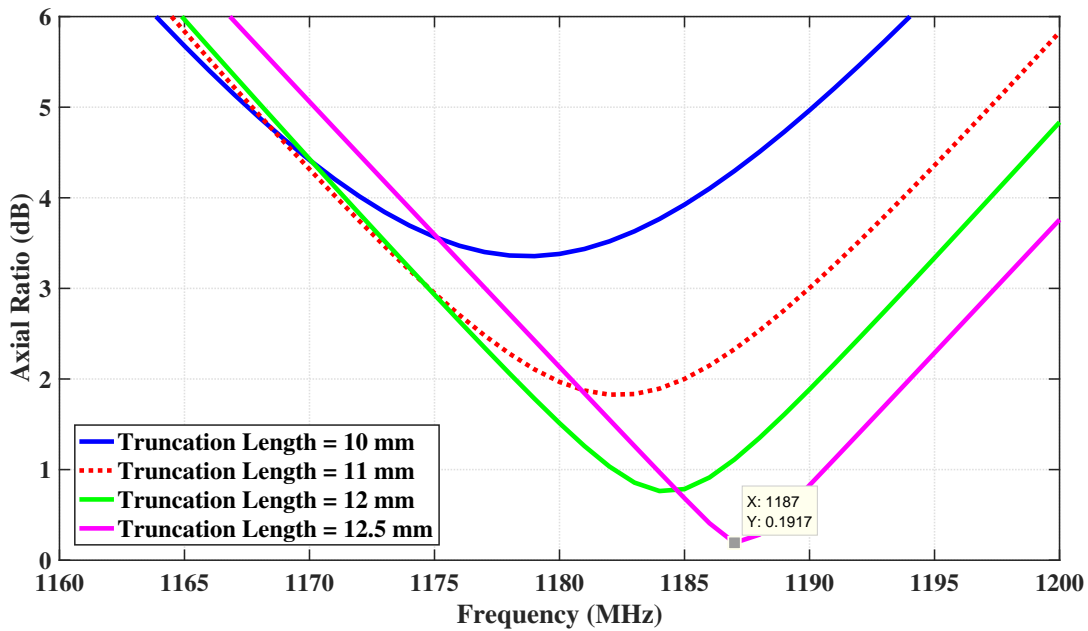


Figure 4.36: Axial ratio versus frequency for different truncation lengths on square patch.

The length of the corner truncation is increased up to 12.5 mm to achieve circular polarization. The change of the axial ratio with respect to truncation length is given in

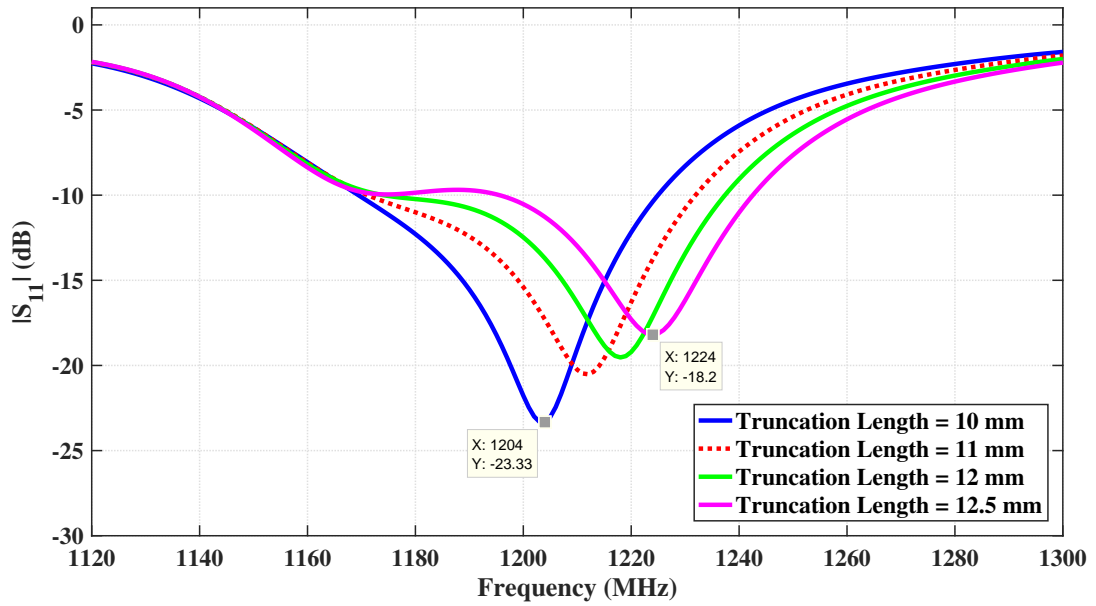


Figure 4.37:  $S_{11}$  versus frequency for different truncation lengths on square patch.

Figure 4.36. The axial ratio of 0.2 dB is obtained when the truncation length is equal to 12.5 mm at 1187 MHz. When the truncation length is increased, the resonance frequency of the antenna is increased as given in Figure 4.37.

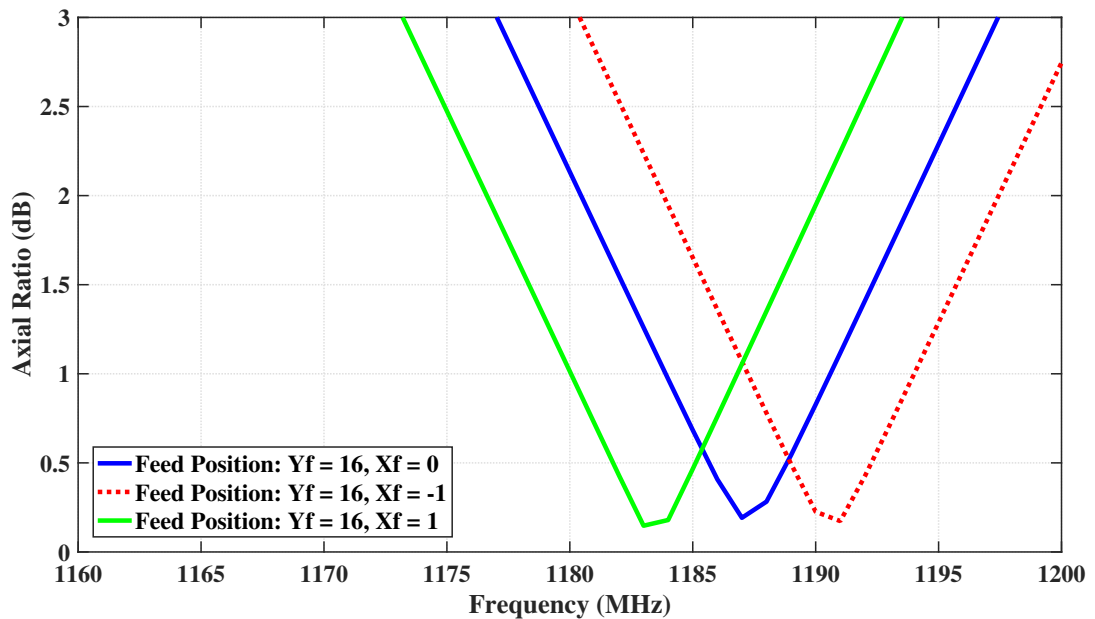


Figure 4.38: Axial ratio graph related to the change of feed position on square patch.

There are two ways to tune the notch frequency of axial ratio on the corner truncated patch antennas. One of these ways is the change of the patch length as performed on

any designs on rectangular patches. The other way is the change of the feed position. Generally, the patch is fed in the direction of the orthogonal axes according to the orientation of the patch. The feed is placed on the y-axis on the antenna ( $X_f = 0$  mm). The change of the feed position on the x-axis causes to a change in the notch frequency of the axial ratio as given in Figure 4.38. If the position of the feed is changed in the positive direction on the x-axis, the notch frequency of the axial ratio shifts to lower frequencies, and vice versa.

Table 4.6: The parameters of the L5 band circularly polarized truncated antenna.

Parameter	Value (mm)	Description
W_Ant	150	Width of the substrate
L_Ant	150	Length of the substrate
W_Bottom	81.54	Width of the bottom patch
L_Bottom	81.54	Length of the bottom patch
T3	13.5	Truncation length of the bottom patch
Xf	4	Distance of the coaxial probe along the negative x-axis
Yf	20	Distance of the coaxial probe along the positive y-axis

The parameters of the bottom patch that radiates circularly polarized at 1176.45 MHz are given in Table 4.6. Graphs of the  $S_{11}$  and the axial ratio are given in Figure 4.39 and Figure 4.40, respectively. According to results, the impedance bandwidth of 82.8 MHz (7%) and the 3-dB axial ratio bandwidth of 21.1 MHz (1.8%) are achieved around the center frequency of 1176.45 MHz. Obtained results meets the requirements of the L5 GPS signal.

The effects of patch length, truncation length and feed position are examined in the study of parameter analysis and this experience is used in design of the whole antenna.

After parameter analysis, a linearly polarized L1/L2/L5 GPS band stacked antenna is designed with the given parameters in Table 4.7.  $S_{11}$  of the linearly polarized L1/L2/L5 GPS band stacked antenna is given in Figure 4.41.

The corners of the bottom patch is cut as the parameter of truncation length (T3). Truncation length is increased up to 11 mm and the change on the axial ratio is given in Figure 4.42. As seen from the Figure 4.42, the axial ratio is reduced up to 1.03 dB at 1176.45 MHz but  $S_{11}$  is changed in an unwanted way as shown in Figure 4.43.

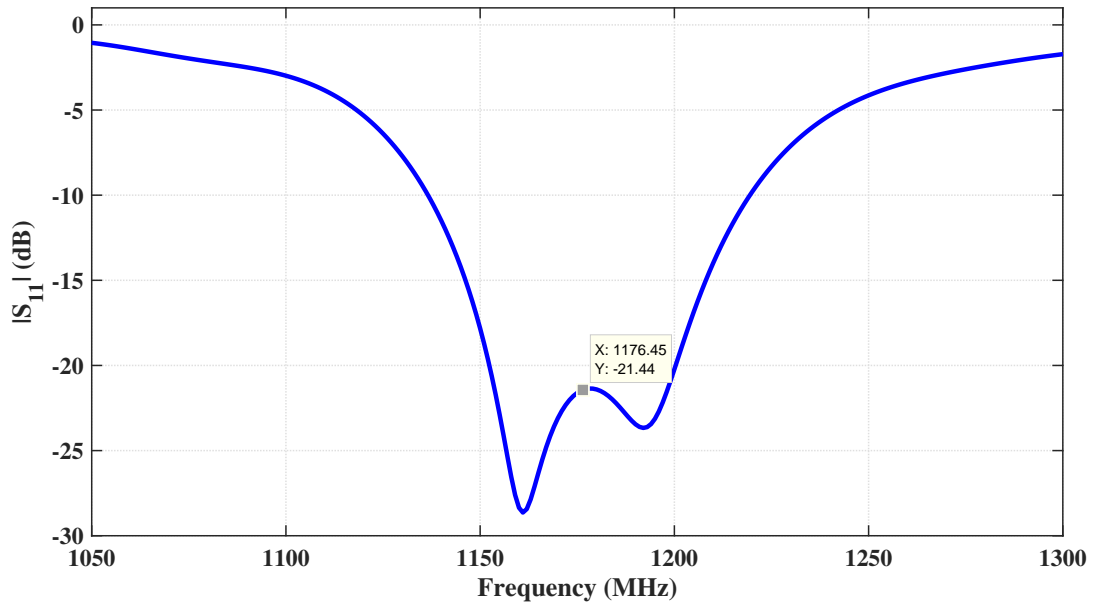


Figure 4.39:  $S_{11}$  of L5 GPS band circular polarized corner truncated antenna.

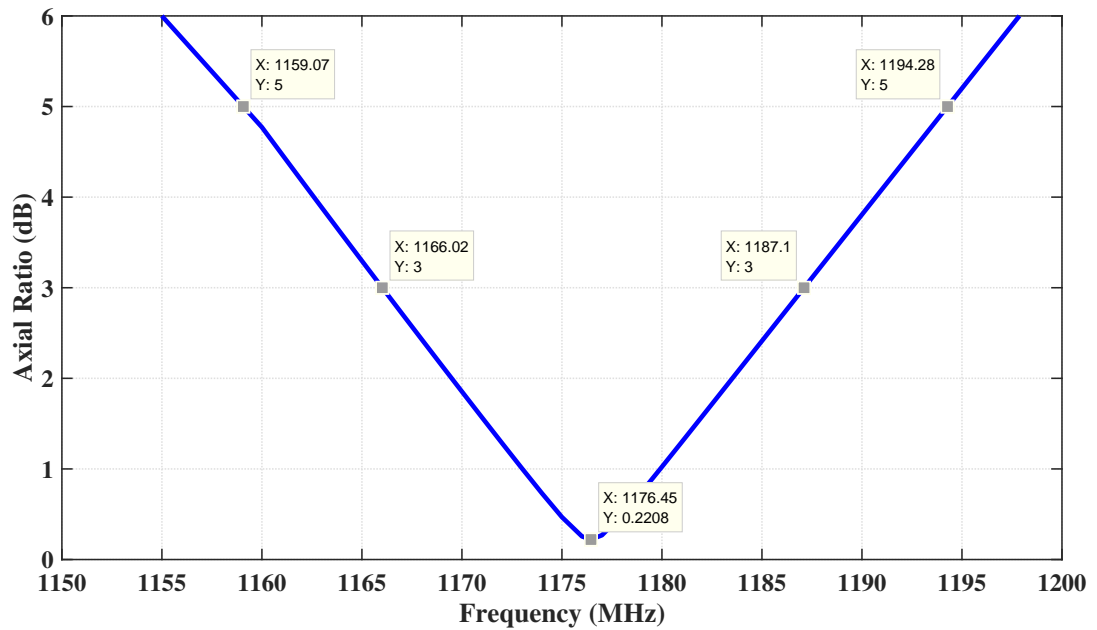


Figure 4.40: Axial ratio of L5 GPS band circular polarized corner truncated antenna.

First, the feed position is changed along the positive y-axis to 22.5 mm but desired changes could not be realized. Then, the feed position is changed along the negative x-axis to 4 mm and  $S_{11}$  is changed as given in Figure 4.44. Therefore, the return loss is enhanced at lower band.

Table 4.7: The parameters of the L5 band circularly polarized truncated stacked antenna

Parameter	Value (mm)	Description
W_Ant	150	Width of the substrate
L_Ant	150	Length of the substrate
W_Bottom	75.2	Width of the bottom patch
L_Bottom	75.2	Length of the bottom patch
W_Middle	62.5	Width of the middle patch
L_Middle	62.5	Length of the middle patch
W_Top	49.37	Width of the top patch
L_Top	49.37	Length of the top patch
T3	0	Truncation length of the bottom patch
T2	0	Truncation length of the middle patch
T1	0	Truncation length of the top patch
Xf	0	Distance of the coaxial probe along the negative x-axis
Yf	18	Distance of the coaxial probe along the positive y-axis
r_FeedOffset	1.5	Feed offset between feed probe and patches

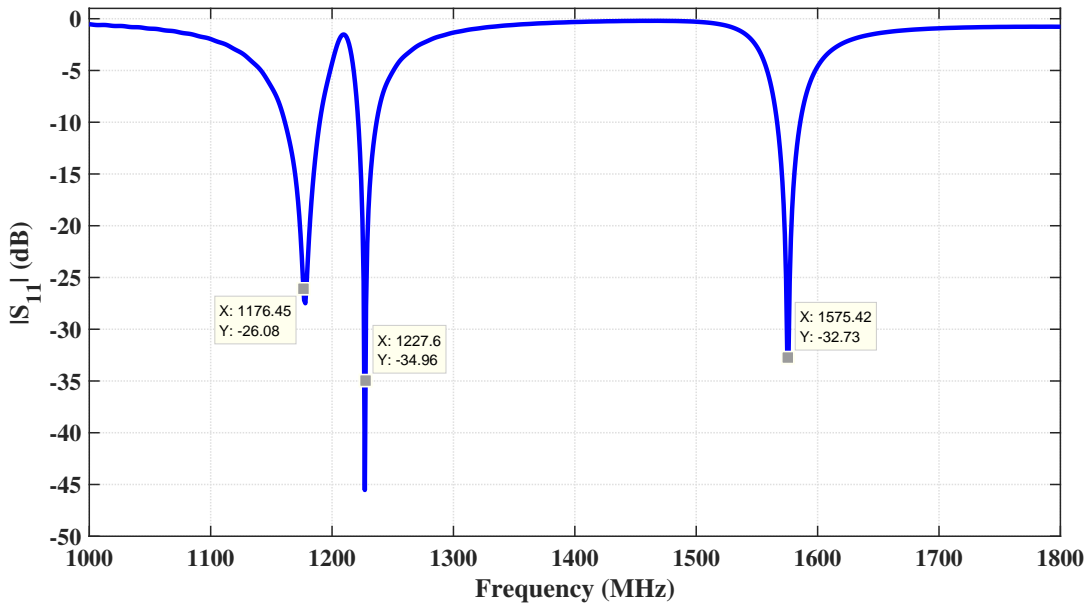


Figure 4.41:  $S_{11}$  of linearly polarized L1/L2/L5 GPS band corner truncated stacked antenna.

$S_{11}$  of the antenna is reduced lower than -10 dB around 1176.45 MHz with the change of the feed along x-axis. As it is learned in parametric analysis, the change of the

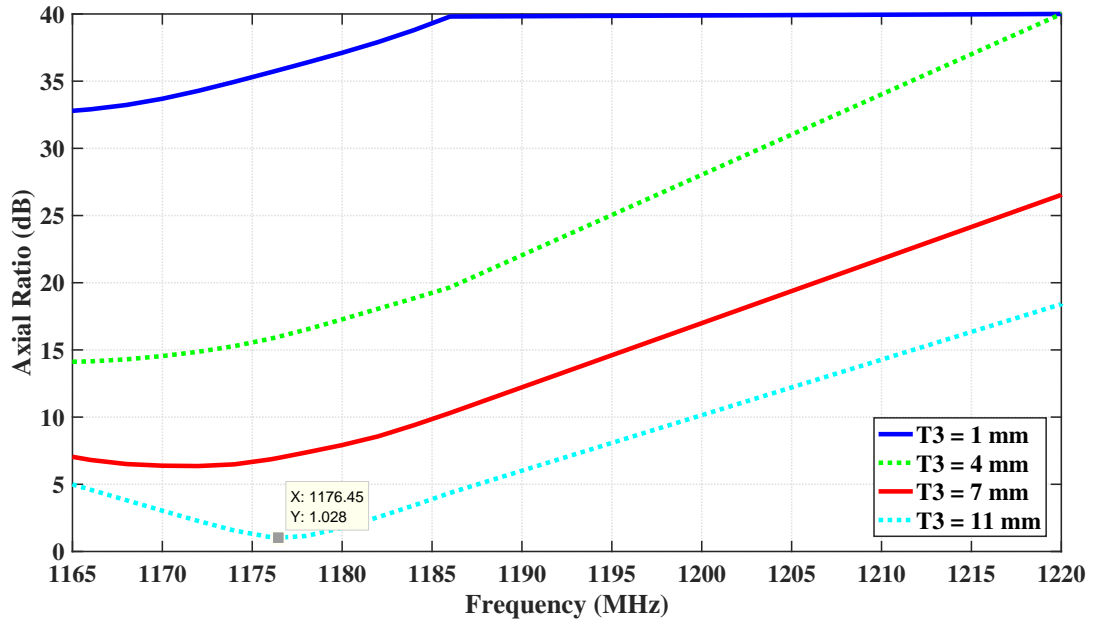


Figure 4.42: Axial Ratio of the change of truncation length on bottom patch in corner truncated stacked antenna.

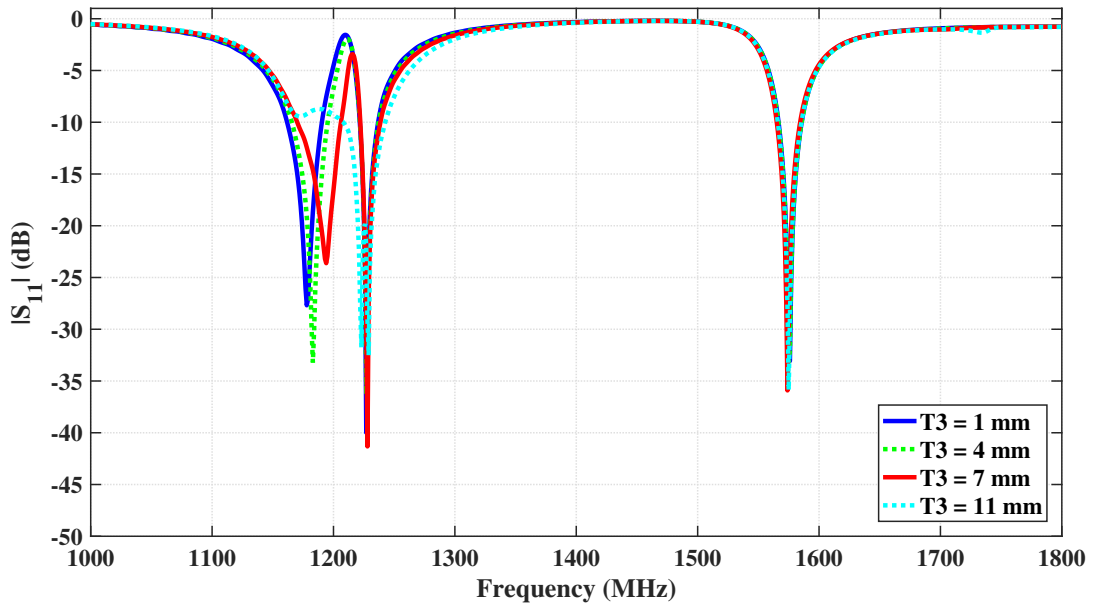


Figure 4.43:  $S_{11}$  of the change of truncation length on bottom patch in corner truncated stacked antenna.

feed position along negative x-axis increases the notch frequency of the axial ratio as shown in Figure 4.45.

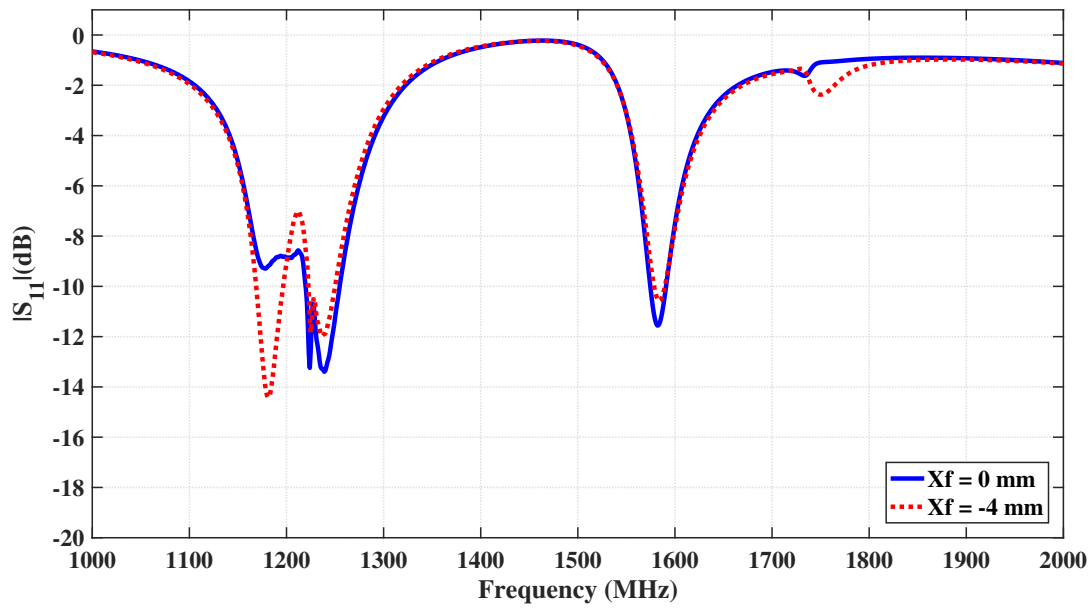


Figure 4.44:  $S_{11}$  of the change of  $X_f$  parameter on bottom patch in corner truncated stacked antenna.

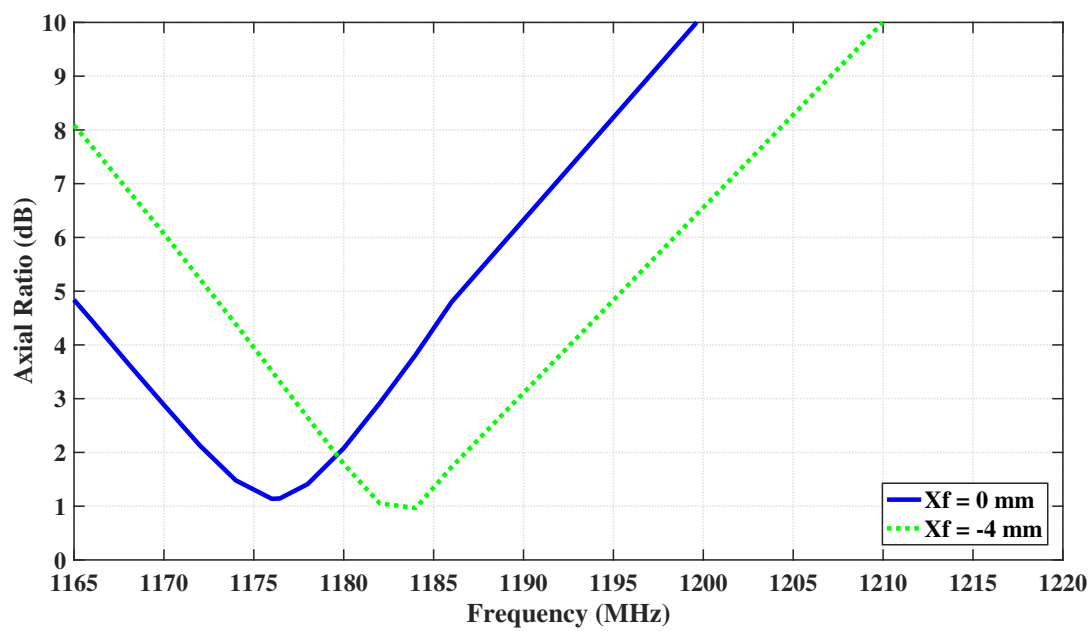


Figure 4.45: Axial ratio of the change of  $X_f$  parameter on bottom patch in corner truncated stacked antenna.

The patch length is increased to decrease the notch frequency of the axial ratio.  $S_{11}$  is changed with the increase of the patch length as shown in Figure 4.46. The notch frequency is tuned to 1176.45 MHz when the patch length is equal to 75.7 mm; thus,

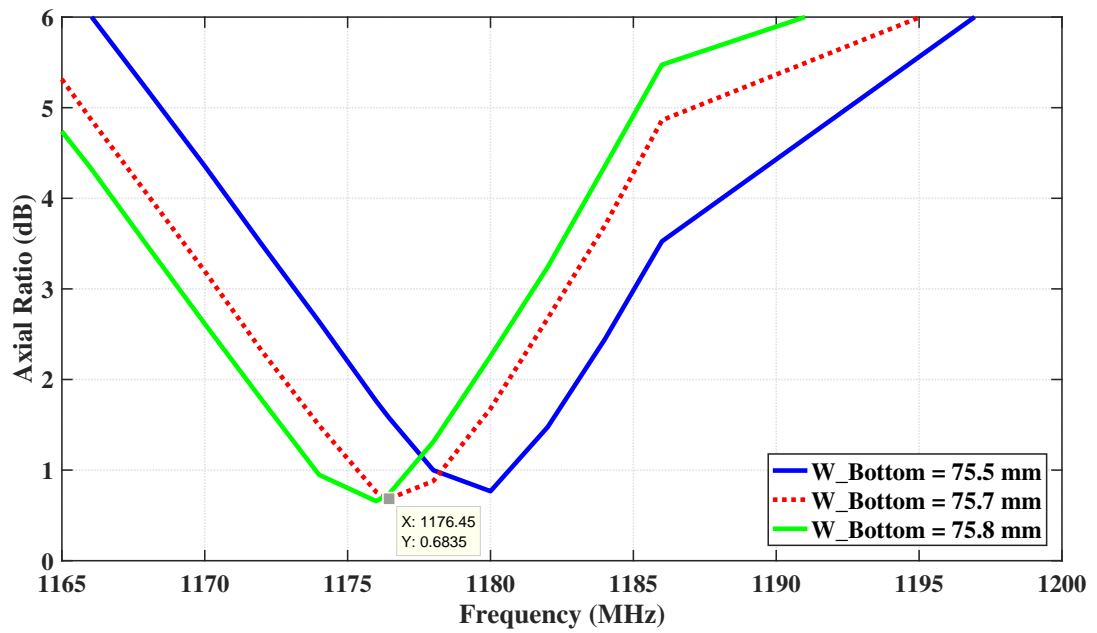


Figure 4.46: Axial Ratio of the change of  $W_{\text{Bottom}}$  on bottom patch in corner truncated stacked antenna.

the antenna becomes circularly polarized at L5 GPS band.

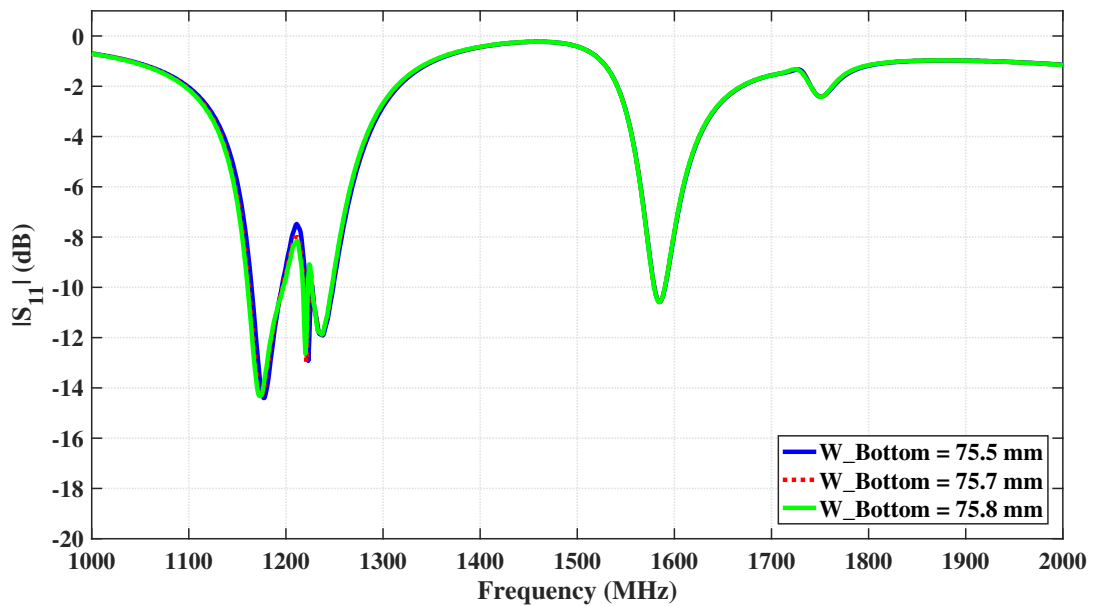


Figure 4.47:  $S_{11}$  of the change of  $W_{\text{Bottom}}$  parameter on bottom patch in corner truncated stacked antenna.

Corners of the middle patch is cut to get circular polarization at L2 GPS band. The

length of the corner truncation is increased from 3 mm to 6.7 mm and the axial ratio graph with respect to the change of corner truncation length is given in Figure 4.48. The axial ratio is decreased to 1.8 dB at 1245 MHz. The middle patch is moved along the negative x-axis to decreased the notch frequency of the axial ratio to 1227.6 MHz.

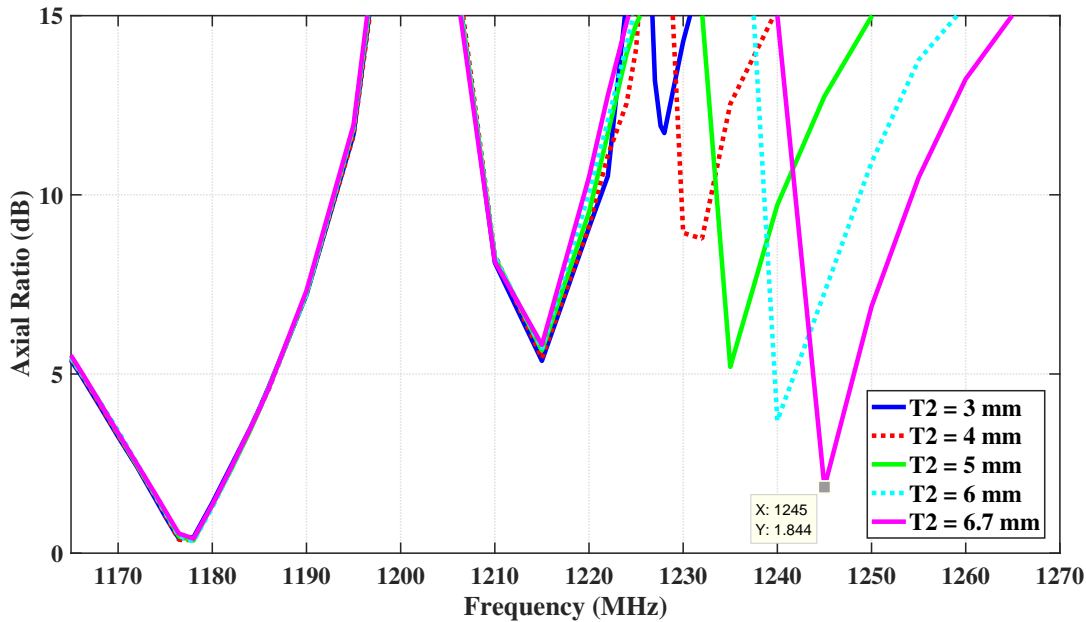


Figure 4.48: Axial ratio of the change of T2 parameter on middle patch in corner truncated stacked antenna.

The parameter of "x\_trans\_middle" is changed in simulations and the notch frequency of axial ratio tuned to 1227.6 MHz when the parameter of x\_trans\_middle is equal to 3.6 mm as shown in Figure 4.49. As seen in Figure 4.49, notch frequency of the first band is shifted to 1178 MHz. Fine tuning is applied on the patch dimensions of the bottom and middle patches to tune the notch frequencies to 1176.45 MHz and 1227.6 MHz, respectively. As seen in Figure 4.50, the notch frequencies are tune to required frequencies when the parameters of W\_Bottom and W\_Middle are equal to 75.85 mm and 63.33 mm, respectively.  $S_{11}$  is changed as shown in Figure 4.51. Therefore, the antenna is become circularly polarized at L5 and L2 GPS bands.

After achievement of circular polarization at L2 and L5 GPS bands, the corners of the top patch are cut to get circular polarization at L1 GPS band. The parameter of T1 is increased up to 5 mm and the axial ratio of 2.6 dB is obtained at 1590 MHz as shown in Figure 4.52. The length of the top patch is increased to decrease the notch

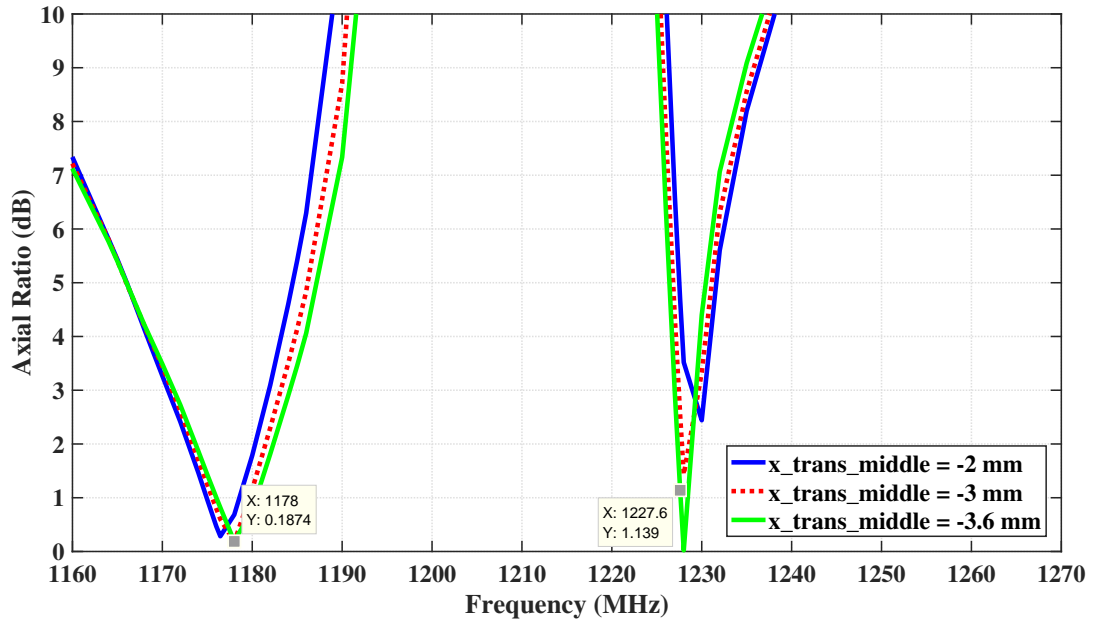


Figure 4.49: Axial ratio of the change of  $x\_trans\_middle$  parameter on middle patch in corner truncated stacked antenna.

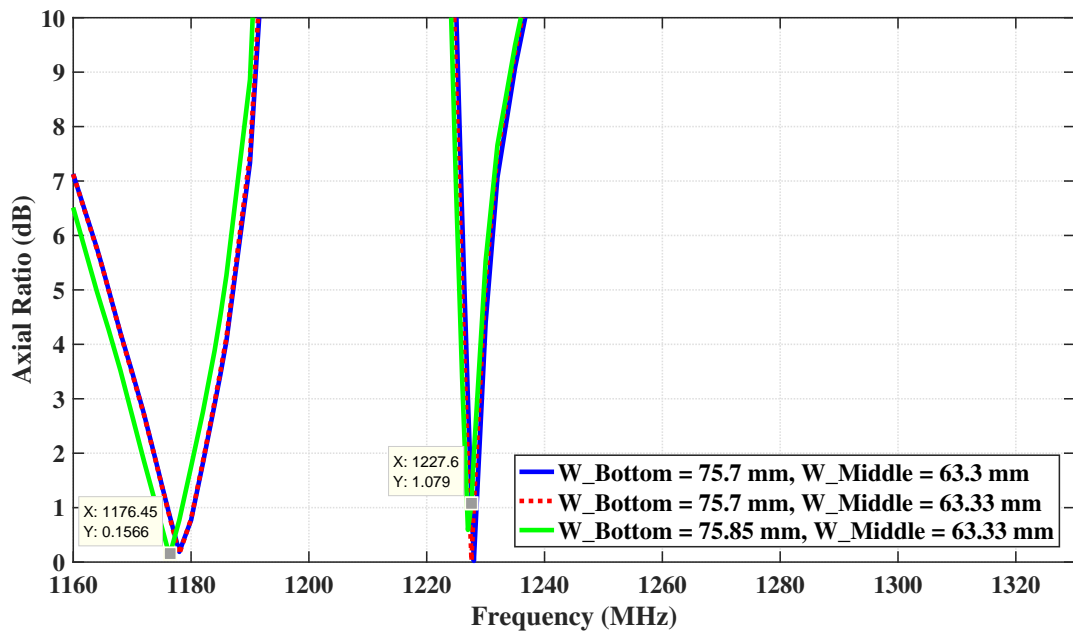


Figure 4.50: Axial ratio of the change of  $W\_Middle$  and  $W\_Bottom$  parameters in corner truncated stacked antenna.

frequency of the axial ratio to 1575.42 MHz. As shown in Figure 4.53, axial ratio is tuned 1575.42 MHz when the length of the top patch is equal to 49.9 mm.

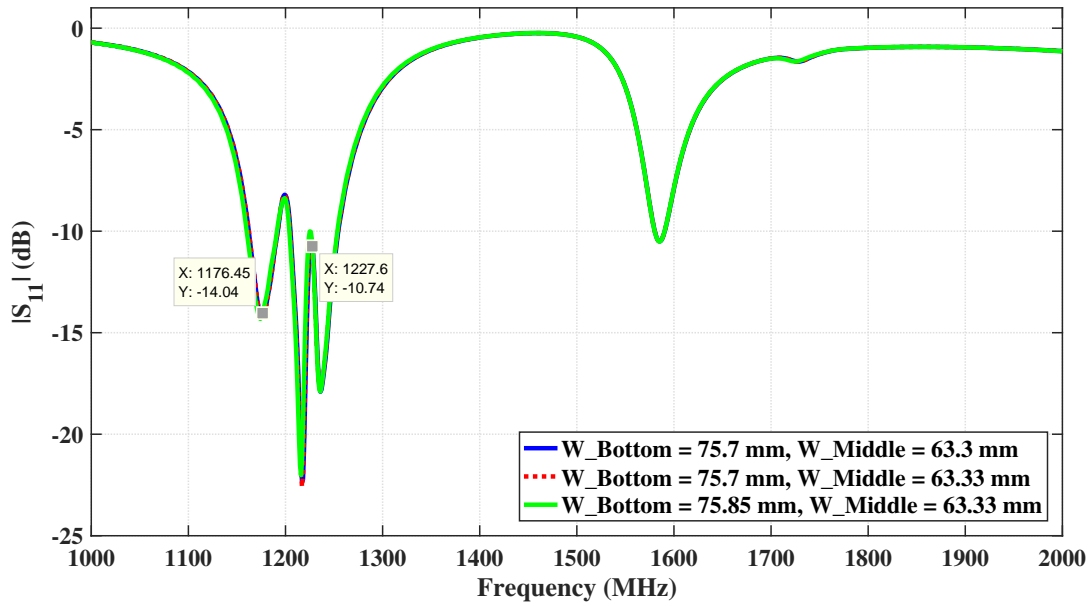


Figure 4.51:  $S_{11}$  of the change of  $W_{Middle}$  and  $W_{Bottom}$  parameters in corner truncated stacked antenna.

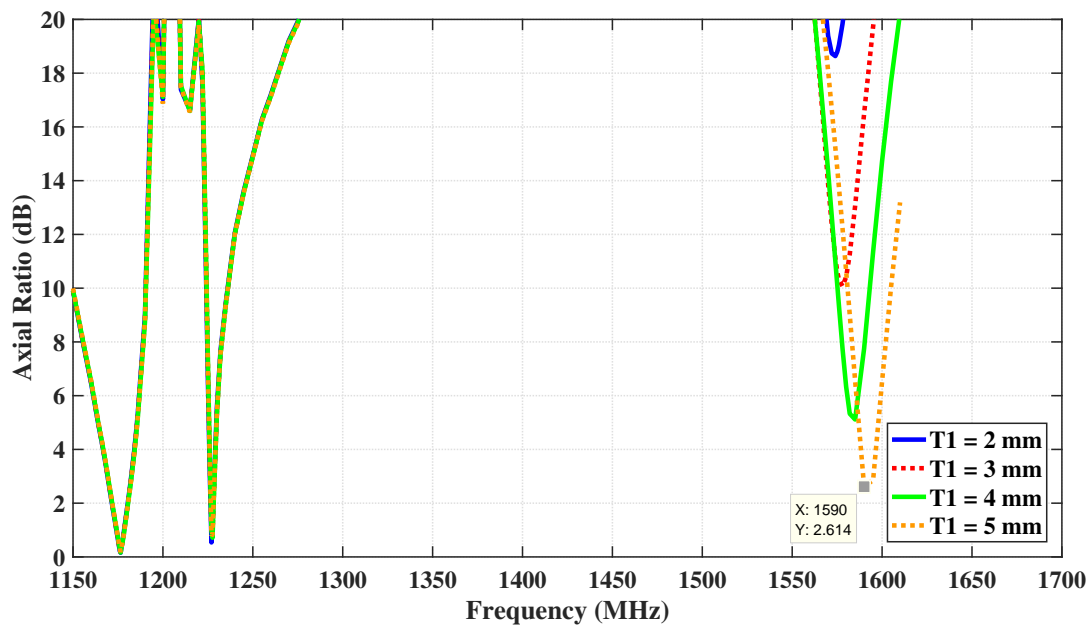


Figure 4.52: Axial ratio of the change of  $T1_{Middle}$  parameters in corner truncated stacked antenna.

Fine tuning is applied on the parameters of  $W_{Top}$  and  $T1$  to enhance the axial ratio at L1 GPS band. Axial ratio and  $S_{11}$  graphs related to the process of fine tuning are given in Figure 4.54 and Figure 4.55, respectively. According to Figure 4.54,

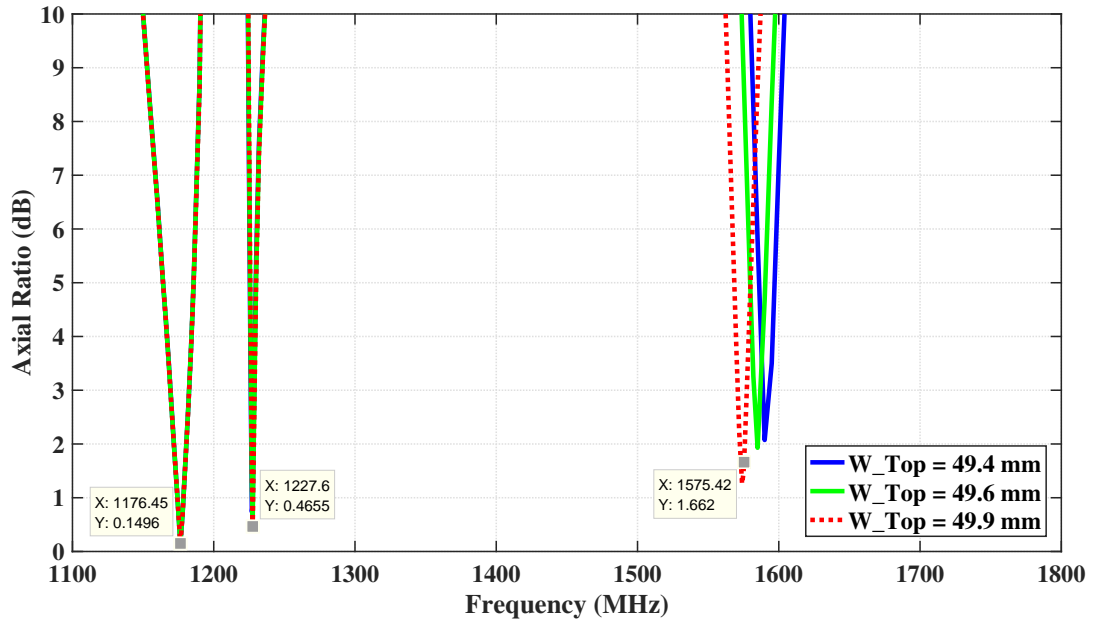


Figure 4.53: Axial ratio of the change of  $W\_Top$  parameters in corner truncated stacked antenna.

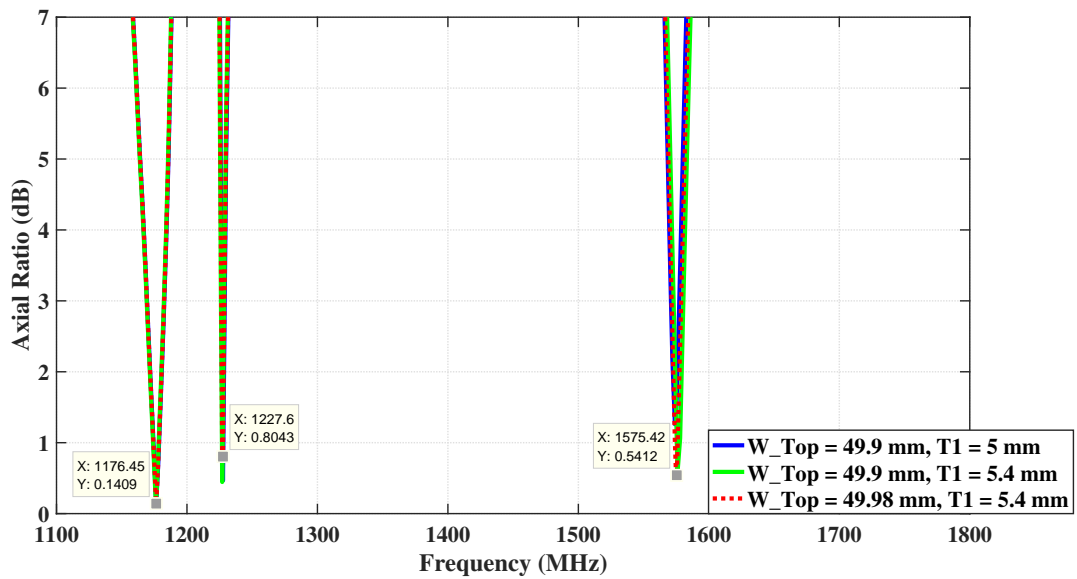


Figure 4.54: Axial ratio of the final tuning of  $W\_Top$  and  $T1$  parameters in corner truncated stacked antenna.

the axial ratios of 0.14 dB, 0.8 dB and 0.54 dB are achieved at L5, L2 and L1 GPS bands, respectively. The 5-dB axial ratio bandwidths of 21.6 MHz, 4.21 MHz and 12.4 MHz are achieved at L5, L2 and L1 GPS bands, respectively. The 3-dB axial

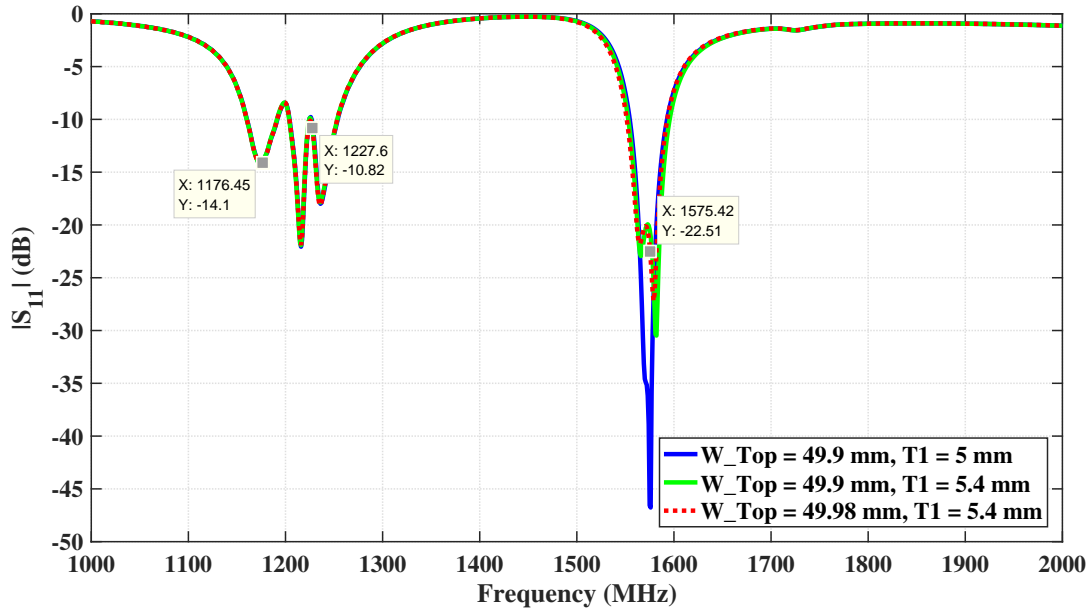


Figure 4.55:  $S_{11}$  of the final tuning of  $W_{Top}$  and  $T1$  parameters in corner truncated stacked antenna.

ratio bandwidths of 13.2 MHz, 2.5 MHz and 7.3 MHz are achieved at L5, L2 and L1 GPS bands, respectively. The impedance bandwidths of 31.3 MHz, 49.3 MHz and 41.7 MHz are achieved at L5, L2 and L1 GPS bands, respectively.

The RHCP and LHCP patterns are given in Figure 4.56 at L1/L2/L5 GPS bands. According to RHCP and LHCP patterns, the cross polarization is obtained as 36.8 dB, 28.9 dB and 30.6 dB at L5, L2 and L1 GPS bands, respectively. Therefore, the antenna radiates RHCP to boresight of the antenna.

#### 4.2.2 Fabrication of the Antenna

Designed microstrip layers are fabricated by PCB prototyping machine as in previous cases. The fabricated bottom patch, middle patch and the top patch are shown in Figure 4.57, Figure 4.58 and Figure 4.59, respectively.

The integration of the microstrip layers is carried out as shown in Figure 4.60. As seen from the Figure 4.60, two Rogers RT5880 substrates (black color) with the height of 3.18 mm are stacked to achieve a single substrate with the height of 6.36 mm. Other microstrip layers which contains of Rogers 4003C substrates (white color) are placed

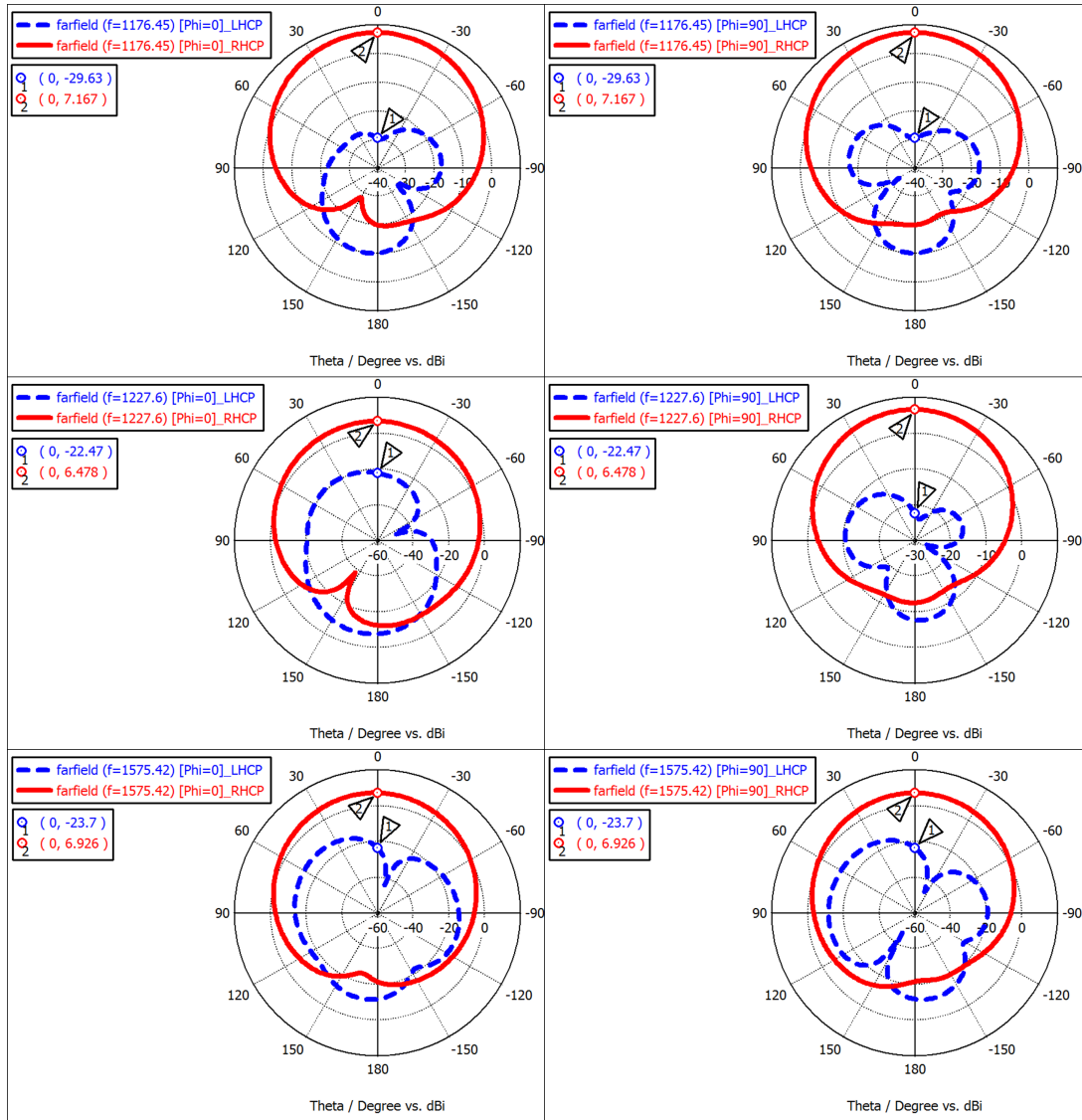


Figure 4.56: Co-polar and cross-polar radiation patterns of the three layered antenna at L1/L2/L5 GPS bands.

respectively on the bottom patch. Corners of the microstrip layers are drilled to place the nonconducting screws at the integration phase of the antenna.

Same kind of coaxial panel connector is used to feed the stacked antenna. The conducting plane of the lowest substrate is used as the ground plane of the antenna. The extending part of the coaxial probe is cut as is at the same level with the top patch. Then, it is soldered to top patch.

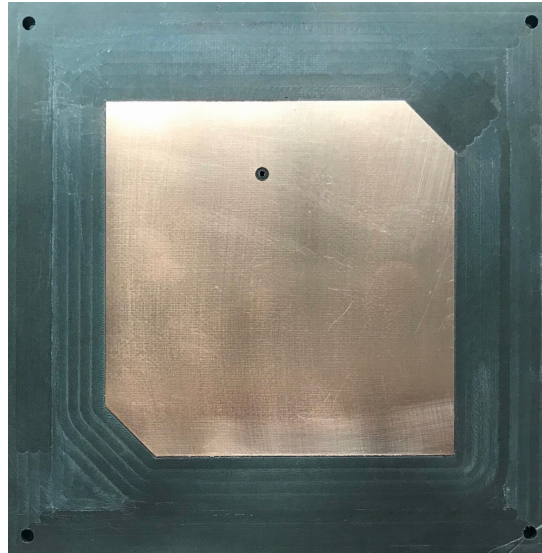


Figure 4.57: Fabricated bottom patch of the three-layer antenna at L1/L2/L5 GPS bands.

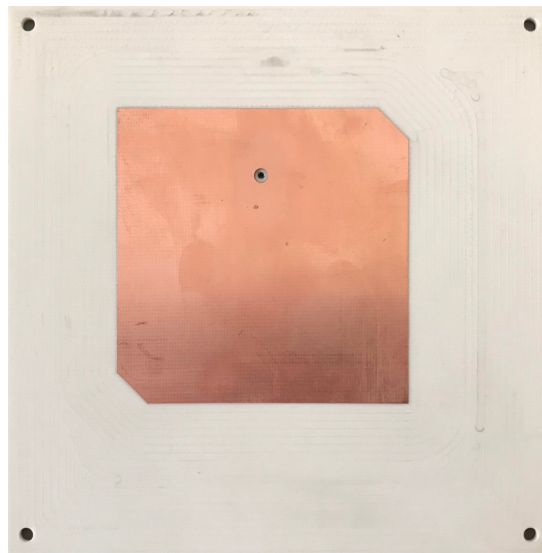


Figure 4.58: Fabricated middle patch of the three-layer antenna at L1/L2/L5 GPS bands.

### 4.2.3 Measurement Results of Fabricated Antenna

First, the measurement of  $S_{11}$  is carried out on the integrated stacked antenna. The result of the  $S_{11}$  measurement is given in Figure 4.61. In this graph, the simulation result is also given to see the difference between simulation and measurement.

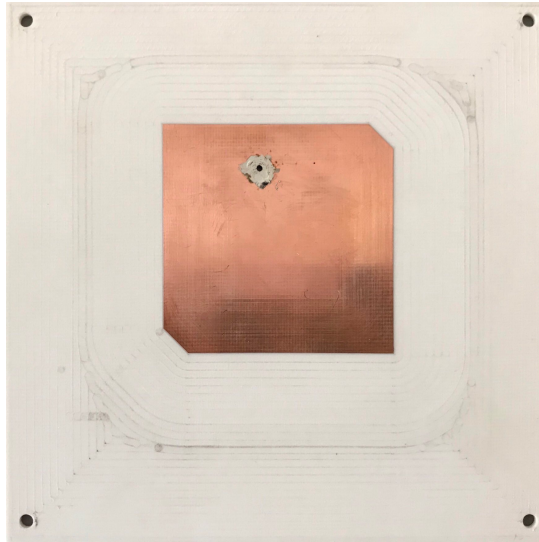


Figure 4.59: Fabricated top patch of the three-layer antenna at L1/L2/L5 GPS bands.

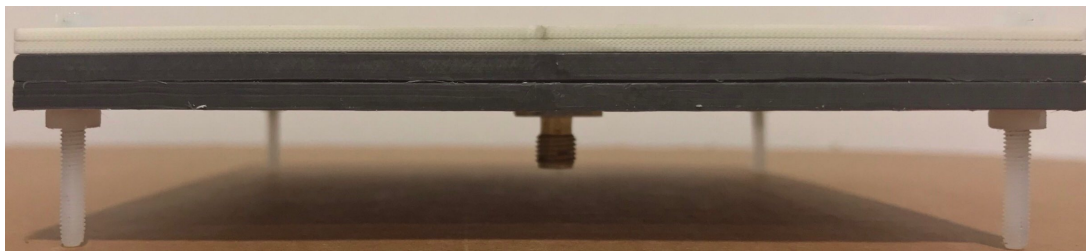


Figure 4.60: Side view of the fabricated three-layer antenna at L1/L2/L5 GPS bands.

According to graph, all three resonance frequencies of the antenna are shifted approximately 60 MHz to higher frequencies. The shift in the resonance frequencies can be occurred from the errors in fabrication and integration of the antenna. Extra milling can cause to shift of the resonance frequencies to higher values. Because, it is known that when the thickness of the substrate is decreased the electrical length of the conducting patch is decreases. Therefore, the resonance frequencies of the antenna increase.

The effects of the material properties of conducting patches are analyzed in simulations to examine the shifts in measurements. The material of the patches were assigned as PEC in design process to decrease the simulation time. The material of the patches is changed to copper and simulations are performed with the final design parameters to simulate the realized antenna materials. The comparison graphs of  $S_{11}$

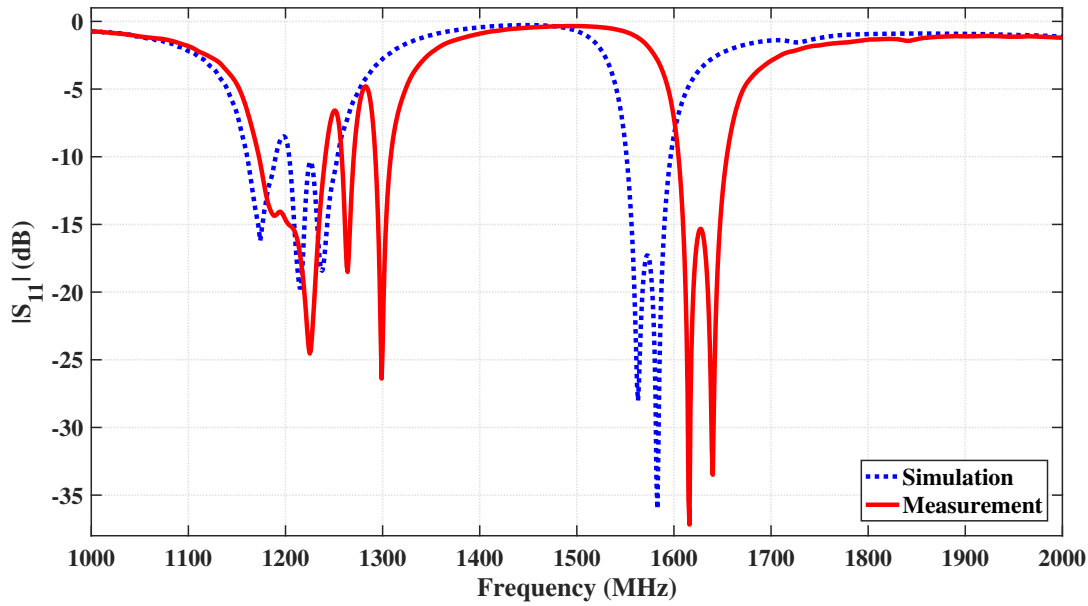


Figure 4.61:  $S_{11}$  comparison of the corner truncated three-layer stacked antenna.

and axial ratio are given in Figure 4.62 and Figure 4.63, respectively. According to comparison graphs, it is seen that the change of PEC material to copper does not effect the return loss and circular polarization performance of the antenna in simulations.

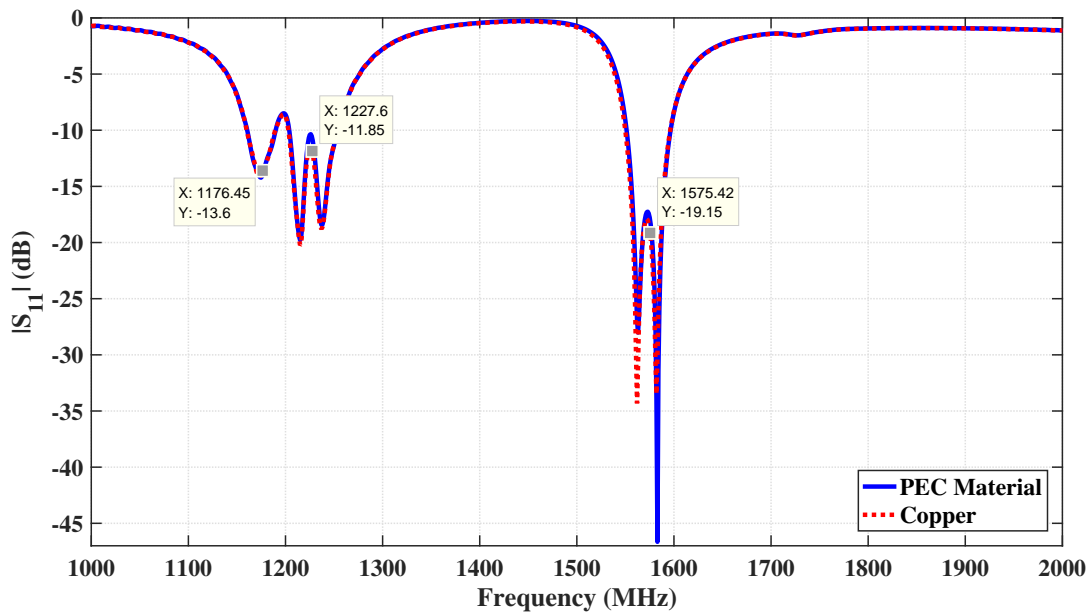


Figure 4.62:  $S_{11}$  comparison between PEC and copper materials on corner truncated three-layer stacked antenna.

Fabricated patches are modified by copper tapes to tune the antenna to L1, L2 and

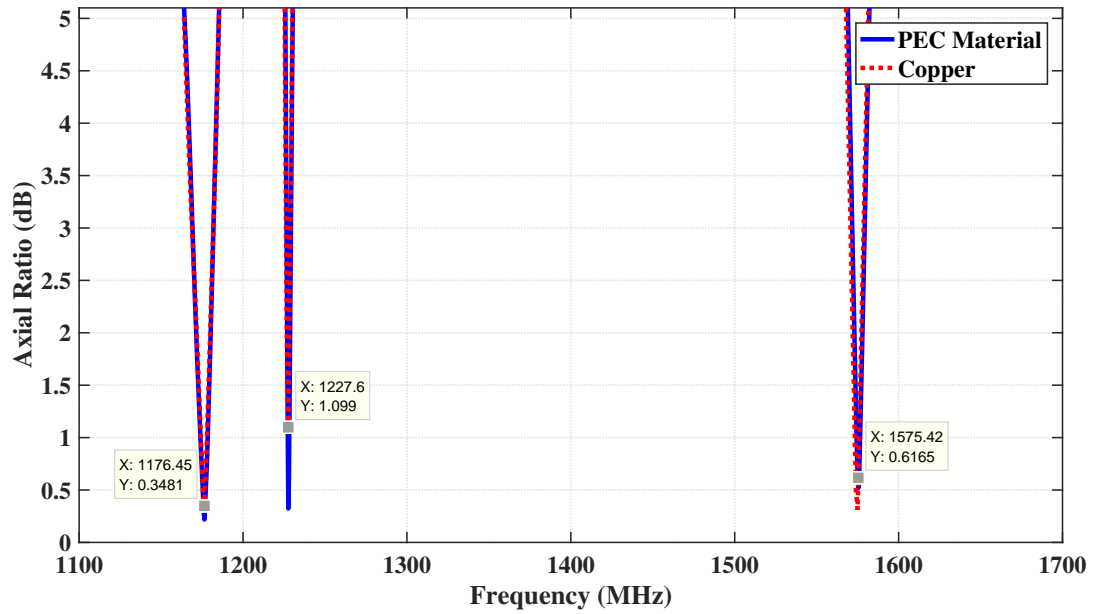


Figure 4.63: Axial ratio comparison between PEC and copper materials on corner truncated three-layer stacked antenna.

L5 GPS bands. The copper tapes are stuck to the edges of the patch. Then, copper tapes are signed by means of a digital caliper as shown in Figure 4.64 and afterwards it is cut. Therefore, the extension of the patches is performed with a controlled way.



Figure 4.64: Tuning studies of the three-layer stacked antenna at L1/L2/L5 GPS bands.

The extension of the bottom patch is performed as shown in Figure 4.65. First, the extension width is changed from 2 mm to 1 mm. The results of  $S_{11}$  measurements are

given in Figure 4.65 for different widths of the copper tapes. As seen in the Figure 4.66, the copper tapes with the extension width of 1 mm tuned the antenna to the center frequency of the L5 GPS band (1176.45 MHz).

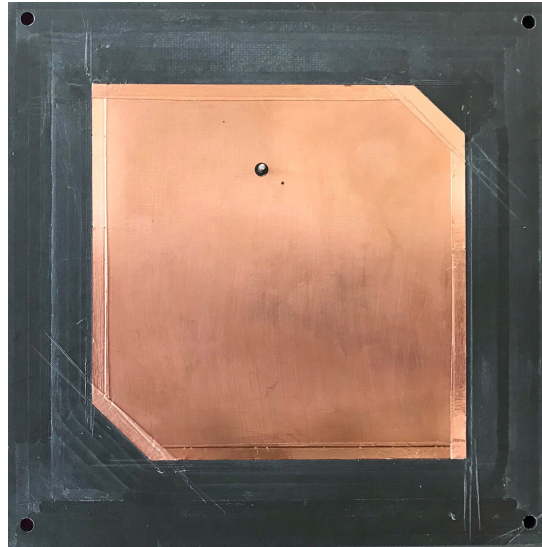


Figure 4.65: Tuned three-layer stacked antenna at L5 GPS band.

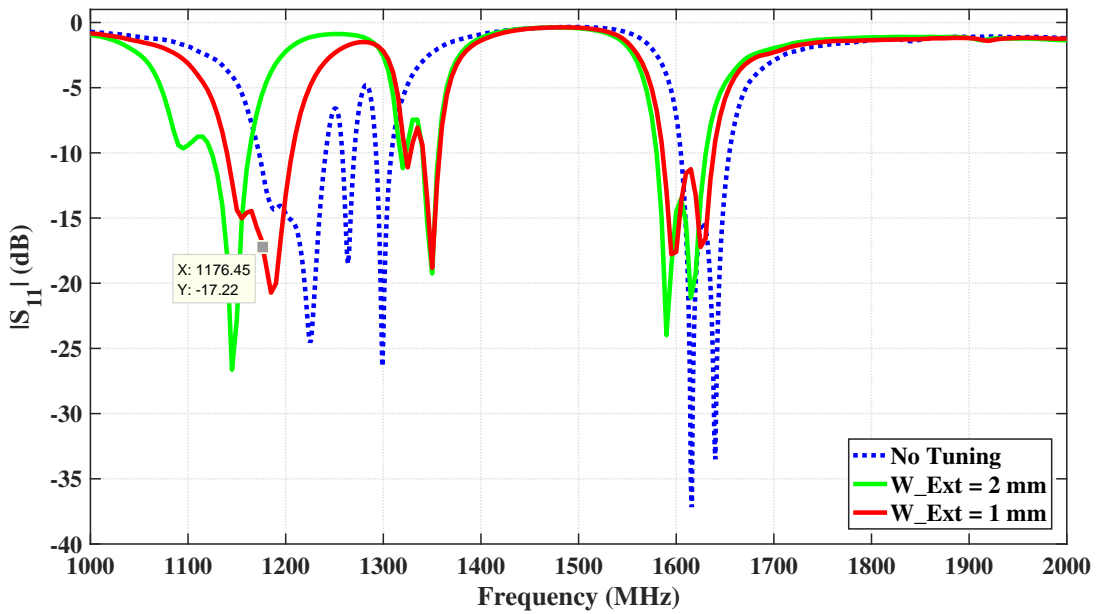


Figure 4.66:  $S_{11}$  measurement results of tuning on three-layer stacked antenna at L5 GPS band.

After adjusting the required resonance frequency, the axial ratio measurements are also performed with the measurement setup shown in Figure 4.67. This measurement

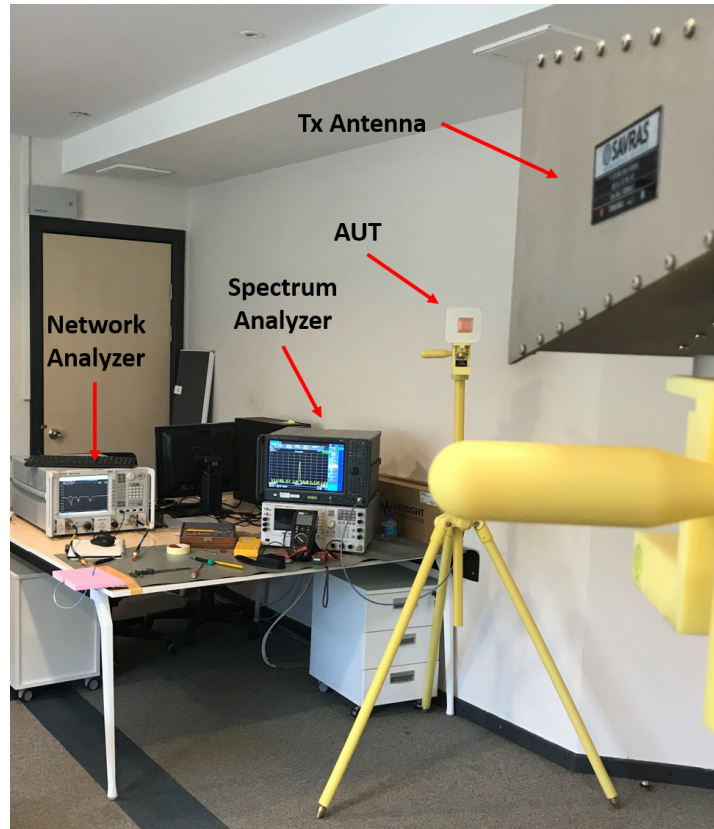


Figure 4.67: Pre-measurement setup for the measurement of axial ratio in tuning studies.

setup is used as a pre-measurement setup before anechoic chamber measurements to give an insight about the circular polarization performance of the antenna. Test signal is transmitted from a signal generator by means of the transmitting antenna (Tx Antenna). The received power by means of the Antenna Under Test (AUT) is measured on the spectrum analyzer on an orthogonal plane. Then, the same measurement is performed for the other orthogonal plane with rotating of the AUT as  $90^\circ$ . The ratio between the measured power levels on orthogonal planes gives the axial ratio. When, the axial ratio measurement is performed at the frequency of 1176.45 MHz, the axial ratio is measured less than 1 dB. Therefore, it is not needed to change the truncation length of the corners.

Tuning is continued with the extension of the middle patch as shown in Figure 4.68. The  $S_{11}$  measurements of the tuned middle patch are given in Figure 4.69. First, the all edges are extended as the extension width of 4 mm and the second band goes into

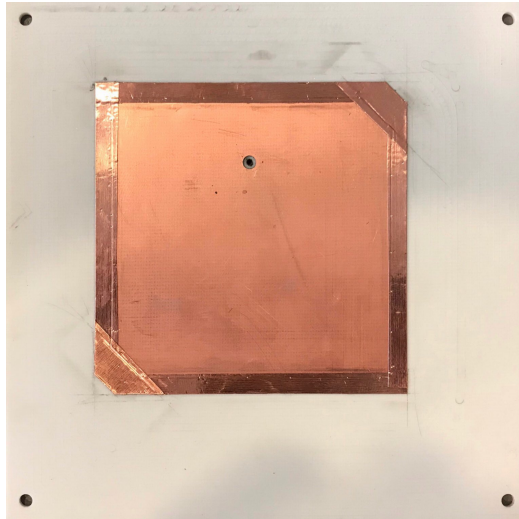


Figure 4.68: Tuned three-layer stacked antenna at L2 GPS band.

the first band as seen in Figure 4.69. The extension width is decreased to enhance the return loss at second band. Therefore, the top edge is cut as 2 mm and the antenna tuned to the center frequency of the L2 GPS band. Then, the measurement of axial ratio is performed. The length of corner truncation is cut as 7 mm on the middle patch and the axial ratio is measured less than 2 dB in pre-measurement setup. This axial ratio is seen acceptable for the circular polarization and tuning continued for L1 frequency band.

The copper tape is stucked over the top patch as shown in Figure 4.70 to tune L1 GPS band. The extension width is changed from 5 mm to 2 mm and the  $S_{11}$  is changed as the given measurement results in Figure 4.71. The tuning of the third frequency band towards higher frequencies is seen with decreasing of the extension width. The third frequency band of the antenna is tuned to the center frequency of the L1 GPS band with the extension width of 2 mm as seen from the Figure 4.71.

The graph of  $S_{11}$  is given in Figure 4.72 to compare the measurement results of early fabricated and final tuned antennas. The impedance bandwidths of 71.1 MHz, 4 MHz and 32 MHz are achieved around the center frequencies of L5, L2 and L1 GPS bands, respectively. The axial ratio of the antenna is measured less than 1 dB at L1 GPS band in pre-measurement setup.

The axial ratio measurements are performed at L2 and L5 GPS bands again with the

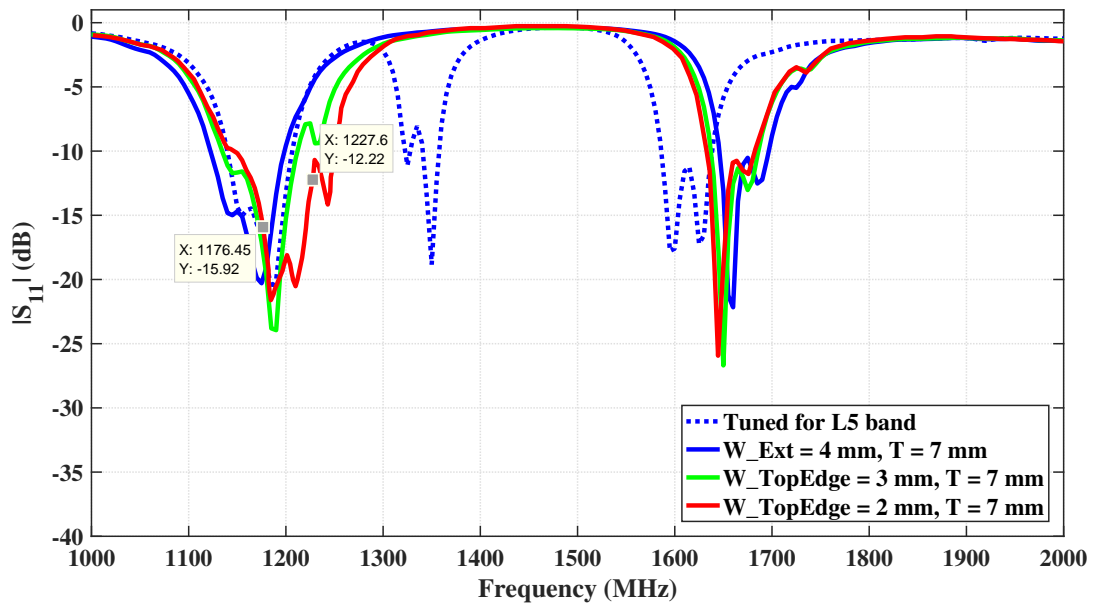


Figure 4.69:  $S_{11}$  measurement results of tuning on three-layer stacked antenna at L2 GPS band.



Figure 4.70: Tuned three-layer stacked antenna at L1 GPS band.

final configuration. The axial ratio is measured less than 8 dB at the center frequency of L2 GPS band and less than 5 dB at the center frequency of the L5 GPS band in pre-measurement setup. It is seen that, the axial ratios are increased at L2 and L5 bands and thus, iterative tuning process causes to disturb the previously tuned bands.

Afterwards, radiation pattern and axial ratio measurements are performed in anechoic

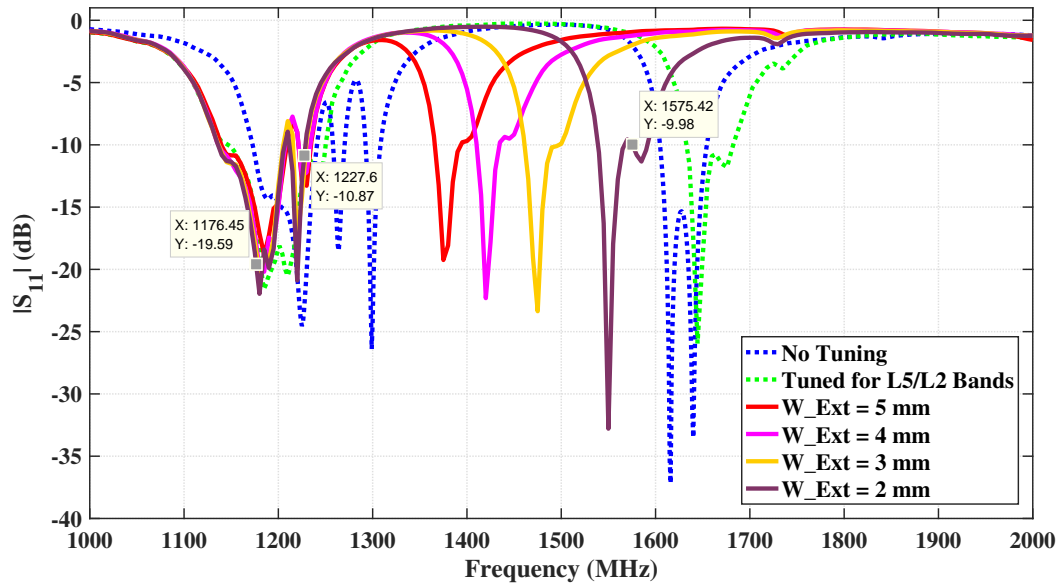


Figure 4.71:  $S_{11}$  measurement results of tuning on three-layer stacked antenna at L1 GPS band.

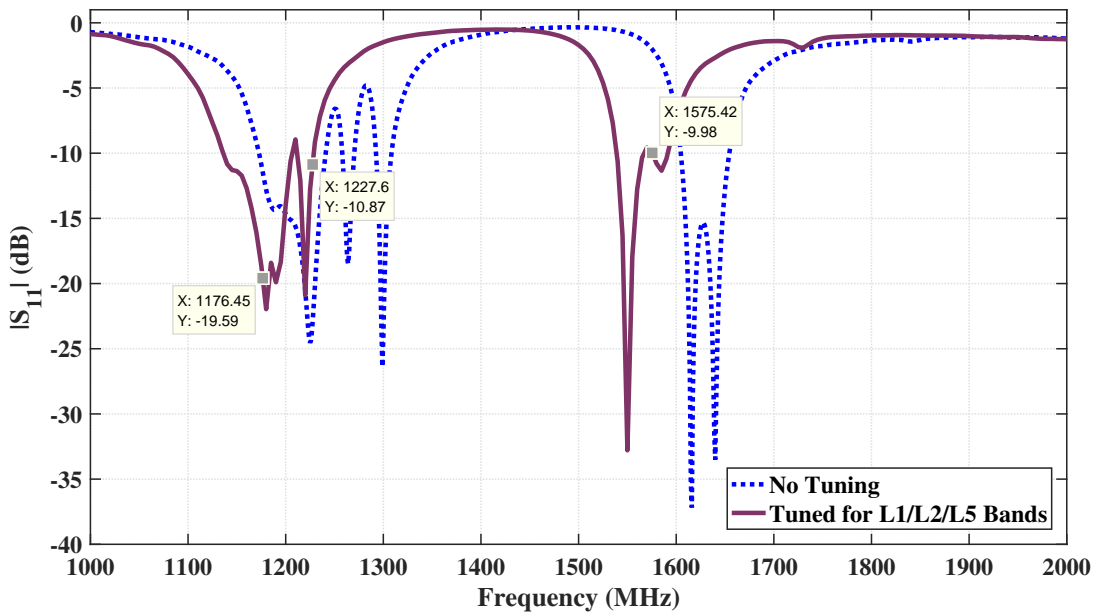


Figure 4.72: Comparison of  $S_{11}$  measurement results of early fabricated and tuned three-layer stacked antennas.

chamber. The measured radiation patterns at the frequencies of 1176 MHz, 1227 MHz and 1575 MHz are given in Figure 4.73, Figure 4.74 and Figure 4.75, respectively. The radiation patterns are measured on azimuth and the elevation planes and com-

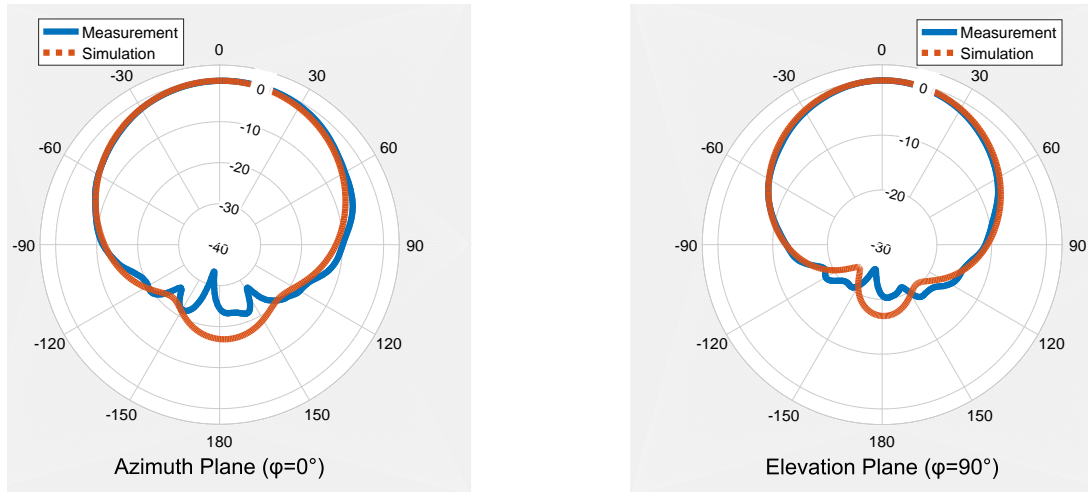


Figure 4.73: Radiation pattern of the first frequency band of three-layer stacked antenna.

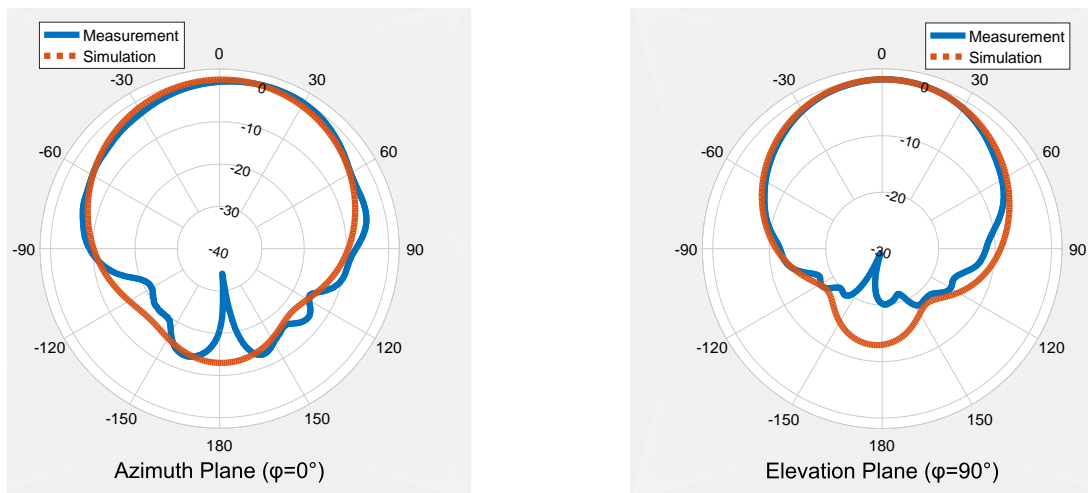


Figure 4.74: Radiation pattern of the second frequency band of three-layer stacked antenna.

pared with the radiation patterns which are obtained in simulations. The measured radiation patterns are seen consistent with simulations. The antenna radiates bore-sight at L1, L2 and L5 GPS bands. In the measurements at L5 GPS band, the HPBW of  $88^\circ$  and  $80^\circ$  are obtained on azimuth and elevation planes, respectively. In the measurements at L2 GPS band, the HPBW of  $84^\circ$  and  $83^\circ$  are obtained on azimuth and elevation planes, respectively. In the measurements at L1 GPS band, the HPBW of  $92^\circ$  and  $83^\circ$  are obtained on azimuth and elevation planes, respectively.

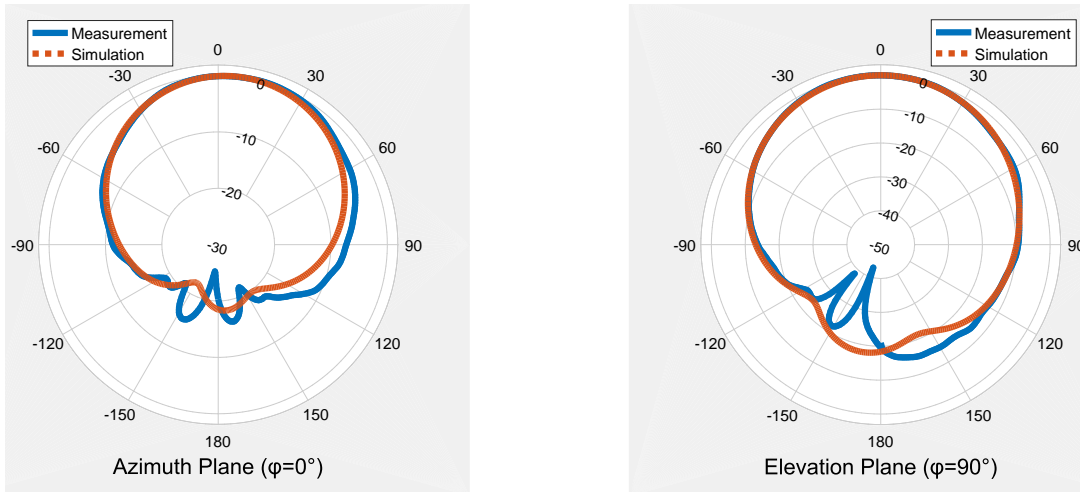


Figure 4.75: Radiation pattern of the third frequency band of three-layer stacked antenna.

The axial ratio measurements are performed around operating bands. The graph which shows the measured axial ratio at different frequencies is given in Figure 4.76. According to axial ratio graph, the tuned antenna has an axial ratio of 0.7 dB at 1575.45 MHz. In addition, 3-dB axial ratio bandwidth of 5 MHz is achieved at L1 GPS band. This results meets the bandwidth requirements of the L1 GPS band.

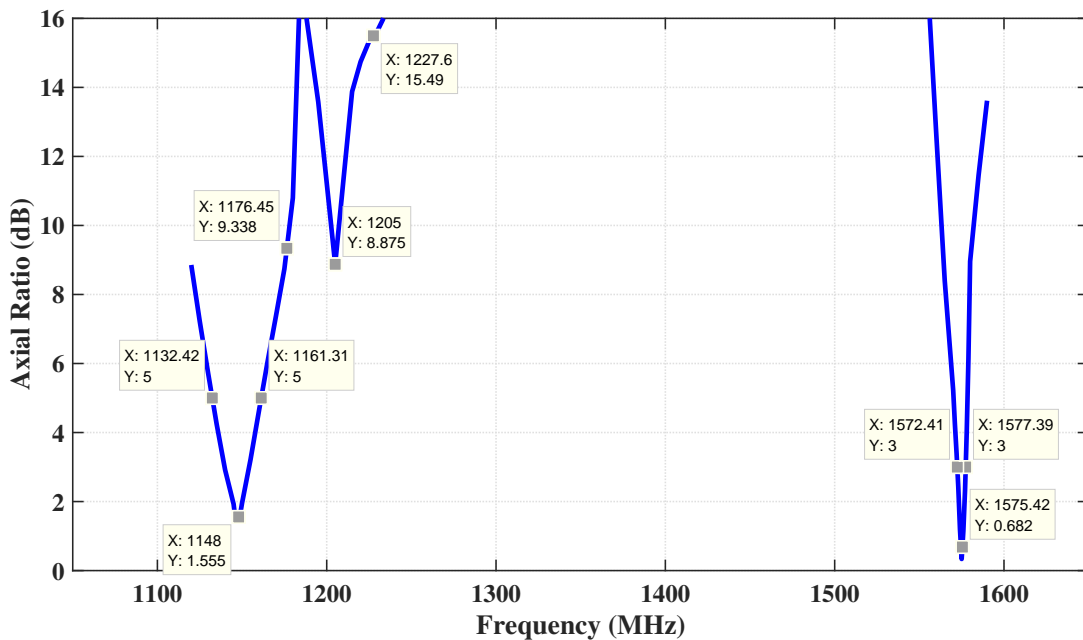


Figure 4.76: Axial ratio measurement result of the tuned three-layer stacked antenna.

It is seen in Figure 4.76, the axial ratios of 9.3 dB and 15.5 dB are achieved at 1176.45 MHz and 1227.6 MHz, respectively. The notch frequencies of the axial ratios are seen as shifted to lower frequencies. The lowest axial ratios of 1.5 dB and 8.9 dB are achieved at 1148 MHz and 1205 MHz, respectively.

5-dB axial ratio bandwidth of 28.9 MHz is achieved at the center frequency of 1148 MHz. According to this output, circular polarization is achieved at the first band of the antenna but the notch frequency is shifted to lower frequencies. However, the circular polarization could not be achieved as required at second band.

### 4.3 SUMMARY and DISCUSSIONS

The studies on L1/L2/L5 triband GPS antennas are given in this chapter. Two kind of antennas are designed to operate at L1/L2/L5 GPS bands as the stacked structure of two-layer and three-layer. Both antennas are fed with a single coaxial probe and circular polarization is achieved at L1/L2/L5 GPS bands in simulations. The bandwidth requirements of GPS signals are also achieved in simulations.

Two-layer stacked antenna consists of a nearly square patch and a coved four-slotted patch. Nearly square patch is used to resonate at L5 GPS band and a novel modified four-slotted patch (coved four-slotted patch) is used to resonate at L1 and L2 GPS bands. A foam substrate is used under the bottom patch antenna to increase the bandwidth at L5 GPS band. Obtained final simulation results are summarized in Table 4.8. According to simulation results, obtained bandwidth requirements meet the specifications of L1/L2/L5 GPS bands.

Table 4.8: Summary of final simulation results of two-layer stacked antenna.

L1 GPS Band		L2 GPS Band		L5 GPS Band	
<b>-10 dB Impedance Bandwidth</b>	12.5 MHz (0.80%)	<b>-10 dB Impedance Bandwidth</b>	33.4 MHz (2.70%)	<b>-10 dB Impedance Bandwidth</b>	43.4 MHz (3.70%)
<b>3 dB Axial Ratio Bandwidth</b>	2.4 MHz (0.15%)	<b>3 dB Axial Ratio Bandwidth</b>	2.8 MHz (0.23%)	<b>5 dB Axial Ratio Bandwidth</b>	26.2 MHz (2.23%)

Designed antenna is fabricated and measured.  $S_{11}$ , axial ratio and radiation pattern

measurements are performed and the measurement results are summarized in Table 4.9. According to measurement results, the operating frequencies of the fabricated antenna are shifted to the frequencies of 1178 MHz, 1259 MHz and 1623 MHz and fabricated antenna radiates to boresight at all three operating bands.

Table 4.9: Summary of measurement results of two-layer stacked antenna.

First Band (Lowest Band)		Second Band (Middle Band)		Third Band (Highest Band)	
<b>-10 dB Impedance Bandwidth</b>	58 MHz (4.92%)	<b>-10 dB Impedance Bandwidth</b>	28 MHz (2.22%)	<b>-10 dB Impedance Bandwidth</b>	11 MHz (0.68%)
<b>5 dB Axial Ratio Bandwidth</b>	27.3 MHz (2.30%)	<b>5 dB Axial Ratio Bandwidth</b>	-	<b>5 dB Axial Ratio Bandwidth</b>	-
<b>Lowest Axial Ratio</b>	0.7 dB (@1187 MHz)	<b>Lowest Axial Ratio</b>	8.06 dB (@1257 MHz)	<b>Lowest Axial Ratio</b>	7.51 dB (@1618 MHz)
<b>Azimuth HPBW</b>	63°	<b>Azimuth HPBW</b>	77°	<b>Azimuth HPBW</b>	82°
<b>Elevation HPBW</b>	69°	<b>Elevation HPBW</b>	71°	<b>Elevation HPBW</b>	88°

According to axial ratio measurements, the axial ratio of 3.9 dB is achieved at 1176 MHz. The lowest axial ratio is measured as 0.7 dB at the frequency of 1187 MHz. The 5-dB axial ratio bandwidth of 27.3 MHz is achieved around the center frequency of 1187 MHz. The lowest axial ratios are measured as 8 dB and 7.5 dB at the frequencies of 1257 MHz and 1618 MHz, respectively. It is seen from the results that the fabricated antenna radiates circularly polarized at L5 GPS band but does not radiate circularly polarized as required at second and third operating bands. In order to tune the third band to L1 GPS band, antenna is tuned by hand and the length of the conducting cove is increased to decrease the frequency ratio and third frequency is also tuned to L1 GPS band.

Three-layer stacked antenna consists of three corner truncated patches which are used to resonate at L1/L2/L5 GPS bands. The microstrip layer which is used to operate at L5 GPS band is placed as the lowest layer and that patch is named as the bottom patch. Rogers RT5880 substrate with the height of 6.36 mm is chosen to get broader bandwidth as the substrate of bottom patch. Rogers 4003C substrates with the height of 1.52 mm are used as the substrates of middle and top patches. Obtained final simulation results are summarized in Table 4.10. According to simulation results, obtained bandwidth requirements meet the specifications of L1/L2/L5 GPS bands.

Table 4.10: Summary of final simulation results of three-layer stacked antenna.

L1 GPS Band		L2 GPS Band		L5 GPS Band	
<b>-10 dB Impedance Bandwidth</b>	41.7 MHz (2.65%)	<b>-10 dB Impedance Bandwidth</b>	49.3 MHz (4.00%)	<b>-10 dB Impedance Bandwidth</b>	31.3 MHz (2.70%)
<b>3 dB Axial Ratio Bandwidth</b>	7.3 MHz (0.46%)	<b>3 dB Axial Ratio Bandwidth</b>	2.5 MHz (0.20%)	<b>3 dB Axial Ratio Bandwidth</b>	13.2 MHz (1.12%)
<b>5 dB Axial Ratio Bandwidth</b>	12.4 MHz (0.79%)	<b>5 dB Axial Ratio Bandwidth</b>	4.21 MHz (0.34%)	<b>5 dB Axial Ratio Bandwidth</b>	21.6 MHz (1.84%)

Designed antenna is fabricated, integrated and measured. It is seen in the s-parameter measurements that all three frequency bands are shifted to higher frequencies. The antenna is tune to L1/L2/L5 GPS bands by copper tapes.  $S_{11}$ , axial ratio and radiation pattern measurements are performed on tuned antenna and the measurement results of the tuned antenna are summarized in Table 4.11.

Table 4.11: Summary of measurement results of three-layer stacked antenna.

First Band (Lowest Band)		Second Band (Middle Band)		Third Band (Highest Band)	
<b>-10 dB Impedance Bandwidth</b>	71 MHz (6.04%)	<b>-10 dB Impedance Bandwidth</b>	4 MHz (0.30%)	<b>-10 dB Impedance Bandwidth</b>	32 MHz (2.03%)
<b>3 dB Axial Ratio Bandwidth</b>	15 MHz (1.28%)	<b>3 dB Axial Ratio Bandwidth</b>	-	<b>3 dB Axial Ratio Bandwidth</b>	5 MHz 0.32%
<b>5 dB Axial Ratio Bandwidth</b>	28.9 MHz (2.46%)	<b>5 dB Axial Ratio Bandwidth</b>	-	<b>5 dB Axial Ratio Bandwidth</b>	8.7 MHz (0.56%)
<b>Lowest Axial Ratio</b>	1.5 dB (@ 1148 MHz)	<b>Lowest Axial Ratio</b>	8.9 dB (@ 1205 MHz)	<b>Lowest Axial Ratio</b>	0.7 dB (@ 1575 MHz)
<b>Azimuth HPBW</b>	92°	<b>Azimuth HPBW</b>	84°	<b>Azimuth HPBW</b>	88°
<b>Elevation HPBW</b>	83°	<b>Elevation HPBW</b>	83°	<b>Elevation HPBW</b>	80°

The impedance bandwidths of 71 MHz, 4 MHz and 32 MHz are achieved around the center frequencies of L5, L2 and L1 GPS bands, respectively. In the axial ratio measurements at L1 GPS band, the axial ratio of 0.7 dB and 3-dB axial ratio bandwidth of 5 MHz are achieved. In the axial ratio measurements at the center frequencies of L5 and L2 GPS bands, the axial ratios of 9.3 dB and 15.5 dB are measured, respectively. The lowest axial ratios of 1.5 dB and 8.9 dB are achieved at 1148 MHz and 1205 MHz, respectively. 5-dB axial ratio bandwidth of 28.9 MHz is achieved at the center frequency of 1148 MHz. According to this output, circular polarization is

achieved at L5 GPS band of the antenna but the notch frequency is shifted to lower frequencies. However, the circular polarization could not be achieved as required at second band. In the radiation pattern measurements, the antenna radiates boresight at L1, L2 and L5 GPS bands.

Some differences are observed between simulations and measurements in both two-layer and three-layer antennas. It is thought that the shift in the resonance frequencies can be occurred from errors in fabrication and integration. Microstrip layers are fabricated with PCB prototyping machine, and therefore extra milling can cause to detune of the resonance frequencies of the microstrip layers. Integration is another important process in stacked antennas. Because, aligning and sticking of the layers are quite challenging issue in integration of the stacked antenna. Misalignment, the unwanted air gaps and double sided tapes can cause to detune the antenna.

The tuning process is also challenging in multiband stacked antennas. Because, it is needed to demount the antenna, modify layer and then mount it again. In tuning process, the resonance frequencies are tuned by cutting of the extending parts of conducting copper tapes. But, the circular polarization performance of the antenna is also needed to be taken into consideration. Therefore, a pre-measurement setup is used to give an insight about the performance of circular polarization during the tuning process of the antenna. In addition, the tuning of a microstrip layer can cause to detune of another layer. Therefore, tuning of staked antennas is a time consuming process.

Shifted resonance frequencies of the fabricated antennas can be tuned with re-fabrication by taking into consideration in the amount of shifts in frequencies.

## CHAPTER 5

### CONCLUSION, ACHIEVEMENTS AND FUTURE WORKS

In this thesis study, it is intended to design multiband circularly polarized microstrip antennas for GPS applications. A circularly polarized L1 band GPS antenna is designed with CMA method to get an insight to circularly polarized microstrip antennas. The theory of characteristic modes, physical explanations and surface currents of characteristic modes are examined within the studies on CMA method. A design flow is proposed for circularly polarized microstrip antennas by interpreting of CMA outputs.

An L1/L2 dualband GPS antenna is intended to designed on a single patch by feeding with a single coaxial probe. According to this purpose, capacitively loaded four-slotted patch is designed to operate circularly polarized at L1/L2 GPS bands. Afterwards, a novel modified slotted patch (zigzag four-slotted patch) is proposed to decrease the frequency ratio in dualband microstrip antennas without using capacitive loading. Proposed zigzag four-slotted patch is designed to operate circularly polarized at L1/L2 GPS bands with a single coaxial feed. Designed antenna is fabricated with PCB prototyping machine and measurements are carried out. In  $S_{11}$  measurements, it is seen that the resonance frequencies are shifted to higher frequencies. The lower band and higher bands are shifted as 11 MHz and 46 MHz, respectively. It is thought that the shifts in resonance frequencies occurred because of extra milling in fabrication process. Therefore, the shifts in the resonance frequencies are analyzed in simulations by increasing the thickness of the milling, and thus it is seen that the resonance frequencies are shifted to higher frequencies as in the measurements. The axial ratio of 8 dB is measured at operating bands.

Two kind of stacked antennas are designed within the studies on triband GPS anten-

nas. Both antennas are designed to operate RHCP at L1/L2/L5 GPS bands and fed by a single coaxial probe. The inner conductor of the coaxial probe is soldered to top patches and the rest of the patches are fed by parasitically in both antennas.

In one of these antennas, triband operation is achieved by using two microstrip layers, and therefore it is named as two-layer stacked antenna. A modified four-slotted patch (coved four-slotted patch) is proposed to operate at L1/L2 GPS bands and a nearly square patch is used to operate at L5 GPS band. A foam substrate is used beneath the lower microstrip patch to meet the broad bandwidth requirement in L5 GPS signal. The microstrip layers of the stacked antenna are fabricated and stacked antenna is integrated. The fabricated antenna is measured and it is seen that the frequency bands are shifted to the frequencies of 1178 MHz, 1259 MHz and 1623 MHz. The radiation pattern and axial ratio measurements are performed in anechoic chamber. The axial ratio of 3.9 dB is achieved at 1176 MHz and the lowest axial ratio of 0.7 dB is measured at 1187 MHz. The 5-dB axial ratio bandwidth of 27.3 MHz is achieved around the center frequency of 1187 MHz. The lowest axial ratios are measured as 8 dB and 7.5 dB at the second and third operating bands, respectively. The third band is tuned to L1 GPS band with copper tapes.

The second triband stacked antenna consists of three microstrip layers, and therefore it is named as three-layer stacked antenna. Corner truncated patches are designed to operate RHCP at L1/L2/L5 GPS bands in the microstrip layers. The bottom patch is used to operate at L5 GPS band, the middle patch is used to operate at L2 GPS band and the top patch is used to operate at L1 GPS band. Bandwidth requirements of L1/L2/L5 GPS bands are met in simulations. The microstrip layers of the stacked antenna are fabricated and stacked antenna is integrated. In  $S_{11}$  measurements, it is seen that all three operating bands are shifted to higher frequencies, and therefore tuning studies are applied to each patch to tune the antenna. The impedance bandwidths of 71.1 MHz, 4 MHz and 32 MHz are achieved around the center frequencies of L5, L2 and L1 GPS bands, respectively. The radiation pattern and axial ratio measurements of tuned antenna are performed in anechoic chamber. The axial ratio of 0.7 dB is obtained at the center frequency of L1 GPS band (1575.42 MHz). In addition, 3-dB axial ratio bandwidth of 5 MHz is achieved at L1 GPS band. The axial ratios of 9.3 dB and 15.5 dB are achieved at 1176.45 MHz and 1227.6 MHz, respectively. The lowest

axial ratios of 1.5 dB and 8.9 dB are achieved at 1148 MHz and 1205 MHz, respectively. 5-dB axial ratio bandwidth of 28.9 MHz is achieved at the center frequency of 1148 MHz.

Multiband circularly polarized microstrip antennas are designed in simulations as meeting the requirements of civilian GPS signals. However, the measurements on fabricated antennas show that the resonance frequencies are shifted to higher frequencies. It is thought that the shifts in resonance frequencies are originated from extra milling in PCB prototyping machine. Because, the electrical length decreases when the height of the substrate decreases. Therefore, simulation results can be achieved with better fabrication methods like PCB processing with UV lasers. Misalignment, air gaps and double-sided tapes can also detune the antennas in the integration of stacked antennas.

It is observed that circular polarization bandwidths were narrow in slotted patches. It is not recommended to use slotted patches in dualband applications which require broader circular polarization bandwidth.

It is seen that the circular polarization bandwidths were narrow in designed antennas. So, increasing the circular polarization bandwidth of operating bands will be performed in future works. It is known that the double fed circularly polarized patch antennas have broader axial ratio bandwidths than single fed ones. Therefore, circular polarization can be applied with double feed and a  $90^\circ$  phase shifter passive component.



## REFERENCES

- [1] S. S. Gao, Q. Luo, and F. Zhu, *Circularly Polarized Antennas*. John Wiley & Sons, 2013.
- [2] B. Hofmann-Wellenhof, H. Lichtenegger, and E. Wasle, *GNSS-Global Navigation Satellite Systems: GPS, GLONASS, Galileo, and more*. Springer Science & Business Media, 2007.
- [3] C. A. Balanis, *Antenna theory: analysis and design*. Wiley-Interscience, 2005.
- [4] R. Garg, P. Bhartia, I. J. Bahl, and A. Ittipiboon, *Microstrip antenna design handbook*. Artech house, 2001.
- [5] A. Kajiwara, "Line-of-sight indoor radio communication using circular polarized waves," *IEEE Transactions on Vehicular Technology*, vol. 44, no. 3, pp. 487–493, 1995.
- [6] S. Kumar, B. K. Kanaujia, M. K. Khandelwal, and A. Gautam, "Stacked dual-band circularly polarized microstrip antenna with small frequency ratio," *Microwave and Optical Technology Letters*, vol. 56, no. 8, pp. 1933–1937, 2014.
- [7] M. H. Dias, B. Franciscatto, E. Nogueira, and T. Vuong, "On the design of a dual-fed aperture-coupled circularly polarized microstrip patch antenna," in *Microwave & Optoelectronics Conference (IMOC), 2013 SBMO/IEEE MTT-S International*, pp. 1–5, IEEE, 2013.
- [8] T. Jayachitra, V. Pandey, and A. Singh, "Circularly polarized microstrip patch antenna with fr4 substrate in dual feed for wlan applications," *International Journal of Advanced Research in Computer Science and Electronics Engineering (IJARCSEE)*, vol. 2, no. 12, pp. pp–765, 2013.
- [9] M.-C. Pan and K.-L. Wong, "Circularly polarized microstrip antenna with dual-cpw feed," in *Antennas and Propagation Society International Symposium, 2000. IEEE*, vol. 2, pp. 996–999, IEEE, 2000.

- [10] X. Ye, M. He, Y. Hao, Y. Wang, and G. Wang, "Analysis and design of dual-feed circularly polarized u-slot microstrip antennas," in *Communication Problem-Solving (ICCP), 2015 IEEE International Conference on*, pp. 300–302, IEEE, 2015.
- [11] P. Sharma and K. Gupta, "Analysis and optimized design of single feed circularly polarized microstrip antennas," *IEEE Transactions on Antennas and Propagation*, vol. 31, no. 6, pp. 949–955, 1983.
- [12] S. L. S. Yang, K. F. Lee, A. A. Kishk, and K. M. Luk, "Design of wideband single feed truncated corner microstrip patch antennas for circularly polarized applications," in *2008 IEEE Antennas and Propagation Society International Symposium*, pp. 1–4, July 2008.
- [13] J. Luo, A. Alphones, and C. Jin, "Microstrip square patch antenna with arc shaped edges for circular polarization," in *Microwave Conference Proceedings (APMC), 2011 Asia-Pacific*, pp. 1710–1713, IEEE, 2011.
- [14] S. Long and L. Shen, "The circularly polarized elliptical printed-circuit antenna," in *Antennas and Propagation Society International Symposium, 1980*, vol. 18, pp. 731–734, IEEE, 1980.
- [15] A. A. Heidari, M. Heyrani, and M. Nakhkash, "A dual-band circularly polarized stub loaded microstrip patch antenna for gps applications," *Progress In Electromagnetics Research*, vol. 92, pp. 195–208, 2009.
- [16] Z. N. Chen, X. Qing, *et al.*, "Asymmetric-circular shaped slotted microstrip antennas for circular polarization and rfid applications," *IEEE Transactions on Antennas and Propagation*, vol. 58, no. 12, pp. 3821–3828, 2010.
- [17] Y. Anjani, A. Alphones, *et al.*, "A wide-beam circularly polarized asymmetric-microstrip antenna," *IEEE Transactions on Antennas and Propagation*, vol. 63, no. 8, pp. 3764–3768, 2015.
- [18] X. Qing, Z. Chen, *et al.*, "Compact circularly polarized symmetric-slit microstrip antennas," *IEEE Antennas and Propagation Magazine*, vol. 53, no. 4, pp. 63–75, 2011.

- [19] K.-F. Tong and T.-P. Wong, "Circularly polarized u-slot antenna," *IEEE Transactions on antennas and propagation*, vol. 55, no. 8, pp. 2382–2385, 2007.
- [20] A. Khidre, K. F. Lee, F. Yang, and A. Elsherbeni, "Wideband circularly polarized e-shaped patch antenna for wireless applications [wireless corner]," *IEEE Antennas and Propagation Magazine*, vol. 52, no. 5, pp. 219–229, 2010.
- [21] W.-S. Chen, K.-L. Wong, and C.-K. Wu, "Inset microstripline-fed circularly polarized microstrip antennas," *IEEE transactions on antennas and propagation*, vol. 48, no. 8, pp. 1253–1254, 2000.
- [22] S.-Q. Wu, S.-B. Liu, and Z. Guo, "Coaxial probe-fed circularly polarized microstrip antenna for beidou rdss applications," in *Microwave and Millimeter Wave Technology (ICMMT), 2010 International Conference on*, pp. 297–299, IEEE, 2010.
- [23] T. Huynh and K.-F. Lee, "Single-layer single-patch wideband microstrip antenna," *Electronics letters*, vol. 31, no. 16, pp. 1310–1312, 1995.
- [24] F. Yang, X.-X. Zhang, X. Ye, and Y. Rahmat-Samii, "Wide-band e-shaped patch antennas for wireless communications," *IEEE transactions on antennas and propagation*, vol. 49, no. 7, pp. 1094–1100, 2001.
- [25] C.-M. Su and K.-L. Wong, "A dual-band gps microstrip antenna," *Microwave and Optical Technology Letters*, vol. 33, no. 4, pp. 238–240.
- [26] O. P. Falade, X. Chen, Y. Alfadhil, and C. Parini, "Quad band circular polarized antenna," in *Antennas and Propagation Conference (LAPC), 2012 Loughborough*, pp. 1–4, IEEE, 2012.
- [27] K. Agarwal, A. Alphones, *et al.*, "Triple-band compact circularly polarised stacked microstrip antenna over reactive impedance meta-surface for gps applications," *IET Microwaves, Antennas & Propagation*, vol. 8, no. 13, pp. 1057–1065, 2014.
- [28] O. P. Falade, M. U. Rehman, Y. Gao, X. Chen, and C. Parini, "Stacked patch circular polarized antenna for gps/galileo receiver applications," in *Antennas and Propagation (EUCAP), 2012 6th European Conference on*, pp. 1992–1995, IEEE, 2012.

- [29] O. P. Falade, M. U. Rehman, Y. Gao, X. Chen, and C. G. Parini, "Single feed stacked patch circular polarized antenna for triple band gps receivers," *IEEE transactions on antennas and propagation*, vol. 60, no. 10, pp. 4479–4484, 2012.
- [30] Y. Wang, J. Feng, J. Cui, and X. Yang, "A dual-band circularly polarized stacked microstrip antenna with single-fed for gps applications," in *Antennas, Propagation and EM Theory, 2008. ISAPE 2008. 8th International Symposium on*, pp. 108–110, IEEE, 2008.
- [31] N. Herscovici, Z. Sipus, and D. Bonefacic, "Circularly polarized single-fed wide-band microstrip patch," *IEEE Transactions on Antennas and Propagation*, vol. 51, no. 6, pp. 1277–1280, 2003.
- [32] S. Maci and G. B. Gentili, "Dual-frequency patch antennas," *IEEE Antennas and Propagation Magazine*, vol. 39, no. 6, pp. 13–20, 1997.
- [33] K.-P. Yang and K.-L. Wong, "Dual-band circularly-polarized square microstrip antenna," *IEEE Transactions on Antennas and Propagation*, vol. 49, no. 3, pp. 377–382, 2001.
- [34] T. Fujimoto, D. Ayukawa, K. Iwanaga, and M. Taguchi, "Dual-band circularly polarized microstrip antenna for gps application," in *Antennas and Propagation Society International Symposium, 2008. AP-S 2008. IEEE*, pp. 1–4, IEEE, 2008.
- [35] S. Kim, K. Yoon, and W. Yang, "Dual-band circular polarization square patch antenna for gps and dmb," *Microwave and optical technology letters*, vol. 49, no. 12, pp. 2925–2926, 2007.
- [36] K.-F. Lee, S. L. S. Yang, and A. A. Kishk, "Dual-and multiband u-slot patch antennas," *IEEE Antennas and Wireless Propagation Letters*, vol. 7, pp. 645–647, 2008.
- [37] X.-B. Sun, "Circular-slotted microstrip antenna for gps," *Microwave and Optical Technology Letters*, vol. 52, no. 5, pp. 999–1000, 2010.
- [38] R. Garbacz and R. Turpin, "A generalized expansion for radiated and scattered fields," *IEEE transactions on Antennas and Propagation*, vol. 19, no. 3, pp. 348–358, 1971.

- [39] R. Harrington and J. Mautz, "Theory of characteristic modes for conducting bodies," *IEEE Transactions on Antennas and Propagation*, vol. 19, no. 5, pp. 622–628, 1971.
- [40] R. Harrington, J. Mautz, and Y. Chang, "Characteristic modes for dielectric and magnetic bodies," *IEEE Transactions on Antennas and Propagation*, vol. 20, no. 2, pp. 194–198, 1972.
- [41] M. Cabedo Fabres, *Systematic design of antennas using the theory of characteristic modes*. PhD thesis, 2008.
- [42] M. Cabedo-Fabres, E. Antonino-Daviu, A. Valero-Nogueira, and M. F. Bataller, "The theory of characteristic modes revisited: A contribution to the design of antennas for modern applications," *IEEE Antennas and Propagation Magazine*, vol. 49, no. 5, pp. 52–68, 2007.
- [43] E. Newman, "Small antenna location synthesis using characteristic modes," *IEEE Transactions on Antennas and Propagation*, vol. 27, no. 4, pp. 530–531, 1979.
- [44] Y. Chen and C.-F. Wang, "Characteristic-mode-based improvement of circularly polarized u-slot and e-shaped patch antennas," *IEEE antennas and wireless propagation letters*, vol. 11, pp. 1474–1477, 2012.